Neurophysiological Biomarkers of Motor Recovery in Severe Chronic Stroke

Neurophysiological Biomarkers of Motor Recovery in Severe Chronic Stroke

Dissertation

der Mathematisch-Naturwissenschaftlichen Fakultät

der Eberhard Karls Universität Tübingen

zur Erlangung des Grades eines

Doktors der Naturwissenschaften

(Dr. rer. nat.)

vorgelegt von

Dipl.-Inform. Andreas Markus Ray

aus Achern

Tübingen

2021

Gedruckt mit Genehmigung der Mathematisch-Naturwissenschaftlichen Fakultät der Eberhard Karls Universität Tübingen.

Tag der mündlichen Qualifikation:	25.02.2022
Dekan:	Prof. Dr. Thilo Stehle
1. Berichterstatter:	Prof. Dr. Andreas Schilling
2. Berichterstatter:	Prof. Dr. Dr. h.c. mult. Niels Birbaumer
3. Berichterstatter:	PD Dr. Ander Ramos-Murguialday

Für meine kleine Familie
Sonja und Valentin

Abstract

The most common repercussion of stroke is disability, affecting millions of survivors globally each year. More than half of the victims develop chronic motor impairments. There is no efficient standardized therapy for this group. The processes in the brain of patients who recover their motor ability are poorly understood, even after decades of research. Finding, observing and tracking neurophysiological correlates of stroke and recovery could facilitate the interpretation of the brain activity before and during treatment. New therapies could be devised and studies designed, based on models and predicitions derived from these biomarkers.

This thesis presents analyses of neurophysiological data of brain and muscles of healthy individuals and chronic stroke patients with severe motor impairments. Candidates for biomarkers are presented and their potential evaluated. First, desynchronization of the Sensorimotor Rhythm was considered. The brain activity of chronic stroke patients was analyzed during movement attempts of the paretic arm. There was a correlation between motor impairment and the evolution of desynchronization strength as well as the hemispheric laterality of the desynchronization. Moreover, the location of the lesion might have an effect on the strength of desynchronization. Furthermore, there was a significant difference of the peak center frequency of the rhythm compared between stroke patients and healthy individuals. Secondly, low-frequency activity of the brain during movement attempts of the stroke patients increased from before to after the intervention, confirming previous work in animal models and patients with less severe impairment. Thirdly, a methodology for the analysis of coherent brain oscillations during movement attempts is presented. First results show that connectivity within the hemisphere of the lesion as well as the communication between the hemispheres increased with the therapy. Finally, an experiment investigating potential effects of intensive robot-based interventions on muscle activity is presented. Results from four stroke patients did not indicate that the rehabilitation training induces muscular fatigue.

The final chapter presents complementary work on enhancing existing Brain-Machine interface therapies. Sensory feedback to the patient is improved by way of displaying a virtual representation of an exoskeleton for training of movements of hand and arm. Furthermore, a rehabilitation training was embedded in a gamified environment for maximizing immersion and motivation of the patient.

The biomarkers presented in these studies could serve as building blocks for modeling neurorehabilitation and to track and visualize recovery in such enriched training environments. The transition of this research to new or improved modern therapeutic approaches in clinical practice could serve millions of stroke victims.

Kurzfassung

Schlaganfälle kommen jährlich millionenfach und weltweit vor. Die Patienten leiden fast immer unter verschiedensten Behinderungen, und mehr als die Hälfte entwickelt chronische Lähmungen. Für diese Gruppe der Patienten gibt es keine wirksame standardisierte Therapie. Die Vorgänge im Gehirn der Patienten, die ihre Bewegungsfähigkeit nach dem Schlaganfall wieder verbessern, versteht man auch nach Jahrzehnten der Forschung nur teilweise. Das Finden, Beobachten und Überwachen von neurophysiologischen Korrelaten des Erholungsvorgangs könnte helfen, die Gehirnaktivität vor und während einer solchen Behandlung besser zu verstehen. Durch die Entdeckung solcher "Biomarker" und davon abgeleiteter Vorhersagemodelle könnten neuartige Therapien entwickelt und gezieltere klinische Studien entworfen werden.
In dieser Dissertation werden mehrere Analysen von neurophysiologischen Daten der Gehirn- und Muskelaktivität von Gesunden und schwerst gelähmten chronischen Schlaganfallpatienten vorgestellt. Das Potential verschiedener Biomarker wird auf Basis dieser Daten bewertet. Zunächst wurde die Desynchronisierung des Sensorimotorischen Rhythmus' untersucht. Die Gehirnaktivität von chronisch gelähmten Schlaganfallpatienten wurde während der Ausführung von Bewegungen des gelähmten Arms analysiert. Es ergab sich eine Korrelation zwischen der Erholung der Bewegungsfähigkeit und dem Verlauf der Desynchronisierung des Sensorimotorischen Rhythmus' sowie dessen Lateralisation zwischen beiden Hemisphären. Die Position der Läsion scheint zudem einen Einfluss auf die Stärke der Desynchronisierung zu haben. Außerdem gab es beim Vergleich von Schlaganfallpatienten und Gesunden Unterschiede in der individuellen dominanten Frequenz des Rhythmus'. In einer weiteren Analyse wurde die Gehirnaktivität in niedrigen Frequenzen des Aktivitätsspektrums untersucht. Diese erhöhte sich bei den Patienten über der Läsion, was Ergebnisse früherer Arbeiten mit Tiermodellen und weniger stark gelähmten Schlaganfallpatienten bestätigt. Darüberhinaus wird eine Vorgehensweise für die Analyse von kohärenten Oszillationen im Gehirn während der Ausführung von Bewegungen vorgestellt. Erste Ergebnisse zeigen, dass sich die Verbindungen innerhalb der beschädigten Gehirnhälfte und zwischen den beiden Gehirnhälften mit der Therapie verstärken. Zuletzt wird ein Experiment vorgestellt, worin die möglichen Effekte der intensiven robotischen Therapie auf die Muskelaktivität der Patienten untersucht werden. Die Ergebnisse zeigten keinen ermüdenden Effekt des Trainings auf die Muskeln.
Im letzten Kapitel werden weiterführende Arbeiten für die Erweiterung von bereits existierenden Brain-Machine interface-Therapien vorgestellt. Ein virtuelles Exoskelett wurde zur Verbesserung des visuellen Feedbacks, das die Patienten während des Bewegungstraining mit dem Roboter erhalten, implementiert. Außerdem wurde hier ein umfassen-

des Training in eine “gamifizierte” Rehabilitationsumgebung integriert, um die Immersion und damit die Motivation der Patienten zu erhöhen.
Die hier vorgestellten Biomarker könnten als Bausteine für Modelle von Neurorehabilitation dienen und den Trainingsfortschritt der Patienten in solchen neuartigen Rehabilitationsumgebungen beobachtbar und visualisierbar machen. Die Übertragung der hier vorgestellten Forschungsergebnisse in neue oder verbesserte moderne Behandlungsmethoden könnten Millionen von Schlaganfallpatienten helfen, in Zukunft ihre Bewegungsfähigkeit wiederzuerlangen.

Acknowledgements

First and foremost I would like to express my sincerest gratitude to Dr. Ander Ramos-Murguialday, who has been teacher, mentor and motivator throughout this whole PhD project. Without his dedication, interest and support completion of this thesis would not have been possible.
I would also like to thank the advisors of the thesis. Prof. Dr. Birbaumer guided me with his wisdom and offered different perspectives. Prof. Dr. Andreas Schilling supported me from my very first instant at University, the first lecture, to my very last, the conclusion of this thesis. He was always curious and open-minded about my ideas.
Furthermore, I must thank Prof. Dr. Ranganatha Sitaram and Dr. Sergio Ruiz Poblete, who lighted the fire of my scientific interest and offered me invaluable opportunities to experience international collaboration.

I would like to thank my colleagues Florian Helmhold, Dr. Thiago Da Cruz Figueiredo, Dr. Farid Shiman and Wala Jaser Mahmoud, from whom I could learn so much, who never let me down and who played a major role in making this seven-year journey a success. Dr. Chiara Fioravanti became a dear friend already at the beginning PhD project. Thank you for countless conversations opening up new perspectives on science and life. Dr. Monika Schönauer, my "running mate", impressed me with her integrity, openness and energy, and I would not have wanted to miss becoming friends. Moreover, getting to know and being accompanied by the "Latinos" aka Carlos Bibián-Nogueras, Dr. Eduardo López-Larraz, Ainhoa Insausti-Delgado, Dr. Nerea Irastorza-Landa, Dr. Andrea Sarasola-Sanz, Dr. Iñaki Ortego-Isasa, Dr. Paulo Rogerio, Dr. Marco Curado and Pilar Urschitz-Duprat throughout these past years was a great gift. I am deeply grateful!

Last but not least, I thank my family for their love, advice and unconditional support: My mother and father – the curiosity you aroused was the spark that led me to where I am now. My sister Clara. I cherish the time we spent together throughout these past years. My mother-, father- and sister-in-law, whose emotional, motivational (and culinary) support was priceless.

I am blessed with having found my love Sonja, who bore with me, believed in me, encouraged me and supported me unconditionally for all these years. Thank you so much! Wir können alles schaffen!

Contents

Chapter 1

Synopsis

1.1 Introduction

1.1.1 Stroke

Stroke remains common: it is the second leading cause of death globally (Feigin *et al.*, 2016b). The cerebrovascular attack occurs when oxygen and nutrient supply of parts of the brain are disturbed. The most common causes are obstructed blood vessels (ischemia: 80% of patients) or internal brain bleeding (hemorrhage: 15% of patients) (WHO, 2001). In 2017 there were 1.5 M stroke cases out of which 438000 people died with the insult. There are 9 M stroke survivors currently living in Europe (Luengo-Fernandez *et al.*, 2019). They suffer from disabilities spanning a wide range of body functions, including paralysis, sensory disturbances and difficulties with cognition and articulation, depending on location and severity of the lesion (WHO, 2001; NIH Fact Sheet authors, 2020). As the lack of blood causes cell death within minutes, emergency care for stroke victims is imperative. Implementation of stroke units across Europe is underway increasing quality and overall access (Stevens *et al.*, 2017). Despite the improvement in immediate response, the disabilities impact the patients' lives. The most common deficit, contralateral upper limb paresis, is seen in 80% of the patients and remains after discharge from acute care in almost 30% of those patients with mild to moderate symptoms. Of patients with complete acute paralysis only 5% regain functional use of their arm (Hatem *et al.*, 2016). The motor deficit remains in nearly two-thirds of patients after discharge (Crichton *et al.*, 2016). At home, they need assistance for carrying out activities of their daily lives. Many cannot return to work, and their participation in society is limited. Secondary diseases such as depression occur in almost 40% of these patients (Stevens *et al.*, 2017). Their overall quality of life is greatly limited. As so many are affected this is not only a great number of dire individual fates but it entails a serious health problem of global magnitude and high economic impact on societies. Healthcare costs directly related to stroke were B€ 20 in Europe. Indirect costs, including loss of productivity and those borne by the families and communities of the patients, are estimated to amount to B€ 25 (Stevens *et al.*, 2017). Projections indicate that costs will increase in the years to come. Application of rehabilitation regimes that help victims regain independence and

mitigate the economic burden are thus imperative.

1.1.2 Motor neurorehabilitation after stroke

The ability of the brain to reorganize is the foundation of rehabilitative efforts after stroke. Various processes occur at different times and on multiple levels in the central nervous system after stroke. They entail changes in strength of existing synaptic connections and formation of new synapses. These processes, referred to as "homeostatic" and "hebbian" synaptic learning, both contribute to changing the brain state after the insult in order to promote repair. As long as some pathways for routing sensory input and motor output remain lost function can shift into new circuits, in most cases structurally close to the lesion (Murphy and Corbett, 2009). This reorganization of the brain is likely to be promoted by basic principles of motor learning: Reduction of kinematic and dynamic error and variation guided by sensory input (Krakauer, 2006). Integration of these principles into rehabilitation schemes has been shown to help patients improve their motor function (Chan *et al.*, 2006). Physical therapy in different forms such as neuro-developmental treatment (NDT, also known as Bobath approach) is the traditional approach to rehabilitation for stroke patients, in all stages of stroke. Extensions have been proposed based on theories of motor learning after stroke. Among these are mirror therapy, constraint-induced movement therapy and high-intensity and high-quality individualized movement therapy aiming at improving performance during day-to-day tasks (Taub *et al.*, 1994; Ward *et al.*, 2019). Increased intensity and engaging practice of motor skills increase retention and generalization (Krakauer, 2006). The dose of upper-limb motor training in currently applied therapy regimes is low (Lang *et al.*, 2009). Therefore, therapies using upper-limb robots have emerged. These motorized exoskeletons could help increase repetitions of the movements that patients train during rehabilitation. They can be used in different modes: (1) rendering the patient completely passive (robot moves the limb of the patient), (2) on an assistance-as-needed basis (e.g. patient tries to move and robot supports arm to mitigate effects of gravity), (3) resistive (patient tries to move and robot tries to hinder certain movements) or (4) including both arms of the patient in the paradigm (e.g. mirroring the movement of the unaffected limb) (Irastorza-Landa *et al.*, 2021). However, randomized controlled trials have not confirmed the potential of this approach to rehabilitation of chronic stroke patients (Lo *et al.*, 2010; Rodgers *et al.*, 2019).

1.1.3 Brain-Machine interfaces for upper-limb motor rehabilitation

The second pillar of improvement of motor skills is engagement in the task. Increased engagement can be achieved by way of enhancing the feedback the patient receives and enriching the training environment. The latter goal was one of the research foci of this thesis and background, and current efforts are presented in more detail in chapter 7. Severely impaired patients with limited or no residual upper-limb movement cannot

benefit from most of the established rehabilitation methodologies. For this patient group especially, but not exclusively, enhanced feedback and guidance play an important role for rehabilitation. In order to elicit neuroplastic changes in the central nervous system (essentially reinforcing connections between neurons) volition needs to be followed by an observable action. In the case of severely paralyzed patients, volition is never followed by action because the damage to the motor pathways caused by the stroke was so severe that commands do not reach the muscles and contractions are not triggered. An emerging approach provides a tool to (re-)implement a closed loop between the will to move and the actual movement: Brain-Machine interfaces (BMI). They register brain signals and interpret the activity. Once the intention to move is detected, an effector is triggered that acts upon the limb of the patient. Such action could be the movement of a robotic orthosis or targeted electrical stimulation of a group of muscles. As the limb moves with the exoskeleton or the muscles contract due to the electrical stimulation, the proprioceptive afferent feedback is sent from the limb to the brain. Adopting the perspective of the brain, the activity in cells representing the intention to move is followed by sensory feedback of an actual movement. Action follows volition, leading to neuroplastic changes. Early works which employed decoding of movement intention non-invasively in humans for the purpose of assisting (in the case of paraplegia) and rehabilitation of stroke patients were published only in the first decade of the 21st century (reviewed in Birbaumer and Cohen (2007)). More studies underlining the potential of the technology to produce changes even in the chronic stage of stroke have been published. In the first randomized controlled trial with a BMI for upper-limb motor rehabilitation small significant reduction of impairment was produced in this patient group (Ramos-Murguialday *et al.*, 2013). The success was replicated by other researchers (Ang *et al.*, 2014; Ono *et al.*, 2014; Leeb *et al.*, 2016; Mokienko *et al.*, 2016; Kim *et al.*, 2016; Leeb *et al.*, 2016; Frolov *et al.*, 2017). Many studies have been published to date, employing a similar methodology. Most use electromagnetic measures of brain activity such as Electroencephalography (EEG) (López-Larraz *et al.*, 2018b). However, some also propose potential ameliorations for improving feedback. Among these are combinations of effectors (e.g. exoskeleton and stimulation) or combinations of EEG with other measures of brain activity or nervous system activity such as Electromyography (EMG) (Sarasola-Sanz *et al.*, 2017).

1.1.4 Electroencephalography and brain rhythms

EEG is widely applied in clinical practice and research. It measures variations of electrical potentials from within the brain summed on the scalp. Pyramidal cells have unique properties in the context of EEG. Their apical dendrites are long and perpendicular to the surface of the cortex, they are located in the upper layers of the cortex and many of these cells are aligned in parallel to each other. Excitatory input far away from the soma of the cells creates extracellular negativity. The excitatory potential spreads along the membrane of the dendrite and causes an efflux of positive charge closer to the soma. The

extracellular space around the cell body becomes positive. A vertical dipole is created. Inhibitory input at the far end of the apical dendrite produces a dipole with the opposite effect. Similar activity of thousands or millions of these neurons (perpendicular to the scalp) will sum up to the waves measured in the EEG over time. The more afferents of pyramidal neurons evoke postsynaptic potentials synchronously, the larger the amplitude of the wave measured in the EEG. Such highly synchronized activity has been observed at various frequencies and locations during different mental states. These synchronized waves have been classified into brain rhythms, visible during sleep (δ and θ waves, 0.5 – 3.5 Hz and 4 – 7.5 Hz) or during the awake resting state (α and β waves, 8 – 13 Hz and 13 – 30 Hz) (Kirschstein and Köhling, 2009). Beside various potential connections of these rhythms to psychological concepts such as mental workload and attention, the latter are of specific interest for Brain-Machine interfaces. The rhythm in the alpha frequency range, if localized around the motor cortex, is termed sensorimotor rhythm (SMR) and plays an important role in decoding motor intention (Pfurtscheller and Lopes da Silva, 1999; Klimesch *et al.*, 2007).

In comparison to other invasive and non-invasive measures of brain-activity utilisation of EEG is inexpensive and not restricted to a specific environment. These are the reasons why it is so widely used in clinical practice and research, which, in turn, made the technique a logical choice for the research focus of this study: Neurophysiological biomarkers of stroke and neurorehabilitation in chronic severe stroke.

1.2 Biomarkers

Biomarkers, short for "biological markers", are defined as indirect measures of processes in the human body that could be used as indicators of certain states (e.g. of a disease) (Boyd *et al.*, 2017). They are in essence accurately and reproducibly measurable medical signs on a functional, physiological, biochemical, cellular or molecular scale (Strimbu and Tavel, 2010; WHO, 1993).

For clinical therapies the outcome is paramount, that is, in the case of acute stroke, survival of the patient and then improvement of function. In clinical studies the endpoints have been oriented at the outcome of treatments: For example, the question if a new treatment approach is effective (i.e. improves function or not) is always measured on motor scales that relate to clinical practice such as ARAT or the WOLF test (for rehabilitation of paralysis after stroke) (Carroll, 1965; Wolf *et al.*, 2001). They reflect motor improvement of the patient and are easily applicable in clinical practice. However, in stroke these might not be the optimal measures because clinical trials for new treatment approaches, specifically in severe chronic stroke, do only achieve small changes on clinical scales (López-Larraz *et al.*, 2018a). Moreover, Krakauer and Carmichael point out that in several studies on chronic stroke there are some patients who do not improve and very few who improve many points on the clinical scales. It is unknown if these patients are just statistical outliers or if they stem from a different distribution (Krakauer and Carmichael,

2017, p. 184). Other markers that reflect processes in the central nervous system might be better suited to indicate changes of disease state, understand these changes and provide a finer granularity of state differences. For example, many severely paralyzed stroke patients cannot actively extend their fingers but still show some voluntary residual muscle activity (Ramos-Murguialday and Birbaumer, 2015). Clinical scales measuring arm function would exhibit low or no scores in this case. However, a biomarker based on EMG activity could uncover some activity, thus provide more insight and guide subsequent actions: Inclusion in a study on stroke rehabilitation that employs EMG activity or pursuit of a specific treatment pathway.

Clinical practice and research alike would benefit from the use of biomarkers. Stroke is heterogeneous in terms of the location and volume of the damage to the brain, which leads to diverse cognitive and behavioural deficits. With an increase of a priori insight through introduction of biomarkers, clinical trials could benefit from informed stratification of patients. Study design would be more focused and efficient and thus outcomes would likely be more easily interpretable (Strimbu and Tavel, 2010). For clinical practice biomarkers could inform triage and help patients and therapists set appropriate goals and choose optimal rehabilitation pathways, including type of training, dose and intensity (Boyd *et al.*, 2017). Furthermore, research and clinical practice could both benefit from collection of (easily obtainable) objective measures at multiple time-points during a treatment.

1.2.1 Electrophysiological biomarkers of motor deficits after stroke

Stroke victims often suffer from multiple repercussions of the damage to the brain: Among these are sleep deficits and increased daytime sleepiness, aphasia, depression, attention deficits, cognition deficits, neglect, language and coordination deficits, all of which are targeted during rehabilitation and could benefit from biomarkers, as has been pointed out by Boyd and colleagues (Boyd *et al.*, 2017). In the present work, there is a focus on motor deficits as for many patients they are the most severe factor limiting participation. There is a variety of measures employing different techniques. Clinical measures of function such as ARAT and the WOLF motor test are widely applied in clinical practice. The Fugl-Meyer scale, which measures impairment, is more elaborate and is mainly administered in clinical trials (Fugl-Meyer *et al.*, 1975). The scale predicts long-term outcome of treatment better than demographic and structural markers (Coupar *et al.*, 2011). Neuroimaging biomarkers are generally more difficult to obtain because of the complexity of the technology involved. With MRI (T1-weighted) structure and integrity of the cortex are measured and can hint at the potential damage, but there is not necessarily a good correlation between lesion volume and location and the paralysis and motor outcome after rehabilitation (Coupar *et al.*, 2011). However, integrity of white matter pathways (using DTI) is an indicator of motor performance and is a better predictor of motor outcome than lesion volume alone (Stinear *et al.*, 2017). Functional MRI provides measures of focal and network activity of the cortex during rest, volun-

tary or passive movements. There are indications that activity more similar to that of healthy controls implies better motor performance (Stinear *et al.*, 2017). Furthermore, laterality of activity between the brain hemispheres might predict motor performance (Ramos-Murguialday *et al.*, 2013).

Combination of non-invasive brain stimulation and myoelectric activity as biomarkers have been investigated, too. During measurement of Motor Evoked Potentials (MEPs) the brain (the motor cortex) is stimulated non-invasively using a strong magnetic field (Transcranial Magnetic Stimulation – TMS), and the response of the limb muscles is captured with EMG. If the forced activation command travels from the cortex to the muscle, a contraction is triggered. In those patients that show an MEP the motor outcome after rehabilitation is better than in those who do not (Stinear *et al.*, 2017).

The use of EEG in clinical practice is common, and data of many patients is potentially available. However, the utilisation of biomarkers for replacing more expensive (resonance imaging) or augmenting less specific (functional clinical scales) markers has not yet had a breakthrough in clinical practice. In research, there is increasing evidence that various features that are captured by the EEG correlate with the acute state of impairment of the patient and with recovery in different stages. These features include Sensory Evoked Potentials (SEPs), cortical oscillatory signals, measures of functional connectivity such as coherence and measures of interhemispheric balance of brain activity. First reviews that focus on the potential of these features as biomarkers were published in the last decade (Finnigan and van Putten, 2013; Rabiller *et al.*, 2015; Tedesco Triccas *et al.*, 2019). In addition to the overview that they provide, table 1.1 lists current research on electromagnetic biomarkers of stroke investigating the aforementioned features in cross-sectional and longitudinal studies at different stages of stroke and with varying degrees of impairment.

Reference	Study design / measured time points	Time since stroke	No. of stroke patients	Severity of the impairment	Measures used
Platz *et al.* (2002)	Cross-sectional	acute, subacute	9	moderate, mild	Spectral analysis
Gerloff *et al.* (2006)	Cross-sectional	chronic	11	moderate, mild	Cortico-cortical connectivity, spectral analysis, TMS for cortico-spinal integrity
Kaiser *et al.* (2012)	Cross-sectional	subacute	29	ESS: mean 69	Spectral analysis

Pellegrino *et al.* (2012)	Cross-sectional	chronic	7	NIHSS: mean 8.4	Spectral analysis, interhemispheric coherence during rest
Ono *et al.* (2014) *	Longitudinal	subacute, chronic	12	severe	Spectral analysis
Tangwiriyasakul *et al.* (2014)	Longitudinal	acute	8	severe, moderate, mild	Spectral analysis
Nicolo *et al.* (2015)	Longitudinal	acute	24	NIHSS mean 13	Connectivity
Pichiorri *et al.* (2015) *	Longitudinal	subacute	28	moderate, mild	Spectral analysis, connectivity
Wu *et al.* (2015)	Longitudinal	chronic	12	moderate, mild	Connectivity
Park *et al.* (2016)	Cross-sectional	subacute	9	severe, moderate, mild	Spectral analysis
Wu *et al.* (2016)	Cross-sectional	acute (ER/ICU)	24	NIHSS 1 to 19	Partial least squares models, Spectral analysis
Chen *et al.* (2017)	Cross-sectional	acute, subacute, chronic	37	severe, moderate, mild	Connectivity, predictive modelling
Philips *et al.* (2017)	Longitudinal	chronic	30	severe, moderate, mild	Connectivity
Pichiorri *et al.* (2017)	Cross-sectional	subacute	30	severe, moderate, mild	Connectivity, TMS for measurment of cortico-spinal tract integrity
Thibaut *et al.* (2017)	Cross-sectional	chronic	55	moderate, mild	Spectral analysis, TMS for measurement of motor threshold
Biasiucci *et al.* (2018) *	Longitudinal	chronic	27	severe, moderate	Connectivity
Mane *et al.* (2019) *	Longitudinal	chronic	19	moderate	Spectral analysis, connectivity
Saes *et al.* (2019)	Cross-sectional	chronic	21	severe, moderate, mild	Spectral analysis

Krauth *et al.* (2019)	Longitudinal	acute, subacute	4	severe, moderate, mild	Cortico-muscular coherence
Bönstrup *et al.* (2019)	Longitudinal	acute, subacute	33	severe, moderate, mild	Spectral analysis

Table 1.1: List of current works investigating features of the EEG with the potential to be used as biomarkers

This overview illustrates the increase of research of biomarkers in this field in the last decade. The longitudinal studies are clinical studies on rehabilitation approaches, often including a neural control paradigm (i.e. a BMI), in which electrophysiological markers can be correlated with behaviour (marked with a * in the table). In acute patients, there are indications that ipsilesional loss of power (i.e. interhemispheric imbalance of power) is an indicator of poor outcome (Finnigan and van Putten, 2013). Furthermore, changes of relative power during movement (sensorimotor desynchronization) correlated with recovery (Tangwiriyasakul *et al.*, 2014). There are indications that laterality of relative power correlates with impairment (Kaiser *et al.*, 2012). Recent works expanded investigations to lower frequencies (δ and θ) and found correlations to motor impairment, too (Bönstrup *et al.*, 2019). Connectivity measures such as coherence, mainly in the beta frequency, correlate with recovery (Nicolo *et al.*, 2015; Chen *et al.*, 2017). More specifically, coherence in the primary motor cortex over the lesion and the rest of the cortex predicted recovery until the subacute stage (Wu *et al.*, 2016). One study found that resting-state coherence in the higher β band correlated best with motor performance (Pellegrino *et al.*, 2012).

Similar investigations have been performed with patients in the chronic stage. However, many included only a small number of subjects and mixed different degrees of impairment severity, which is likely to confound correlations. The group of patients with severe chronic upper-limb impairment is especially dependent on the development of a biomarker different from the ones in use today, because these patients do not show the ability to actively extend some or all of their upper-limb joints, which means that clinical scores do not capture potential improvement. No improvement (on a clinical scale and of function) implies in most health systems of the world that the patients do not receive sufficient (if any) therapy any more. This neglect in the chronic phase leads to cessation of application of any therapeutic tools.

Establishing biomarkers that predict outcome in these patients reliably, that track recovery with finer granularity and that can be captured using inexpensive electrophysiological techniques is not trivial but necessary to overcome disregard of this patient group.

1.3 Objectives and overview

This thesis has two main objectives: (1) Exploring the potential of electromagnetic biomarkers for predicting outcome and tracking recovery in this specific subgroup of patients and (2) advancing the state-of-the art of rehabilitation paradigms employing neural control by enhancing the feedback to the patients.

The first objective was pursued by investigating various features of the EEG in two unique datasets of severely impaired chronic stroke patients. The efforts are arranged into five chapters and grouped by electromagnetic features of the neurophysiological signals, the aptitude of which as biomarker for stroke and/or recovery is discussed.

Chapter 2: Desynchronization of the Sensorimotor Rhythm Two studies are presented in this chapter. They both focus on relative power of the sensorimotor motor rhythm during movements. The publication "Brain oscillatory activity as a biomarker of motor recovery in chronic stroke" (Ray *et al.*, 2020) investigated how movement-related desynchronization of sensorimotor oscillations track recovery during the course of a rehabilitation intervention based on BMI. The results emphasize the importance of lateralization of sensorimotor brain activity. The peer-reviewed conference paper "Movement-related brain oscillations vary with lesion location in severely paralyzed chronic stroke patients" (Ray *et al.*, 2017) focussed on the relation between the location of the lesion and the strength of desynchronization of oscillations.

Chapter 3: Spectral characteristics of the Sensorimotor Rhythm A previous conference publication, investigating the stability of sensorimotor oscillations over the course of a rehabilitation intervention, was a precursor to the study presented here (Ray *et al.*, 2018). Results indicated notable differences in the central peak frequency of the sensorimotor oscillations between subgroups of stroke patients. The chapter "Sensorimotor oscillations in severe chronic stroke" describes a more concise processing pipeline to automatically parametrize broad-spectrum oscillations. These parameters are shown descriptively, their aptitude as biomarkers for stroke is evaluated and they are compared to those of a healthy population. This study pooled data from five datasets in order to create a larger data basis.

Chapter 4: Low-frequency oscillatory brain activity Studies in animal models of stroke and human stroke victims have only recently indicated that low-frequency oscillations, i.e. oscillations between 3 and 5 Hz, could serve as a biomarker for recovery in stroke and even as a target for rehabilitation. The chapter "Low frequency oscillations in upper limb motor recovery in severe chronic stroke" investigated a chronically and severely impaired population and found dualities to previous studies. The most important finding is that low-frequency oscillations increase from before to after an intervention, which adds to current knowledge. However, correlations with clinical measures of

impairment are less clear and need further investigation.

Chapter 5: Coherent brain oscillations This chapter describes the effort to extract various connectivity measures from the brain activity of stroke patients and to investigate their potential as biomarkers for stroke and motor recovery. The study was initially based on numerous previous studies that indicated correlations between recovery and connectivity measures. The approach that has been proposed in literature is parametric. The connections between different areas of the brain are modelled as a multivariate autoregressive process. However, the implementation of the chosen approach proved to be challenging and had some methodological drawbacks. The merit of the work presented in the chapter lies in exploring a non-parametric approach for deriving meaningful connectivity measures using a statistical threshold for significant coherence values between different sources. This methodology has not been widely used before but has several advantages over the parametric approach.

The second objective was pursued within the framework of a comprehensive pilot study where a hybrid electroencephalographic and electromyographic interface (hBMI) for training of severely impaired patients was created, advancing the state of the art of neural interfaces for rehabilitation. The chapters present works carried out towards increasing engagement in the training by enhancing feedback to the patient.

Chapter 6: Muscle fatigue in stroke rehabilitation using neural interfaces This chapter presents the peer-reviewed conference paper "Electromyographic indices of muscle fatigue of a severely paralyzed chronic stroke patient undergoing upper limb motor rehabilitation" (Ray *et al.*, 2019). It is well-known that dose and intensity have an effect on motor learning. Increasing the intensity for rehabilitation training for impaired patients whose limbs have not been used in a long time could lead to effects such as muscular fatigue. As has been reported in a healthy population, fatigued muscles exhibit electromagnetic signals different from rested ones. If the signals captured from a muscle change due to fatigue this could have implications for decoding in the context of interventions based on hBMIs that exploit EMG. The study presented shows a methodology for comparing muscle activity of chronically impaired stroke patients and of a healthy population for training tasks used in a very specific setting.

Chapter 7: Increasing engagement - Enhancing feedback The chapter presents two complementary projects on enhancing existing Brain-Machine interface therapies.

Section 7.3: Improving visuo-proprioceptive feedback: Interactive 3D visualization of the orthosis In the study on the hBMI (Dataset 2, section 1.3.1, see below) the patients were asked to move the exoskeleton that was connected to their arm towards individual previously specified targets on the experimental table using their brain activity and residual muscle activity. Steering the system to the exact position proved to be

challenging as the patients hat do memorize the target position. To solve this issue a virtual three-dimensional representation of the exoskeleton and the target positions was developed and used in the experiments with the patients. The section describes the implementation and features of this software.

Section 7.4: Improving immersion and training motivation: The AMoRSA setup The AMoRSA setup is an augmentation of the hBMI system. It includes a gaming environment with which the patients can interact. Patients shape a virtual garden to their liking while performing the tasks of the rehabilitation training. The section motivates this project and provides details on the implementation.

The dissertation is concluded by a short chapter that provides auxiliary information supporting repeatability of the results obtained and providing meta-data on the work. It comprises a description of the general structure of the code produced for the analyses, which is partly publicly available and some details on the implementation of algorithms employed. Moreover, the software development project "Multicam" is introduced, which allows recording audio and video of experiments from multiple points of view and can be triggered programmatically over the network. Its main purpose is to integrate functionality for recording experimental sessions in the laboratory into the experimental software.

1.3.1 Datasets

This section provides a summary of the nature and origin of the data analyzed for this work. Both are unique datasets of chronic stroke patients undergoing a rehabilitation intervention. The specifics of the portion of the datasets analyzed is presented in detail in each chapter and the studies.

Dataset 1: BMI in chronic stroke This comprehensive study was conducted by one of the advisors of this thesis, Dr. Ramos-Murguialday. It was published as Ramos-Murguialday *et al.* (2013) and was the first randomized controlled trial showing motor improvement of the upper limb of severely impaired chronic stroke patients after BMI rehabilitation training. Patients used their brain activity to drive a robotic exoskeleton that was connected to their arm. The orthosis initiated a one-dimensional movement on a pre-defined trajectory (extending the arm and/or extending the fingers) once the patients exhibited the "desired" brain activity. In the rehabilitation period they trained approximately two hours per weekday for four weeks in a row. The dataset comprises a plethora of clinical scales, self-reports, questionnaires, structural and functional imaging data, electroencephalographic and electromyographic recordings and kinematics. Most of the measures were recorded at multiple time-points (before, immediately before, after and sixth months after the intervention). Kinematics, EEG and EMG were registered continuously during the intervention. The focus of this thesis are electromagnetic biomarkers and their correlation to clinical scales. That is why the four main components of all analyses were: the Fugl-Meyer scale (FMA), resting-state EEG, EEG and EMG

of self-paced finger extension attempts of the healthy and the paretic hand and EEG and EMG during control of the exoskeleton. The clinical scale, the resting-state EEG and EEG and EMG of the finger movements were recorded in screening sessions before and after the intervention.
The clinical scale was recorded according to the manual (Fugl-Meyer *et al.*, 1975). The scale measures the degree of impairment by asking the patient to perform various movements of isolated joints. If the movement is perfect (similar to a completely healthy limb) two points are added to the score. If there is some imperfect movement one point is added. If there is no movement no points are added. The lower the sum of scores the greater the impairment (more information on the movements can be found in section 2.6.6).
The resting-state EEG was recorded while the patients kept there eyes open and focused on a marker on a screen or on the wall for two minutes or more. They refrained from any movement during that time. This paradigm is necessary for assessing spontaneous brain activity, e.g. oscillatory activity or connectivity between different centers in the brain. Parts of the analyses also include resting-state data that was recorded in the same manner but in multiple shorter intervals in alternation with the finger extension task.
EEG and EMG activity during finger extension (attempts) was recorded while patients were asked to try to actively extend and release their fingers after an audiovisual cue. The task was repeated for both hands (paretic and unaffected).
EEG and EMG activity during control of the exoskeleton was recorded continuously in the rehabilitation period. Relative power differences between resting (not trying to move) and movement (trying to move the paretic arm/hand) triggered the movement of the orthosis. In each repetition the patients rested around 4 seconds, they were then cued to prepare for the movement. Subsequently, a cue prompted them to try to move and they could control the exoskeleton for 5 seconds. Then the cycle repeated.
More information on the neurophysiological recordings can be found in section 8.1.6.

Dataset 2: Hybrid EEG-EMG BMI in chronic stroke The data of this comprehensive study are comparable to the ones described before in dataset 1. The main publication presenting this study is in preparation. There were screenings before and after a rehabilitation period. During the intervention patients trained with the system over a period of four weeks in similar fashion (there was a break of two weeks after ten days of training). However, there are some notable differences: The exoskeleton used here enabled the patients to control seven degrees of freedom including two-dimensional reaching and finger movements. The study evaluated an enhanced decoding strategy that included EMG activity from 14 muscles for high-dimensional control. Conditions such as EEG during sleep and TMS priming were added to the paradigm in order to answer additional research questions.

The clinical scales, resting-state EEG, EEG and EMG during finger extension and EEG and EMG during hybrid control of the exoskeleton were recorded the same way as

in the previously described study. It is noteworthy, though, that the EEG signals were sampled from twice the number of channels, and activity of 14 muscles of the paretic arm were included instead of only four. Section 7.2 provides more details on the procedures.

1.4 Results and discussion

Almost one third of stroke patients show long-lasting severe paralysis. In therapy these patients are largely neglected since they do not benefit from current approaches to rehabilitation due to their severe impairment. However, according to recent research this patient group has the potential to improve (López-Larraz *et al.*, 2018a). Even though the total number of patients included in those trials is small, there is variety in the outcomes. Some patients improve many points on clinical scales while others show no improvement (see Ramos-Murguialday *et al.* (2013) as an example). Changes that are meaningful for activities of the daily lives of the patients have not been achieved yet for the severely paralyzed. Clinical scores do not uncover the differences between those who benefit and those who do not. The studies presented in chapters 2 through 6 present puzzle pieces of the bigger picture hidden beyond the coarseness of the clinical scales.

All of the studies on EEG focused on the analysis of the frequency domain. They are categorized below by the features investigated. Results are presented in summary and the implications discussed. The last publication focussed on electromyography and is also presented and discussed briefly here.

1.4.1 Event-related Desynchronization – Relative power changes of the Sensorimotor Rhythm during movement

Event-related Desynchronization (ERD) is a change of ongoing EEG activity that is specific to the alpha frequency range. During wakeful resting an oscillation with power considerably larger than the underlying noise floor of the EEG is measurable. During planning and execution of movements, foremost of the limbs, the power of this oscillation over the contralateral motor areas is reduced (Pfurtscheller and Lopes da Silva, 1999). The reason for this phenomenon is synchronous activity of hundreds of thousands of cortical cells, mainly triggered by a feedback loop with thalamic afferents and efferents (Steriade *et al.*, 1990). Synchronous membrane potentials are summed to the recorded gross potentials in the EEG. As soon as more specific activity of subgroups of cells takes place, for example during execution of a limb movement, less cells fire in synchrony and the power of the summed potential in the EEG is reduced (hence the term Event-related Desynchronization). The relative change of power between the resting condition and the activity condition is expressed as percentage. ERD was a major research focus two decades ago. In the last decade, several studies investigated the effect of stroke on ERD. Early after stroke ERD is reduced over the lesion and progresses towards normal activity

during recovery (Tangwiriyasakul *et al.*, 2014). In subacute patients with mild to moderate impairment motor improvements were also accompanied by an increase of ERD (Platz *et al.*, 2002), and patients with severe motor deficits showed higher probability for motor improvements with increased ERD (Pichiorri *et al.*, 2015). A first characterization of ERD in chronic stroke has been attempted (Kaiser *et al.*, 2012). These studies indicated that recruitment of more cells specific to the task during spontaneous recovery or rehabilitation training is measurable by ERD. These results encouraged the two investigations. The aim of Study 1 (Ray *et al.*, 2020) was to generalize the previous discoveries to the chronically and severely paralyzed. We analyzed the evolution of ERD throughout a BMI-based rehabilitation intervention (Dataset 1, section 1.3.1). We found a significant correlation between the change of ERD and motor improvement. Most importantly, we showed that the initial ability to desynchronize (relative to the median of the group of patients analyzed) modulated this correlation: In those patients who had a stronger ERD in the beginning, increase of the ERD was accompanied by motor improvement. In the patients with relatively weaker initial ERD, the opposite was the case: weakening of the ERD was accompanied by motor improvement. At first this result partly contradicted our hypothesis that stronger ERD would indicate better motor improvement. However, inclusion of the unaffected hemisphere in the analysis revealed that those patients who reduced their ERD and still improved reduced contralesional ERD even more. This discovery supports the importance of the lateral (im)balance of brain activation, also found with resonance imaging (Ramos-Murguialday *et al.*, 2013).

Imaging studies have also indicated that the location and volume of the lesion correlates with function after stroke (Lindenberg *et al.*, 2010; Pineiro *et al.*, 2000). In study 2 (Ray *et al.*, 2017) we investigated how the generation of ERD during movement is influenced by the location of the lesion. Stratification of the patients was carried out by separating those with damage to the motor cortex from those with only subcortical lesions. Due to the relatively low number of patients compared to the heterogeneity of the lesion volumes this is a coarse separation. However, the results showed a trend towards weaker average ERD (mean difference: 16 percentage points) in the group with inclusion of the motor cortex in the lesion. The reason might be that due to the damage to cortex there are less cells contributing to the synchronous activity. The difference between synchronous and desynchronized activity is thus smaller, leading to lower average ERD.

These studies showed that ERD is an interesting candidate for a biomarker of stroke and recovery. The results have implications for the design of BMI interventions based on ERD (most are). Firstly, initial ERD could inform the course of the intervention: either strengthening ipsilesional ERD or increasing interhemispheric imbalance of the ERD towards the lesion. Secondly, ERD could be used to track recovery. Thirdly, even though location of the lesion did not influence the results of the first study, the observations of the second study should be considered for the stratification of patients in future studies as ERD might be an indicator of cortex integrity.

1.4.2 Parameterization of the Sensorimotor Rhythm during resting

Characteristics of the SMR have been investigated since the inception of human EEG recordings. The average peak frequency of the SMR for humans was determined, and later also the stability of the peak frequency for individuals over time (Kuhlman, 1978). Studies also found an average slowing of the rhythm with age (Scally *et al.*, 2018).

Despite the abundance of research, characterization of the sensorimotor rhythm was still lacking in chronic stroke patients. In the chronic stroke patients peak center frequency and absolute power of the sensorimotor rhythm might differ between patients depending on factors such as lesion location and progress in the rehabilitation training. Preliminary results were presented at FENS 2018 (Ray *et al.*, 2018). Study 3 is an extension and completion of this work, using a more advanced methodology. The chapter presents a pipeline for fully automatic analysis and comparison of characteristics of the SMR within and between patients: Peak center frequency and absolute power. The pipeline is employed to extract these characteristics from data of chronically impaired stroke patients and healthy volunteers (Dataset 1 and 2, section 1.3.1 and additional datasets).

The processing pipeline employs an algorithm for fitting of fractal noise and gaussian bell curves to model the noise and the peaks of the EEG power spectrum. The center frequency of the SMR was parametrized in all patients (and healthy volunteers). There was no statistical difference of center frequency between hemispheres, which confirms the observation of "mirrored" oscillation characteristics present in healthy subjects. Similarly, the absolute power of the SMR was not different either. Moreover, there was no significant change of the center frequency or the power from before to after the intervention.

These results confirm what has been found in healthy populations: In stroke, the (deterministically identified) peak center frequency of the SMR is stable within subject and over time. This is particularly interesting in the context of BMI-based interventions. In these studies control frequencies are often chosen based on the individual frequency of the SMR. The present study shows that the SMR does not change due to the intervention and does not need to be adapted. Moreover, decisions about the SMR of the hemisphere of the lesion (such as the choice of the individual feedback band in a BMI-based intervention) can be sanity-checked by comparison to the unaffected hemisphere.

Another interesting result of the study was that the peak center frequency and the absolute power of the SMR were significantly lower in stroke patients than in healthy volunteers. The control-group was not age-matched, but due to the large age range in the stroke group "age" could be ruled out as the only factor for this effect. The damage to the thalamocortical circuits could, after all, have had an influence on the EEG, as quantified by the generally lower peak center frequency.

1.4.3 Low frequency oscillations in upper limb motor recovery in severe chronic stroke

Low frequency oscillations (LFO) have been shown to be disturbed after stroke and to reappear with recovery. The works of Ramanathan and colleagues and Bönstrup and colleagues presented evidence that low frequency oscillations could serve as a biomarker of stroke and recovery (of motor function) (Ramanathan *et al.*, 2018; Bönstrup *et al.*, 2019). Their investigations focused on animal models and acute and subacute stroke patients, respectively. In the present study (chapter 4) LFOs increased significantly from before to after a BMI-based intervention in severely paralyzed chronic stroke patients. Bönstrup et al. correlated the mean power of the LFOs with clinical scales and found weak correlations. In the analysis presented, no correlation between LFOs and motor recovery was found. However, I show that it is the group of patients receiving contingent feedback who contributes most to the *pre-post* difference of LFOs. These patients were also the ones who improved their motor function with the intervention. This observation hints at an effect of the intervention. A correlation with impairment might thus be observed in a larger cohort.
In those patients with lower initial LFO a larger difference of LFO from before to after the intervention was observed. This larger "repairing" effect could be an indication of LFO being an indicator of the damage to the motor networks (which is under debate).

The study of Ramanathan et al is a great example of how investigation of biomarkers could increase understanding of recovery processes after stroke (Ramanathan *et al.*, 2018). Furthermore, in their study LFOs were exploited as a target for electrical brain stimulation. LFOs can thus directly be used to induce (or boost) recovery. Together with the works of Bönstrup and colleagues (Bönstrup *et al.*, 2019) the results presented in chapter 4 are encouraging for biomarker research in human stroke victims.

1.4.4 Coherent oscillations - Brain connectivity in chronic stroke

Brain function relies on localized and large-scale activity of neurons in ensembles and networks. The concept of connectivity is an umbrella term comprising all measures that capture the interaction within these networks (Horwitz, 2003). Unilateral limb movements rest upon a complex network of inhibitory connections between and excitatory connections within the hemispheres that is disrupted after stroke. Recent studies have shown that connectivity features extracted from EEG recordings predict motor recovery in the acute, subacute and even in the chronic phase to some extent (Nicolo *et al.*, 2015; Pichiorri *et al.*, 2015; Pellegrino *et al.*, 2012). Functional changes due to lesions have also been described (Aerts *et al.*, 2016). These findings motivated the present study which aimed at describing connectivity within the brain under the stroke pathophysiology in the chronic patients. A method that allows assessment of directional communication within networks of nodes (i.e. EEG channels) was implemented together with an appropriate estimator for a critical value (i.e. a significance threshold). Partial Directed Coherence

as presented by Baccalá and colleagues relies on modelling the data as an autoregressive process (Baccalá and Sameshima, 2001). If the model order is unknown, which is the case in real-world EEG data, noise can lead to spikes in coherence, which might lead to false conclusions about connections between nodes. Schelter and colleagues proposed a significance threshold for Partial Directed Coherence that is derived from the statistical properties of the auto-regressive model (Schelter *et al.*, 2005).

This combination of methods was implemented and used on Dataset 1 (section 1.3.1). Connectivity was assessed in the longitudinal data of patients activating an exoskeleton with their brain activity to move their paretic arm in a total of 17 training sessions.

The results were encouraging at first. In parts, however, the results remained obscure: in cases in which the unit of the EEG data was different (mV instead of V) the algorithm failed and could not provide proper estimation of the significance threshold. This shifted the focus of the study towards methodological exploration. First, the method for computing the significance threshold was assessed using example data from the original paper. Different implementations in Python and Matlab were compared. The example of the original paper of Schelter and colleagues could not be replicated exactly, no matter the method. This called the applicability of the method into question and encouraged the implementation of a different approach that does not depend on modelling the data as autoregressive process. It was described in the paper of Dhamala et al (Dhamala *et al.*, 2008). The noise covariance matrix and transfer function necessary for arriving at Partial Directed Coherence values are derived directly from the spectrally transformed data. This methodology is less widely used but comparison to the parametric method using the same example data confirmed its validity. The nature of the EEG data enables comparison of two conditions such as “movement” and “no movement”. The significance threshold for the PDC obtained was computed by comparing these conditions using permuation clustering (Maris and Oostenveld, 2007).

The first results are in line with previous findings. Connectivity increased within the hemisphere of the lesion in the higher β band and the communication of the hemisphere of the lesion and the healthy hemisphere increased, too.

These results encourage further investigation that should address the following points:

1. The general structure of the nodes in the system: which brain areas communicate with each other? How does communication change from before to after the intervention?

2. Quantification and statistical testing of these changes

3. Comparison between the patients and healthy volunteers to underline the significance of the changes found

1.4.5 Fatigued muscles during chronic stroke rehabilitation training

Intensive exercise such as weight lifting fatigues muscles. The causes are a smaller amount of recruited motor units in the nervous system, an accumulation of metabolites and altered conduction velocity of fibers in the muscle. It is well known that these changes influence amplitude and spectrum of the EMG (González-Izal *et al.*, 2012). In rehabilitation employing classification of myoelectric signals and hBMI studies (such as the one described as Dataset 2, section 1.3.1) the decoding and subsequent orthotic control rely on accurate extraction of features from EMG. Changes of these features due to fatigued muscles could have detrimental effects on performance. The phenomenon might emerge particularly in severely paralyzed patients who are not able to move there limbs. Lack of use weakens muscles and causes them to get fatigued more easily when exercising.

In Study 6 (Ray *et al.*, 2019) a framework for comparing myoelectric measures of stroke patients with those of healthy volunteers was created. The focus lay on a very specific task type. In the hBMI study (Dataset 2, cf. section 1.3.1) and in many other studies stroke patients performed forward reaching movements. When reaching a target centered in front of them, they extend the elbow using combined contractions of various muscles. One major contributor to this movement is the Deltoidus Anterior muscle on the shoulder.

Healthy volunteers would normally not become fatigued while performing the reaching movement. Therefore, an apparatus was designed and built that allowed performing controlled forward elbow extension with an opposing force. Healthy volunteers were asked to use the apparatus until they could not extend their elbow any more while EMG was measured form the Deltoidus muscle. Evaluation showed that the apparatus induced fatigue in most subjects. We applied two myoelectric measures of muscle fatigue to the data recorded: Mean spectral frequency (Bigland-Ritchie *et al.*, 1981) and the Dimitrov Spectral Index (Dimitrov *et al.*, 2006). We did not find a significant average difference of these EMG measures compared at the beginning and at the end of the fatiguing session. However, for half of the subjects, regression over the fatigue indices computed for each individual contraction showed an overall linear decrease. This finding shows that the setup can induce muscle fatigue and that the methodology of analysis captures fatigue even though the contractions are dynamic and the muscle under observation is small.

After testing the EMG measures on healthy participants, the fatigue indices were computed for four patients. Each movement with the exoskeleton was analyzed and averaged over multiple sessions. Two of the patients showed an average increased mean spectral frequency and the other two did not show any change. This might indicate that the experimental setup is in fact not inducing fatigue. On the contrary, the increase indicates that the muscles of the patients might even be more activated after the training.

Due to the pilot nature of this study it is not possible to generalize the findings. However, the likelihood of muscle fatigue disturbing the hBMI setup can be considered low

since there was no patient showing muscle fatigue. So far, in the hBMI study (dataset 2, cf. section 1.3.1) no obvious changes of the EMG activity and subsequent detrimental effects were observed (analysis pending). With the framework developed for the present study such effects can be tested in the future.

1.4.6 Increasing engagement - enhancing feedback

Researchers and clinicians seek to build enriched rehabilitation environments that integrate different technologies and principles of motor learning to optimize rehabilitation outcome. Increasing engagement of the patient, i.e. focus on the task as well as long-term motivation and enhancing the feedback to the patients, are two aspects of building enriched rehabilitation paradigms that have been implemented and investigated here. Enhanced visual feedback to the patients using the interactive 3D visualization of the exoskeleton turned out to be crucial for the patient. With this additional perspective on the exercise their sensory feedback was improved and it was easier for them to control the movements they had to perform to successfully reach the targets. Observation of the patients during the experiments showed that they relied on the visual feedback during the training. Their subjective feedback confirmed the usefulness and necessity of the 3D visualization.

In the AMoRSA project a repetitive and demanding rehabilitation training paradigm was successfully integrated into a gaming environment. The training system was tested on five patients and their subjective feedback confirmed that the game was engaging and motivated them to train more.

The response of the patients using both systems underlines the immediate benefit of enhanced feedback and supports the positive effect of gaming principles on motivation. However, during the AMoRSA project the importance of careful planning and thought for integrating rehabilitation into a game also became clear. Understanding (patho-) physiology and psychology of the patients is paramount.

The work is a foundation for future projects where other markers of rehabilitation (e.g. those presented in chapters 2,4,5 and 6) could be integrated to track and visualize the otherwise abstract progress.

1.5 Conclusions

The five studies on EEG data all underline the importance of **laterality of brain activity**. The study on the evolution of the ERD shows that the relation of brain activity of both hemispheres correlates with recovery. Reduction of the ERD on the contralesional hemisphere was accompanied by an increase of motor function. The analysis of the Low-frequency oscillations uncovered power differences between hemispheres. Only on the hemisphere of the lesion LFO power was smaller during movement attempts of the paretic limb before the intervention than after the intervention. Moreover, more balanced

laterality of LFO power was an indicator of better motor impairment. The connectivity analysis is inherently suited to assess lateral variations of brain activity. The pilot results presented show that lateralized activity within the hemisphere of the lesion and from one hemisphere to the other changes throughout the intervention. Increased intrahemispheric connectivity in the higher β band follow previous reports. Increased connectivity towards the healthy hemisphere indicates more communication from the lesion. The SMR analysis showed no hemispheric imbalance of peak center frequency or the power of the rhythm during rest.

Both studies on ERD underlined the **heterogeneity of stroke**. The cross-sectional study showed a tendency of lesion volume and lesion size influencing the magnitude of the ERD. The longitudinal analysis revealed that patients exhibit different strategies: Some improve while strengthening their ERD and some improve while weakening desynchronization. More detailed stratification could even reveal other strategies. The study on SMR adds to these discoveries, showing that there is an effect on the peak central frequency of the rhythm that is not exclusively attributable to age but also to stroke. The three studies support the idea of individualized treatments (and more effective stratification of clinical trials). In the study on LFOs the patients in the group receiving contingent feedback were identified as main contributors to the *pre-post* difference of LFO power. These were the patients who benefitted from the intervention as they improved their motor function. However, there was no correlation between LFO power and recovery. Just as the three other studies, this one also calls for an extension and validation of the results in larger cohorts.

Kim and colleagues have recently argued that analysis of brain networks is becoming state-of-the-art for models of stroke and recovery using biomarkers (Kim *et al.*, 2016). The results presented in the Coherence analysis are only a first step but they are promising. The study compared the non-parametric approach to the widely used parametric approaches and showed in the application to the comprehensive stroke dataset (Dataset 1, cf. section 1.3.1) that the method is readily applicable. The use of non-proprietal open-source software improves comparability of studies employing the technique and paves the way towards further improvements (of methodology and performance). One of the merits of the work is the presentation of the data-driven threshold estimation based on experimental conditions. This approach is applicable to similar experiments using EEG.

Correlation of potential biomarkers with clinical scales could be assessed. Some measures correlated well (ERD progression and laterality), others did not. However, that does not mean that there is no connection of the measures to recovery. Other works have shown that increase of LFO is accompanying spontaneous recovery in early stages of stroke and moderate to mild cases. The mismatch between these findings and the ones presented here calls for further validation in a larger cohort. After all, neurophysiological markers have the potential to improve prediction of outcome when combined with clinical scales (Kim *et al.*, 2016).

Implementation of the two neurorehabilitation projects, the three-dimensional visualization of the exoskeleton and the rehabilitation gaming environment of AMoRSA,

underline the importance of **feedback tailored to the patient in BMI-based interventions**. The investigation of the characteristics of the SMR showed that stroke has an effect on both hemispheres and slows the sensorimotor rhythm, but the rhythm itself is stable over time. This means that the feedback on the SMR (e.g. as a control signal for an exoskeleton) needs to be tailored to the patient at the beginning of the intervention. The rhythm recorded from the healthy hemisphere could support selection of the appropriate frequency range.
The interventions might cause muscle fatigue in some patients. The extent remains unclear. With the work presented here a framework is available for assessing these effects in the recordings of the ongoing rehabilitation training without further effort. If muscle fatigue is detected in patients, the training could be modified automatically, for example by increasing the duration of break times.
The combination of the biomarkers explored here and the rehabilitation gaming environment could provide a way of giving the patient feedback (and prospect) while there is no or only little observable change of behavior. Neurophysiological changes could be integrated in the game as distinct elements or graphs and make abstract progress tangible.

Observation and responses of the patients using the gaming rehabilitation environment confirmed that **enhanced feedback and carefully designed virtual worlds lead to immersion and motivation** to take part in and carry on the demanding and repetitive training exercises.

1.6 Outlook

The reward of the research efforts on neurophysiological biomarkers will be two-fold: Knowledge about the mechanisms of plasticity and neurorehabilitation will be gained and models of the processes will be created. The insights will help stratify patients for further clinical studies and they will also inform treatment pathways in the future.

There are two levels at which modelling of rehabilitation research develops: Simple (regression) models relating individual markers or sets of markers to clinical outcome and models of actual neurorehabilitation that provide dynamic and potentially more accurate predictions.
Despite the simplicity, the **regression models** already have prognostic value for stratification in clinical studies and might even prove helpful in the future for choosing the appropriate course of intervention. The number of (clinical) studies on biomarkers is increasing and consequently more data is becoming available (Tedesco Triccas *et al.*, 2019). The biomarker candidates in these studies, just as the ones under investigation in this thesis, can be correlated with clinical outcome. In addition to potential prognostic ability regressions such as presented here might raise questions on the processes going on during rehabilitation, just as we have seen here: Patients use two strategies when modulating the ERD. What is the physiological reason behind that?

The data of comprehensive studies such as Dataset 1 and Dataset 2 will be pooled

in the future to include regressions of combinations of electrophysiological biomarkers and clinical / behavioral markers. As an example, in a study of our work group on Dataset 1 we used a linear combination of several markers for a prognostic regression model (Figueiredo, Ray et al, unpublished). In the model the five best predictors of motor improvement were (1) feedback group (experimental group or sham group), (2) interhemispheric connectivity from the lesion to the healthy hemisphere in the θ band, (3) connectivity between the SMR band and the muscle activity and (4 & 5) connectivity from both hemispheres to the muscle activity. The model was tested in a permutation test and performed significantly better than chance (in terms of root-mean-squared error). Correlation between predicted and actual Fugl-Meyer scores was $r^2 = 0.38$.

It is clear that all the models presented need to be validated on new data and with larger datasets than currently done in order to decrease false positive or random correlations and to uncover effects of potentially influential unknown variables. There are initiatives in the field that aim at pooling similar data of BMI-based stroke rehabilitation for validation of previous findings such as the Enigma data sharing initiative (http://enigma.ini.usc.edu/ongoing/enigma-stroke-recovery/).

The prognostic potential and clinical validity of electrophysiological biomarkers, namely the Motor Evoked Potential, has recently been shown by Stinear and colleagues (Stinear *et al.*, 2017). Figure 1.1 shows a flow chart of the algorithm, which predicted motor outcome for patients with 75% accuracy. Their report shows that biomarkers can already be introduced to clinical practice and could help decrease application of functional MRI, which is costly and strenuous for the patients (Stinear *et al.*, 2017).

The second level of developments will move modelling beyond regression and prognosis. **Models of neurorehabilitation** will not only contribute to understanding the processes in the brain of patients undergoing rehabilitation treatment. They also aim at providing causal mappings of brain plasticity in neural networks and the behavioral change due to rehabilitation. The models are dynamic and have internal states that have biological or functional meaning. In their enlightening work Reinkensmeyer and colleagues state that such models of neurorehabilitation consist of three building blocks (Reinkensmeyer *et al.*, 2016):

1. a quantitative description of sensorimotor activity of the patients (such as the biomarker candidates described here)

2. a computational model of plasticity that explains recovery

3. a quantitative description of the behavioral change

The authors argue that these models would help understand and predict outcome of rehabilitation interventions more quickly than with the current trial-and-error-based approach. They summarize various modelling approaches as examples. In one of these models the production of force in the wrist was modelled by an artificial neural network

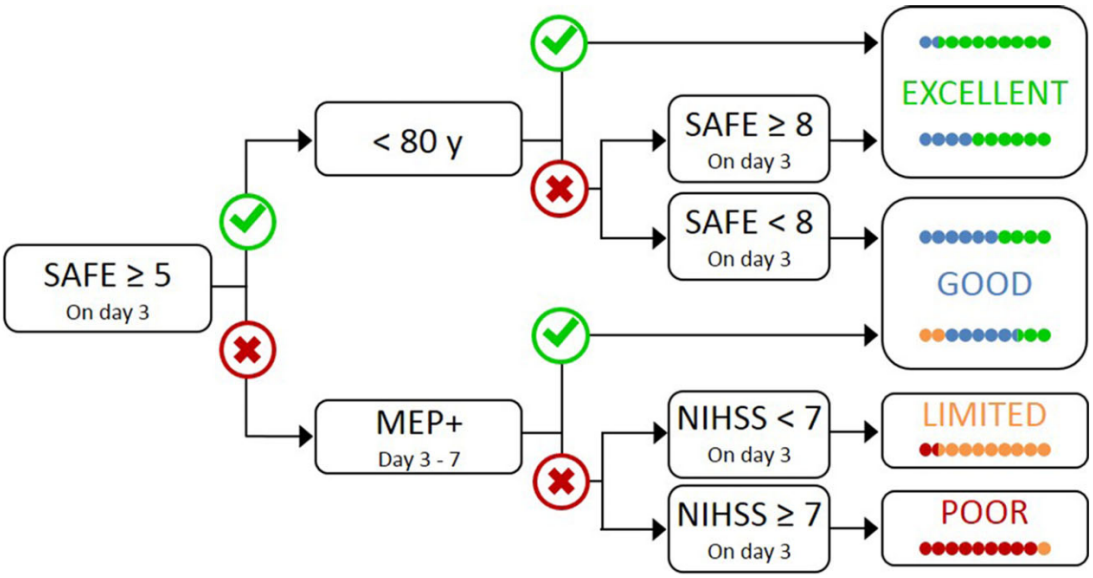

Figure 1.1: The PREP2 algorithm predicts uper limb functional outcome (excellent, good, limited, poor) at 3 months post stroke. SAFE is a clinical scale that is administered first. The path within the flow chart unfolds depending on the demographic marker age and the electrophysiological biomarker MEP (Taken from Stinear *et al.* (2017) [Licensed under CC-BY 3.0 https://creativecommons.org/licenses/by/3.0/])

of corticospinal cells (those that remained after a stroke), which was based on observations from experiments with primates. The basic assumption is that output force is proportional to the summed firing rate of corticospinal cells. The cells fired randomly, and activation patterns that produced force were strengthened (as in a reinforcement learning paradigm). This single learning mechanism alone was able to predict features of stroke recovery such as a dose-response curve, the influence of the strength of impairment and the influence of the timing of administration of a certain dose. Other models predicted the spontaneous use of the paretic arm in a bimanual task as a function of the dose or predict decay of (re-) learned motor control over time using kinematic data from robotic interventions (Reinkensmeyer *et al.*, 2016). With increased understanding of the pathophysiology of stroke and the increased amount of available data from BMI-based trials, models can be devised that provide a basis for stratification and choice of treatment pathways. These models could even pave the way towards completely new approaches to rehabilitation training.

The AMoRSA project showed that **integration of a very complex rehabilitation training into a gaming environment is feasible**. This research project is only a small piece of a whole sector that is changing: motor rehabilitation will be integrated into virtual environments and serious games in the future. Companies are forming all over the world and new approaches are being tested. Gamification of rehabilitation follows ubiquitous gamification in many other areas. The majority of smartphone apps contain at least a few gamified elements. A great example are health apps with step counters. Simply displaying a discrepancy between a movement goal (y number of steps) and the objectively measured state (x number of steps) motivates hundreds of thousands of people daily to walk a little bit further or to climb stairs instead of taking the elevator.
For the rehabilitation sector and especially including BMI more and more studies and even real-world applications and therapies are launched. The data acquired there will help understanding pathophysiology and psychology of the stroke patients and allow researchers and health entrepreneurs improve treatments.

When more data leads to better understanding the enhanced rehabilitation environments can be enriched and progress can be monitored and visualized using neurophysiological biomarkers. At the same time patient models and disease models improve predictions and inform treatment pathways.

In the context of these developments in the field the results of this work are very encouraging and research will hopefully thrive for the benefit of the victims of stroke.

1.7 List of scientific publications and contributions

Parts of chapters 2 and 6 were taken from peer-reviewed publications as shown below and as stated at the beginning of the respective chapter.

1. **Ray, A. M.**; López-Larraz, E.; Figueiredo, T. C.; Birbaumer, N. & Ramos-Murguialday, A.: *Movement-related brain oscillations vary with lesion location in*

severely paralyzed chronic stroke patients, Published in the proceedings of the 39th Annual International Conference of the IEEE Engineering in Medicine and Biology Society (EMBC), 2017, pp. 1664-1667 (peer-reviewed)

2. **Ray, A. M.**; Maillot, A.; Helmhold, F.; Jaser Mahmoud, W.; López-Larraz, E. & Ramos-Murguialday, A.: *Electromyographic indices of muscle fatigue of a severely paralyzed chronic stroke patient undergoing upper limb motor rehabilitation*, Published in the proceedings of the 9th Annual International IEEE EMBS Conference on Neural Engineering, 2019, DOI 10.1109/NER.2019.8717165 (peer-reviewed)

3. **Ray, A. M.**; Figueiredo, T. D. C.; López-Larraz, E.; Birbaumer, N. & Ramos-Murguialday, A.: *Brain oscillatory activity as a biomarker of motor recovery in chronic stroke*, Human Brain Mapping, 2020, 41, 1296-1308

All analyses presented in this work have been performed by me and it was I who wrote all texts. However, the domain of this work, neural interfaces for stroke rehabilitation, is inherently interdisciplinary. Conducting the studies and obtaining the results presented here could only be realized by collaboration and concentrated effort of a team of scientists with experience in neuroscience, physiotherapy, informatics, physics, biomedical engineering and psychology. Any contributions of others are disclosed in section 8.2. Please note that I used the pronoun ”we” throughout most of the dissertation, referring to me and the team who played a part in the realization of the respective study. This is in accordance with the scientific writing style used in journal publications and it reflects the interdisciplinary nature of the work.

Chapter 2

Desynchronization of the Sensorimotor Rhythm

The greatest part of this chapter has been published in a peer-reviewed journal paper as (Ray et al., 2020). Section 2.5 presents the results and conclusions of a peer-reviewed conference paper published as Ray et al. (2017). The material presented in section 2.6 provides additional information on procedures, data and results in this chapter. The contents of this section are taken from the supporting information of the publications. For disclosure of contributions see section 8.2.

2.1 Introduction

Changes in sensorimotor brain oscillations involved in planning and execution of movements were used as control signals for the BMI in the studies cited in the synopsis (chapter 1). The sensorimotor rhythm (SMR) is an oscillation within the alpha frequency range of the EEG during a motionless resting state over the central-parietal brain regions. Movement planning, imagination and execution lead to its suppression. In the present work, we investigated EEG brain oscillations of the alpha frequency, ranging from 8 to 12 Hz, over the motor cortex, and we termed them "alpha oscillations".

Alpha brain oscillations have been evaluated as markers of ischaemia and predictors of clinical outcome in acute patients (Finnigan and van Putten, 2013; Rabiller *et al.*, 2015). Desynchronization in the alpha frequency range has also been investigated as a marker of stroke and a predictor of recovery in the same patient group. Tangwiriyasakul and colleagues showed that the recovery of motor function was accompanied by an increase of alpha desynchronization on the ipsilesional side (Tangwiriyasakul *et al.*, 2014). In subacute patients presenting mild to moderate motor deficits recovery lead to a similar increase of alpha desynchronization on the affected hemisphere (Platz *et al.*, 2002). Furthermore, first attempts investigated correlations of alpha desynchronization with motor improvements in chronically impaired patients (Kaiser *et al.*, 2012). In a controlled study, a group of subacute patients with severe deficits used motor imagery, guided by a brain-computer interface, in addition to their regular physiotherapeutic rehabilitation

protocol. They showed a higher probability for motor improvements with increased alpha desynchronization (Pichiorri *et al.*, 2015).

In the present work, we investigated what changes in the oscillatory activity of the brain a proprioceptive BMI coupled with physiotherapy produces over the course of a training intervention and if these correlate with recovery in severely paralyzed chronic stroke patients. We hypothesized that functional motor improvements are accompanied by an ipsilesional increase and a contralesional decrease in alpha desynchronization indicating reorganization of compensatory brain activity from the contralesional to the ipsilesional hemisphere. We intend to establish alpha oscillatory activity as a biomarker of motor impairment and as a building block of statistical models of stroke neurorehabilitation. Furthermore, the potential influence of the location of the lesion in the brain on alpha desynchronization is explored in section 2.5.

2.2 Methods

2.2.1 Data

The analysis presented in this chapter was performed on the data of dataset 1 recorded during the movements of the exoskeleton (section 1.3.1). Patients were randomly divided into an experimental group (n=16) and a control group (n=14). In both groups, electric brain activity was recorded using electroencephalography (EEG). Changes in the sensorimotor rhythm (SMR) of the ipsilesional hemisphere during movement attempts of fingers and arm were contingently translated into movement of the arm and hand orthosis only in the experimental group. Decrease of the power of the SMR with respect to baseline led to movement of the arm or the hand and a relative increase stopped the movement. In the control group, the setup was similar but the movements executed by the robot were independent of brain activity. The movements were triggered randomly but the period of time the orthosis was moving was approximately equivalent to that of the experimental group. Both groups received identical physiotherapy after the BMI training.

The individual SMR frequency was obtained from EEG recorded in a calibration session on the day before the training. The power of the EEG signal while the patients rested and while they were trying to open and close the paretic hand was compared. The frequency range showing the maximum variance between the two conditions as measured by the coefficient of determination was defined as individual SMR frequency. The most discriminative electrodes in the central-parietal region were selected.

2.2.2 Movement-related features of the EEG power spectrum

Movement planning, imagination and execution lead to suppression of brain oscillatory activity over the motor cortex. It has been shown that stroke patients can (re-) learn to voluntarily modulate this rhythm to control movements of their paretic limbs by way of

robotic orthoses (Buch *et al.*, 2008; Ramos-Murguialday *et al.*, 2013). The phenomenon is often defined as μ rhythm or as sensorimotor rhythm (SMR). There are various works describing the effect within the alpha frequency range of the EEG (Klimesch *et al.*, 2007; Kuhlman, 1978; Pfurtscheller and Lopes da Silva, 1999). Similar synchronization and desynchronization effects have been reported with other functional relevance in the beta frequency range (van Wijk *et al.*, 2012). Peak frequency and amplitude of the SMR vary between individuals but movement-related desynchronization in healthy populations spreads across the whole alpha range (Pfurtscheller, 2003). As alpha oscillations may also constitute indicators of underlying processes not related to movements it may be difficult to discern alpha central oscillations from genuine sensorimotor oscillatory activity in patients involved in visuo-proprioceptive motor tasks (Klimesch *et al.*, 2007). However, since firstly, significant power decreases in healthy subjects during execution of a BMI lasting several seconds have mainly been found in the alpha frequency range (Ramos-Murguialday and Birbaumer, 2015) and, secondly, the SMR frequency (defined as the frequency range with the largest difference between movement attempts of the paralyzed limb and resting state) in the original trial, were also centered in the alpha frequency band (mean 10.6 Hz $\pm$ 4.8) we focused our analysis on the progression of alpha desynchronization. Furthermore, to disentangle effects of individualized SMR values used for BMI interventions from the general alpha band, we also evaluated the progression of desynchronization in the individual SMR frequency. More information can be found in section 2.6.5.

Nevertheless, recent work has identified beta oscillations as potential therapeutic target for stroke rehabilitation because these oscillations are involved in cortical disinhibition and have been suggested as the rhythm connecting brain and muscles (Mima *et al.*, 2001; Naros and Gharabaghi, 2015; Rossiter *et al.*, 2014; Ward *et al.*, 2019). Therefore, we also analyzed the progression of desynchronization in the beta frequency band (12 to 25 Hz) (see section 2.6.5).

A previous work of our group on a similar dataset involving movement attempts in chronic stroke showed the adverse influence of low frequency (1 to 4) and high frequency (30 to 48 Hz, i.e. γ band) artifacts on time-frequency analysis of movement-related desynchronization and classification of EEG signals (López-Larraz *et al.*, 2018b). Therefore, γ oscillations (30 to 48 Hz) were not considered in the present analysis.

Event-related desynchronisation (ERD) was calculated following Pfurtscheller and colleagues (Pfurtscheller and Lopes da Silva, 1999) as the proportional decrease of EEG power in a movement attempt interval, M, relative to a reference interval, R:

$$ERD = \frac{M-R}{R} x100\% \tag{2.1}$$

ERD over the sensorimotor cortex was extracted from both hemispheres separately using the EEG signal of the electrodes C3, Cp3, P3 and C4, Cp4, P4, respectively, and within the alpha frequency band (8-12 Hz). The power spectral density was computed using Welch's method and the mean power of that frequency range was extracted. Fur-

thermore, the EEG power was averaged over the three channels on each hemisphere. No additional spatial filters were used. Mean ERD was computed as described in equation (1) over all trials of each session using the EEG data of the last 4 seconds of the inter-trial interval as reference R and the EEG data of the movement attempt phase as M.

It is important to note that a larger relative difference between neural activity during rest (synchronized, larger EEG power) and action (desynchronized, smaller EEG power) is represented by a numerically smaller, more negative ERD value (Eq. 1) and vice-versa. We thus report "strong" ERD when the ERD values are more negative and "weak" ERD when they are less negative.

Works on brain oscillatory biomarkers of stroke rehabilitation were often limited to predicting behavioral changes by brain activity measured before and after spontaneous recovery or intervention (Stinear, 2017). Here, a comparison of ERD during movement attempts of the upper limb without the afferent input of the orthosis before and after the intervention indeed did not reveal a generalized change of ERD. For each patient a *pre* measurement and a *post* measurement involving movement attempts of the paretic arm without the orthosis were performed. The patients were asked to perform up to 85 repetitions of 3s of resting and 4s of movement attempts. The EEG data was preprocessed and the mean ERD of each patient before and after the intervention (*pre* and *post*) was computed. A difference of the ERD values between groups and time points could not be found (see section 2.6.4). In the present work, however, we make use of the large amount of longitudinal neurophysiological data gathered during dozens of training sessions to infer on the relationship of progression of changes of brain activity and behavioral improvements. All the analysis was performed using EEG and EMG data acquired during the interventional sessions, in which the patients tried to move their paretic limb avoiding compensatory movements and the limb moved according to the brain-controlled robotic orthosis. During the intervention proprioceptive feedback usually lead to an increased SMR desynchronization.

2.2.3 Artifact detection

Even though the participants were instructed to minimize movements of head and body during the recordings, contamination of the EEG by movement artefacts could not be completely prevented as the experiment involved movements of the body. Detection and rejection of artefacts in the data were carried out using a fully automated process (fig. 2.1). First, artefacts caused by eye movements were removed from the EEG signal by way of extracting the independent components representing these artefacts identified in the EOG (Halder *et al.*, 2007). Then, trials contaminated by cranial muscle artefacts were detected. The EEG signal of all channels was filtered between 110 Hz and 140 Hz and the signal in each channel was z-scored and the z-values were averaged per sample. A threshold of 4 standard deviations was applied to remove trials containing artefacts. Afterwards, a similar procedure was performed on the broadband EEG signal with a threshold of 20 standard deviations to remove trials containing offset artefacts. The fieldtrip

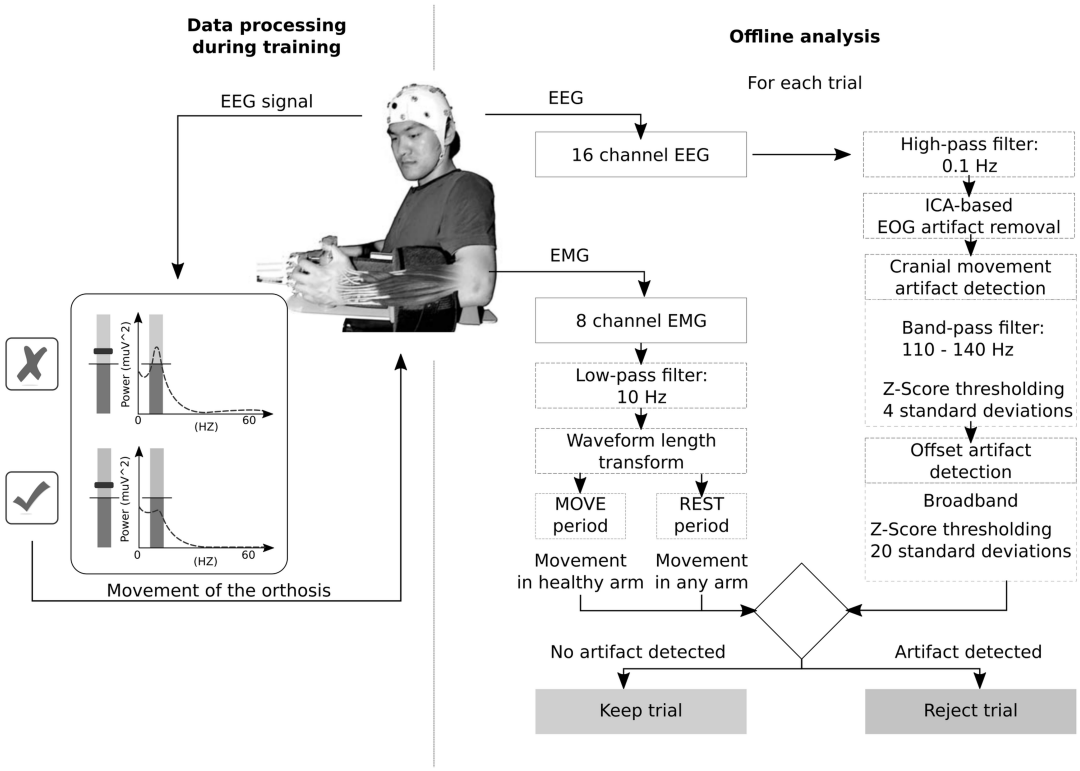

Figure 2.1: Schematics of the data acquisition phase and the offline analysis for EEG and EMG. Neurophysiological data was acquired using a 16 channel EEG cap and 4 bipolar EMG electrodes on each arm. EEG data were cleaned from eye movement artifacts and trials containing other artifacts (e.g., cranial EMG, head movements, and so on). EMG data were analyzed to detect compensatory muscle contractions on the healthy upper limb and on the paretic side during resting intervals to identify these trials as contaminated because the muscle activity is a sign of undesired EEG activity. Only data free of artifacts were used for the final analysis of EEG oscillatory activity.

toolbox was used for rejection of EEG artefacts (Oostenveld *et al.*, 2010). Finally, the EMG activity was analyzed. The Waveform length of the EMG was computed (Ramos-Murguialday *et al.*, 2013). Muscle contractions were identified by the Waveform length exceeding 3 standard deviations of the data. Any such arm or hand movement during the rest period or movements of the healthy limb during the phase of the movement attempt led to removal of the trial from the analysis.

A session was excluded from the analysis if less than 10% (16 trials) of all trials remained. If half of the total number of sessions of a patient were removed, the subject was excluded from the analysis. Table 2.1 shows a summary of the rejection procedure. Descriptive statistics on the rejection of trials and an overview of the number of trials, sessions and subjects removed is presented in 2.6.1.

To further improve interpretability and generalizability the R function *dfbetas* was used to investigate the linear models for influential data. The function computes the standardized difference of parameter estimates between a regression model based on the full data and a model from which a subset of potentially influential data is removed.

Dfbetas is defined as:

$$Dfbetas_{pZ} = \frac{b_Z - b_{-bZ}}{se(b_{-bZ})} \tag{2.2}$$

where the denomiator is the difference between the slope estimate of one of the predictors (Z). The first term (b_Z) is the estimate using the full sample and the second term (b_{-pZ}) is the estimate after excluding a patient (p). The value is normalized by dividing the standard error of the second term (Van der Meer *et al.*, 2010). Here, one out of all subject is left out in each iteration. A DFBETAS value is computed for each parameter in the model. For the linear model the parameter "slope" of the data of the α-band was strongly influenced by subject 12 (see description of the modeling procedure in the next section). Removing the subject would change the slope coefficient of the model almost one order of magnitude more than removing the next most influential data point. Moreover, the inspection of the mean power values of the EEG revealed that this patient had, on average, larger power during the movement phase than during the resting period in all training sessions except one (fig. 2.2). This might indicate that the patient consistently synchronized the SMR during movement attempts or produced SMR synchronization due to an unfiltered artifact (e.g. subtle contractions of the neck or face muscles). On top of that, the patient was part of the control group, which received sham feedback. In the first three sessions, this patient received contingent negative feedback because of a technical issue. In this type of feedback the robot moved whenever the patients did not desynchronize or synchronized their ipsilesional SMR. Synchronization thus could have been rewarded in this patient in the beginning of the intervention. We thus conclude that the patient was not able to and did not learn to produce the desired SMR desynchronization throughout the course of the intervention, which would explain the odd coefficients of the linear mixed model.

We considered the patient an outlier and decided to remove this subject from the analysis.

The rigorous rejection procedure led to a final pool of 22 subjects. This conservative procedure facilitates interpretability of the results.

2.2.4 Statistical modeling

In order to model the cross-sectional response (the clinical outcome measure ΔcFMA) with the longitudinal predictors (progression of the ERD across training sessions) we employed a two-stage modeling process. First, the individual time courses of the ERD of all patients were modelled using a linear mixed-effects model. In the second step,

Subject ID	Total number of sessions	Number of sessions removed	Total number of trials	Number of trials removed	Feedback group	Was the subject part of the analysis?
1	16	4	2731	2296	C+	yes
2	17	10	2828	2617	Sham	no
3	19	5	3188	2619	Sham	yes
4	16	2	2680	1913	Sham	yes
5	16	7	2570	2102	C+	yes
6	19	18	2978	2908	Sham	no
7	17	6	3401	2845	C+	yes
8	16	8	2553	1870	C+	yes
9	17	1	3430	2139	C+	yes
10	19	3	3158	2466	C+	yes
11	16	2	2766	2146	C+	yes
12	18	9	2920	2544	Sham	yes
13	17	2	3003	1948	Sham	yes
14	17	11	2889	2688	C+	no
15	17	14	2405	2252	C+	no
16	11	1	1780	1524	Sham	yes
17	12	7	1926	1800	Sham	no
18	17	16	2540	2419	C+	no
19	18	4	2776	2307	C+	yes
20	18	0	2998	1856	C+	yes
21	16	5	2555	1554	C+	yes
22	19	4	3184	1910	Sham	yes
23	15	6	2500	2225	C+	yes
24	19	15	2820	2628	Sham	no
25	16	5	2624	2219	Sham	yes
26	17	3	2666	2097	C+	yes
27	18	0	2700	2018	Sham	yes
28	17	1	2902	1813	Sham	yes
29	18	5	3236	2848	C+	yes
30	18	7	2850	1777	Sham	yes

Table 2.1: the total number training sessions and the total number of movement attempt trials carried out in the whole training per patient. Moreover, the number of trials and the number of sessions that have been removed from the analysis during the preprocessing are shown. The rightmost two columns indicate the feedback group the patients belonged to and whether or not they were included in the analysis.

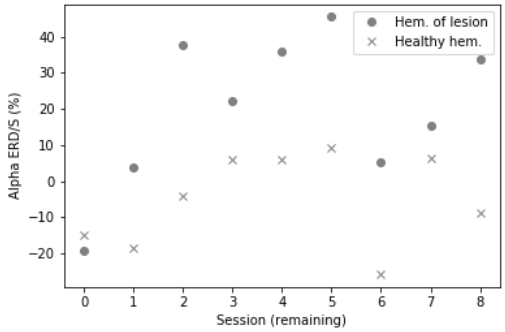

Figure 2.2: Averaged event-related desynchronization / synchronization in the sessions remaining after the preprocessing (re-indexed from 0 to 8) on both hemispheres of subject 12. The subject only desynchronized in one of the nine sessions.

the coefficients of these modelled time courses were used to predict each patients' motor improvement (fig. 2.3).

Linear mixed-effects models are suited for describing longitudinal physiological data because (1) they allow to reflect individual differences of intercepts and slopes with respect to population means; (2) data may be modelled even though measurements are unequally timed; (3) the number of measurements per subject is not required to be equal (Lang *et al.*, 2016) (Verbeke and Molenbergs (2001) provide a thorough description of linear mixed models). Shetty and co-workers showed that estimating the value of the explanatory variable(s) with a linear-mixed model (LMEM) approach leads to the best regression parameters for predicting a clinical outcome (Shetty *et al.*, 2009).

Using this approach, in the first step of modeling a LMEM is constructed to estimate two coefficients per patient which describe the initial state and the progression of the ERD of each patient throughout the course of the intervention. The response variable (ERD) is thus modelled by a general intercept (representing the mean initial ERD value of all patients) and the general change over time (mean unit change of the ERD per BCI-training session of all patients) as fixed effects. Both intercept and change over time may vary for each patient, and are therefore also introduced as random effects in the linear mixed model. The model thus yields two coefficients per patient: the individual progression of the ERD over time (the individual model slope), and the subject-specific initial value of the ERD (the individual model intercept). In the second step of the procedure a linear regression model (LM) is constructed that predicts the change of the clinical outcome (ΔcFMA) by the patients' individual dynamics of the ERD, which are represented by the coefficients modeled in the first step of the procedure. From this model an inference can be made if and how the initial state of the ERD of each patient, the progression of the ERD throughout the training and the interaction between these two factors predict the motor improvement. Please also see listings 10 and 11 for implementation details in R.

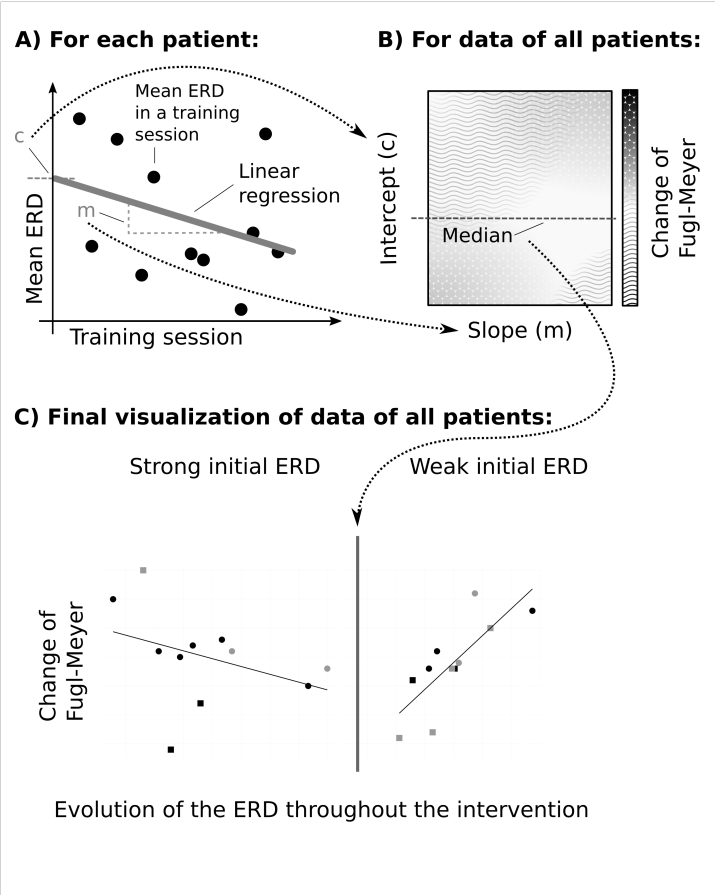

Figure 2.3: The two-step modeling approach for describing the relationship between brain activity (session-wise mean ERD) and the clinical outcome (cFMA). Step (A): Longitudinal modeling and coefficient extraction. First, the coefficients "intercept" and "slope" are extracted from a linear mixed-effects model for each patient. The linear mixed model provides the best (least squares) estimates of these coefficients. As the initial ERD values and their progression vary for each patient, the factors time and subject are considered as random effects in the model. Therefore, the two coefficients represent the patient-specific estimated initial value and the progression of the ERD throughout the intervention. Step (B): Two-dimensional visualization of the interaction in the model. The extracted coefficients of (A) are used in a linear model predicting the clinical outcome (cFMA). The model includes an interaction term. The model thus can capture modulation of the outcome variable by both independent variables. One of the variables might predict the outcome variable depending on the other independent variable. Here, for example, large Fugl-Meyer values are predicted by large slopes if the intercept is large, too. Step (C): Visualization for interpretation. The median of the intercept values is used to form cross-sections of the data that are visualized in separate panels to increase interpretability of the linear model.

To assess the interhemispheric asymmetry of brain activation during recovery, the laterality coefficient is often used (Kaiser *et al.*, 2012; Pivik *et al.*, 1993; Tangwiriyasakul *et al.*, 2014; van Putten, 2007). The sign of the coefficient represents the laterality of the desynchronization, i.e. which of the hemispheres is more active during a certain condition such as the movement of the paretic arm. In order to assess the progression of the asymmetry of the interhemispheric oscillatory activity of the brain, we expanded the laterality coefficient to encompass the temporal component (training progression). The progressive laterality coefficient (*pLC*) is computed as:

$$pLC_{ERD} = S_H - S_L \tag{2.3}$$

The change (i.e. slope) of the ERD for each patient, was extracted from the LMEM from the data of both hemispheres (healthy hemisphere: S_H, hemisphere of the lesion: S_L) and subtracted from each other to form the *pLC*. This measure describes the progression of the asymmetry of the desynchronization between both hemispheres over the course of the training. It may reveal if the change of desynchronization throughout the intervention was stronger on one hemisphere than on the other. The values of the pLC_{ERD} were correlated with the primary clinical outcome ΔcFMA to investigate the relevance of progressive brain activity asymmetry for motor improvement.

2.3 Results

2.3.1 Prediction of ΔcFMA from contralateral (ipsilesional) EEG

The linear models for the ERD in the alpha frequency range were constructed, each predicting ΔcFMA using the coefficients extracted from the corresponding linear mixed effects model: the progression of the ERD throughout the intervention sessions and the initial ERD magnitude. An interaction term was included in the LM to investigate if the initial ERD modulated the progression of the oscillatory activity. An F-test of the regression equation was significant: $F(2,18) = 6.96$, $p = 0.0026$ and an adjusted $r^2 = 0.46$.

In linear models with interaction terms two independent variables might exert an effect on the dependent variable. They might also modulate each other. In order to understand and interpret the interaction the data is usually separated into smaller subsets (Aiken and West, 1991). One variable is "fixed" and defines these subsets while the other variable is investigated independently within each subset. This procedure allows to observe whether the value of the "fixed" variable influences the "free" variable depending on the subset or not. If the "fixed" variable is categorical the subsets are naturally defined. However, here, the variable of interest, initial ERD, is a continuous variable and the separation is defined based on prior knowledge and the characteristics of the data (Aiken and West, 1991). Given the amount of data points a division into few subsets is the best choice. Furthermore, even though there is no standardized definition, "strong initial ERD" and

"weak initial ERD" may be meaningful for the interpretation. For these reasons, we split the data into equal subsets at the median. The procedure supports intuitive visualization of the linear model (Breheny and Burchett, 2016). Moreover, it facilitates interpretation of the analysis of the brain activity on the healthy hemisphere because we saw that the ipsilesional brain activity of the patients is modulated differently in the subgroups. We thus show the correlation of the progression of ERD and ΔcFMA for two subgroups presenting relatively strong and relatively weak initial ERD (higher and lower than the median). The median value of the initial ERD is -29.96 (fig. 2.4). Those patients presenting a relatively strong ERD at the beginning of the intervention (fig. 2.4, panel on the left) improved if their ERD progressively increased throughout the training. In contrast, those patients whose ERD was already relatively weak at the beginning of the intervention (fig. 2.4, panel on the right) improved if their ERD progressively decreased throughout the training.

These relationships are also reflected in visualization of time-frequency representations. Here, time-frequency plots of two patients of the subgroup with relatively strong and two patients of the subgroup with relatively weak initial desynchronization are shown. The chosen subjects represent the extremes of the modeled ERD progression (fig. 2.5). The plots show the time-frequency representation of an early and a late session (fig. 2.6). The sessions that are plotted here reflect the modeled progression of the ERD. Plots of other sessions might not reflect the modeled progression because the ERD values vary around the slope of the model. The plots were created using Morlet wavelets for the time-frequency decomposition with a resolution of 0.5 Hz from 2 Hz to 36 Hz. The data of the instruction phase of the trials were disregarded and is shown here in light grey. It is important to note that the ERD/S values for the plots were obtained using time-frequency decomposition with Morlet wavelets rather than Welch's method, which has been used to obtain the ERD/S values for the statistical tests. Furthermore, the ERD/S values were computed using the full last four seconds of the rest period as baseline. Here, the baseline period was truncated by 250 ms at the beginning and at the end to alleviate potential aliasing effects of the wavelets.

It is noteworthy that four patients of the control group presented a negative change of their cFMA score regardless of their ERD progression throughout the intervention (four squares below the zero line in fig. 2.4).

The progression of the ERD in the beta frequency range (11 – 25 Hz) and the individual SMR frequency were also analyzed in the same way as the data of the alpha frequency range to complement the analysis. The results and plots are presented in section 2.6.5. In summary, the F-test of the regression equation of the model of the β band was not significant. The linear model for the individual SMR frequency was significant ($F(3,18) = 3.475, p = 0.038$). The fit was lower than that of the model for alpha: $r^2 = 0.26$.

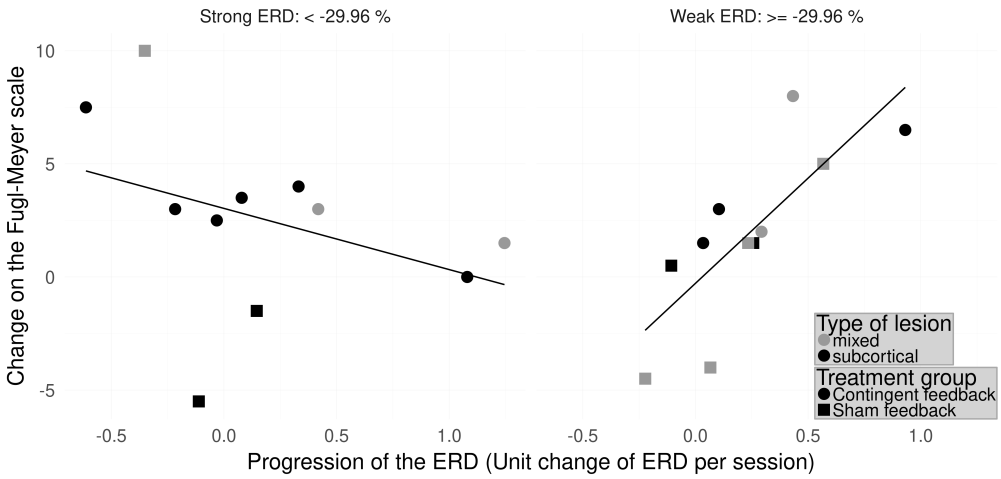

Figure 2.4: Linear model predicting the improvement of motor function (ΔcFMA) on the hemisphere of the lesion by the initial ERD and the progression of the ERD of the alpha frequency range on the ipsilesional hemisphere over sessions: Adjusted $r^2 = 0.46; F(3,18) = 6.96, p = .0026$. For improved visualization of the effect of both explanatory variables in the model the patients are separated into two cross-sections showing relatively strong ERD (left panel) and a second group showing relatively weak initial ERD (panel on the right). For the patients showing strong ERD the inverse linear relationship of the variables suggests that the more these patients increase their ERD the larger the improvement. For the patients showing a relatively weaker ERD at the beginning of the training, the opposite relationship is apparent.

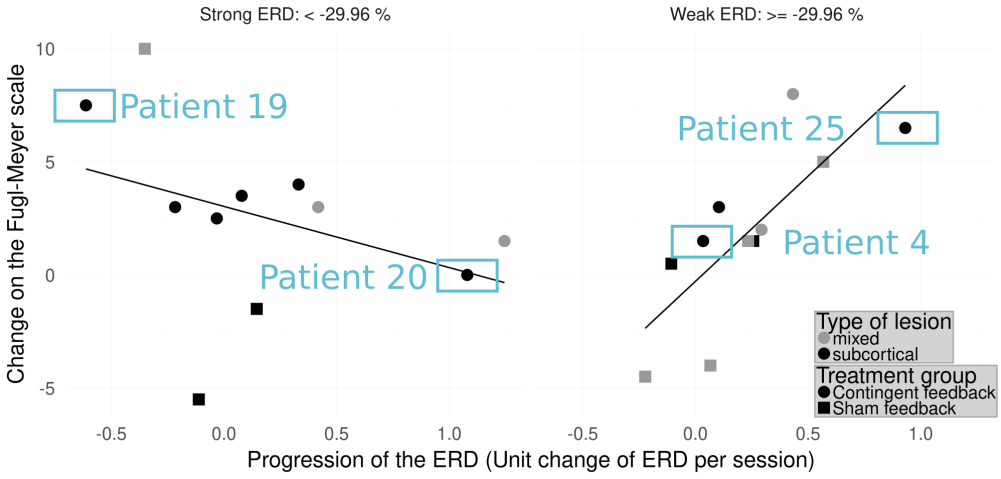

Figure 2.5: The time-frequency plots in figure 2.6 are presented for the patients marked here. This figure is otherwise identical to figure 2.4.

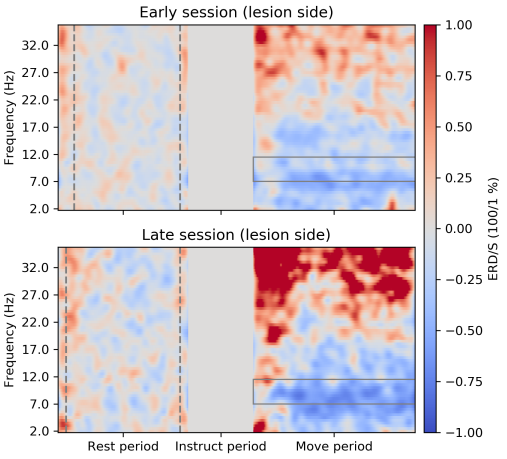

(a) Patient 18: Alpha desynchronization is stronger in the late session (sessions 1 and 16 out of 18 retained sessions presented)

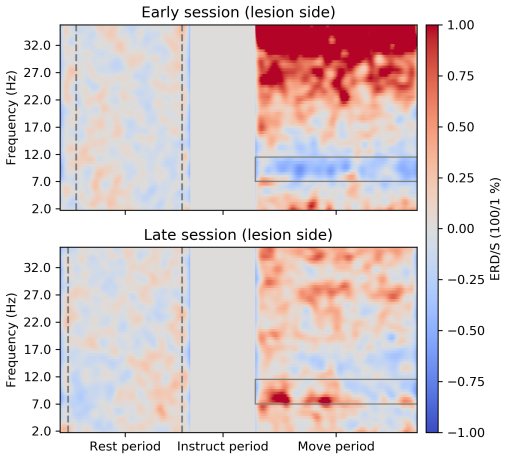

(b) Patient 19: Alpha desynchronization is weaker in the late session (sessions 1 and 11 out of 11 retained sessions presented)

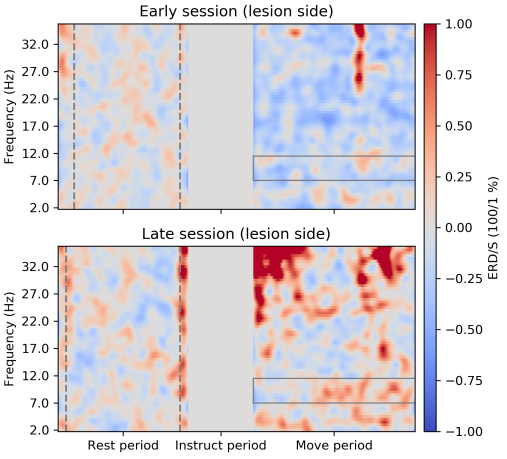

(c) Patient 24: Alpha desynchronization is weaker in the late session (sessions 1 and 11 out of 14 retained sessions presented)

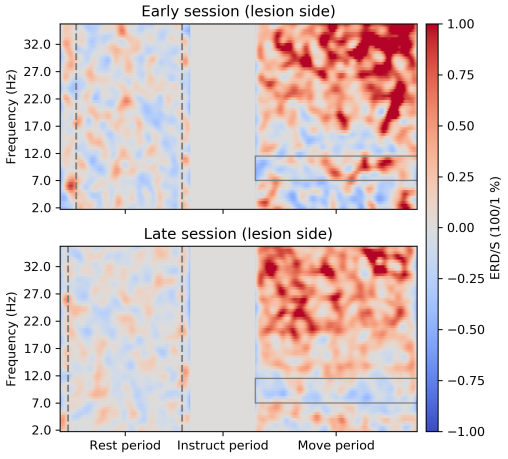

(d) Patient 3: Alpha desynchronization did not change on average (sessions 2 and 8 out of 9 retained sessions presented)

Figure 2.6: Activity from all channels of interest on the hemisphere of the lesion has been averaged (i.e. average of channels C3, CP3, P3 or average of channels C4, CP4, P4). The duration of the *Rest* period is four seconds. The duration of the *Move* period is five seconds. The *Instruct* period has been disregarded in the analysis and is shown in light grey. The grey dashed lines mark the interval that was used to compute the baseline for ERD/S. The rectangle with the grey outline in the *Move* period shows the time and frequency range that was used to compute the ERD/S values.

2.3.2 Prediction of ΔcFMA from ipsilateral (contralesional) EEG

We examined how the progression of the ERD of the healthy hemisphere relates to the clinical improvement depending on the initial ERD of the lesioned hemisphere. Knowing that the initial ERD on the ipsilesional hemisphere interacts with the ERD progression patients were again separated into the same two subgroups accordingly (relatively strong and relatively weak ipsilesional ERD). The progression of the ERD on the healthy hemisphere during movements of the paretic arm and hand were modeled for both subgroups. These linear models predicted the change of the clinical outcome measure ΔcFMA. For the subgroup showing relatively weak ERD at the beginning of the intervention on the ipsilesional hemisphere the model showed a significant positive linear relationship: Adjusted $r^2 = 0.47; F(1,9) = 9.05, p = 0.0148$. For the other subgroup, the patients showing relatively strong initial ERD, however, the F-test for the regression equation was not significant: Adjusted $r^2 = -0.11; F(1,9) = 0.0072, p = 0.93$ (fig. 2.7).

In summary, the patients presenting a relatively weak ipsilesional ERD at the beginning of the intervention, presented a larger motor improvement if their ERD decreased on the healthy hemisphere (i.e. activating their contralesional hemisphere less) during paretic hand movements using the BMI.

2.3.3 Prediction of ΔcFMA from interhemispheric asymmetry of brain activation

To investigate the interhemispheric asymmetry during motor recovery, the progressive laterality coefficient *pLC* was used to predict the clinical change ΔcFMA. The F-test for this linear regression equation was significant: $F(0,20) = 9.11, p = 0.007$ with an adjusted $r^2 = 0.28$ (fig. 2.8). The analysis thus demonstrated that the patients who progressively produce more ipsilesional relative to contralesional brain oscillatory activity (stronger desynchronization) in the alpha band during the course of training improved motor function.

Since the model predicting change on the Fugl-Meyer scale from the ERD of the contralateral/ipsilesional hemisphere was significant for the individual SMR frequency, we also analyzed the interhemispheric asymmetry in this frequency band. The results and plots are shown in section 2.6.5. In summary, the F-test for this linear regression was not significant but showed a trend ($F(0,20) = 3.76, p = 0.067$). The fit of the model to the data was low: $r^2 = 0.1161$.

2.4 Discussion and conclusions

We investigated how the brain oscillatory activity of severely impaired chronic stroke patients changes throughout a brain-controlled robotic intervention for motor rehabilitation of the upper limb and how it relates to the functional motor improvement. We

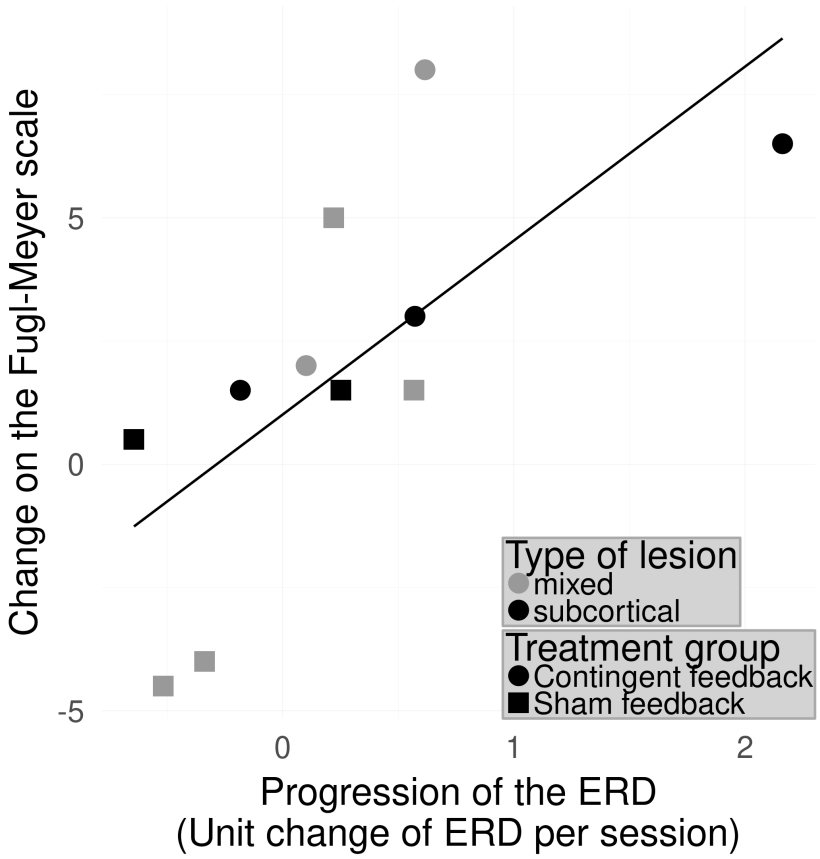

Figure 2.7: Linear model predicting the improvement of motor function (ΔcFMA) by the progression of the ERD of the alpha frequency range on the healthy hemisphere over all sessions for the patients showing relatively weak initial ERD on the ipsilesional hemisphere: Adjusted $r^2 = 0.45; F(1,9) = 9.05, p = .015$. Better recovery was achieved when the ERD on the healthy hemisphere decreased in the course of the training

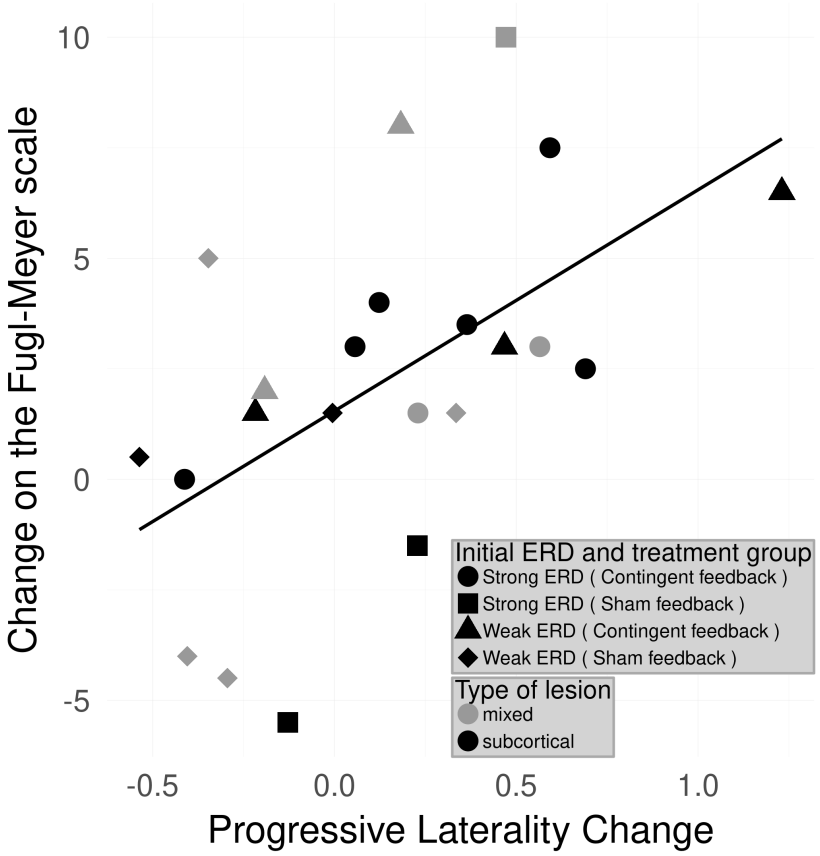

Figure 2.8: Relationship between improvement and interhemispheric difference of changes of the ERD in the α band. Relationship between improvement and interhemispheric difference of changes of the ERD in the α band: Adjusted $r^2 = 0.279; F(1,20) = 9.11, p = .0068$. Values on the x-axis express the difference between the progression of the ERD on the healthy hemisphere and the ipsilesional side. Positive values on this axis indicate that throughout the training patients exhibited stronger ipsilesional ERD, negative values indicate a stronger ERD on the healthy hemisphere. The regression indicates that the larger a difference towards the hemisphere of the lesion is found the better the motor improvement.

found that dynamics of event-related desynchronization in the alpha frequency range (ERD) significantly correlate with motor improvement. Most notably, patients showing a relatively strong ERD on the side of the lesion at the beginning of the intervention improved when progressively increasing ERD during movements of the paretic arm in the course of the intervention. Patients showing a relatively weak ERD on the affected hemisphere improved when progressively decreasing ERD. Furthermore, we found larger motor improvements in patients with a progressively larger ERD on the hemisphere of the lesion as compared to concomitant ERD on the healthy hemisphere. The results indicate that the patients might have used two strategies to gain control over the orthoses to link brain oscillatory activity and upper limb movement. Their success rebalancing ipsi-/contralesional activity plays an important role in impairment reduction.

Considering that the proprioceptive feedback was initiated based on the individual SMR ERD, patients who could elicit a strong ERD at the beginning could learn to control the robotic orthosis BMI more easily. We show that a strong ERD on the ipsilesional side during movement attempts of the paretic limb and a subsequent further increase of the ERD was linked to recovery whereas a strong ERD on the healthy hemisphere was not. The results indicate that generating a strong ERD on the hemisphere of the lesion may suffice to regain control of the paretic limb via BMI and to reduce motor impairment. It was indicated that patients without transfer of ERD from the contra- to the ipsilesional hemisphere do not improve as predicted by the concept of learned non-use (Daly and Wolpaw, 2008). A linear relationship between the relative progressions of the ERD on both hemispheres was observed. The modeling presented, links greater improvement of motor function to stronger ERD on the affected hemisphere than on the healthy hemisphere during BMI intervention. Patients with weak ERD during movement attempts of the paretic arm at the beginning of the intervention improved if they showed progressively reduced ERD on the hemisphere of the lesion and an even more pronounced progressive reduction of desynchronization on the healthy hemisphere. One additional explanation to the learned non-use model of rehabilitation for this phenomenon is that when having acquired proficiency in performing the motor task, reduced ERD represents more efficient inhibition of systems that are not task-relevant on the ipsilesional side (Klimesch *et al.*, 2007; Taub *et al.*, 1994). Moreover, a connection between alpha synchronization of the EEG and focalized suppression of areas involved in generation of movements irrelevant to the task is assumed (Klimesch *et al.*, 2007; Pfurtscheller and Lopes da Silva, 1999). The reduction of desynchronization on the healthy hemisphere as compared to the affected hemisphere indicates less recruitment of the healthy hemisphere during the course of the training as predicted by the model of learned non-use (Taub *et al.*, 1994). Experiments have shown that interhemispheric inhibition from the healthy to the affected hemisphere is associated with deficient motor recovery (Murase *et al.*, 2004). Concordant with this interpretation the increased desynchronization of the healthy hemisphere is associated with poorer recovery (Kaiser *et al.*, 2012).

The stratification of the patients into two subgroups (relatively strong and weak ERD) after investigating the linear model paved the way to a concise interpretation of the re-

sults obtained. Learning to control a BMI involving proprioceptive feedback modulates desynchronization of the SMR (Ramos-Murguialday *et al.*, 2012)). The group receiving sham feedback might have had a lower or no effect of the practice on the modulation of their SMR. Nevertheless, random correct feedback was sometimes administered, because the orthoses might have also moved while patients correctly produced ERD and both groups received identical physiotherapy after BMI training. Since almost all patients showed some behavioral change, we assumed that the neurophysiological data could explain these changes, which was the main goal of this investigation. The number of patients analyzed did not allow for a robust analysis including stratification by feedback group. There was no difference in number of trials rejected due to EEG or EMG artifacts between the feedback groups. For these reasons we collapsed the analysis across both feedback groups. The oscillatory signature of recovery was our target. A study with a larger number of participants than presented here could potentially uncover whether or not there are differences of the progression of alpha ERD throughout the training depending on if the patients received correct or sham feedback. Behavioral effects of the feedback group have already been investigated in the primary analysis (Ramos-Murguialday *et al.*, 2013). Moreover, for generalizing it is important to reduce variance in the data caused by noise. Previous work of our group clearly showed the adverse effects of artifacts on the analysis of EEG power where gamma band activity overshadowed activity in the lower bands and suggested ways to avoid or minimize their influence on BMI control and posterior analyses (López-Larraz *et al.*, 2018b). We ensured robustness of the results presented by way of employing the conservative fully automatic rejection procedure.

The longitudinal analysis of the desynchronization of beta oscillation does not allow concise interpretation because the model is not significant. An explanation could be that beta desynchronization is not upheld throughout the whole trial, as has been shown in a healthy population (Ramos-Murguialday and Birbaumer, 2015). There, significant beta desynchronization only occurred in the beginning of the movement period of the trials. In the present analysis the spectral activity was computed over the whole movement period of trials. Furthermore, we might not be able to capture the dynamics of beta oscillations in terms of linear modeling of desynchronization. More complex metrics such coherence might be more suited (Nicolo *et al.*, 2015). The longitudinal analysis of the individual SMR frequency band shows weaker fits of the model than the analysis of the α band. An explanation might be that this analysis included some patients that were rewarded for SMR desynchronization in the beta frequency range during the intervention (cf. table 2.3). In healthy populations significant power decreases during execution of a BMI task lasting several seconds have mainly been found in the alpha frequency range (Ramos-Murguialday and Birbaumer, 2015) and movement-related activity is known to spread across the whole alpha range (Pfurtscheller and Lopes da Silva, 1999). This result underlines the potential of alpha desynchronization as a biomarker as it explains the variance of the changes in the Fugl-Meyer scores better than the other frequency ranges.

Alpha ERD was also evaluated in the *pre* and *post* assessments of the trial. The patients performed repeated movement attempts of their paralyzed arm. We found no difference of alpha ERD between the *pre* and the *post* assessment and between groups (section 2.6.4). The fact that alpha ERD did not change from *pre* to *post* despite the behavioral changes could be attributed to the lack of proprioceptive feedback in the assessment and the difference in the task (one is controlling the hand open/close movements of an orthosis by way of modulation of their SMR and the other one is a natural attempt to open and close the hand). Since the patients only performed movement attempts and they did not use the exoskeleton that provided them with proprioceptive input (their hands were completely paralyzed) during the *pre* and *post* assessments, the sensorimotor activity differs, as this type of feedback influences the modulation of brain rhythms (Ramos-Murguialday and Birbaumer, 2015). Furthermore, the classifier used in the BMI rewarded differences from the inter-trial interval (considered as rest) and the task (attempt to move to down-regulate the SMR power and move the orthosis) SMR power using the last 15 seconds of data for both cases to create the two data distributions (more information can be found in the Supplementary information of the original trial (Ramos-Murguialday *et al.*, 2013)). Therefore, they could efficiently move the orthosis by either increasing power during inter trial interval, decreasing power during BMI task or both, to decrease variability of the distributions. This fact allowed each patient to choose their own strategy implicitly. These reasons and their initial ERD modulation ability make a general *pre-post* comparison of ERD values complicated without the use of a robotic orthosis. Probably a stratification of this comparison should be done, and unfortunately, the number of patients in the present work limits that comparison and does not allow drawing any conclusion. Due to these results, it might be difficult to generalize or use alpha as biomarker if the screening is not executed with a brain-controlled orthosis. This finding suggests investigation of alpha ERD in *pre-* and *post*-assessments of movement-attempts that include proprioceptive feedback in future trials, as passive movements modulate desynchronization (Ramos-Murguialday and Birbaumer, 2015). Inclusion of passive movements via orthoses could be a complementary measure for assessment of ERD with proprioceptive feedback (as has been already suggested using electrical stimulation, e.g. in Cho *et al.* (2011)) that would need to be tested in future trials.

Even smallest improvements on the Fugl-Meyer scale could mean a relevant behavioral change especially in these severely chronically paralyzed patients, in which no spontaneous behavioral improvements are expected. The FMA changes are particularly meaningful for modeling and they are preserved in the long-term (Ramos-Murguialday *et al.*, 2019). The test-retest reliability of the Fugl-Meyer test is very high (Platz *et al.*, 2005), but its sensitivity especially in severe patients might not be sufficient. Therefore, several measures were taken to ensure that the changes in the original study are adequately captured. Firstly, the assessors were blinded to group allocation to avoid a potential retest bias. If there had been a general repetition effect all patients should have improved, which is not the case. Secondly, the mean of both baseline Fugl-Meyer assessments was used to measure improvement (Whitall *et al.*, 2010). Statistical analy-

sis of the Fugl-Meyer values of arm and hand of the two baseline assessments for the present cohort showed that the distributions are not different (Wilcoxon signed-rank test: $p = 0.30$). This underlines that the test-retest reliability of the Fugl-Meyer assessment is high in our sample. Thirdly, the assessment focused only on the upper limb motor scores of arm and hand without coordination and speed, and without scores related to reflexes, further reducing variability (Crow and Harmeling-van der Wel, 2008). Further trials with longer treatment duration or refined methods should boost the behavioral effects to skills of functional relevance. To better understand our results, we repeated the statistical modeling for the arm and hand motor skills separately and observed significant models only for the arm part. This was expected, as most patients had larger motor improvement in the proximal part of the arm. This larger variability in the arm scores is explained by the progression of the ERD in the α band, confirming the results obtained with the combined arm and hand Fugl-Meyer scores. The hand scores alone could not be explained by the linear model, probably because of the lower variability of motor improvement scores (section 2.6.4). In this case, the large impairment of our patients (part of the inclusion criteria) and the low sensitivity and ordinal origin of the Fugl-Meyer scale limits our modeling. However, trials in acute or low-to-mild-to-severe patients, and/or longer and refined trials might also increase recovery of hand limb motor skills, which then might also be explainable by ERD progression.

Although cortical integrity is reflected in oscillations of the sensorimotor network measured by ERD, the cortical or subcortical location of the lesion was not a confounder of the modeling procedure (Park *et al.*, 2016; Ray *et al.*, 2017). Firstly, inclusion of the lesion location as factor did not affect the predictive power of the linear mixed models. A likelihood ratio test of a model comparison of a model with and a model without the factor lesion location did not show a significant difference ($\chi^2 = 4.25, p = 0.12$). Secondly, linear mixed models allow for individual variations of intercept and slope of the progression of the ERD. That is why the relative individual change of ERD throughout the training can be compared between patients with different lesion characteristics. Moreover, in the patients with mixed lesions (subcortical and cortical) damage of the precentral gyrus and the postcentral gyrus did not lead to differences in expression of alpha ERD during the *pre* measurement (section 2.6.7).

Linear mixed-effects models are suited for describing physiological data because they acknowledge individual deviations from the population mean and account for unequal number and unequal spacing of data points (Lang *et al.*, 2016). However, each model is a simplification of the data. Learning processes in Neurofeedback have also been described with much higher orders (Gunkelman and Johnstone, 2005). The model coefficients provide the best description of the data in a least squares sense and the linear mixed model including subject-specific slopes describes the data significantly better than a model not allowing deviation from the general slope. A likelihood ratio test of a model comparison shows a significant difference ($\chi^2 = 6.57, p = 0.038$). However, even with the flexibility that linear-mixed effects models allow, assuming linear progression of the ERD values could be an oversimplified description of the true time course. Moreover, the

two-staged linear modeling employed in the present work could introduce further simplification due to the second modeling step, which might blur the results. On the other hand, linear models allow for the description of the underlying processes with only a few parameters, which is an advantage for intuitive interpretation and quantitative comparison of the models and necessary for the two-stage analysis employed here.
Four patients of the control group showed a decline of their motor function regardless of the dynamics of their ERD throughout the intervention (four squares below the zero line in fig. 2.4). It has been suggested that the contingency of brain-activity and visuo-proprioceptive feedback is key to cortical reorganization and recovery (Ramos-Murguialday *et al.*, 2013). Non-contingent feedback interfered with learning and thus could worsen motor impairment (e.g. reinforcing maladaptive synergies), which could happen with open-loop control of body actuators (e.g. robotics and electromagnetic stimulation) or during physiotherapy.
The present results in severe chronic stroke indicate that EEG oscillatory activity can predict recovery of these patients and links its progression to functional motor recovery, and therefore mark it as a promising biotarget for rehabilitation interventions. In heterogeneous conditions such as stroke, biomarkers could play an important role in informing treatment pathways (informed patients stratification). Mane et al have recently shown that the predictive power of EEG-based markers may be specific to the intervention methodology (Mane *et al.*, 2019). Studies of oscillatory brain activity during motor imagery and movement of the paretic hand of moderately to severely affected chronic stroke patients (Kaiser *et al.*, 2012) as well as subacute patients of mild to moderate (Platz *et al.*, 2002) and severe impairment (Pichiorri *et al.*, 2015) support our findings suggesting that the level of impairment is negatively correlated to the desynchronization of alpha oscillations on the ipsilesional hemisphere. Moreover, an increase of ipsilesional ERD was observed after spontaneous recovery in acute stroke (Tangwiriyasakul *et al.*, 2014) with concomitant lack of ERD on the healthy hemisphere, which indicates our results might generalize those of acute and sub-acute stroke patients. The sensorimotor ERD magnitude has also been shown to correlate with recovery in spinal cord patients (López-Larraz *et al.*, 2015), supporting the validity of this metric as a viable and easily obtainable biomarker of clinical progress in patients suffering from motor impairments and as a measure of brain plasticity (Takemi *et al.*, 2015). Moreover, the presence of alpha oscillations at cortical sites of the sensorimotor systems reflects the intact balance of thalamic circuits, particularly reticular thalamic recurrent inhibition of thalamocortical afferents (Steriade *et al.*, 1990). Lack of these oscillations in relaxed wakefulness and sleep thus does not allow the excitatory blockade of inhibitory reticular-thalamic and centro-thalamic circuits at the ipsilesional thalamo-cortical system. Reappearance of the delicate excitatory-inhibitory balance in the thalamocortical circuits after stroke in the course of a learning process directly targeting this oscillatory mechanism, clearly supports the neurophsyiosological logic of Brain-Machine interface strategies (Birbaumer and Cohen, 2007; Birbaumer *et al.*, 1990).

It is important to emphasize that models as the one presented here only show corre-

Lesion type	Sex	Age (years)	Time since stroke (months)	Lesion side	cFMA score
LM	8M/5F	53.7±13.2	58.4±50.5	9R/4L	11.2±7.8
LS	10M/7F	53.7±11.2	73.1±65.6	8R/9L	12.9±9.7

Table 2.2: Patient demographics for the patients investigated in the study on ERD and lesion location

lations to outcome variables, which do not allow causal inference. However, our results constitute a building block of more generalizable statistical models of the process of motor recovery in chronic stroke. As pointed out in the synopsis, quantitative statistical comparison of performance of different markers and different combinations and sequences of markers employing more data could eventually yield the optimal procedure and best outcome for the individual patient.

2.5 Lesion location

Previous works have shown that location and volume of the lesion might be indicators of function after stroke. ERD magnitude has been shown to be lower in stroke patients as compared to healthy individuals (Tangwiriyasakul *et al.*, 2014; Park *et al.*, 2016). These differences in brain oscillations can also be observed in stroke patients suffering from moderate or mild paralysis presenting different grades lesions severity (Park *et al.*, 2016).

EEG recordings of 30 patients undergoing the BMI training described above (Dataset 1, section 1.3.1) were preprocessed. Only the data of the first training session was considered here, as no between-group effects of the training were expected on the first day of the intervention. The artifact rejection did not lead to exclusion of any subject (as data only from one session was considered).

The Event-related desynchronization was computed as in equation (2.1) in the alpha and beta frequency range.

The patients were stratified into two groups depending on lesion location: patients with lesions involving the primary motor cortex and the primary sensorimotor cortex were assigned to group LM (n=13) and the rest to group LS (n=17) (table 2.2). For the statistical evaluations non-parametric tests were used. As the samples were independent a Wilcoxon rank-sum test was used for the comparison between the two groups to assess the mean difference in ERD values between them using a significance level of 0.05. The effect size was computed using the rank-biserial correlation (Wendt, 1972).

2.5.1 Results

The mean±SD of the alpha-ERD values of the patients suffering from a lesion that extends to the primary motor cortex (LM) was -17.0 ± 22.6. For the other patients (LS), the values were lower on average with mean±SD of -32.9 ± 18.4. When performing the Wilcoxon rank-sum test, which resulted in $U = 155$ and $p = 0.065$, we did not find enough evidence to conclude that the observed difference of the ERD values in the alpha range is statistically significant. The effect size, of $r = 0.40$, however, is moderate. Those patients suffering from a lesion that extends to the primary motor cortex (LM) tendentially show a lower activation on average (i.e. less negative ERD magnitude) than the patients that do not have their primary motor cortex affected (LS) (fig. 2.9a). The mean±SD of the beta-ERD values was -15.6 ± 16.0 for group LM and -25.4 ± 17.6 for the patients whose primary motor cortex was not affected (LS). The same type of statistical test was applied to the ERD values of the β band of the two groups. It did not show a statistically significant difference with $U = 148$ and $p = 0.1227$. The effect size, however, was moderate with $r = 0.34$. We thus conclude that at least a similar tendency of lower average activation (i.e. less negative ERD magnitude) in the β band can be observed for patients with inclusion of the motor cortex (fig. 2.9b).

2.5.2 Discussion

There were no significant differences of the ERD magnitude of the two groups of patients. The results only show a tendency towards ERD as a measure of relative EEG power being less pronounced if the motor cortex is affected by the lesion but production of ERD is not generally impeded.

It has long been known that ERD is an electrophysiological correlate of ongoing cortical processing of sensory information and generation of motor behavior (Niedermeyer and Lopes da Silva, 2005). Patients with motor deficit due to stroke exhibit less pronounced ERD as compared to healthy controls (Tangwiriyasakul *et al.*, 2014; Park *et al.*, 2016). Motor output and control of movements of these patients are reduced. Their limb strength and their ability to control and direct movements of the paralyzed limb are lower than in a healthy population (Broetz *et al.*, 2014). Lesion volume and location, on the other hand, have shown to be correlated with behavioral outcome in imaging studies (Lindenberg *et al.*, 2010; Pineiro *et al.*, 2000). Our findings point in the direction of closing the argumentational loop: inclusion of the primary motor cortex in the lesion might also be correlated with less pronounced ERD. As ERD of the α band potentially represents a biomarker of the excitability of cortical and spinal levels (Takemi *et al.*, 2015; López-Larraz *et al.*, 2015), less ERD due to involvement of the primary motor cortex in the lesion could imply impeded progress in a rehabilitation scenario.

The results show a certain degree of heterogeneity of ERD generation between patients that might depend on the location of the lesion, i.e. the inclusion of the sensorimotor cortex in the lesion, among other factors. For this reason, they support the idea of designing

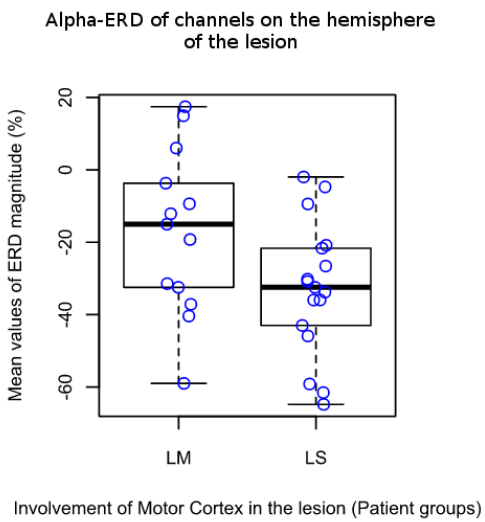

(a) Boxplot showing how the values of the alpha-ERD magnitude differ between the two groups of lesion locations. Those patients suffering from an involvement of the motor cortex show less negative alpha-ERD magnitude on average than those patients whose motor cortex is not touched by the lesion. The mean values of the alpha-ERD magnitude of each patient are overlayed as blue circles. They are randomly jittered around the vertical center of the boxes to increase clarity. The difference is not statistically significant, when employing a Wilcoxon rank-sum test.

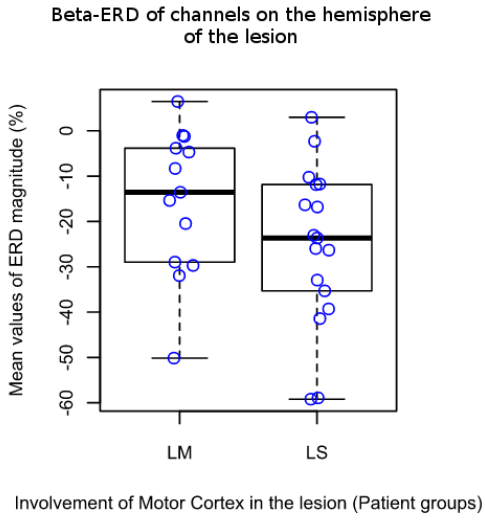

(b) Boxplot showing how the values of the beta-ERD magnitude differ between the two groups of lesion locations. Those patients suffering from an involvement of the motor cortex show slightly less negative beta-ERD magnitude on average than those patients whose motor cortex is not touched by the lesion. The mean values of the beta-ERD magnitude of each patient are overlayed as blue circles. They are randomly jittered around the vertical center of the boxes to increase clarity. The difference is not statistically significant, when employing a Wilcoxon rank-sum test.

Figure 2.9: Distributions of ERD values in the two groups in the two frequency bands under investigation.

intervention schemes that are better tuned to the individual characteristic of the stroke of the patient, which could increase efficiency of the rehabilitation intervention. SMR-based classifiers driving a rehabilitation robot could be adjusted to the less pronounced ERD signals of patients showing lesions that extend to the motor cortex, e.g. by increasing the sensitivity and thus allowing more subtle changes in the signal to produce larger effects in the control of the robot.

2.6 Materials

This section presents auxiliary information for the analyses presented in this chapter.

2.6.1 Rejection procedure

In the following supporting information on the rejection procedure during preprocessing of the data analyzed in this chapter is presented.

Figures 2.10 to 2.13 show the number of trials that were removed from each training session of each patient and the percentage of trials remaining.

2.6.2 Descriptive statistics on rejection

The following figures show descriptive statistics on the number of rejected trials. Figure 2.14a shows the distribution of the total number of trials. Figure 2.14b shows the distribution of the total number of rejected trials. Figure 2.15 shows the distribution of the percentage of trials remaining per session.

2.6.3 Descriptive statistics on reasons for rejection

The following figures show descriptive statistics on the number of rejected trials. Figure 2.16 shows the distribution of the total number of trials showing EEG artifacts. Figure 2.17a shows the distribution of the total number of trials showing ipsilateral EMG artifacts and figure 2.17b shows the distribution of the total number of trials showing ipsilateral or bilateral EMG artifacts.

2.6.4 *Pre* and *post* comparison of primary outcome measures with the new cohort

In this section *pre* and *post* comparisons of the primary outcome measures are shown for completeness. Only the 23 subjects used in the main analysis were considered.

Figure 2.18 shows the comparison of mean event-related desynchronization (ERD) during the *pre* measurement and the *post* measurement. At these two time points subjects were seated and they performed cued opening attempts of the paretic hand and resting

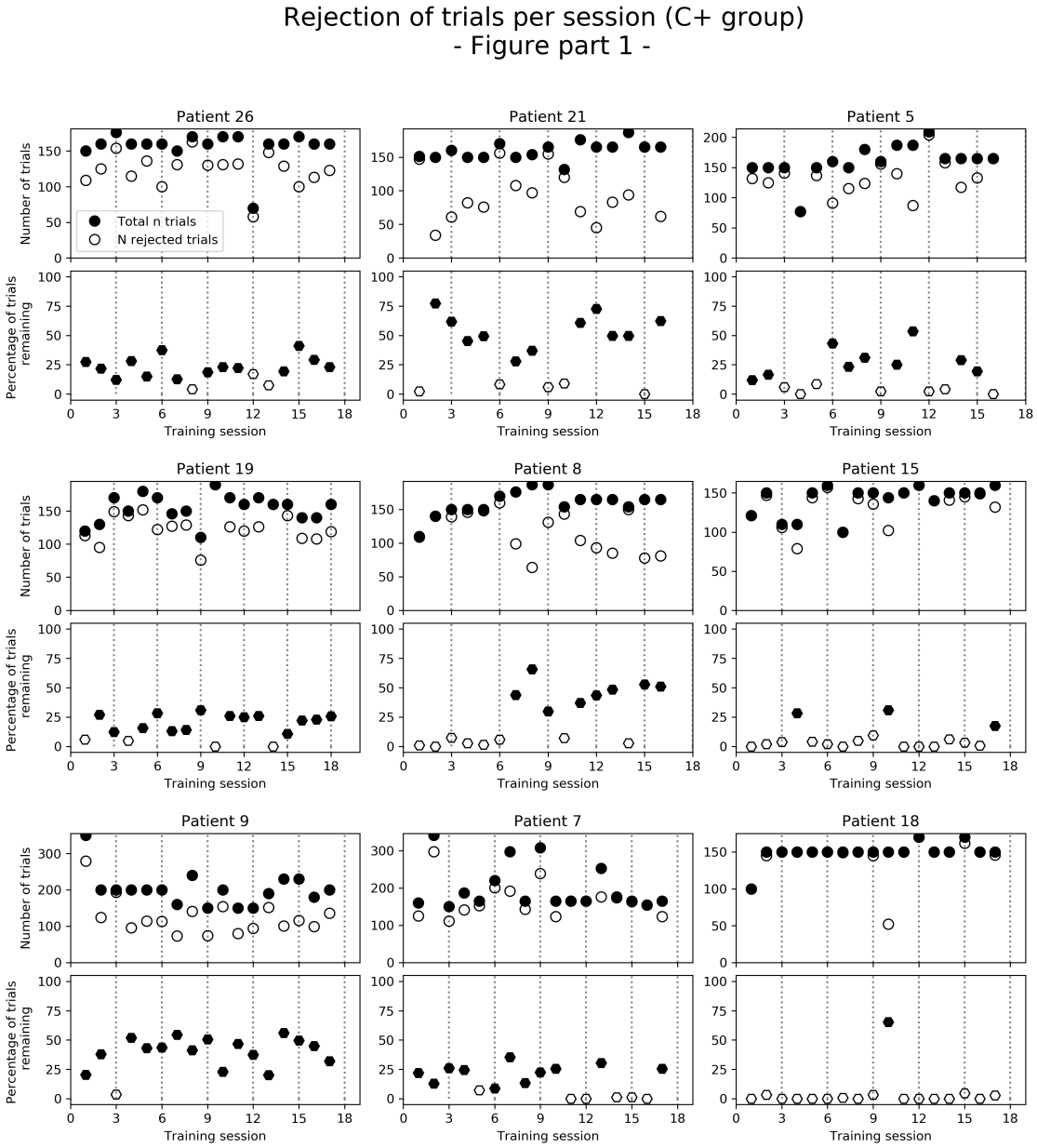

Figure 2.10: The number of trials that have been removed in each training session for each patient (contingent positive feedback group). The subplots on the top show the total number of trials (full circles) and the number of trials rejected (empty circles) per session. The bottom subplots show the percentage of trials remaining after the rejection procedure. The globally defined minimum number of trials necessary for a session to remain in the analysis is 15. The sessions having less than 15 ”good” trials remaining have been rejected. Rejection is indicated by empty hexagons. The percentage threshold for trial rejection varies between sessions because of the total number of trials varies per session.

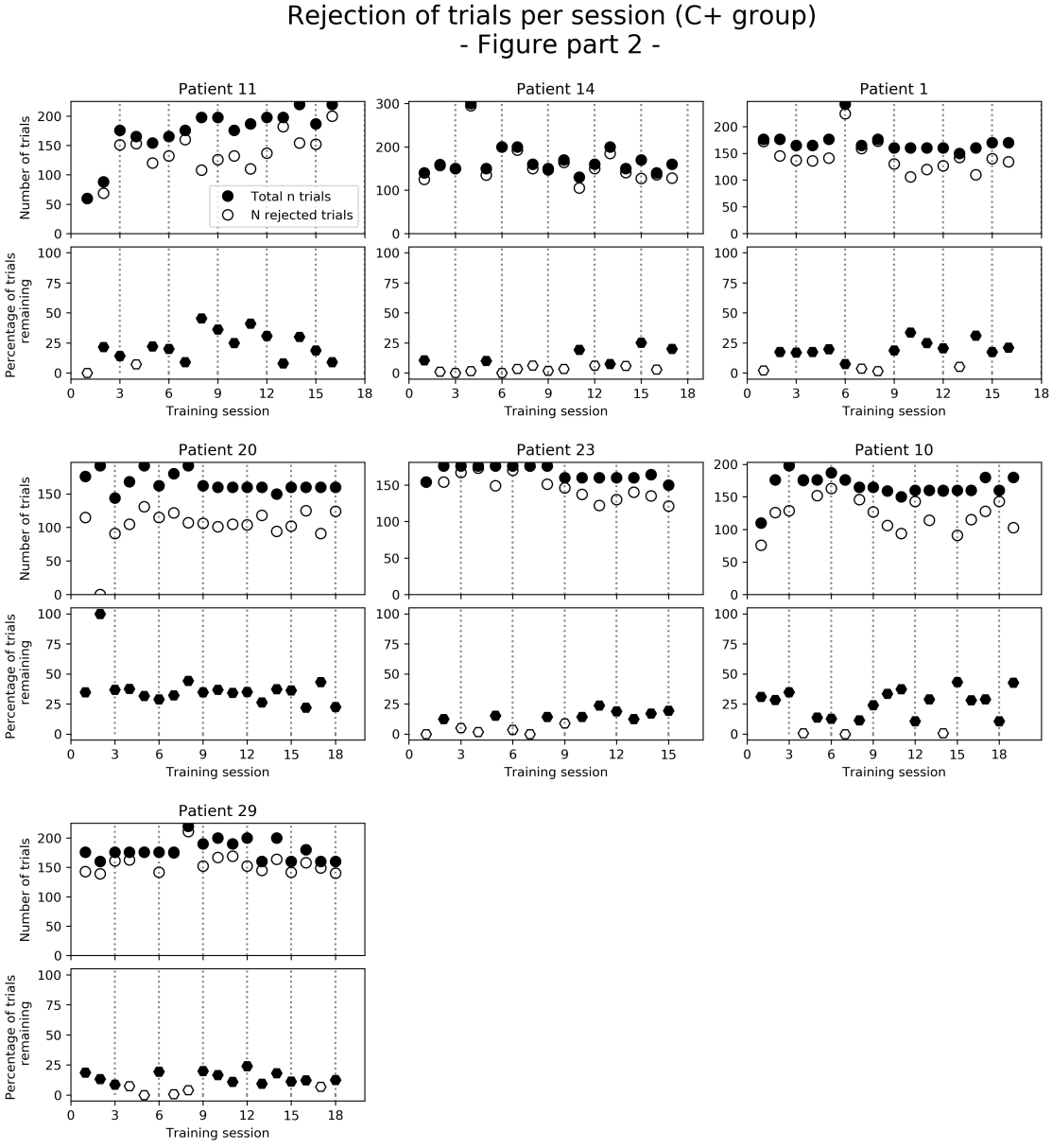

Figure 2.11: (continued)

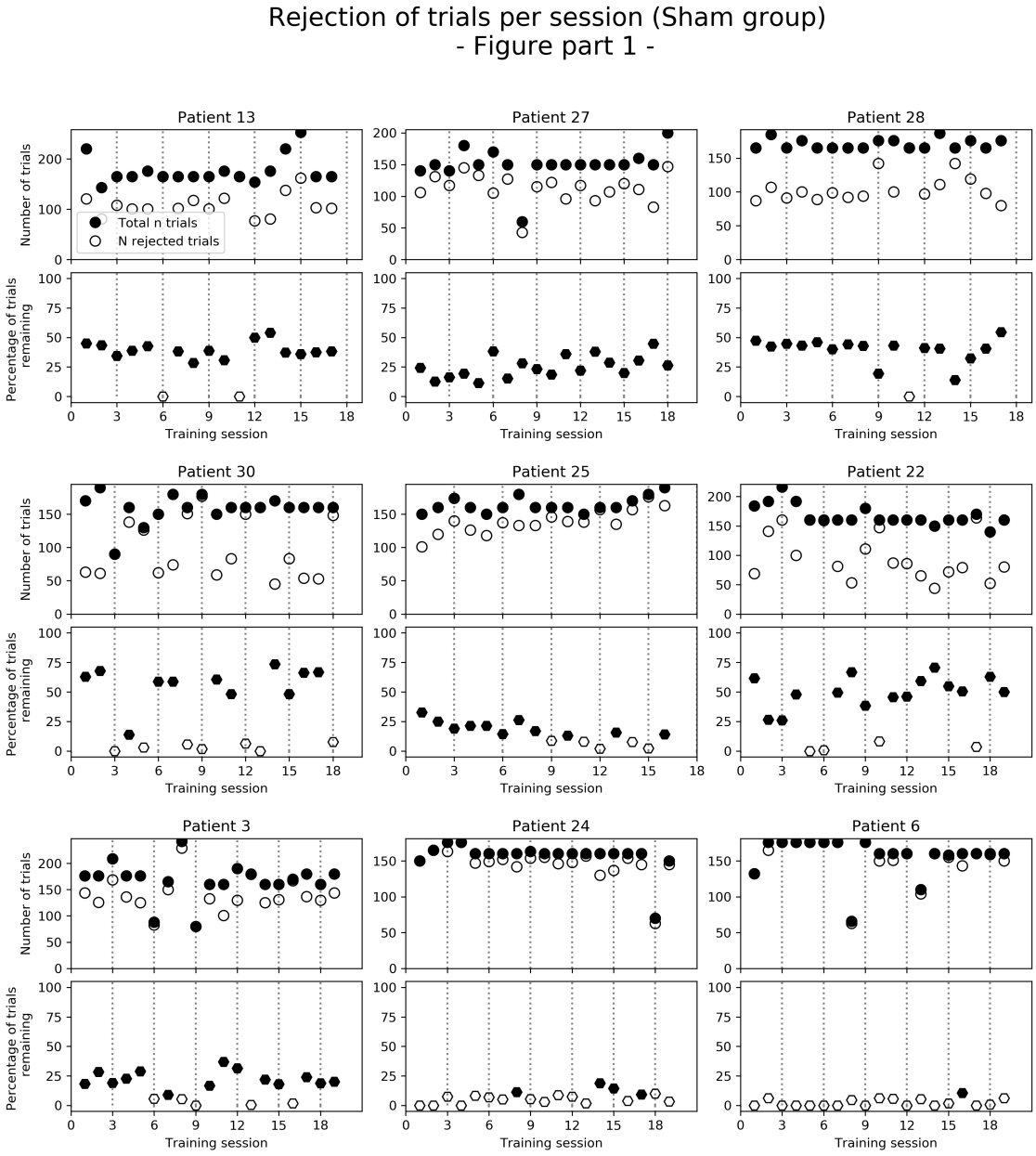

Figure 2.12: The figure shows the number of trials that have been removed in each training session for each patient (Sham feedback group). The subplots on the top show the total number of trials (full circles) and the number of trials rejected (empty circles) per session. The bottom subplots show the percentage of trials remaining after the rejection procedure. The globally defined minimum number of trials necessary for a session to remain in the analysis is 15. The sessions having less than 15 ”good” trials remaining have been rejected. Rejection is indicated by empty hexagons. The percentage threshold for trial rejection varies between sessions because of the total number of trials varies per session.

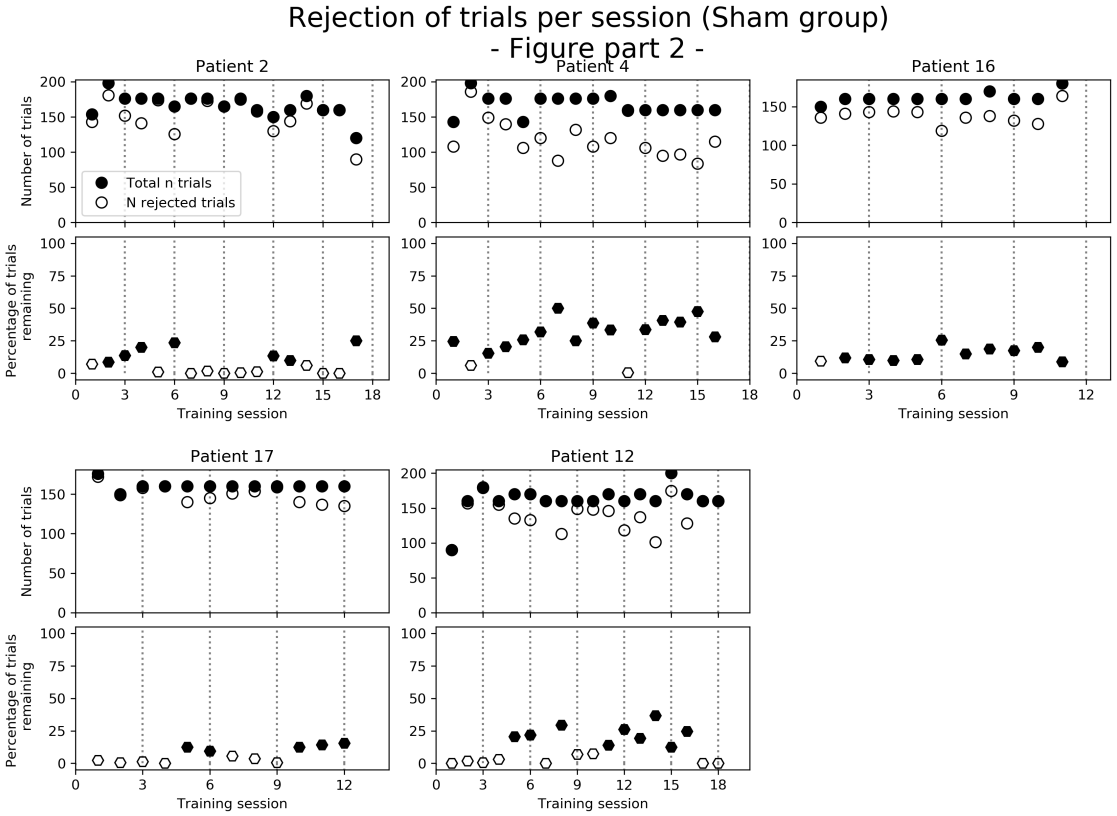

Figure 2.13: (continued)

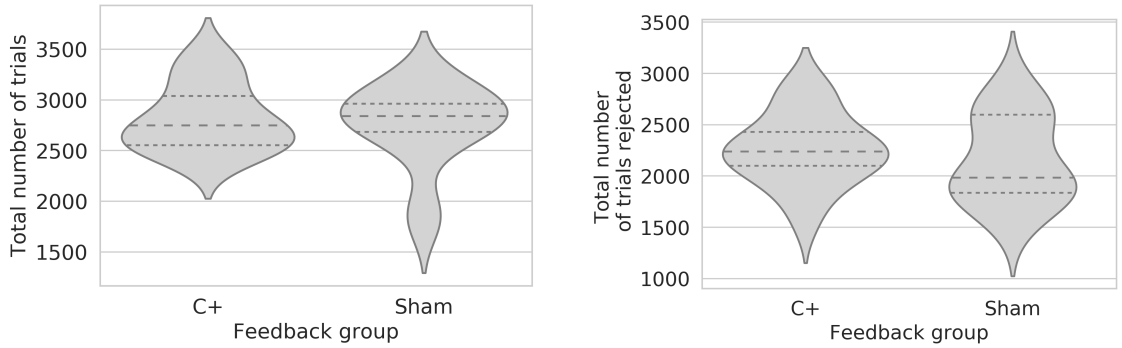

(a) The violin plot displays median and first and third quartile of the data and a density estimation of the distributions of the data. There is no difference between the groups in the total number of trials. There are two Sham patients who had only 11 sessions in total which explains the bottom tail of the plot on the right.

(b) The violin plot displays median and first and third quartile of the data and a density estimation of the distributions of the number of rejected trials of both groups.

Figure 2.14: Distributions of trials and rejected trials per group.

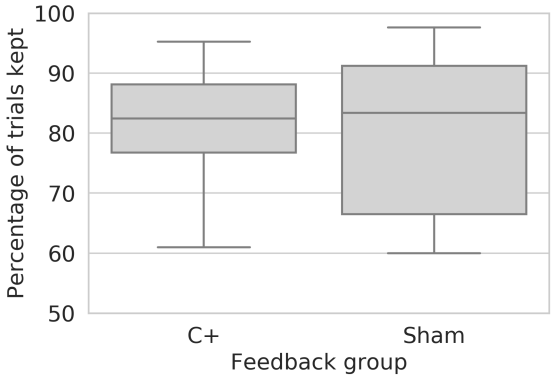

Figure 2.15: The box plot indicates that there is no difference in the percentage of trials remaining per session after preprocessing between the feedback groups. This is confirmed by the result of a t-test: $t = -1.19, p = 0.84$.

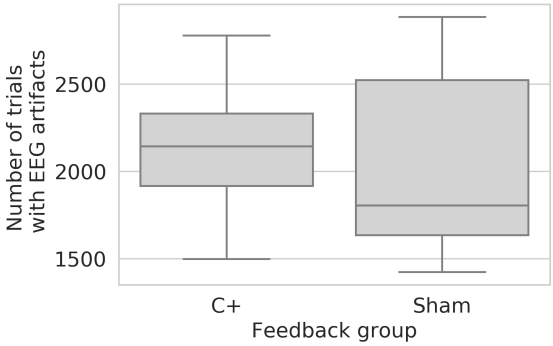

Figure 2.16: The box plot shows the distribution of the total number of trials per subject with artifacts in the EEG. A t-test does not show a difference between groups: $t = -1.79, p = 0.44$.

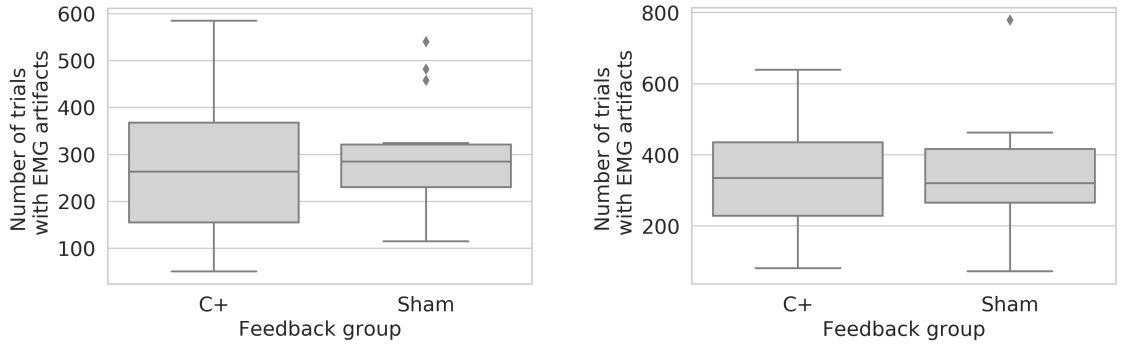

(a) The box plot shows the distribution of the total number of trials removed per subject with artifacts caused by movements of the unaffacted arm during movement attempts of the paralyzed arm. There is no difference between groups.

(b) The box plot shows the distribution of the total number of trials per subject with artifacts caused by movements of any arm during the rest period. There is no difference between groups.

Figure 2.17: Distribution of trials rejected because of EMG artifacts.

in randomized order. Data acquisition and processing was the same as for the main analysis. However, there was no minimum number of trials remaining after the analysis and no subject was removed. In an additional preprocessing step ERD values below -100 and above 100 were considered artifacts and were discarded (mean±sd 3.6 ± 2.6 trials per subject contained such values).

Figure 2.19 shows the comparison of the difference of the modified Fugl-Meyer assessment scores from *pre* to *post* stratified by feedback group. A t-test reveals a trend towards a difference between groups ($t = 2.05, p = 0.057$).

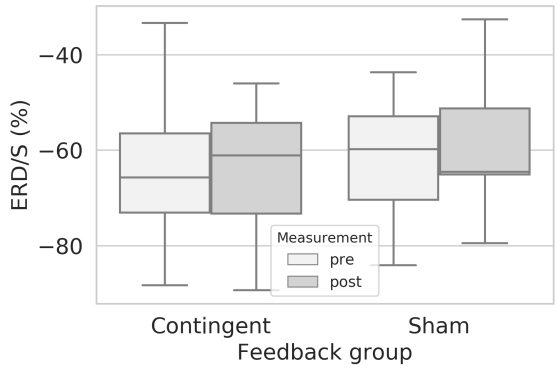

Figure 2.18: Comparison of alpha ERD values of patients in the two feedback groups during *pre* and *post* assessments

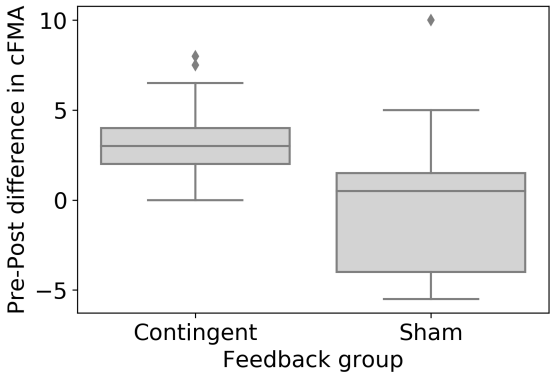

Figure 2.19: Comparison of the difference of the modified Fugl-Meyer assessment scores from pre to post by feedback group

2.6.5 Progression of desynchronization in other frequency ranges than alpha

In the following the main analysis is repeated on data of the β and the individual μ frequency band.

Beta frequency range

The linear model for the ERD in the beta frequency range (11 - 25 Hz) was constructed in the same way as the model of the ERD in the alpha frequency range presented above. ΔcFMA is predicted by the coefficients extracted from the corresponding linear mixed effects model: the progression of the ERD throughout the intervention sessions and the initial ERD magnitude. An interaction term was included in the LM to investigate if the initial ERD correlated with the progression of the oscillatory activity. The F-test of the regression equation was not significant and the fit of the model was very low: $F(3,18) = 1.23$, $p = 0.3278$ and an adjusted $r^2 = 0.032$. Figure 2.20 shows the linear model predicting the improvement of motor function (ΔcFMA) on the hemisphere of the lesion.

μ frequency range

The linear model for the ERD in the individual SMR frequency range (μ) was constructed in the same way as the model of the ERD in the alpha frequency range presented above. ΔcFMA is predicted by the coefficients extracted from the corresponding linear mixed effects model: the progression of the ERD throughout the intervention sessions and the initial ERD magnitude. An interaction term was included in the LM to investigate if the initial ERD correlated with the progression of the oscillatory activity (fig. 2.21). Table 2.3 shows the frequency range selected for each subject for control of the

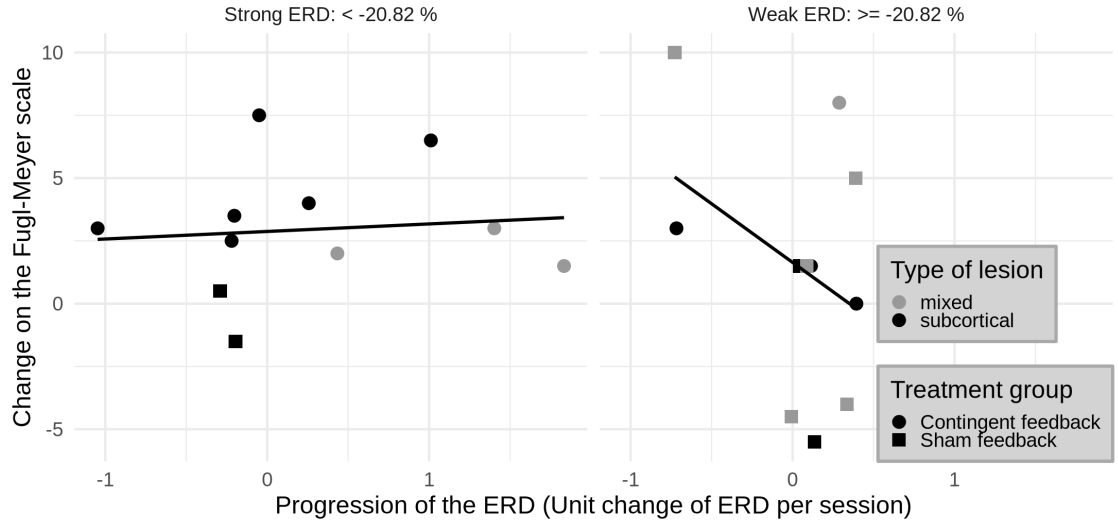

Figure 2.20: Linear model predicting the improvement of motor function (ΔcFMA) by the initial ERD and the progression of the ERD of the beta frequency range on the ipsilesional hemisphere over sessions. For improved visualization of the effects of both explanatory variables in the model the patients are separated into two cross-sections showing relatively strong initial ERD (left panel) and a second group showing relatively weak initial ERD (panel on the right). The F-test of the regression equation was not significant.

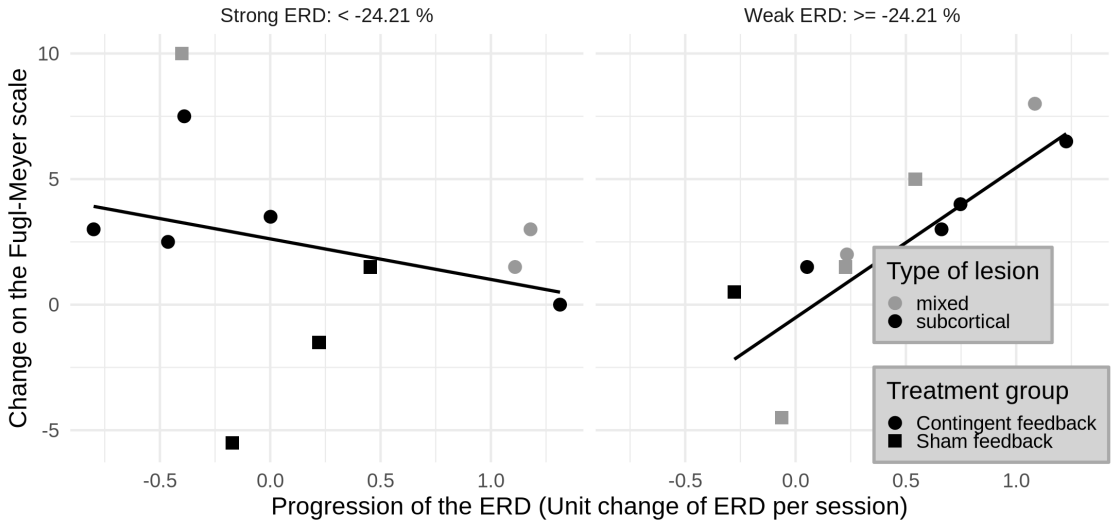

Figure 2.21: Linear model predicting the improvement of motor function (ΔcFMA) by the initial ERD and the progression of the ERD of the individual SMR frequency range on the ipsilesional hemisphere over sessions. For improved visualization of the effects of both explanatory variables in the model the patients are separated into two cross-sections showing relatively strong initial ERD (left panel) and a second group showing relatively weak initial ERD (panel on the right).

exoskeleton. The F-test of the regression equation was significant: $F(3,18) = 3.475$, $p = 0.038$ and an adjusted $r^2 = 0.26$.

The analysis of the interhemispheric asymmetry in the SMR frequency investigated if the progressive laterality coefficient predicts the clinical change ΔcFMA (fig. 2.22). The F-test for this linear regression equation was not significant but revealed a trend. However, the fit of the equation is low. $F(1,20) = 3.76$, $p = 0.067$ and an adjusted $r^2 = 0.1161$.

2.6.6 Progression of desynchronization of alpha oscillations with breakdown of FMA scores

Breakdown of the Fugl-Meyer assessment

The Fugl-Meyer Assessment evaluates impairments in sensorimotor function. Here, the scale was modified to exclude coordination, reflexes and speed. These measures introduce variability since the patients could not actively extend their fingers (Ramos-Murguialday *et al.*, 2013).

The evaluation took into account the motor skills of upper arm and forearm. 15 items were tested with a maximum score of 30 points. Furthermore, the motor skills of hand

Subject ID	Frequency range of the individual μ
1	5.5 - 8.5 Hz
2	8.5 - 11.5 Hz
3	14.5 - 17.5 Hz
4	8.5 - 11.5 Hz
6	11.5 - 14.5 Hz
7	14.5 - 17.5 Hz
8	5.5 - 8.5 Hz
9	5.5 - 8.5 Hz
10	8.5 - 11.5 Hz
12	23.5 - 26.5 Hz
15	8.5 - 11.5 Hz
18	8.5 - 11.5 Hz
19	5.5 - 8.5 Hz
20	8.5 - 11.5 Hz
21	8.5 - 11.5 Hz
22	17.5 - 20.5 Hz
24	8.5 - 11.5 Hz
25	8.5 - 11.5 Hz
26	5.5 - 8.5 Hz
27	8.5 - 11.5 Hz
28	5.5 - 8.5 Hz
29	8.5 - 11.5 Hz
Average	**9.6 $\pm$ 4.8 Hz**

Table 2.3: Frequency ranges of the individual SMR

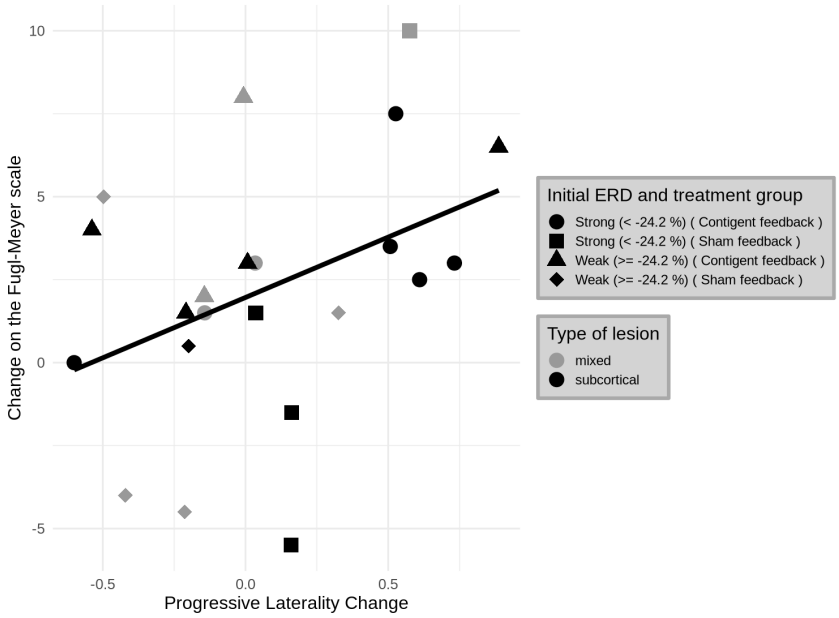

Figure 2.22: Relationship between improvement and interhemispheric difference of changes of the ERD in the individual SMR-band. Values on the x-axis express the difference between the progression of the ERD on the healthy hemisphere and the ipsilesional side. Positive values on this axis indicate that throughout the training patients exhibited stronger ipsilesional ERD, negative values indicate a stronger ERD on the healthy hemisphere. The regression indicates that the larger a difference towards the hemisphere of the lesion is found the better the motor improvement.

and fingers were tested comprising 12 items with a maximum score of 24 points. The total maximum score was 54 points.

The movements of the arm test The following 15 movements were assessed:

- Movements 1 ot 6: Synergies of the flexors („touch the ipsilateral ear“):
  - elevation
  - shoulder retraction, abduction, external rotation
  - forearm supination
- Movements 7 to 9: Synergies of the extensors (”touch the contralateral knee“):
  - shoulder adduction, internal rotation
  - elbow extension
  - forearm pronation
- Movement 10: „Move the hand to lumbar spine“
- Movement 11: Shoulder flexion 0-90°
- Movement 12. Pro/supination while elbow is in flexion
- Movement 13: Shoulder abduction 0-90°
- Movement 14: Shoulder flexion 90-180°
- Movement 15: Pro/supination while elbow is in extension

The movements of the hand test The following twelve movements were assessed:

- Movement 1: Stabilitby of the wrist in 15° extension while elbow is at 90°
- Movement 2: Stability of the wrist in flexion and extension while elbow is at 90°
- Movement 3: Stability of the wrist in 15° extension while elbow is at 0°
- Movement 4: Flexion/extension of the wrist while elbow is at 0°
- Movement 5: Circumduction of the wrist
- Movement 6: Flexion of the fingers
- Movement 7: Extension of the fingers
- Movement 8: Grasping against resistance with metacarpophalangeal joints of digit two and flexion of the proximal interphalangeal joints

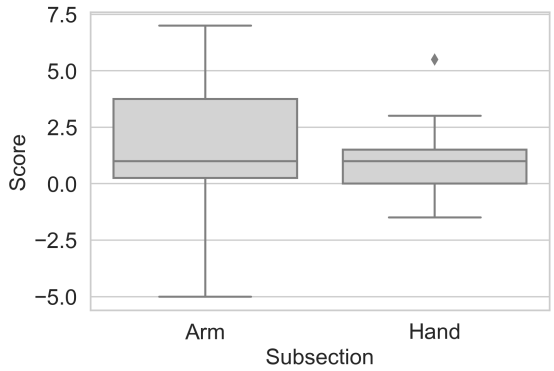

Figure 2.23: Distribution of the changes of the scores of the FMA from *pre* to *post* separated into arm and hand subsections

- Movement 9: Grasping of a scrap of paper
- Movement 10: Grasping of a pencil
- Movement 11: Grasping of a cylinder
- Movement 12: Grasping of a tennis ball

Improvement in arm and hand The figure shows that the range of improved points on the arm subscore of the Fugl-Meyer assessment is greater than that of the hand subscore (fig. 2.23).

Statistical modeling

The statistical modeling analysis described above was repeated with a breakdown of the Fugl-Meyer assessment into arm subscores and hand subscores.

The linear models for the ERD in the alpha frequency predicted the change in the arm scores of the Fugl-Meyer assessment (ΔFMA_{arm}, fig. 2.24) but not for the hand scores (ΔFMA_{hand}, fig. 2.25). For the arm scores the F-test of the regression equation was significant: $F(3,18) = 5.15$, $p = 0.0096$ and an adjusted $r^2 = 0.37$. The F-test of the regression equation of the hand scores was not significant: $F(3,18) = 0.59$, $p = 0.6293$ and an adjusted $r^2 = -0.06$.

Linear models predicting both FMA subscores from the contralesional hemisphere were constructed. Only the F-test for the regression of the arm subscores for those subjects with relatively weak initial ERD was significant: $F(0,9) = 6.4$, $p = 0.032$ and an adjusted $r^2 = 0.35$ (fig. 2.26).

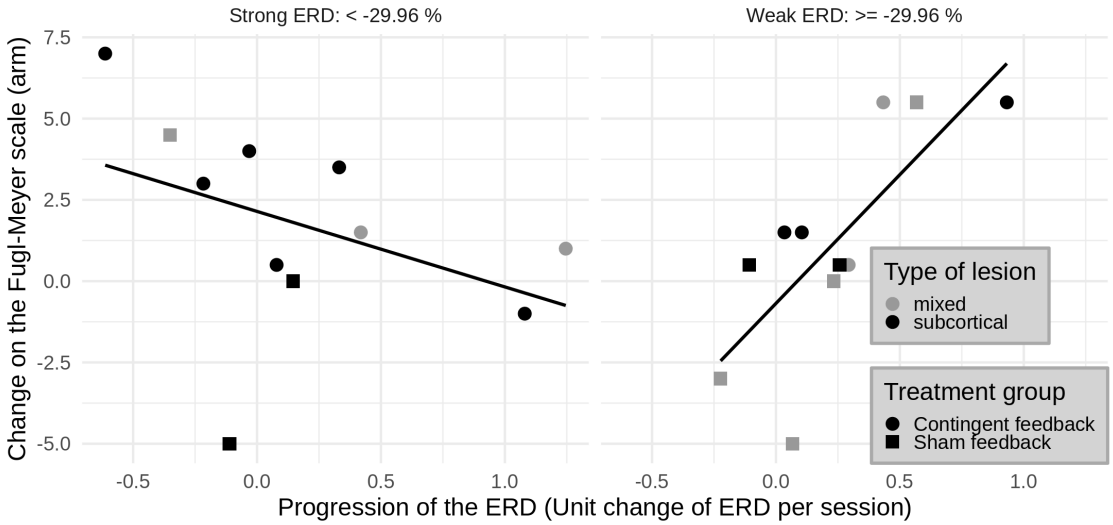

Figure 2.24: Linear model predicting the improvement of motor function (ΔFMA_{arm}) by the initial ERD and the progression of the ERD of the alpha frequency range on the ipsilesional hemisphere over sessions. For improved visualization of the effects of both explanatory variables in the model the patients are separated into two cross-sections showing relatively strong ERD (left panel) and a second group showing relatively weak initial ERD (panel on the right).

2.6.7 Lesion characteristics: Involvement of the pre/postcentral gyrus

The precentral and the postcentral gyrus are the locations of the primary motor cortex and the primary somatosensory cortex. Previous works showed that cortical integrity is reflected in oscillations of the sensorimotor network measured by ERD if stroke patients with damaged cortex are compared to patients with subcortical lesions (Park *et al.* (2016) and section 2.5).

Of those subjects who had cortical involvement of the stroke there were eight with and one without involvement of the precentral gyrus. The same numbers apply to the subjects regarding the postcentral gyrus. There were seven subjects who had both gyri affected and only two who did not (fig. 2.27).

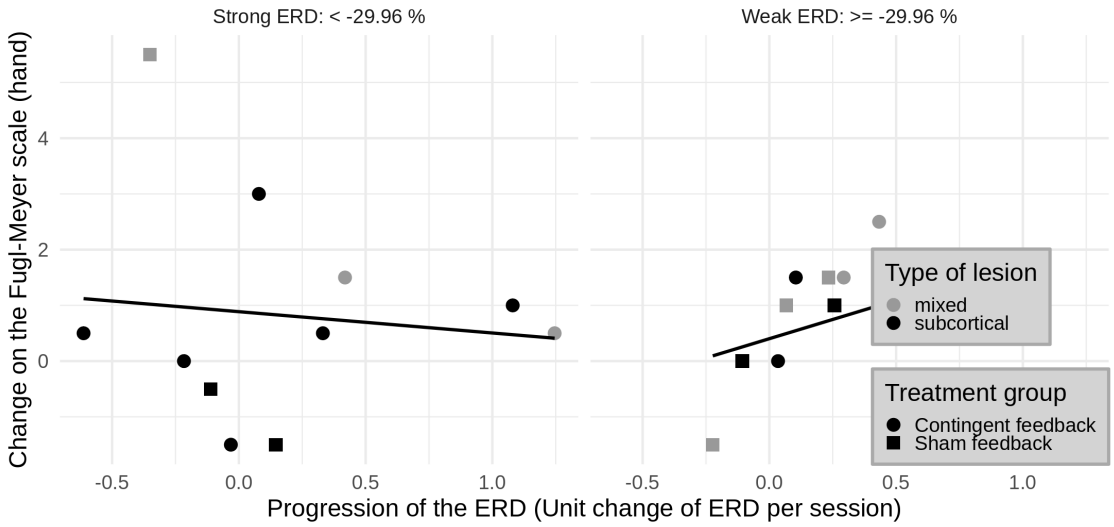

Figure 2.25: Linear model predicting the improvement of motor function (ΔFMA_{hand}) by the initial ERD and the progression of the ERD of the alpha frequency range on the ipsilesional hemisphere over sessions. For improved visualization of the effects of both explanatory variables in the model the patients are separated into two cross-sections showing relatively strong ERD (left panel) and a second group showing relatively weak initial ERD (panel on the right).

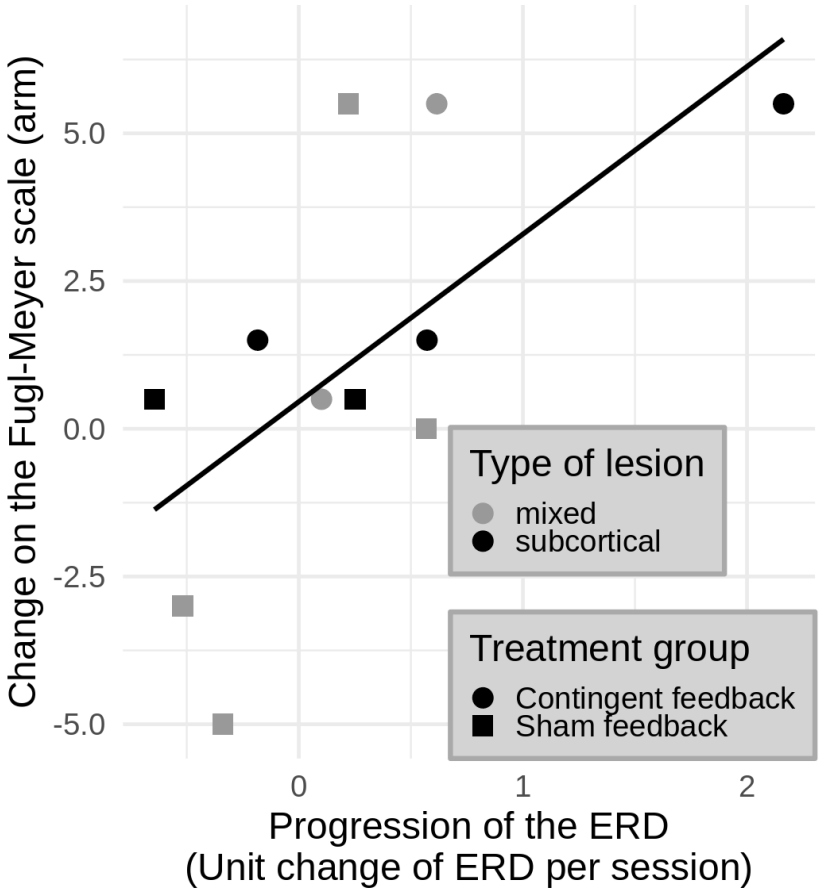

Figure 2.26: Linear model predicting the improvement of motor function (ΔFMA_{arm}) by the progression of the ERD of the alpha frequency range on the healthy hemisphere over all sessions for the patients showing relatively weak initial ERD on the ipsilesional hemisphere. Better recovery was achieved when the ERD on the healthy hemisphere decreased in the course of the training.

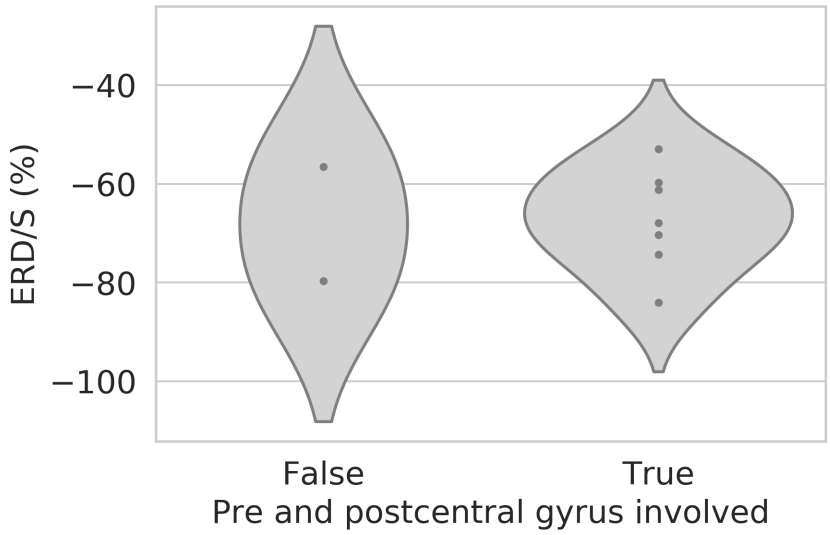

Figure 2.27: There is no difference of the alpha-ERD over the lesion between those subjects with cortical involvement in which the pre/postcentral gyrus is affected by the lesion and those in which it is not. Please note, however, that there are only two subjects in the left distribution.

Chapter 3

Sensorimotor oscillations in severe chronic stroke

3.1 Introduction

Stroke causes focal perturbations in brain function that influence local properties of sensorimotor oscillations (SMR). This rhythm oscillates in the alpha frequency range of the EEG and has the largest amplitude over central-parietal brain regions during resting. SMR is extensively used in studies on movement-related Brain-Machine interfaces. Moreover, it was shown to be a measure of cortical excitability (Takemi *et al.*, 2015).

In acute stroke power and ability to modulate the rhythm are reduced but increase over time (Tangwiriyasakul *et al.*, 2014). Similarly, modulation of the SMR power is related with motor recovery in chronic stroke and location and extent of the lesion influence SMR power, as was shown in chapter 2 and Ray *et al.* (2020, 2017); Wijngaarden *et al.* (2016). Not only is the power of the rhythm reduced, but the frequency of the oscillations in the alpha range of the EEG are slowed in acute stroke as compared to a healthy population (Wijngaarden *et al.*, 2016). The oscillations are generated in a loop connecting cortex and thalamic structures (Steriade *et al.*, 1990). The interactions between the involved structures are complex. Any disturbance within this system leads to a disturbance of the oscillations visible on the cortex (Hughes and Crunelli, 2005). During wakefulness thalamic relay cells usually fire every 100 ms (10 Hz). If feedback from the cortex is reduced, the hyperpolarized relay cells are less likely to fire because of inhibition from the reticular thalamic nucleus (Jones, 2002). This leads to slower re-occurring signals from the thalamus to the cortex.

Slowing of SMR oscillations has been reported in stroke patients in the acute phase (Dubovik *et al.*, 2012; Wijngaarden *et al.*, 2016). These findings indicate that assumptions on peak center frequency and power derived from healthy populations are not directly transferable to stroke patients, especially not to those with severe paresis and in the chronic state. Their cortico-thalamic-spinal networks are anatomically and functionally compromised and stabilized after a long period of time. Moreover, it is unclear how SMR changes are affecting interhemispheric networks.

Current approaches to effective treatment of chronic stroke encompass intensive neu-

rorehabilitation approaches (Ward *et al.*, 2019) and approaches exploiting different properties of oscillations related to motor activity, like Brain-Machine interfaces (BCI) (Ramos-Murguialday *et al.*, 2013) or closed-loop brain stimulation (Ziemann *et al.*, 2018).

In order to uncover some of the remaining unclarity of the characteristics of SMR in chronic stroke, we present an investigation of peak center frequency and power of the sensorimotor oscillations in a large cohort of chronically and severely impaired stroke patients (n = 41) and compare them to a younger group of healthy volunteers. Furthermore, we extend the analysis to a comparison of these properties to the effects of a BCI-based intervention. We employ a fully automatic, deterministic methodology for extracting these parameters of the SMR from electroencephalographic (EEG) resting-state data.

3.2 Methods

This study pooled data from multiple previously published and ongoing studies. Overall, data of 41 patients was considered (table 3.1). All of them had a singular cortical or subcortical stroke and were chronically and severely impaired. Only three showed limited residual hand movements. All the others were not able to voluntarily extend their hand. 30 of the patients took part in a previously published study. Half of these patients had the motor cortex included in the lesion, the other half had a subcortical stroke. Detailed exclusion and inclusion criteria are provided elsewhere (Ramos-Murguialday *et al.*, 2013). Data from the other eleven patients was recorded in two ongoing studies. A total of 36 of the patients took part in a rehabilitation intervention based on Brain-Machine interfaces that aimed at improving motor skills and capabilities of the paralyzed upper limb. 30 of the patients were part of the study presented in 2013 (Ramos-Murguialday *et al.* (2013), dataset 1 in section 1.3.1) and six patients were part of an ongoing study with the same aims and a similar protocol (unpublished, dataset 2 in section 1.3.1). All of these patients received a battery of clinical, behavioral and neurophysiological assessment tests before and after the intervention. The primary clinical outcome measure was the modified Fugl-Meyer assessment with a maximum score of 54. This test comprises the sum of the arm and hand motor scores excluding scores related to coordination, speed and reflexes. The assessment was performed at the *post* test and two tests prior to the intervention. The mean of both baseline FMA values was used to calculate the difference between the values of the *pre* intervention and the *post* intervention measurement.
The remaining five patients were not part of these interventional studies. Their data is thus not considered for assessing the correlations between oscillation parameters and motor improvement.

Data of 55 healthy volunteers (table 3.1) were recorded in two studies, of which one is yet to be published, whereas the other has already been published (Bolinger *et al.*, 2019).

The participants performed two minutes of resting-state EEG recordings in total before the intervention and after the intervention, where applicable. They were instructed not

Study	Number of participants	Type of participants	Age (mean ± sd years)	Sex	Excluded
Stroke motor intervention (upper limb) I	30	Chronic severe stroke	53.5 +/- 12.1	12 F 18 M	3
Stroke motor intervention (upper limb) II	6	Chronic severe stroke	55.5 +/- 9.7	2 F 4 M	0
Stroke motor study (lower limb)	3	Chronic severe stroke	65.3 +/- 11.6	3 M	2
Stroke motor study, no intervention	2	Chronic severe stroke	65 and 70 years	1 F 1 M	1
Healthy participants I	30	Healthy volunteers	24 +/- 3.1	16 F 20 M	6
Healthy participants II	25	Healthy volunteers	27.4 +/- 4.6	7 F 22 M	0

Table 3.1: Demographics of participants considered in this investigation. The last column shows the number of subjects excluded from the analysis per study due to the model fit criterion.

to move and to focus their attention on a cross mark on the wall or on a screen. Some of the healthy volunteers only performed 30 seconds of continuous resting-state EEG.

3.2.1 Neurophysiological recordings and data analysis

EEG data was recorded from between 8 and 32 electrodes. However, for the present analysis only the electrodes directly above the motor cortex, i.e. C3 and C4, were considered. The EEG data from these channels were filtered at 0.1 Hz and 48 Hz and ocular artifacts were removed using linear regression between the EEG and the vertical and horizontal EOG, which was also recorded (Schlögl *et al.*, 2007). Subsequently the continuous recordings were split into epochs of four seconds. Artifacts in the gamma (30 to 48 Hz) and the delta (1 to 4 Hz) frequency band related to motion and cranial muscle activity were discarded from the EEG data using a statistical methodology presented previously (López-Larraz *et al.*, 2018b). Each epoch containing artifacts, which were defined by mean EEG power in the central channels C3 and C4 larger than three standard deviations of the mean of the EEG power, was rejected. This procedure was performed twice (yielding a new rejection threshold the second time).

The EEG data free of artifacts was filtered spatially using a Laplacian derivation as described by Perrin and colleagues (Perrin *et al.*, 1978, 1989; Yilmaz *et al.*, 2015), thus reducing the impact of volume conduction and improving spatial resolution. Using

the surface Laplacian filter also attenuated influence of occipital alpha oscillations on the sensorimotor oscillations. The implementation used is available in the open source MNE-python toolbox (Gramfort *et al.*, 2013).

The final step of the processing procedure was the parameterization of the oscillations using the "Fitting Oscillations & One-Over F" algorithm ("FOOOF"). The toolbox is freely available for python (from https://fooof-tools.github.io/fooof/) (Haller *et al.*, 2018). The FOOOF algorithm first fits an exponential function against the power spectrum of the EEG to parameterize the aperiodic noise underlying the spectrum. Afterwards multiple gaussian models are fit against the power spectrum in order to parameterize the oscillations that protrude from the noise floor as bell-shaped peaks. The parameters of the power spectrum obtained are intercept and exponent of the fractal noise, the central frequency of a peak, as well as its width and power (i.e. the vertical distance between the aperiodic component and the central point of the peak). A maximum of two peaks were searched within a frequency range of four to 25 Hz (theta, alpha and beta frequencies). That way, alpha and beta peaks or even secondary peaks in the alpha range could be captured. The accepted width was between 1 and 8 Hz as the beta peaks are usually wider than the alpha peaks.

Figures 3.1 and 3.2 show examples of parameterized oscillations.

Exclusion of subjects

The signal that was modelled with FOOOF was correlated with the original signal after estimation of the parameters of the aperiodic and periodic components. If the model fit was lower then a strong correlation of $r^2 = 0.6$ for the patients and $r^2 = 0.7$ for the healthy participants, the subject was excluded from further analysis, assuming that the low model fit would result in wrong estimations of periodic parameters (i.e. the oscillations). In fact, more than 75% of the models of the patients were in the range of 80% correlation or higher (fig. 3.3).

Out of the 36 patients participating in the interventional studies, three were removed from the analysis due to low model fit and one of them was removed due to technical issues with the resting-state recording (see table 3.1).

Out of the five patients not taking part in the interventional studies three were removed due to low model fit.
In addition to that two subjects of the interventional studies were removed due to a technical issue with the *post* recording. One further subject was removed due to artifact rejection leading to only a few trials remaining in the *post* recording.

Out of the 55 healthy volunteers six were removed due to low model fit, which might have been attributable to the short duration of the recording. All six patients only recorded 30 seconds of resting-state EEG.

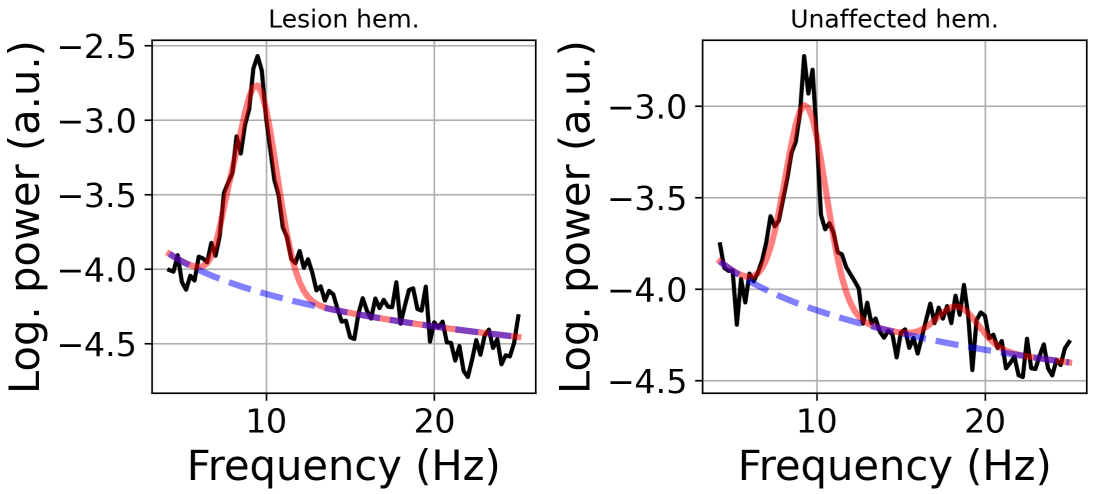

(a) Automatic peak detection between 5 and 25 Hz. The oscillation in the alpha range is correctly modeled (line in light red). On the unaffected hemisphere there is also a smaller peak in the beta range. The dashed line represents the modeled non-oscillatory component.

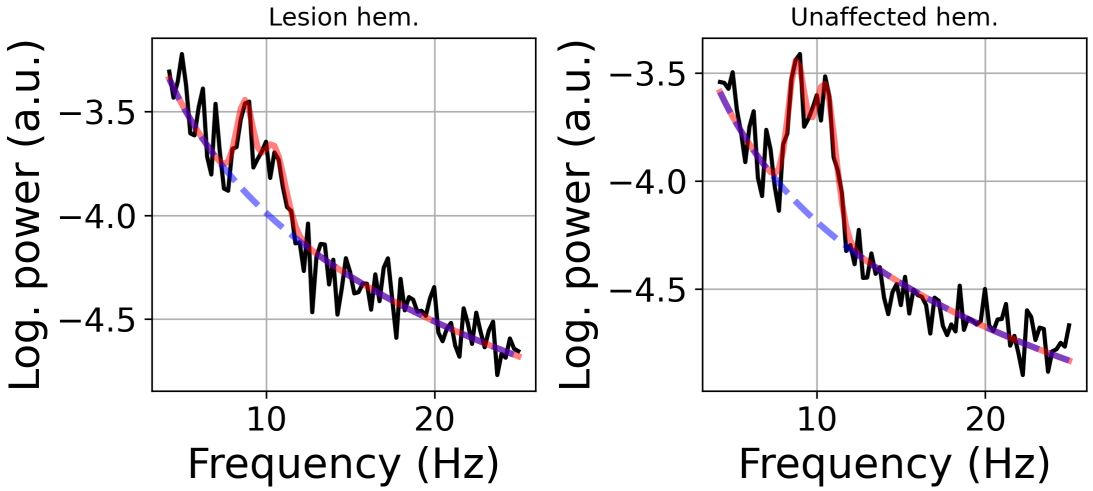

(b) Automatic peak detection between 5 and 25 Hz. There are two peaks within the alpha range.

Figure 3.1: Examples of oscillations parameterized automatically with FOOOF.

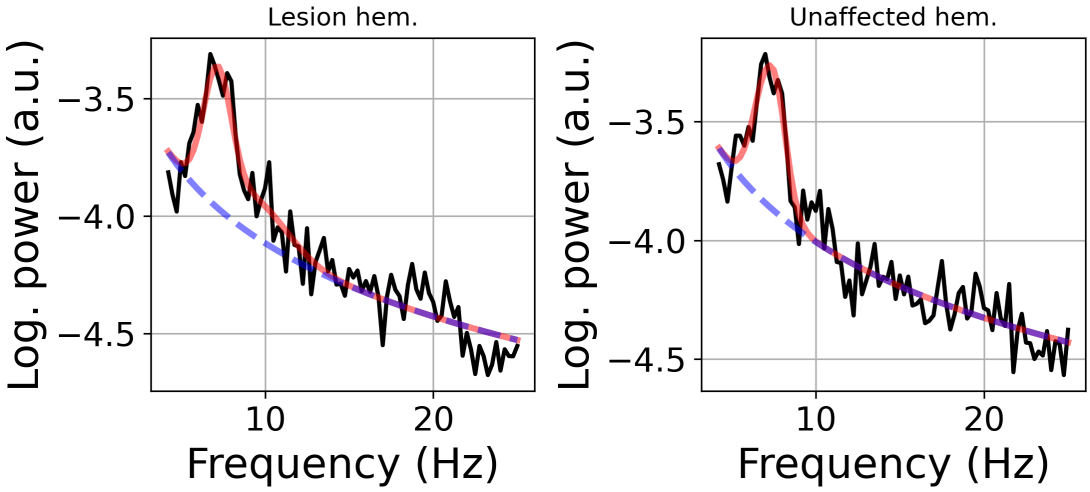

Figure 3.2: Examples of oscillations parameterized automatically with FOOOF (continued). Automatic peak detection between 5 and 25 Hz. The sensorimotor oscillation is so slow that it is in the theta range.

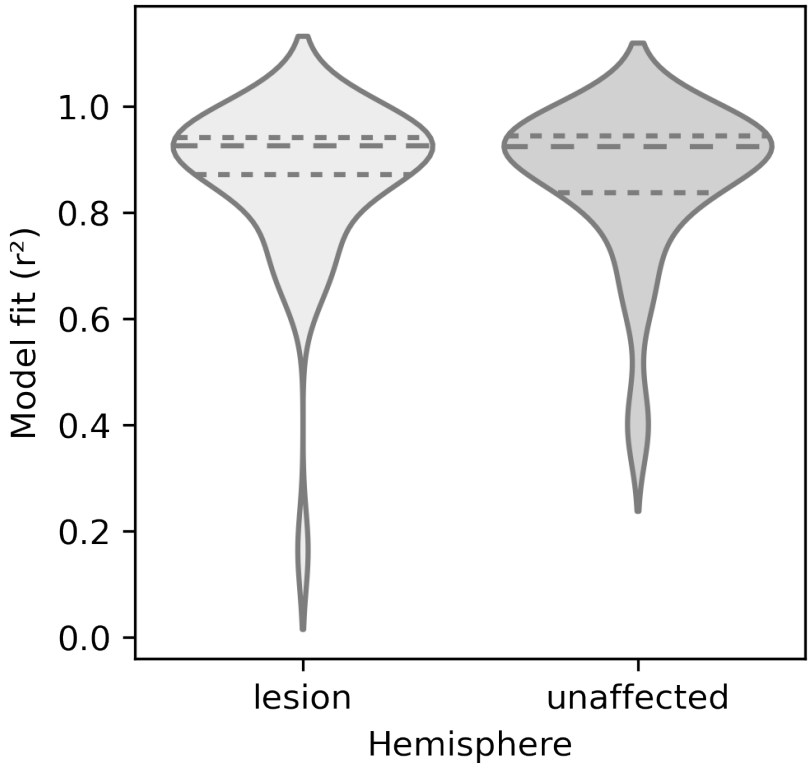

Figure 3.3: Distribution of model fit according to the hemisphere. There is no difference between hemispheres. The great majority of patients showed a high model fit.

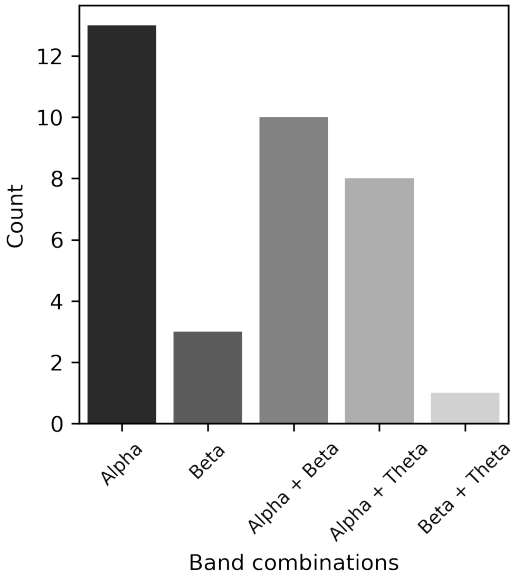

(a) Occurrences of all possible combinations of locations of the major peaks (there was no subject with only a peak in the theta range).

(b) Distributions of center frequencies of peaks within the alpha range on both hemispheres. There is no difference.

Figure 3.4: Peak locations in different frequency bands and peak center frequencies within the alpha range

3.3 Results

3.3.1 Estimated parameters of the oscillations

The peaks of the oscillations directly above the motor cortices of both hemispheres were parameterized. Out of all the peaks found for all subjects 15% were in the theta range, 59% were in the alpha range and 26% were in the beta range. The great majority of patients showed alpha peaks (only 4 did not) (fig. 3.4a). More than 1/3rd of patients did show one peak only in the alpha range, 1/4th presented peaks in alpha and beta and 1/5th in alpha and theta. If a secondary peak was found within the alpha range the one with lower power was discarded (n=5 patients showed a secondary peak in the alpha frequency range: 8.34 Hz $\pm$ 0.52 mean $\pm$ SD). The alpha peaks found on the hemisphere of the lesion were centered at 9.63 $\pm$ 1.06 Hz (fig. 3.4b) and on the contralesional hemisphere were located at 9.76 $\pm$ 0.91. There is no significant difference of the means ($p > 0.05$) (fig. 3.4b). The difference in power of the peaks on both hemispheres was not significantly different either (independent sample t-test: $p > 0.05$).

Since the majority of the patient group underwent a neurofeedback intervention based on ipsilesional EEG SMR, we analyzed specifically if the alpha peaks changed over time but no significant difference was found in the frequency or amplitude of the peaks in

the lesion hemisphere. The peak frequency of the oscillations on the hemisphere of the lesion did not change from before to after the treatment: 9.71 $\pm$ 1.04 Hz (before) and 9.79 $\pm$ 1.23 Hz (after) (paired sample t-test: $p > 0.05$). The power of the oscillation did not change, either (paired sample t-test: $p > 0.05$).

The 30 patients taking part in the published Brain-Machine interface study (Dataset 1, section 1.3.1) were stratified according to involvement of the motor cortex in the lesion. Expert-segmented MRI images of the damaged brain areas are available for these patients. The type of the lesion was not a predictor of peak center frequency nor of peak power (independent sample t-tests: $p > 0.05$).

3.3.2 Correlation of oscillations and impairment

Peak center frequency of the SMR did not correlate with motor function before the intervention and neither did it predict improvement (fig. 3.5a). SMR peak power did not correlate significantly either. However, a DFBETA test revealed an influential outlier (removal of this subject would change the intercept and the slope of the model one order of magnitude more than the next most influential subject, cf. 2.2.3). Removing this outlier yielded a significant model ($F : 4.6; p = 0.04$). The correlation, however, is very small ($r^2 = 0.17$) (fig. 3.5b). No correlation between individual interhemispheric differences of sensorimotor peak frequency and peak power and motor function were found when trying to predict the Fugl-Meyer values before the intervention using an ordinary least squares regression (F-test: $p > 0.05$).

Descriptive analysis shows that the combination of the frequency band of occurrence of the major peaks did not have a systematic influence on motor improvement (fig. 3.6). However, the patients with only beta peaks show no improvement.

3.3.3 Comparison of oscillations in stroke patients and healthy participants

We compared the sensorimotor oscillations of the patients under investigation here with a younger healthy control group. Since there were no differences of the peak center frequency between hemispheres in either of the two groups, we considered peaks from both sides of the brain in one comparison. Secondary peaks in the alpha frequency range have been removed in the patients (n=5) and the healthy population (n=12). The mean sensorimotor peak center frequency in the patients was 9.67 $\pm$ 0.97 Hz and in the healthy participants it was 10.43 $\pm$ 0.93 Hz (fig. 3.7). The difference was significant (independent samples t-test: $p < 0.0001$).

Moreover, the power of the sensorimotor oscillations was significantly higher in the healthy participants (0.64 $\pm$ 0.33 a.u.) than in the patients (0.51 $\pm$ 0.26 a.u.): $p = 0.01$. The groups were not age-matched. However, the patients who participated in this investigation had a large age range from just below 30 years to 75 years. We correlated

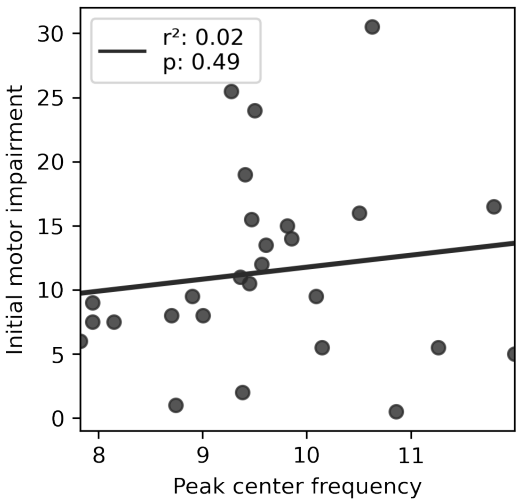

(a) The correlation between peak center frequency and motor impairment cFMA.

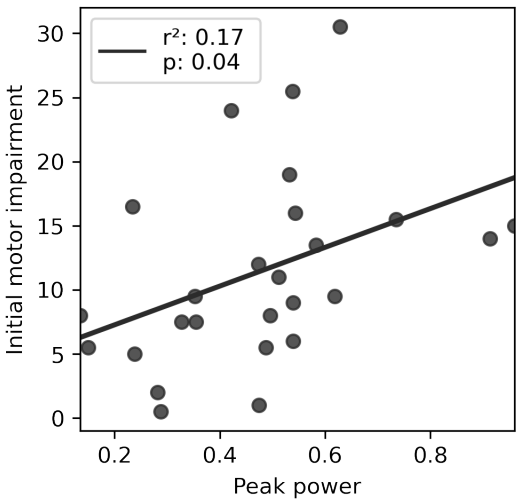

(b) The correlation between peak power and motor impairment cFMA.

Figure 3.5: Regressions assessing the correlations between metrics of the sensorimotor rhythm and motor impairment before the intervention.

sensorimotor oscillation peak frequency in the patients with their age. There was neither a correlation for the peak frequency on the hemisphere of the lesion nor the unaffected hemisphere (fig. 3.8).

3.4 Discussion

In the present work we investigated SMR peak center frequency and power in chronically and severely impaired stroke patients during resting-state. We found that the oscillations are slowed as compared to a younger group of healthy volunteers. SMR peak center frequency did not differ between hemispheres in the patient cohort and it did not change from before to after the interventions. There was a small correlation between power of the SMR and initial impairment.

Our results confirm previous work indicating that these slower rhythms persist in the chronic stage of stroke. For one patient the rhythms were so slow that their center frequency was in the theta range (cf. fig. 3.2). We suspected lesions involving the cortex caused oscillations slower than those only affecting subcortical structures. However, the location of the lesion, which we could investigate for the patients that took part in the published interventional study, did not correlate with the SMR peak center frequency over the lesion. Any damage to the thalamocortical loop might influence SMR oscillations. Investigation of more subgroups in a larger cohort of chronic stroke patients with more detailed identification of damaged structures would help further investigations.

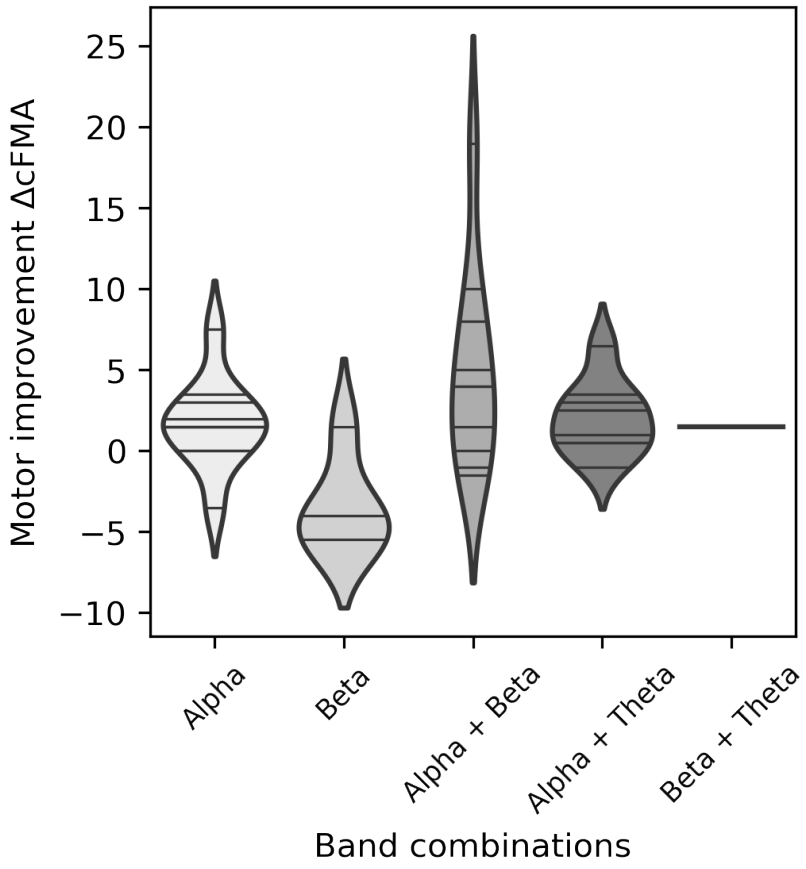

Figure 3.6: Peak band combinations and motor improvement.

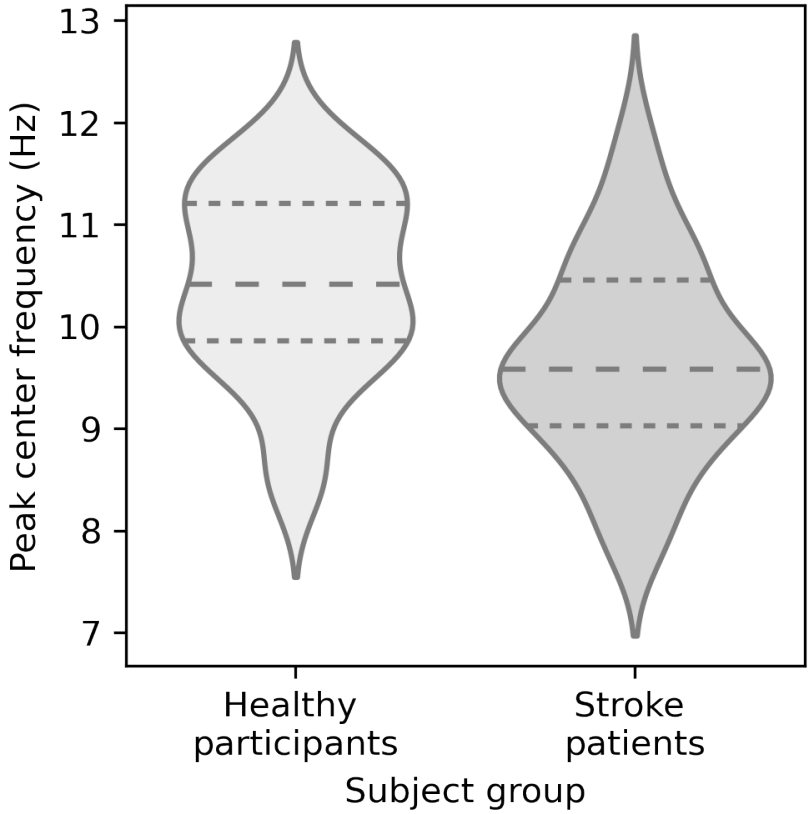

Figure 3.7: Difference of alpha peak center frequency between the healthy participants and the stroke victims.

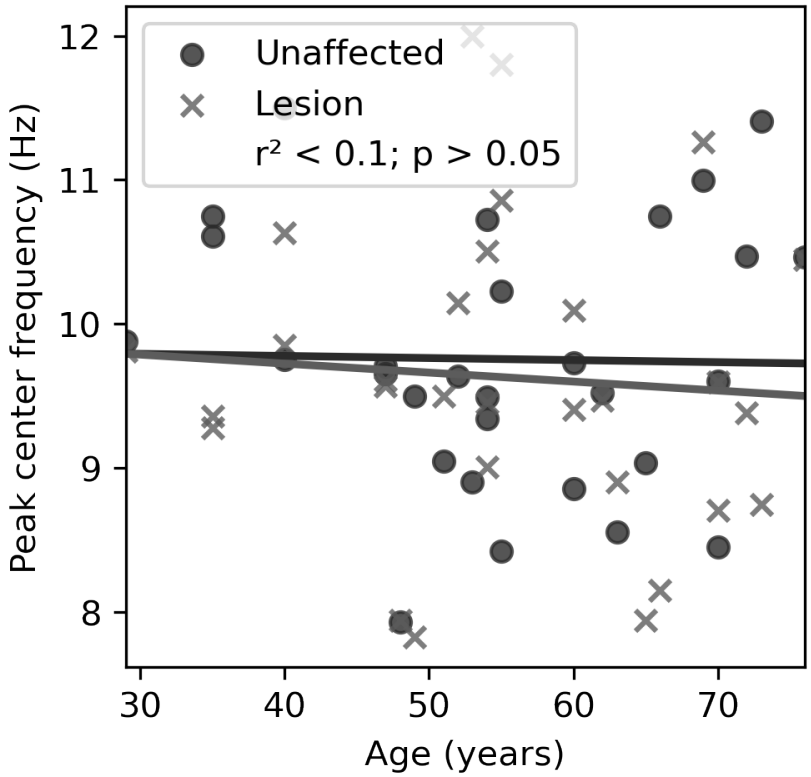

Figure 3.8: There is no correlation between age of the stroke patients and the sensorimotor peak center frequency

Furthermore, the current mental and psychological state of the subject might modulate peak center frequencies of the brain rhythms. A transition to sleep leads to a slowing of the oscillations, too (Ribary *et al.*, 2014). The resting-state data was recorded at the beginning of the experiments, when the patients were generally not tired or exhausted and great care was taken by the experimenters to observe signs of sleepiness, as some chronic stroke patients show signs of increased daytime fatigue in general.

The oscillations in the stroke victims are more than 1 Hz slower than in the healthy volunteers. Previous works have reported effects of age on brain rhythms: The older the subject, the slower the rhythm (Scally *et al.*, 2018). The average age difference between the groups we compared was 30 years and the observed difference of peak center frequency could thus be attributable to age alone. However, the age-range within the patient cohort of our study is large (30 to 76 years). Therefore, an effect of age on the oscillations should have also become apparent in this data. However, we show that age is not correlated to the peak frequency in the stroke patients. For younger subjects the peak center oscillations clearly discriminate stroke victims from healthy persons. The disturbance of the thalamocortical loop caused by the stroke might have a stronger slowing effect on the oscillations than age alone. Interestingly, there was no difference of the center frequency between hemispheres in the stroke patients. The perturbation caused by the lesion somehow "transcends" to the unaffected hemisphere, probably through thalamic and transcallosal circuits.

Power of the SMR might be a direct indicator of the degree of damage to the system involved in generating the SMR. This system is part of a larger system that generates limb movements and processes sensory input from the periphery (Scott, 2004). The positive correlation of power of the SMR and the initial motor impairment thus could simply reflect this direct connection: More damage leads to larger motor impairment and at the same time hinders the expression of the rhythm on the cortex.

All our findings in this study are relevant for interventions where an appropriate individual frequency band for feedback or control is chosen prior to the training, such as Brain-Machine interface training. Firstly, inclusion of the EEG of the healthy hemisphere could inform the choice of this band, since there is no interhemispheric difference. Secondly, the findings underline the necessity of choosing the individual SMR prior to interventions, supporting previous works, where individual alpha center frequency (Pichiorri *et al.*, 2015) or the individual frequency exhibiting the largest difference of SMR modulation (Ramos-Murguialday *et al.*, 2013) have been used throughout the intervention. Such interventions also depend on the stability of the SMR peak center frequency (if no adaptive method is used compensating for potential changes of SMR properties). Our results show that the peak center frequency of the SMR in chronic stroke patients is stable from before to after the intervention. This is in line with findings in a healthy population where the peak center frequency of the sensorimotor oscillations did not change in recordings carried out on multiple days (Kuhlman, 1978). Interventions exploiting peak center frequency thus do need not to use a methodology that adapts to physiological changes the SMR peak frequency throughout an intervention.

Chapter 4

Low frequency oscillations in upper limb motor recovery in severe chronic stroke

4.1 Introduction

Recent work identified low-frequency oscillations of the cortex in rodent stroke models as marker for the degree of spontaneous recovery of motor skills of limb movements. Targeted electrical cortical stimulation triggered by these oscillations improved accuracy of reaching and grasping movements (Ramanathan *et al.*, 2018). The existence of these markers of recovery has been confirmed in a longitudinal study on human stroke victims in the acute and subacute phase (Bönstrup *et al.*, 2019). In that work the power of oscillatory activity in the upper delta and lower theta range at motor cortical sites around the onsets of upper-limb movements was diminished immediately after the insult as compared to healthy controls and reappeared with recovery.

It is not known whether this normalization occurs only in the acute and subacute phase as part of spontaneous recovery or if it can be induced and is generalizable to recovery in the chronic state, especially in the severely impaired.

We conducted a longitudinal investigation of low-frequency oscillations time-locked to the onset of hand movements in chronically severely paralyzed stroke patients who underwent an intervention of four weeks employing brain-machine interface training and adjuvant physiotherapy. The main effects (motor improvement) have already been published (Ramos-Murguialday *et al.*, 2013). In this chapter the brain activity of 28 chronically and severely paralyzed stroke patients was investigated while attempting to execute hand opening and closing (cf. dataset 1: section 1.3.1). We compared the oscillatory brain activity generated while executing the same movements of the unaffected limb and correlated the low-frequency oscillations and motor recovery.

4.2 Methods

Data of 28 patients of dataset 1 (section 1.3.1) was analyzed in the following. The subset of data used for this analysis comprised movement attempts of the paretic arm and movements of the healthy arm. The patients opened (or tried to open) their hands at their own pace after a cue.

The full dataset contained EEG data of 30 chronic and severely impaired stroke patients. However, after preprocessing for the present analysis, two subjects had to be excluded due to technical issues with either the *pre* or the *post* recording. In two other subjects the preprocessing procedure removed too many trials of the pre recording such that instead of using the second baseline measurement ("Pre2"), the first baseline measurement was used ("Pre1").
In two subjects the occipital channel Oz was not recorded and they are not included in figure 4.12.

4.2.1 Neurophysiological data analysis

For the EEG processing we followed the procedure previously presented by our group, which is especially suited for combined EEG and electromygraphic (EMG) recordings involving limb movements (López-Larraz *et al.*, 2018b). After filtering the EEG data at 0.1 Hz and 48 Hz ocular artifacts were removed using linear regression between the EEG and the EOG (vertical and horizontal) activities (Schlögl *et al.*, 2007). The EMG data was filtered at 20 Hz and the waveform length feature was computed in 200 ms windows with a sliding step of 20 ms (Ramos-Murguialday *et al.*, 2010). The average waveform length of the resting state interval was used to compute a threshold of three standard deviations from the mean. Those trials presenting a waveform length larger than the threshold were discarded. Subsequently, the threshold was recomputed with the remaining trials. The new threshold represents activation of a muscle if the threshold was exceeded 200 ms or more. Trials with muscle activation of the limb not cued were discarded.

Artifacts related to motion and cranial muscle activity were discarded from the EEG data in a similar statistical way, based on the gamma frequency band (30 to 48 Hz). In preparation for the further analyses on low-frequency oscillations, it is especially important to identify artifacts in low spectral bands (delta: 1 to 4 Hz). The mean power of the EEG in these bands was computed to define the rejection threshold as three standard deviations during the resting interval of the trials. Trials containing such artifacts in the resting interval were removed. The procedure was repeated, and a second threshold was computed similarly. Trials in which mean EEG power exceeded the new threshold in either the resting period or the movement (attempt) period were removed, too. Two patients of the experimental group had to be removed due to data quality issues with the *post* recording. The final pool of patients was 28, out of which exactly half were part of the experimental group in the original clinical trial.

The subsequent analysis of the EEG data was carried out following parameters and

procedures from Bönstrup et al (Bönstrup *et al.*, 2019). In that work source localization was used to identify motor cortical sources of activity. In the case of our data, source localization was not applicable because of the limited amount of EEG channels available. Instead, we carried out a sensor-space analysis. After the careful artifact rejection procedure a time-frequency representation was computed directly from the data of the two channels above the motor hand cortices (C3 and C4). We used multiple Hanning tapers with a time-window length of 5/frequency within a spectral band of 1 and 22 Hz. The implementation used is available in the open source MNE python toolbox (Gramfort *et al.*, 2013).

Since our patient cohort presented severe paresis, a gripping task with force measurement was not applicable because the patients did not present active finger extension before brain computer interface treatment and only some, limited flexion. Moreover, only a few patients showed consistent task-related EMG activation in the hand extensors and flexors in the pre-assessments. The onset latency of the movements of the paretic limb could thus not be extracted reliably. However, for the control condition (opening and closing of the unaffected hand), the onsets were clearly detectable.

Figures 4.1 shows the distributions of the median latencies of the EMG onset after the audiovisual cue at the *pre* measurement. EMG data of all electrodes of the unaffected limb were highpass-filtered at 10 Hz and the onset of the movement was precisely detected in each trial using the AGLRamp method (Werner *et al.*, 2001). For the movements of the healthy hand, onsets could be detected in all patients and they ranged from 408 ms to 985 ms. For the movement attempts of the paretic hand, the EMG channels of the hand extensor muscles and flexor muscles and the electrodes on biceps and triceps were used for detecting movement onsets. However, they could be detected only in 10 out of 28 subjects. The mean onset latency for these patients was 1.2 s (twice as long as the latency on the healthy hand). One reason for this larger latency might be that the patients took longer to activate the appropriate muscles due to the pathophysiology. However, another reason might simply be that the detected EMG onsets come from a flexion movement rather than the extension (the task was self-paced opening and closing attempts). Since there were so few subjects with detectable EMG onsets and their origin was not certain, the individual average onset of the healthy side was used for computing the low-frequency power time-courses.

Bönstrup and colleagues used the audiovisual cue as anchor point for their analysis of chronically impaired patients. As the generation of low frequency oscillations is assumed to be a top-down process whose timing of initiation is important for the investigation at hand (and not the actual muscle contraction) We think that using the control condition with the healthy limb is a much better estimator of the initiation of the LFO power phenomena of interest than the paralyzed limb. Therefore, the “EMG onset” (i.e. ramping up of the EMG activity) of activity of both hands was defined as the onset of the muscle contraction of the unaffected hand. The onset latency was averaged across trials for each subject individually. These averaged EMG onsets of the unaffected hand were used as ”EMG onset” for movements of the unaffected limb and for movement attempts of

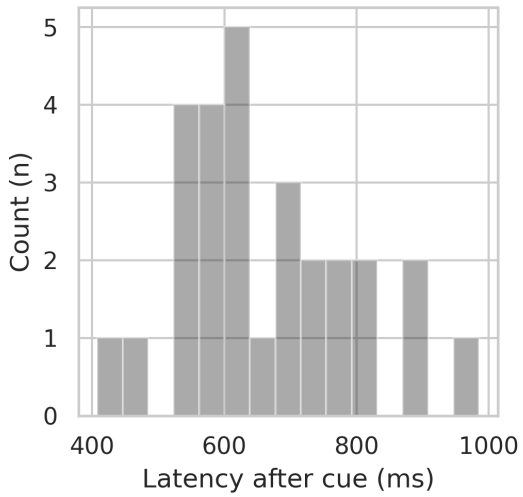

(a) Unaffected side. The mean value of the onset was 665 ms.

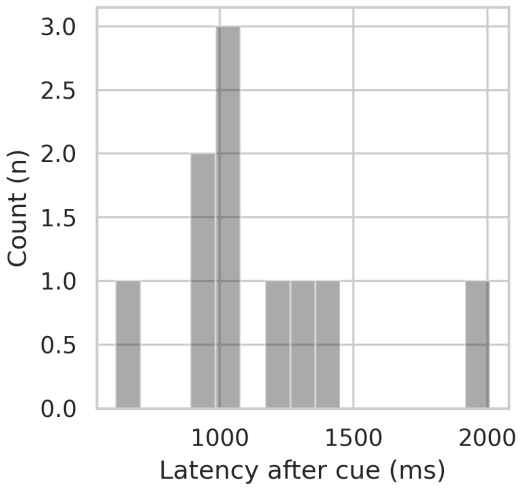

(b) Paretic side. The mean value of the onsets was 1.2s

Figure 4.1: Distributions of the median latencies of the EMG onsets across trials.

the paretic limb. In the following, "EMG onset" always means this individual average latency with respect to the imperative cue.

Bönstrup and colleagues showed that the power in the low frequency oscillations of interest starts to ramp up 200 ms before the onset of the EMG (Bönstrup *et al.*, 2019). We thus averaged the power of the low frequency range of interest from 3 to 5 Hz in the EEG channel over the motor cortex of both hemispheres (central spatially filtered electrodes C3 and C4) from 200 ms before EMG onset to 400 ms after. The averaged EEG power was baseline corrected using the mean power of -2500 to -500 ms of the resting interval with respect to the audiovisual cue. This procedure yielded the **task-related power:** LFO_{TR}.

4.2.2 Statistical analyses

In order to asses statistical difference of the averaged time-courses of task-related power between the *pre* and *post* measurements a permutation clustering test was performed (Maris and Oostenveld, 2007). First, t-values are computed for each sample of the difference between the *pre* and *post* power time-courses. These are thresholded and clustered. The sum of the t-values in each cluster is the test statistic used for the permutation test where the conditions (*pre* and *post*) are randomly flipped for each sample. This procedure yields a distribution of summed t-values that is used for testing of statistical significance of individual clusters (i.e. temporally adjacent samples of power values).
We used paired sample t-tests for comparing the mean difference of the averaged task-related power at the *pre* and the *post* measurement.

Ordinary linear regression was used to correlate changes of the average task-related power and motor improvement as well as to predict *initial* LFO_{TR} and the *change of* LFO_{TR}.

4.3 Results

4.3.1 Time-course of task-related LFO power LFO_{TR}

We investigated the time-course of task-related LFO power (LFO_{TR}) during hand opening and closing attempts of the paretic limb and during hand opening and closing of the healthy limb on both hemispheres in all subjects (fig. 4.2). A comparison from before (pre) to after (post) the intervention revealed significant changes only on the hemisphere of the lesion during movements of the paretic limb (cluster threshold: $p < 0.05$). There are two significantly different clusters between -892 ms to 454 ms and 784 ms to 1000 ms with respect to the EMG onset in (fig. 4.2 upper right).

The time-frequency dynamics of the activity in the central channels (C3/4 depending on lesion location) show a similar pattern (fig. 4.3). The temporo-spectral area (time/frequency range) of interest (-200 ms to 400 ms between 3 to 5 Hz) is marked by a black rectangle. The overall activity is similar during movements of both limbs and on both hemispheres. The strongest activity during movement attempts of the paretic limb are visible around movement onset. During movements of the unaffected limb the activity seems to diminish slightly quicker after the EMG onset. In all panels activity can also be seen prior to the black rectangle (the onset of the LFO ramp derived from previous reports) and also in higher frequency bands. The decrease of power in the higher ranges (9 Hz) before EMG onset indicates movement-related desynchronization.

4.3.2 Comparison of mean LFO_{TR} on both hemispheres during hand opening/closing of either limb

Investigation of averaged LFO_{TR} confirms that there is a *pre-post* difference during movement attempts of the paretic limb on the hemisphere of the lesion (fig. 4.4) (paired samples t-test, corrected for two comparisons, $p = 0.03$). Testing the difference between LFO_{TR} on the two hemispheres during movement (attempts) of the respective contralateral limb did not reveal any difference (paired samples t-test, corrected for two comparisons, $p > 0.05$).

Patients with distinct types of lesions took part in the study, which were matched in numbers. All patients presented involvement of subcortical structures. Half of the patients, however, had an additional involvement of the cortex. We stratified the patients into these two groups in order to investigate if lesion type had an effect on LFO_{TR} (fig. 4.5). There was no pre-post difference in either of the groups (independent samples t-test: $p > 0.05$, corrected for multiple comparisons).

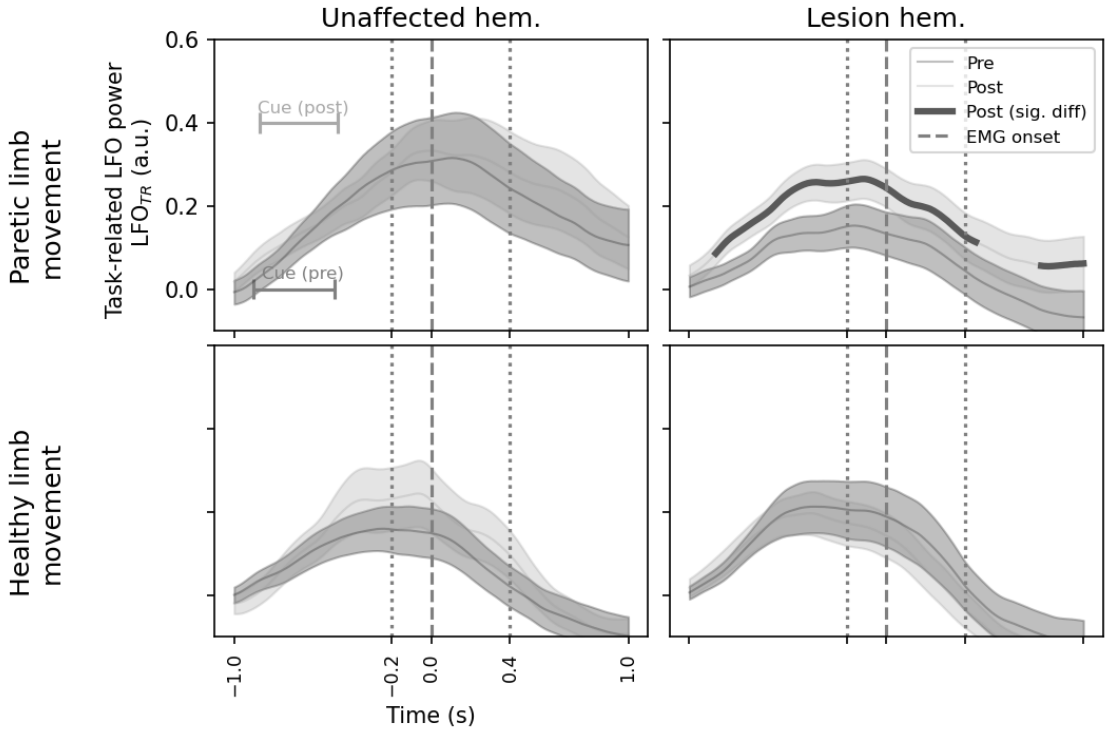

Figure 4.2: Time-course of the task-related power LFO_{TR} around the individual movement onset (mean $\pm$ standard error) in the central channel (C3 or C4, depending on lesion side) at the *pre* measurement and the *post* measurement on both hemispheres during both movement types for all subjects. The thick line represents significant difference between *pre* and *post*.
The latency ranges of the presentation of the audiovisual cue are shown for *pre* and *post* (whiskers mark 5 and 95 percentiles of the cue latency with respect to to the EMG onset of the healthy limb).

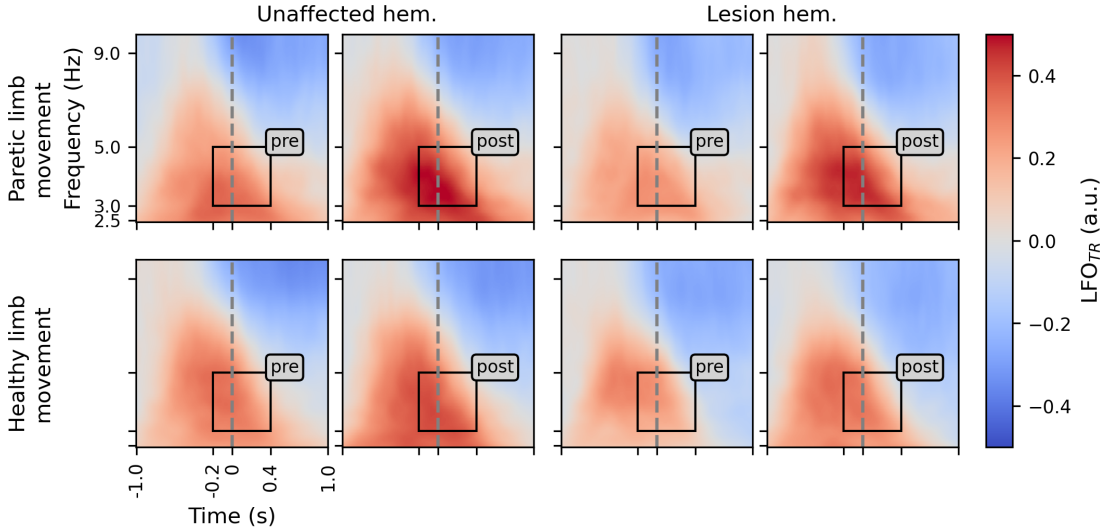

Figure 4.3: Time-frequency plots of LFO power on both hemispheres during both movements in the central channels (C3 and C4, depending on lesion side). The black rectangle marks the time-period of interest around movement onset and the bands of the low frequency oscillations under investigation. There is an increase in LFO power around movement onset during movement of the paretic limb that is stronger at the post measurement. There is no difference between *pre* and *post* during movements of the healthy limb.

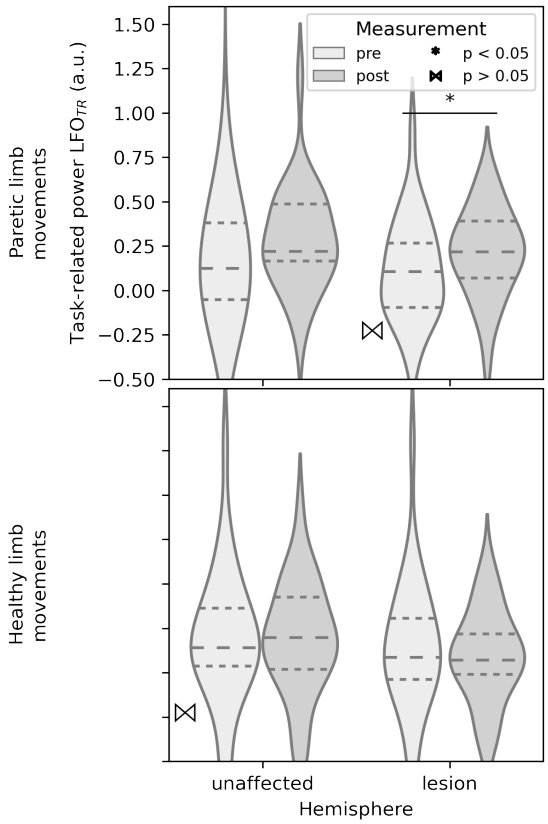

Figure 4.4: Average LFO on both hemispheres during movement attempts of the paretic limb and movements of the healthy limb including all subjects. The difference of the average LFO_{TR} on the hemisphere of the lesion from pre to post is significant.
Furthermore, there is no difference between LFO_{TR} at pre during movements of the healthy limb on the unaffected hemisphere and movement attempts of the paretic limb on the hemisphere of the lesion.

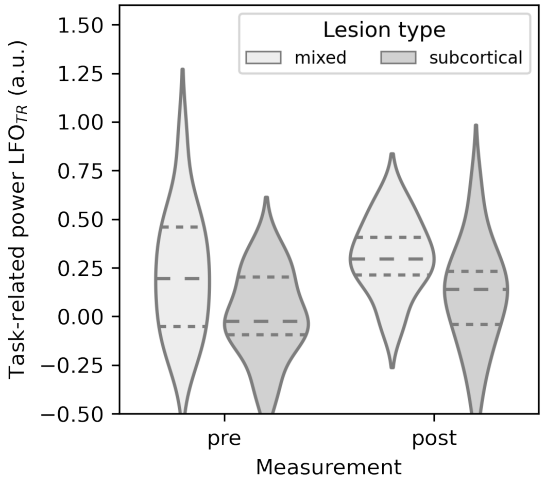

Figure 4.5: Average LFO_{TR} on the hemisphere of the lesion during movement (attempts) of the paretic limb. Neither of the two subgroups stratified by lesion types increased power significantly from before to after the intervention. There is no statistical difference between LFO_{TR} of the two subgroups at either measurement.

4.3.3 Initial LFO power predicts change of LFO power

LFOs are an indicator of functioning of the motor circuit, which includes thalamocortical activity. It has been argued that paresis and recovery are functions of network plasticity rather than local effects of the damaged motor cortex (Ramanathan *et al.*, 2018). The disrupted network may impair synchronization of populations of neurons involved in generating LFOs. However, as presented above, there are *pre-post* differences of the oscillations just as previous works showed that all patients increased LFO_{TR} from the acute to the subacute stage following motor recovery (Bönstrup *et al.*, 2019). The question thus remained how the reduced power of the LFO prior to activation of presumed repair mechanisms due the intervention is related to the change of the LFO power. As LFO power might represent a measure of how disturbed motor circuits are, the intervention could yield larger influence on networks expressing low LFO power than those showing larger LFO power. Indeed, we found a low negative correlation between initial LFO_{TR} and the power change (fig. 4.6).

4.3.4 Effect of the intervention on LFO_{TR}

The *pre-post* differences we show here suggest that the intervention had a general effect on LFO_{TR}. We hypothesized that the effect is larger in the group receiving proprioceptive feedback linked to oscillatory activity (experimental group, C+). These subjects were those showing significant motor improvement. We investigated the time-course of task-related LFO power (LFO_{TR}) during hand opening and closing attempts of the

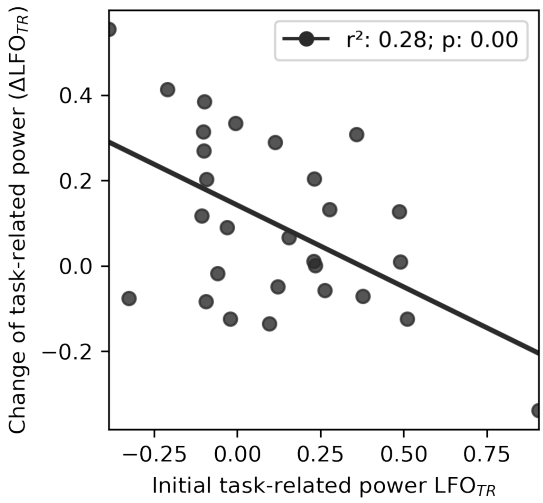

Figure 4.6: Prediction of the change of LFO power from *pre* to *post* by the initial LFO power. There is a significant negative correlation. The subjects showing a smaller LFO power show a larger increase from before to after the intervention.

paretic limb on the hemisphere of the lesion and during hand opening and closing of the healthy limb on the unaffected hemisphere (fig. 4.7). The subjects were stratified by feedback group. A comparison from before (pre) to after (post) the intervention revealed significant changes only on the hemisphere of the lesion during movement attempts of the paretic limb (cluster threshold: $p < 0.05$) in the experimental group. We also found a significantly different cluster in the control group but it is outside the time-period around EMG onset and within the window of cue presentation. It might be attributable to an effect of the cue: for example, habituation at *post*.

We also show the difference between averaged LFO_{TR} of both groups at the *pre* and the *post* screening during movement attempts of the paralyzed limb (fig. 4.8). Statistical tests reveal no difference between the power distributions at either measurement. However, there is a trend towards a difference of power increase from the *pre* measurement to the *post* measurement in the C+-group, only (paired samples t-test: $p < 0.1$, corrected for multiple comparisons), which is not present in the Sham-group. There is no difference between the feedback groups at *post*.

4.3.5 There is no correlation of average LFO_{TR} and motor improvement

Previous work reported weak correlations between LFO_{TR} and motor improvement in a less severe and acute/subacute population (Bönstrup *et al.*, 2019). We tested if LFO_{TR} correlates with motor impairment before and after the intervention. There is no correlation (F-test: $p > 0.05$ in all six regressions) (fig. 4.9). Furthermore, we tested if there

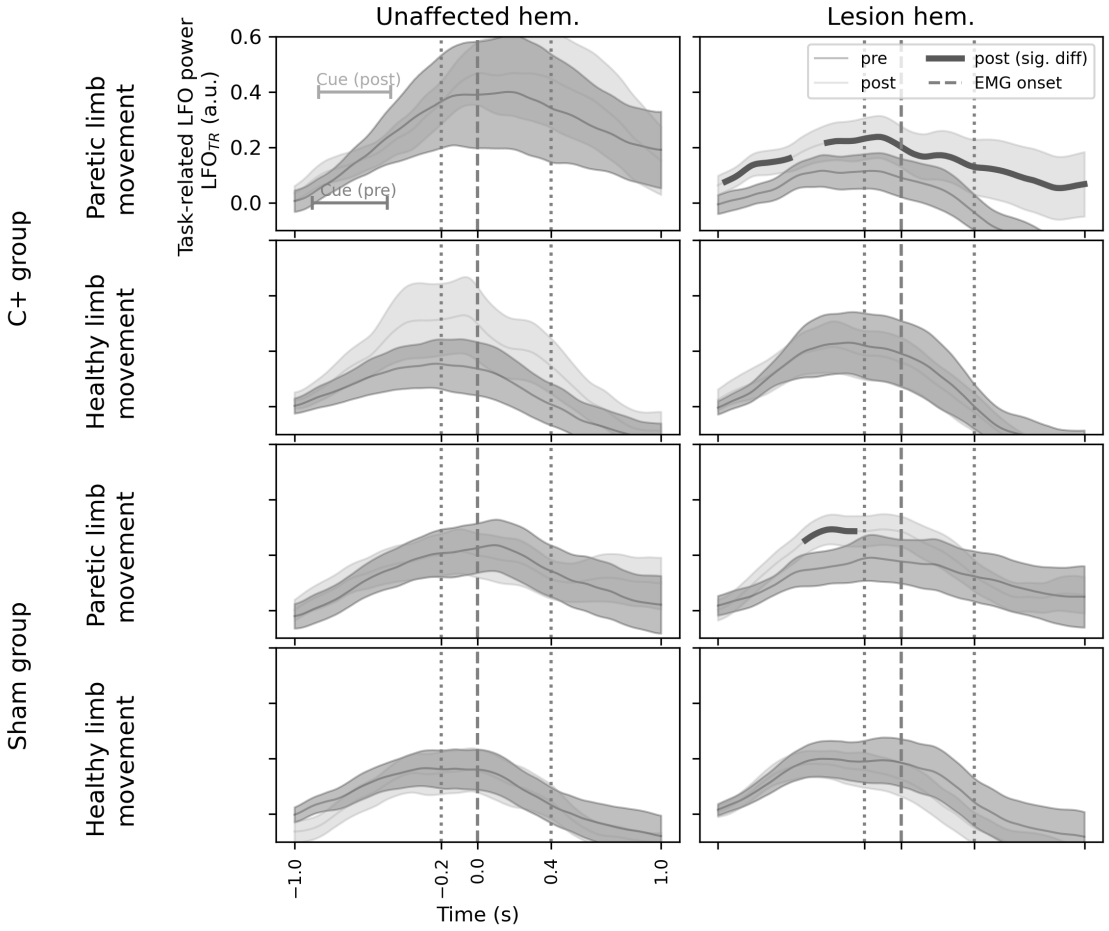

Figure 4.7: Time-course of the task-related power LFO_{TR} around the individual movement onset (mean $\pm$ standard error) in the central channel (C3 or C4, depending on lesion side) at *pre* and at *post* on both hemispheres during the limb movement (attempts) stratified by feedback group. The thick line represents significant difference between *pre* and *post*. Only the experimental group shows a significant increase in task-related LFO power from *pre* to *post* during movements of the paretic limb. The Sham group shows significant activation only outside of the period of interest, which could be related to the presentation of the cue. The latency ranges of the presentation of the audiovisual cue are shown for *pre* and *post* (whiskers mark the 5 and the 95 percentiles of the cue latency with respect to the EMG onset of the healthy limb).

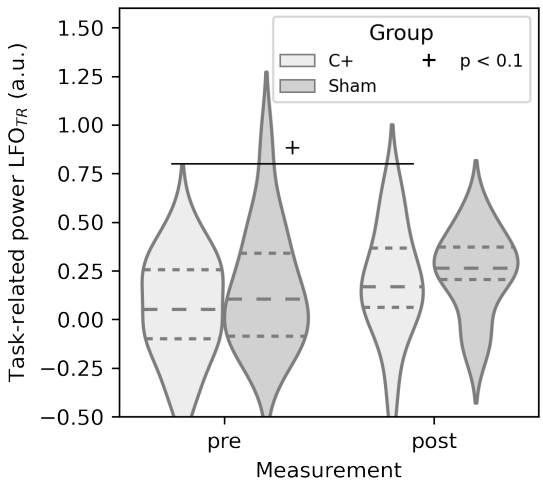

Figure 4.8: Average LFO_{TR} on the hemisphere of the lesion during movement (attempts) of the paretic limb. Only the experimental group (C+) shows a trend towards increase of LFO power from *pre* to *post*.

is a correlation between the differences of LFO_{TR} and motor impairment from before to after the intervention. Figure 4.10 shows that in the severe and chronic patient population under investigation there is no such correlation.

Other investigations on this dataset such as the change of event-related desynchronization and fMRI showed the importance of bilateral balance of movement-related brain activity (Ray *et al.* (2020); Ramos-Murguialday *et al.* (2013), and chapter 7). As previously shown here we saw that LFO power during movements of the paretic limb on the hemisphere of the lesion became more similar to the contralesional activity at post. We computed the difference of LFO_{TR} between the two hemispheres to describe the change of the bilateral balance of LFO_{TR} from *pre* to *post* during movements of the paretic limb (fig. 4.11). Negative values represent stronger LFO power on the unaffected hemisphere and vice versa. A value of zero would represent a perfect bihemispheric balance. In the upper panel the laterality change is shown in relation to the motor improvement. The Gaussian distribution around 0 (balanced power) is slightly skewed towards the unaffected hemisphere at *post*. The patients around the center (balanced LFO power) show the largest motor improvements. Those in the extremes show lower improvements.

4.4 Discussion

We show that bouts of LFO activity occur at motor cortical areas in chronically severely impaired stroke victims before and at onset of upper-limb movement (attempts). We found a significant increase of LFO power from before to after the intervention on the hemisphere of the lesion during movement attempts of the paretic limb that is not present

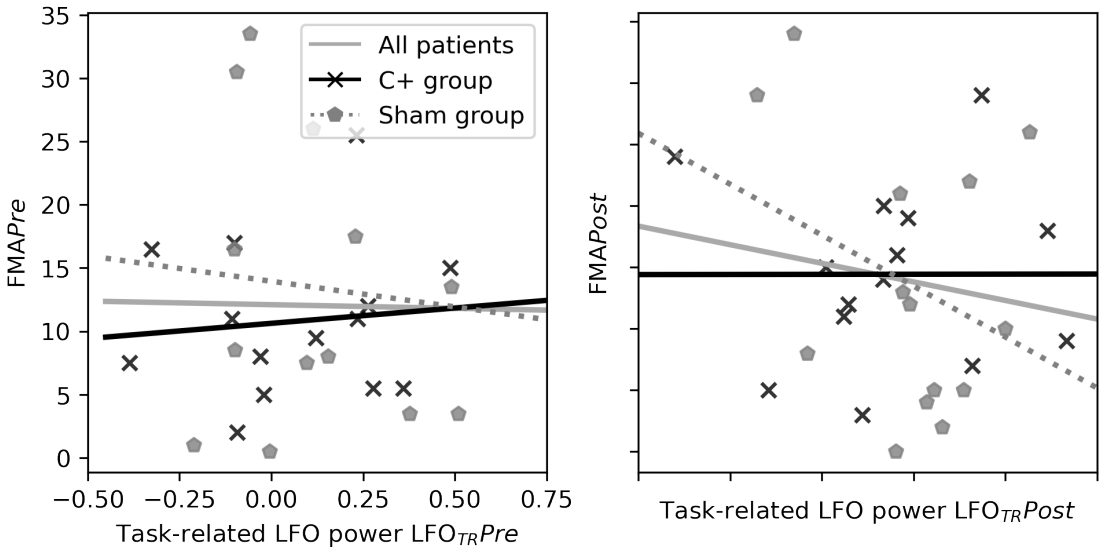

Figure 4.9: Linear relation between the task-related LFO power at *pre* and at *post* and motor impairment at *pre* and *post*. There is no significant correlation.

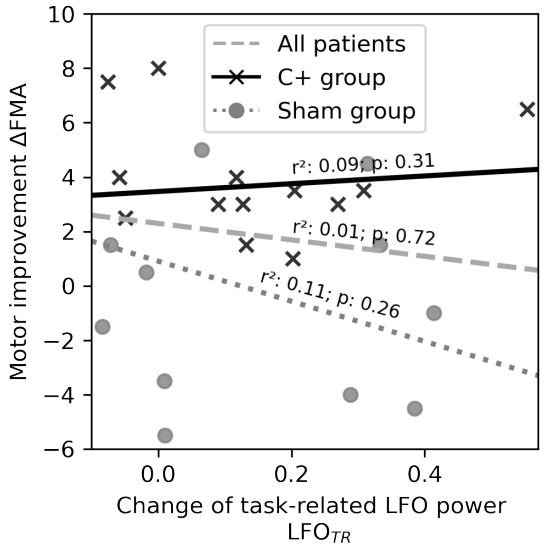

Figure 4.10: Linear relation between the change of task-related LFO power from *pre* to *post* and motor improvement in all subjects and stratified by feedback group. There is no significant correlation.

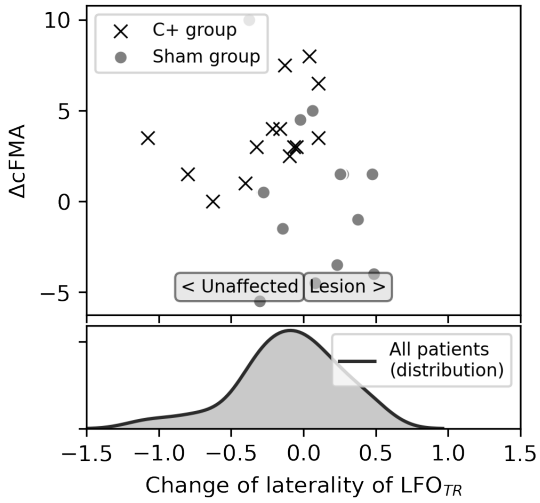

Figure 4.11: Distribution of the change of task-related LFO power from *pre* to *post* vs. motor improvement for all patients (stratified by group).

on the unaffected hemisphere. The main contributors to this increase were the patients in the experimental group who received contingent feedback and improved. This finding suggests that the intervention based on brain-computer interfaces might induce an effect through change of LFO power.

Previous studies have sparked interest in low-frequency oscillations in human stroke victims. Low-frequency oscillations are involved in the control of different parameters of movements such as speed, trajectory and velocity (Bansal *et al.*, 2011; Mollazadeh *et al.*, 2011). Particularly the work of Ramanathan and colleagues supports a mechanistic role of LFOs for motor control as it links diminished LFOs and their re-emergence with skilled reaching in rodent stroke models (Ramanathan *et al.*, 2018). Bönstrup and colleagues showed similar spatiotemporal dynamics of LFO power in healthy humans and acute and subacute stroke victims and linked changes in power to spontaneous motor recovery (Bönstrup *et al.*, 2019). The data presented here is the first demonstration that the mentioned results can be partially generalized to chronic stroke patients with severe paralysis.

4.4.1 Movement-related LFOs in chronic stroke

In the present work we show a significant increase of task-related power of low-frequency oscillations before and at onset of movement attempts of the paralyzed limb. We used the report of Bönstrup and colleagues as reference and focused our investigation on similar spectral and temporal ranges and spatial regions. The time frame for investigating LFO_{TR} was thus from -200 ms and +400 ms with respect to the onset of the EMG. We found an increase of LFO activity (3 Hz to 5 Hz) well preceding motor onset during

movements of both limbs on both hemispheres on the electrodes over the motor cortex. The similarity of the LFO power time-courses to those previously reported in healthy humans and stroke patients confirms that this activity persists in chronic stroke, even in patients with severe hand paresis. The latency of the audiovisual cues prompting the patients to perform the movements ranges from almost a second to half a second before the onset of the EMG. This large variation is evidence that the observed time-course of the LFO power is related to the movement onset and not to the sensory input from the imperative cues, which suggests an intrinsic (top-down) origin of the LFO dynamics. LFOs seem to contribute to setting a brain-state preparing the movement and sensorimotor integration (Bönstrup *et al.*, 2019; Cruikshank *et al.*, 2012).

In a time-frequency analysis we showed activity in temporal relation to the EMG onset. The temporo-spectral area of main interest (around movement onset and between 3 to 5 Hz, as suggested by Bönstrup and colleagues) shows major activity, especially during movements of the paretic limb. The overall pattern of spectral activity resembles that shown in previous works, especially the increase and decrease of low-frequency power in relation to the EMG onset and the decreased activity at higher frequencies (9 Hz) during the movement (Bönstrup *et al.*, 2019; Ramanathan *et al.*, 2018). Since we show a larger time window before and after EMG onset we see activity around 5 Hz just before the onset of LFO_{TR} ramp-up (left end of black box in fig. 4.3). Moreover, the activity during movements of the unaffected limb diminishes quicker than during movement attempts of the paretic limb. We contemplate two potential explanations: Firstly, the EMG onsets of the movements of the unaffected limb are precisely timed. Those of the paretic limb are estimated from the individual average latency of movements of the unaffected limb of each patient. This might lead to temporal blurring of the true onsets, which in turn eves out power in the low frequencies when averaging across all subjects. Secondly, the fixed ratio between frequency and time during computation of the time-frequency representation leads to lower temporal (higher spectral) resolution in the lower frequencies and lower spectral (higher temporal) resolution in the higher frequencies. We did not adjust the time-window and frequency range of interest for the averaged comparisons of LFO_{TR} to encompass the observed differences for the benefit of making our results comparable to those of the previous works.

Bönstrup et al found a propagation of LFOs from posterior to anterior locations, which they interpreted as a further argument for LFOs as a top-down rather than a bottom-up process. In an analysis of four channels at frontal, central, posterior and occipital sites we found a similar pattern (fig. 4.12).

4.4.2 Differences of LFOs due to interhemispheric balance and cortical integrity

The previous studies cited above have reported that LFOs were significantly diminished comparing acute stroke patients and healthy controls. Here, we add to this comparison

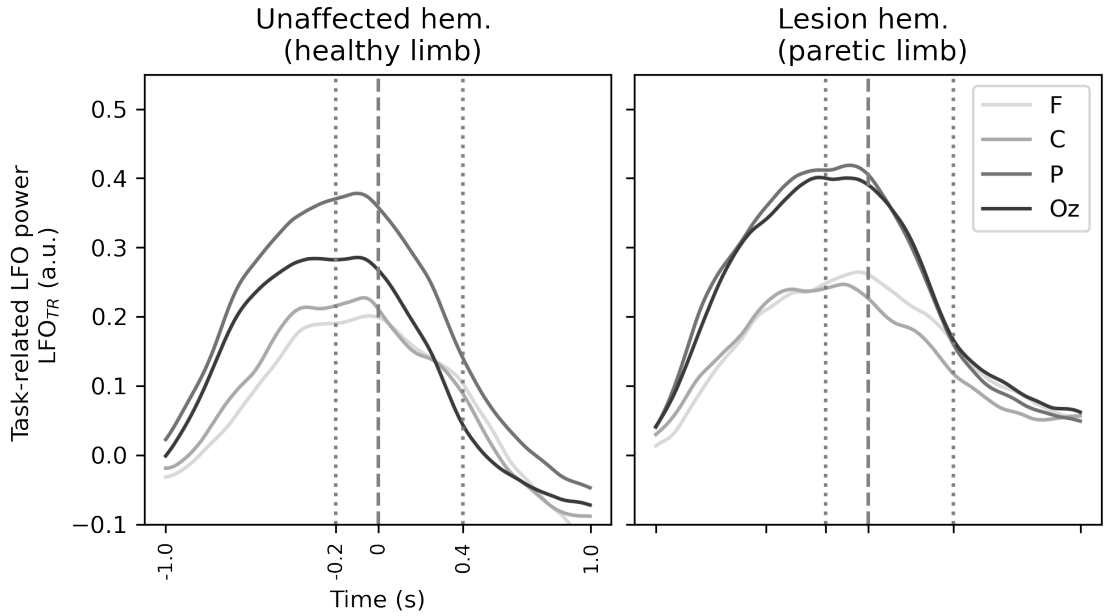

Figure 4.12: Average time-courses of LFO power at frontal (F3/4), central (C3/C4), posterior (C3/C4) occipital (Oz) sites.

by also showing within-subject differences during movements of the ipsilateral and contralateral limb on either hemisphere. We did not find a significant difference of average LFO_{TR} between the hemisphere of the lesion and the healthy hemisphere during the respective contralateral movement. However, while the time-courses of the activity during movements of the unaffected limb are smooth and steady between *pre* and *post*, the ones on the hemisphere of the lesion during paretic movement attempts are not. Inter-subject differences might be one reason. Nevertheless, the difference between *pre* and *post*, which is not present during movements of the unaffected limb (on both hemispheres), might stem from processes in networks unique to movements of the paretic limb on the hemisphere of the lesion.

It would be interesting to compare this observation to bi-hemispheric data in acute patients to see if a similar activation pattern is also visible on the hemisphere of the lesion during movements of the healthy limb. The re-emergence or increase of the LFOs after the intervention, or the difference between *pre* and *post*, might be a marker of plasticity due to the training in the chronically paralyzed stroke patients.
Our analysis based on the type of the lesion (subcortical or subcortical and cortical), suggests that the latter is not a factor that influences LFO_{TR} in the different conditions. However, the number of patients in the groups is small and interpretation of this result has to be cautious.

Investigation of the change of the bihemispheric balance of LFO power during movement attempts of the paretic limb showed a Gaussian distribution around 0 (balanced

power) slightly skewed towards the unaffected hemisphere at post. The patients around the center (balanced LFO power) show the largest motor improvements. Those in the extremes show lower improvements. This observation is in line with the plots of the LFO time courses where we saw that LFO power is similar on both hemispheres during the movement of the healthy limb.

4.4.3 Influence of the intervention on low-frequency oscillations

The patients of the experimental group (C+) (who received contingent proprioceptive feedback during the intervention during the self-induced - by increased event related desynchronization of the ipsilesional brain - movement of the orthosis) contributed most to the changes of LFO power. The control group (sham) did not show significantly different LFO power during the time and frequency range of interest. It has been previously reported that LFO re-emergence accompanied recovery. Moreover, the magnitude of the LFO power increase was found to be higher in patients with more recovery (Bönstrup *et al.*, 2019). Interestingly, our finding suggests the contingency of feedback as the factor that differentiates patients which had significantly different LFO power time-courses before and after the intervention on average and those that did not. The random feedback that the sham group received might have not led to any or minimal changes in the brain circuits responsible for generation of movement-related LFOs. The contingent feedback that the other patients received, on the other hand, might have led to plastic changes within the networks generating LFOs preparing movements of the paretic limb. Influence of the intervention on other oscillations in this dataset has been investigated before (Ray *et al.* (2020), chapter 2). The C+ patients were also those who improved motor function most in the original trial (Ramos-Murguialday *et al.*, 2013).

From the perspective of LFOs as a biomarker, it is worthwhile noting that the initial low-frequency oscillations predict their change throughout the intervention. Those patients with lower initial LFO power have more potential for increasing LFOs throughout the intervention. If LFO power is an indicator of the damage to the motor networks, which is still under debate, the intervention might yield a larger "repairing" effect on the network for those patients with lower LFO power. However, the results presented must be interpreted cautiously because the correlation found is weak.

4.4.4 Limitations and methodological differences

One goal of the present work was to generalize previous findings in human acute and subacute stroke to chronic stroke. Therefore, we tried to employ similar methodology and parameters as Bönstrup and colleagues where applicable.

One methodological difference is the use of a cued self-paced hand opening and closing task instead of a gripping task. None of the patients participating in this study could actively extend the hand, and most of them were not able to reliably generate EMG activity related to the hand movement before intervention. A gripping task was thus not

applicable, and neither was calculation of a precise movement onset in the EMG of the paralyzed limb possible. Even though some of the participants might have been able to forcefully flex fingers, a gripping task would not have been optimal. Some patients can indeed flex their fingers but are not able release the force quickly due to spastic muscle tone. The movement chosen here was extension (or more precisely, extension attempts) followed by flexion of the fingers (and repeated in a self-paced rhythm for five seconds). This design allows for comparison between the patients because none of them could actually perform the first type of movement. However, despite the use of a different movement type comparison to the study by Bönstrup and colleagues and Ramanathan and colleagues is still valid since many properties of movements are subsumed and reflected in low-frequency oscillations (Bansal *et al.*, 2011; Mollazadeh *et al.*, 2011). Furthermore, our protocol could be potentially generalized to the less impaired patients.

In addition to the movements the patients tried to perform with their paretic hand, they performed them with their healthy hand in a separate condition. Movement onsets on the unaffected side were similar for all patients and the shape and range of the time-course of LFO power proved to be very similar to results presented before (Bönstrup *et al.*, 2019). On the other hand, EMG onsets of movements of the paretic side were detected much later (if possible at all). Instead of resorting to the cue as defining anchor-point for computation of LFO power we mirrored the mean EMG onset latency from the healthy arm of each individual to the paretic movement attempts.

Another methodological difference is the use of sensor-space data instead of localized sources. The availability of only 16 EEG channels limits the applicability of source-localization algorithms. We limit our main analysis to only one sensor directly over the motor cortex. Due to the direct computation of LFO_{TR} through time-frequency representations of the data avoiding distortion of the data by application of filters and appropriate baseline correction we believe that the results are comprehensible and comparable.

4.4.5 Concluding remark

LFO_{TR} can be an interesting biomarker of stroke and recovery, as argued in the work of Bönstrup and colleagues despite the correlations reported in that work not being particularly strong. Nonetheless, we show here that the intervention had an effect on low-frequency oscillations. The power was increased at *post*. This work adds to the very interesting predecessors that LFOs also change in chronic patients (with severe paresis). A similar investigation in a larger cohort might shed more light on this effect and correlations to recovery might yet be uncovered in this patient group.

Chapter 5

Coherent oscillations in stroke

5.1 Introduction

Brain function relies on localized and large-scale activity of neurons in ensembles and networks. The concept of connectivity is an umbrella term comprising all measures that capture the interaction within these networks. It can be measured using various recording modalities on different scales in space and time (Horwitz, 2003). The correlation of EEG signals from different brain sites in the frequency domain is termed coherence and is a common basis for electromagnetic connectivity measures of interaction of different brain areas.

Unilateral limb movements rest upon a complex network of inhibititory connections between and excitatory connections within the hemispheres that is disrupted after stroke. Studies employing various imaging techniques such as FMRI (Grefkes *et al.*, 2008; Rehme *et al.*, 2011; Wu *et al.*, 2011; Pellegrino *et al.*, 2012) and stimulation techniques such as TMS (Murase *et al.*, 2004) show that multiple mechanisms are involved in motor deficit after stroke. Inter- and intrahemispheric networks play a role and changes of these networks could promote recovery. Interventions such as bilateral movement therapy (Cauraugh and Summers, 2005) and bihemispheric brain stimulation (Lindenberg *et al.*, 2010) point in this direction and were already shown to induce limited recovery in chronic stroke patients with residual movement.

Recent studies have shown that connectivity features extracted from EEG recordings predict motor recovery in the acute, subacute and even in the chronic phase to some extent (Nicolo *et al.*, 2015; Pichiorri *et al.*, 2015; Pellegrino *et al.*, 2012). Functional changes due to lesions have been described (Aerts *et al.*, 2016). Further exploration of connectivity mechanisms in the chronically and severely impaired is still lacking and might shed some light on the processes of functional recovery in these patients.

This chapter presents the effort to extract neurophysiological connectivity measures from brain activity of the chronically and severely impaired. The patients analyzed all underwent a BMI-based rehabilitation training (Dataset 1, section 1.3.1). The training rewarded ipsilesional desynchronization of the sensorimotor rhythm while they tried to move their paretic limb. The training produced functional recovery and an ipsilesional increase in brain-activity, as shown by fMRI (Ramos-Murguialday *et al.*, 2013). The

goal of the analysis was to better understand and predict rehabilitation outcome. The hypothesis was that the proprioceptive neurofeedback is associated with a decrease in effective connectivity towards the lesion. That means that the unaffected hemisphere carries less inhibition towards the hemisphere of the lesion during movement attempts, which would lead to higher ipsilesion activation. Furthermore, connectivity is key to sensorimotor integration during learning and performance of a motor task (Schoffelen *et al.*, 2005; Womelsdorf and Fries, 2006). Motor improvement reflects learning. We thus hypothesized that measures of brain connectivity correlate with motor recovery.

5.2 The parametric approach

5.2.1 Methodology

Connectivity can be assessed using different imaging techniques and is most frequently used with fMRI, MEG and EEG. For electromagnetic signals, there is a plethora of connectivity metrics with different characteristics. Dynamic Causal Modelling, Phase Locking Value and Partial Directed Coherence are popular examples that all have different characteristics (Sakkalis, 2011). The focus of this investigation were unilateral limb movements, which depend on directed influences from one hemisphere to the other. The Phase Locking Value assesses the synchronization of the phase of two signals, which is inherently non-directional. Dynamic Causal Modelling would allow for assessment of direction. However, it also requires the definition of model parameters for describing the neural physiology. This is difficult in the case of stroke where the lesion has disrupted communication within the brain on all scales.

Partial Directed Coherence

Partial Directed Coherence (PDC) is a data-driven approach that enables observation of directional interactions among brain regions (Baccalá and Sameshima, 2001). It does not depend on a neurophysiological model and choice of appropriate parameters and it accounts for volume conduction by taking the influence of all signals under consideration. PDC essentially measures covariation of time-series based on frequency domain testing of Granger causality, a method from econometrics. A time-series x is defined to "Granger-cause" another series y if the knowledge of the past values of x improves prediction of y. The series y on the other hand does not necessarily "Granger-cause" x. PDC extends previous directed coherence measures to more than two sources and is defined as (Baccalá and Sameshima, 2001):

$$PDC_{ij}(f) = \frac{\bar{A}_{ij}(f)}{\sqrt{(\sum_k |A_{kj}(f)|)^2}} \tag{5.1}$$

This formulation is based on the description of the EEG activity as a multivariate autoregressive process (MVAR). The matrix in the numerator is

$$\bar{A} = I - A(f) \tag{5.2}$$

The matrix A_r is the matrix of coefficients of the multivariate autoregressive process for timelag r. Each entry of that matrix a_{ij} represents the interaction effect of source j at time lag $n-r$ onto i at the final time lag n (the time lag under observation). In order to arrive at the function $A(f)$ all coefficients a_{ij} are fourier-transformed and the coefficient matrices are summed over all time lags as in

$$A(f) = \sum_{r=1}^{p} A_r e^{-i2\pi fr} \tag{5.3}$$

The $\bar{a}_i$ are entries of $\bar{A}$. The numerator is the "outflow" from channel j to the "sink" channel i. The denominator normalizes the fraction by the total outflow to all sinks k. The values of PDC are within a range of 0 and 1.

Threshold for statistical significance for PDC

We saw in equation (5.1) that PDC relies on the choice of an appropriate model order. In high-dimensional and complex data such as EEG the optimal model order is unknown and high orders might be required to describe the interactions of the multivariate process adequately. However, with increasing model order, larger variability is introduced and detection of causal influences becomes more difficult. Small real influences could be overshadowed by larger random noise and noise could be mistaken for influence. For this reason, Schelter and colleagues have discussed statistical properties of PDC. They showed that PDC yields (random) values of up to 0.15 for an autoregressive process using model order 200 where the real order is only 2. The discussion and this example motivated the presentation of a method for deriving a significance level of PDC. The method is tested on simulated and real data (Schelter *et al.*, 2005).

The statistical properties of PDC are derived from the estimates of the MVAR coefficients. The α-significance level for PDC is approximated by

$$\sqrt{\frac{\hat{C}_{ij}(f)\chi^2_{1,1-\alpha}}{N\sum k(|\bar{A}_{kj}(f)|^2)}} \tag{5.4}$$

The $\hat{C}_{ij}$ represent the noise and the covariance of the MVAR process. The $\chi^2_{1,1-\alpha}$ is the $1-\alpha$ quantile of a χ^2-distribution. N is the number of data points available for estimating the process and the $\bar{A}_{kj}(f)$ are the estimates of the MVAR coefficients. The variable j is the source and i the sink of brain activity currently investigated. The k are all sinks. The main argument brought about by Schelter and colleagues is that commonly used estimates of the MVAR coefficients (such as least squares) are normally distributed. The

sum of their squares is then χ^2-distributed with one degree of freedom, which defines the critical value used in formula (5.4). The derivation of this formula is quite elaborate and not trivial but sufficiently well described for implementation. The reader is thus kindly referred to the original paper for detailed explanation of all steps and the mathematical proof (Schelter *et al.*, 2005).

5.2.2 Application of the parametric approach

The methodology described above has been implemented using Matlab and the FieldTrip open source toolbox (MATLAB, 2020; Oostenveld *et al.*, 2010). The analysis was run on Dataset 1, which comprises longitudinal data of patients activating an exoskeleton with their brain activity to move their paretic arm.

Methods

The following preprocessing was applied to the data of Dataset 1 which was recorded during the intervention (movements of the orthosis) (section 1.3.1). The EEG and EMG channels were high-pass filtered (2 Hz EEG, 10 Hz EMG), notch filtered to remove power line noise and epoched according to the task periods of rest (last 4 seconds of the inter-trial-interval) and movement attempt and BMI control (5 seconds). Additionally, the EMG signals were low-pass filtered (3Hz) and rectified in order to get the envelope of the signal. Eye movement artifacts detected with two EOG channels (vertical and horizontal) were removed from the EEG using linear regression (Schlögl *et al.*, 2007). Muscle activity on the unaffected limb during movement attempt of the paretic arm could influence the brain activity patterns that we wanted to analyze. Hence, trials in which the waveform length extracted from the EMG signal at any location on the nonparetic arm exceeded the baseline EMG threshold (mean EMG during movement preparation phase) by three standard deviations during a period of 250 milliseconds or more were regarded as contaminated by compensatory movement and rejected from posterior analysis. Both EMG and EEG signals were downsampled to 100 Hz.

Cortical connectivity patterns were analyzed in three discrete frequency bands (θ: 3-7 Hz, μ: the individually specified sensorimotor band and the β-band: 14-30 Hz). The analysis of θ corticocortical connectivity was motivated by earlier studies that reported changes in θ intrahemispheric inhibition associated with recovery in stroke patients (Nicolo *et al.*, 2015). The analysis of the β band on the other hand aimed at studying descending corticomuscular pathways that were previously reported to be impaired after hemiplegic stroke (Nielsen and Conway, 2008; Mima *et al.*, 2001). The analysis of the SMR was based on the assumption that frequency bands used during the proprioceptive BMI control of the robotic orthoses might result in connectivity changes in those same frequency bands.

Coherence between channels was assessed by first estimating the EEG activity as a multivariate autoregressive process with model order 15, which has been found suffi-

cient for this application and sampling frequency (Florian and Pfurtscheller, 1995). Afterwards, several cortical connectivity metrics were computed based on PDC (fig. 5.1). The first connectivity metric represented the connectivity of the whole network for which PDC was computed in all EEG channels. Moreover, connectivity within the hemispheres and between hemispheres was computed, only including the channels over the motor areas. For all the measures the number of significant connections between channels within each frequency band was counted to quantify the strength of connectivity. The significance was assessed using the approach of Schelter et al as briefly described above.

Results and challenges

The main finding of the (unpublished) study was a decrease of connectivity within the contralesional hemisphere over the course of the training (Multilevel analysis: $p < 0.05$; Marginal $r^2 = 0.007$; Conditional $r^2 = 0.403$). This effect may contribute to the hypothesized disinhibition of the ipsilesional motor cortex during movement attempts.

After completing the analysis on the longitudinal data (movement attempts during training), I used the same pipeline to analyze data of the *pre* and *post* measurements of Dataset 1. The patients were asked to open and close their hand as cued. EEG was recorded while they performed the task but they were not connected to a brain-machine interface. The hypothesis was that the changes found during the training would also be visible in the *post* test.

Inclusion of this additional data lead to surprising and unclear results. The units of the data were different than those of the data of the training (mV instead of V). The scale does not matter for estimation of the MVAR coefficients since the parameter estimates and noise covariance are also scaled. However, this was not the case as the covariance of the noise seemed to depend on the order of magnitude of the input data in the MVAR estimator of the Fieldtrip toolbox. This lead to a propagation of errors and caused a mismatch between the coherence values and the significance threshold values computed.

This discovery firstly called the results obtained so far in question. Furthermore, it motivated a closer investigation of the significance threshold method proposed by (Schelter *et al.*, 2005), which is described in the next section.

Example

The following equation system defines a multivariate autoregressive process as presented in (Schelter *et al.*, 2005). Figure 5.2 shows the structure of the process.

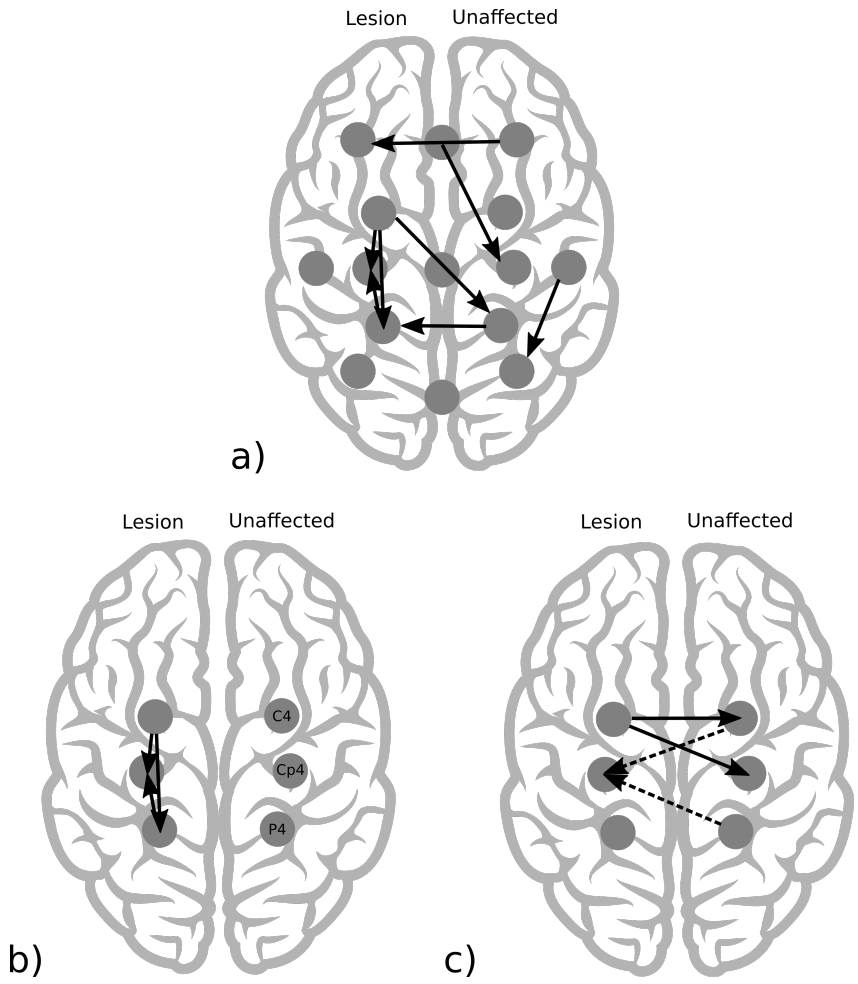

Figure 5.1: Connectivity metrics assessed in the analysis using PDC in pairs of channels. A) All channels in the network. B) Channels within one hemisphere (restricted to motor areas). C) All connections from one towards to other hemisphere (restricted to motor areas)

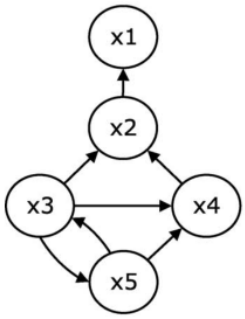

Figure 5.2: Flow chart of the nodes and their influence onto each other within the simulated system. (taken from Schelter *et al.* (2005))

$$
\begin{aligned}
x_1(t) &= 0.6x_1(t-1) + 0.65x_2(t-2) + \varepsilon_1(t) \\
x_2(t) &= 0.5x_2(t-1) - 0.3x_2(t-2) - 0.3x_3(t-4) + 0.6x_4(t-1) + \varepsilon_2(t) \\
x_3(t) &= 0.8x_3(t-1) - 0.7x_3(t-2) - 0.1x_5(t-3) + \varepsilon_3(t) \\
x_4(t) &= 0.5x_4(t-1) + 0.9x_3(t-2) + 0.4x_5(t-2) + \varepsilon_4(t) \\
x_5(t) &= 0.7x_5(t-1) - 0.5x_5(t-2) - 0.2x_3(t-1) + \varepsilon_5(t)
\end{aligned} \tag{Ex1}
$$

Figure 5.3 shows a matrix of figure panels of the original publication. The panels on the diagonal show the power spectral density of the individual components (auto-spectra). The other panels show the spectra of PDC of the component identified by the column j on the component identified by the row i. The plots illustrate the strength of directed influence in each frequency band from one node (j) to the other (i).

The peaks in the auto-spectra reflect the number of upstream nodes influencing the current node. The PDC spectra correctly reveal which nodes influence which other nodes. It is noteworthy that the captured influence is exclusively direct. Indirect influence, e.g. from node 3 to node 1 via node 2 is disregarded by PDC, a feature that is valuable for the analysis of activity of brain networks.

In the following I show that the results of the examples obtained and presented by Schelter and colleagues cannot be replicated. I generated 50000 samples of data from the MVAR process (eq. (Ex1)) using python (generated with the code in listing 12). The data is evaluated three times: (1) with the known coefficients of the data in python (fig. 5.5), (2) with the Matlab pipeline used in the analysis presented above and the correct model order (fig. 5.4) and (3) with the python VAR function (estimation of MVAR coefficients of the statsmodels toolbox using the correct model order) (fig. 5.6). All approaches yield similar results. However, none of them exactly reflects the example presented in the original paper.

The structure of influences is generally captured. There is one exception, which is a

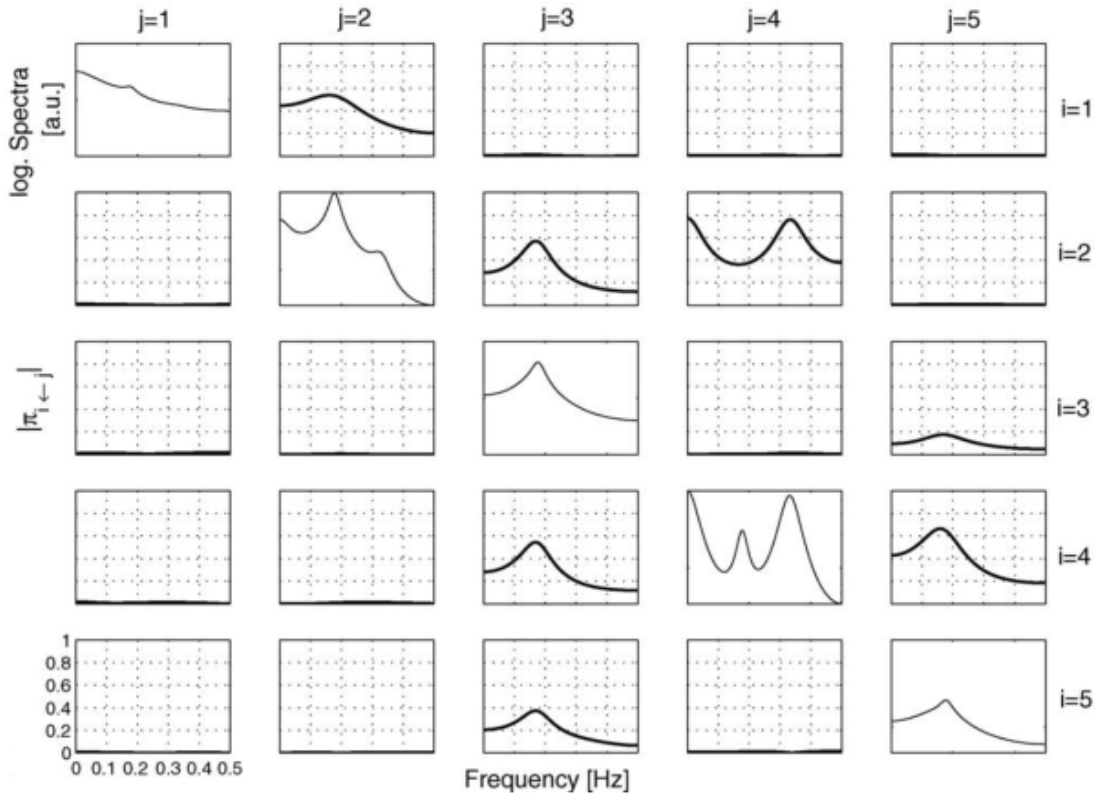

Figure 5.3: Matrix of auto-spectra and Partial Directed Coherence of the MVAR process of equation (Ex1) (taken from Schelter *et al.* (2005))

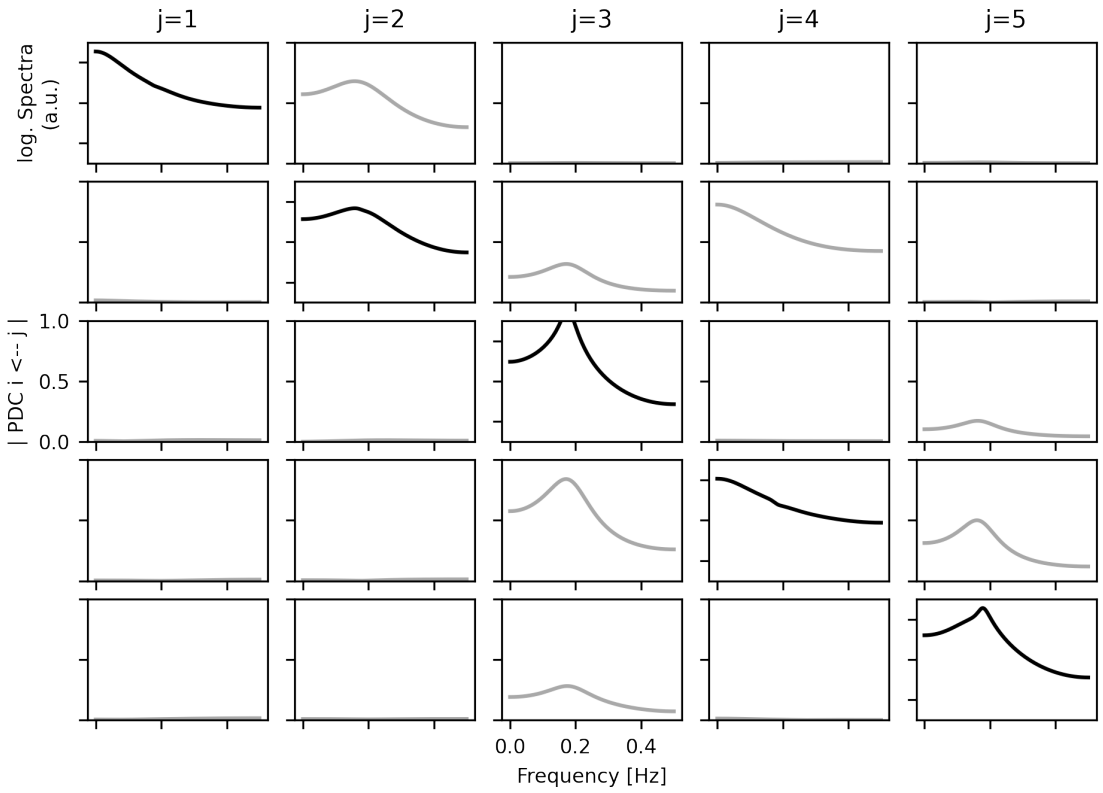

Figure 5.4: Matrix of auto-spectra and Partial Directed Coherence of the MVAR process of equation (Ex1). Evaluated in python with the known coefficients (exact reproduction)

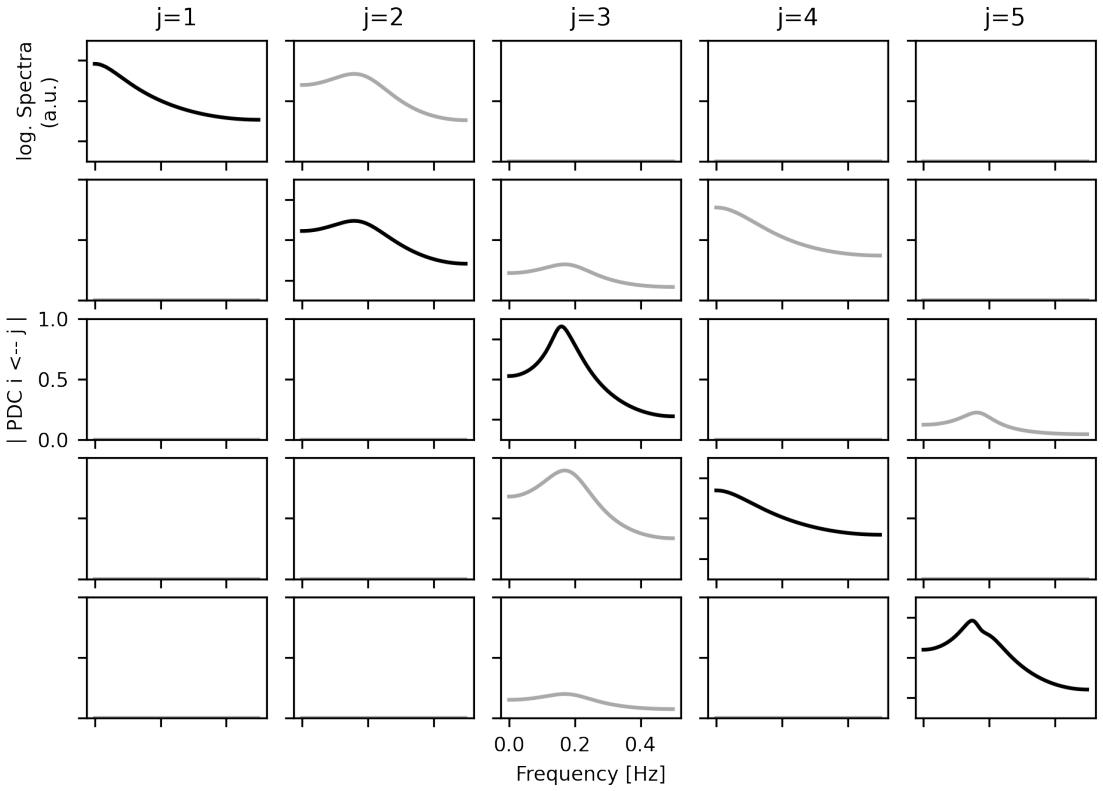

Figure 5.5: Matrix of auto-spectra and Partial Directed Coherence of the MVAR process. Evaluated using the MVAR estimation procedure of Fieldtrip in Matlab.

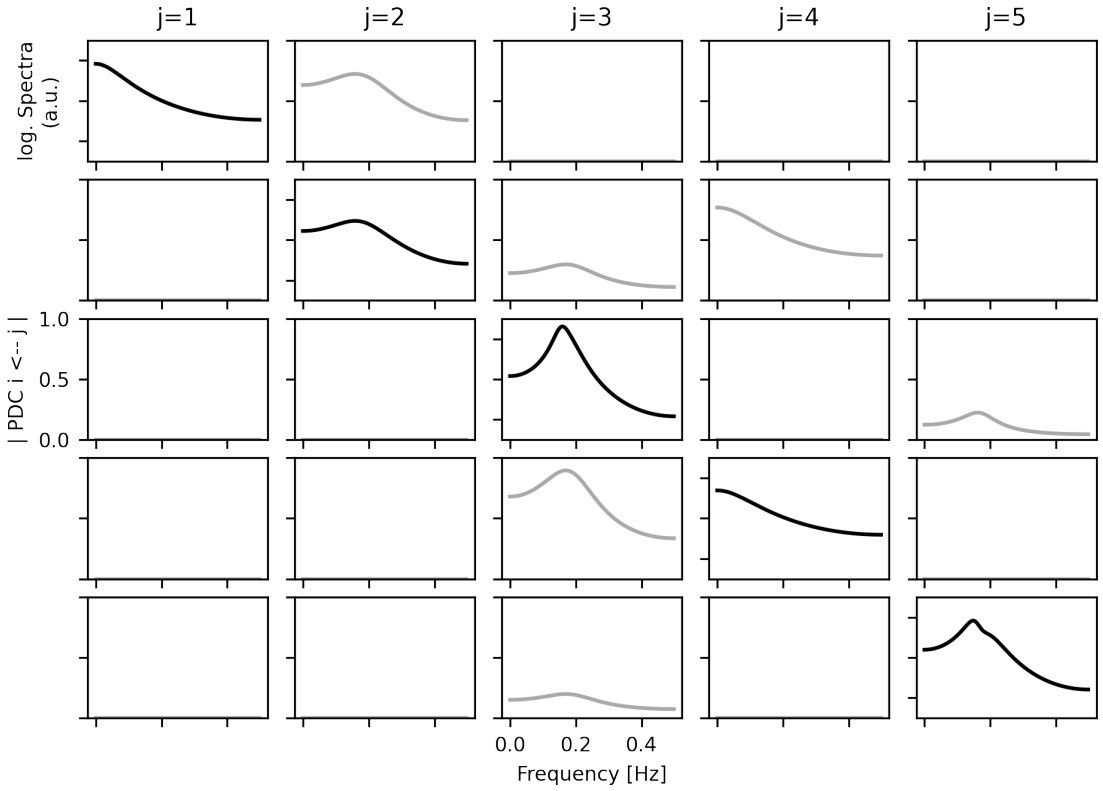

Figure 5.6: Matrix of auto-spectra and Partial Directed Coherence of the MVAR. Evaluated using the VAR estimation procedure of Python Statsmodels.

missing double peak at 0.4 Hz showing the influence of node 4 onto node 2. Furthermore, the peaks in the auto-spectra are not exactly reproduced. In node 4, for example, the original figure shows two distinct peaks that are missing in all other estimations.

The reason for the failed exact replication of the example in the paper could be a small mistake in the equation system provided (mismatch between the equation system describing the MVAR process and the estimation of the process). Schelter and colleagues did not provide details on how the MVAR was estimated for their examples. There might be a difference in their method and the methods used here. However, it is unlikely that two widely used MVAR estimation procedures (Matlab Fieldtrip and Python Statsmodels) both contain errors leading to the observed difference. Despite the differences, the example can be largely reproduced and the example data can be used for evaluating the method of computing the significance threshold.

In the next exemplary analysis I tried to validate the implementation for the computation of the significance threshold. Schelter et al present a model of order 200 fitted to the MVAR process described in equation (Ex1). The model order is much greater than the actual order of four. Therefore, the spectra are noisy (fig. 5.7). The significance threshold is shown in the panels of the PDC spectra.

In the analysis of coherence presented above the proposed method was implemented in Matlab following the algorithm described in the original paper precisely. I implemented the algorithm again in Python for validation of function and comparison of performance and plotted the resulting PDC spectra (fig. 5.8).

Again, the results of Schelter et al could not be reproduced exactly. The structure of node influences in the original MVAR process is largely captured by the PDC and the auto-spectra are comparable with the exception of node 4. The significance threshold estimation showed (grey lines) is similar to the ones in the original paper in the lower frequency ranges and captures the characteristic dip around 0.19 Hz (seen in fig. 5.7 and fig. 5.8, e.g. in node 3). More importantly, though, the significance threshold ramped up in all PDC spectra towards the higher ranges of the frequency bands considered. The reason for this behavior remained unclear. A potential culprit is the inversion operation that might introduce small numerical errors but this is speculation.

In summary, the replication study presented here called the applicability of the whole parametric pipeline in question and showed two main disadvantages. Firstly, the estimation of the MVAR process is dependent on a good choice of model order, which is difficult. If the order is too low, some dynamics of the signal might be missed. If the model is too high noise might be amplified (Sakkalis, 2011).

Secondly, the computation of the significance level was not reliable. Moreover, the significance level is pointwise, so some random crossings will occur, especially with high model order. This is seen in the examples of the original paper (fig. 5.7, e.g. node 5 on node 2). On top of that, the computational demand of the approach should not be underestimated. It proved to be substantial because some operations of the algorithm functions used four nested for-loops ($O(n^4)$, where $n = max(number\ of\ nodes,\ model\ order)$). Optimization techniques such as just-in-time-compilation for the python code improved

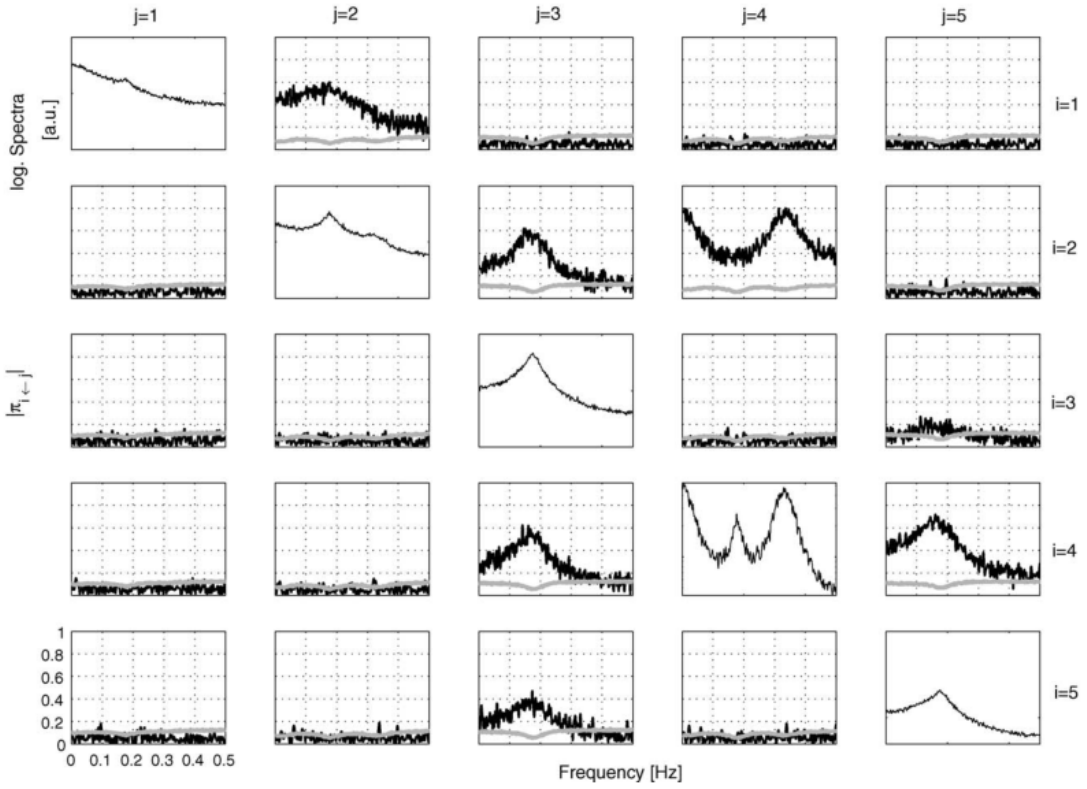

Figure 5.7: Matrix of auto-spectra and Partial Directed Coherence of the MVAR process of equation (Ex1). Model order is 200. The grey lines represent the frequency-dependent significance threshold of PDC (taken from Schelter *et al.* (2005)).

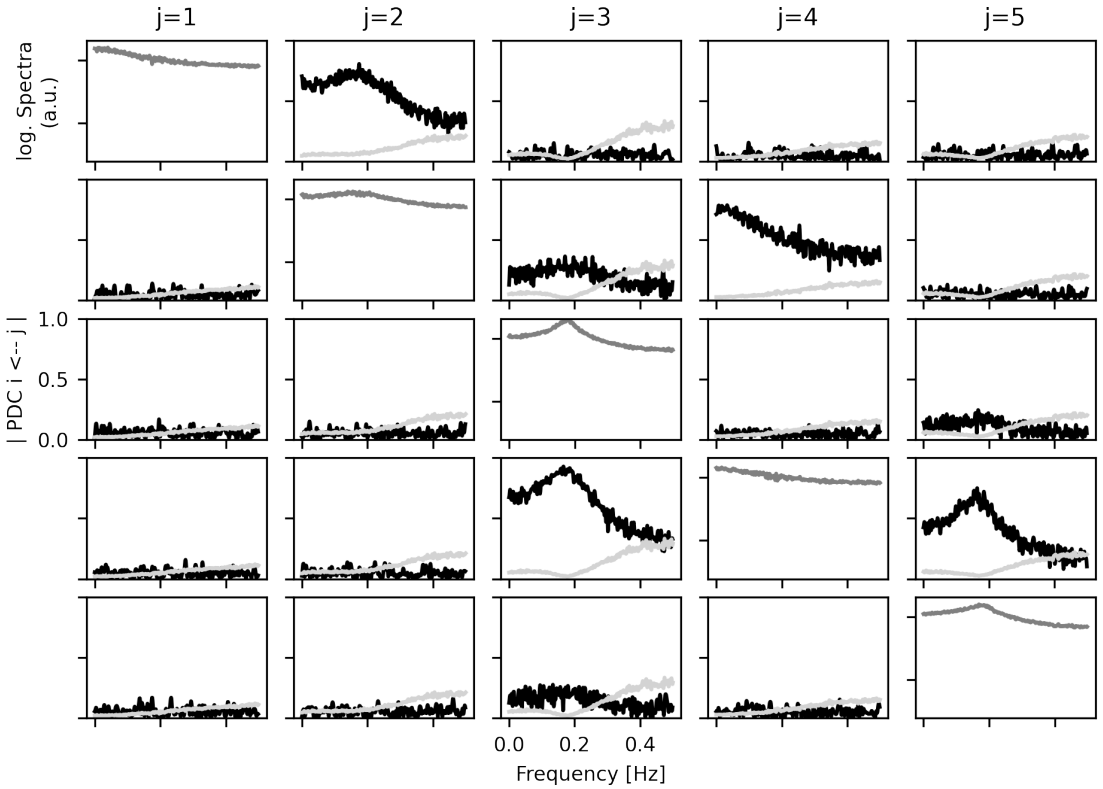

Figure 5.8: Matrix of auto-spectra and Partial Directed Coherence of the MVAR process. Model order is 200. The grey lines represent the frequency-dependent significance threshold of PDC as computed with my implementation of the algorithm of Schelter et al.

performance (see listing 14 for an example).

These disadvantages motivated the implementation and application of a different approach to the problem of assessing connectivity during movement in chronic stroke: A non-parametric approach.

5.3 The non-parametric approach

The key quantity of multivariate spectral analysis is the spectral matrix that relates the spectra of different channels. This matrix is the source for deriving power and coherence. In the parametric approach, as we have seen in the previous section, the data is described as a multivariate autoregressive process. The model transfer function and the noise covariance matrix are obtained from the model and used for deriving coherence. The non-parametric approach employs Fourier transforms of the data directly, which yields the spectral matrix. In order to derive coherence, the spectral matrix is factorized for obtaining the transfer function and the noise covariance matrix (Dhamala *et al.*, 2008).

The methodology is briefly described in the next section. It follows a publication of Dhamala, Rangarajan and Ding (Dhamala *et al.*, 2008).

5.3.1 Methodology

PDC derived from the Cross Spectral Matrix

The cross spectral matrix is computed from the data using either Multitapers or Wavelets. The multitaper spectral and cross-spectral method provides smooth estimation of spectral density (Dhamala *et al.*, 2008).

The estimate of the cross-spectrum between two channels l and m at frequency f is:

$$S_{lm}(f) = \frac{\Delta}{K} \sum_{k=1}^{K} \{ \sum_{s=1}^{n} w_s(k) x_{ls} e^{-i2\pi f s \Delta} \} \{ \sum_{t=1}^{n} w_t(k) x_{mt} e^{i2\pi f t \Delta} \} \tag{5.5}$$

The time-series of the two channels are multiplied by orthogonal tapers w and the result is Fourier transformed. These transforms are then cross-multiplied and averaged over tapers K of length n. The procedure is repeated for multiple realizations (i.e. trials) and averaged over these, too. Repetition for all channel combinations yields the cross-spectral matrix $S(f)$.

In the next step the noise-covariance matrix and the transfer function needed for computation of PDC are derived by factorization of the spectral matrix such that

$$S(f) = H(f) \Sigma H^H(f) \tag{5.6}$$

where H is a minimum-phase transfer function and Σ is the noise covariance matrix.

These quantities can be used in the formulation of the PDC, where the total power of a channel is put into relation to the intrinsic power (i.e. the total power minus the causal contribution of the other channel).

The equations are taken from the publication and for more details the reader is referred to (Dhamala *et al.*, 2008). For the analyses performed in the following, a readily available implementation was used. The open-source toolbox *Spectral Connectivity* follows the methodolgy of Dhamala and colleagues. For spectral matrix factorization the numerically stable algorithm of Wilson is implemented in the toolbox (Eden and Kramer, 2020).

I validated the implementation of Eden and Kramer using the autoregressive process shown above.

Example

Figure 5.9 shows the auto-spectra and the PDC spectra of the example process given by equation (5.5). The spectra were estimated using the implementation of Eden and Kramer of the non-parametric methodology proposed by Dhamala and colleagues. The result is similar to the ones obtained before using the parametric approach. The auto-spectra are even closer to the ones originally shown by Schelter et al than with the Matlab and Python implementation shown above.

Significance threshold

The final step of the methodology is computation of a significance threshold for PDC. Instead of deriving the threshold from the properties of the distribution of the estimates of the MVAR coefficients, significance is evaluated comparing two different conditions. In the EEG data of interest (Dataset 1) two appropriate conditions are available for comparison: Each movement attempt of the paretic limb is preceded by an inter-trial interval during which the patients did not have a specific task. Significant PDC in adjacent frequency bins during the movement attempt is thus defined as a significant difference to a "PDC noise floor" computed on the unspecific condition. This comparison is carried out using a permutation clustering procedure (Maris and Oostenveld, 2007). The difference of PDC is expressed in terms of t-values (i.e. the difference relative to the variation across all trials) (fig. 5.10b). PDC is computed twice for each trial: Once for the movement period and once for the period before the audiovisual cue in which the patients did not have a specific task other than avoiding movements. PDC computed in the first part of the trial is considered random, since no task was given. These t-values are thresholded at the 95-percentile of the distribution of all differences of the sample under investigation. The remaining frequency bins are clustered if they are located in adjacent bins. The sum of the t-values in the largest cluster is the test statistic used for the permutation test with 1000 repetitions where the labels of the condition (PDC_{mov} and PDC_{notask}) are randomly flipped for each sample. The procedure yields a distribution of summed t-values that is

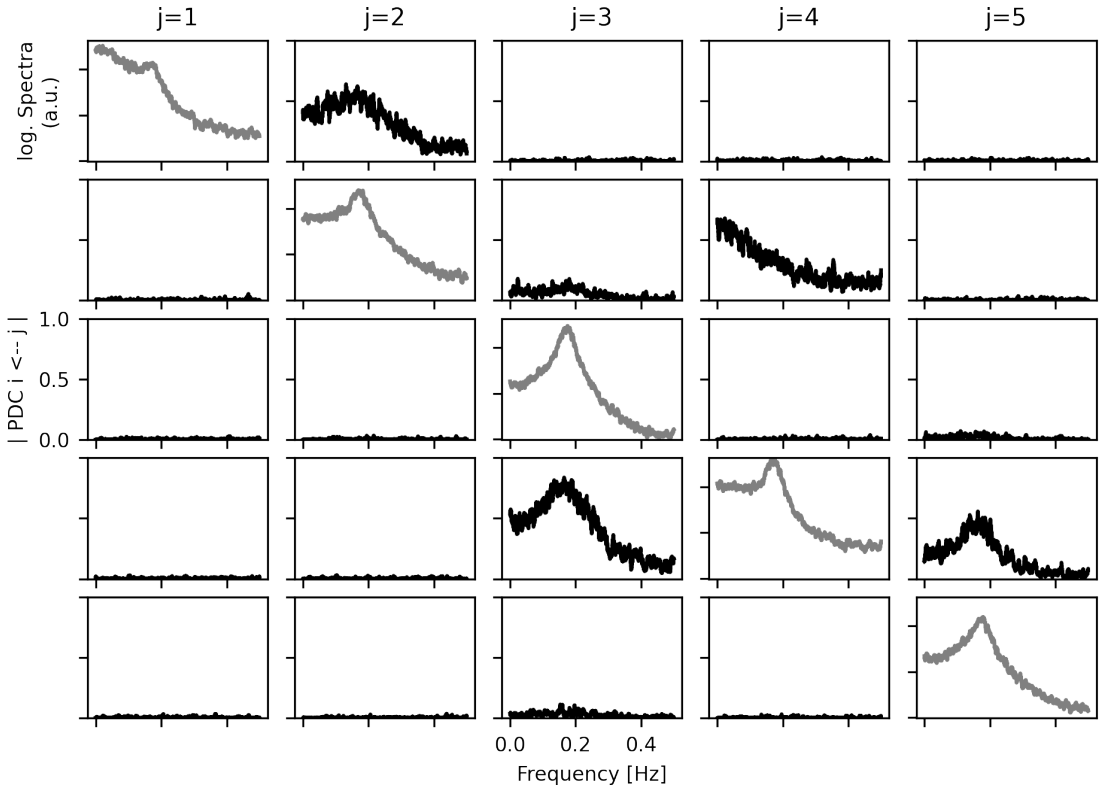

Figure 5.9: Matrix of auto-spectra and Partial Directed Coherence of the MVAR process. Evaluated using the non-parametric approach.

used for testing if the actual PDC value of the movement attempts are above the noise floor (i.e. above the 90-percentile of the t-distribution). The frequency bins within the clusters that fit this criterion are considered statistically significant clusters showing Partial Direct Coherence in the direction of the channel pairs, e.g. from channel C3 towards channel C4 (fig. 5.10c).

Compared to the parametric approach this methodology depends on larger computational resources because of the spectral matrix factorization and the permutation clustering. However, these resources are readily available nowadays and the advantages of not having to guess the model order and having a more reliable significance threshold make up for the increased computation time.

5.4 Application of the non-parametric approach to Dataset 1

After validation of the non-parametric approach using the examples the methodology was used in the data of Dataset 1 that was recorded at the *pre* and *post* screening: Opening (attempts) of the patients' hands. Preprocessing of the EEG data was performed similarly to section 5.2.2. The main purpose of this investigation was to describe changes of three connectivity measures during movement attempts of the paretic limb of the patients from *pre* to *post* intervention. Figure 5.11 shows the connectivity metrics evaluated here.

Figure 5.12 shows the extracted PDC and the significant PDC values obtained using the non-parametric methodology. In the multi panel plot each row of panels represents one connectivity measure and the columns represent the conditions pre and post. The panels show PDC in the frequency bins from 0.1 to 50 Hz for the channel combination of interest (e.g. Directed Coherence from channel C3 to channel P3). The thick parts of the lines mark all those frequency bins within which PDC is significant.

5.4.1 Results

The significant PDC values were extracted and counted. The resulting histogram is shown in figure 5.13. Both the alpha and beta frequency ranges are well represented. There are also some clusters in a lower range (θ, from 3 to 6 Hz). The number of significant clusters in the higher β band within hemisphere (fig. 5.13, panel on the left) has increased from the *pre* measurement to the *post* measurement, which is in line with previous works, where the association of connectivity in the β band (Nicolo *et al.*, 2015) or more specifically the high β band (Pellegrino *et al.*, 2012; Wu *et al.*, 2015, 2016) and motor recovery have been reported. All frequency bands contribute to interhemispheric connections, however, the α frequency range shows the largest number of clusters (fig.5.13, panels in the middle and on the right). The overall number of interhemispheric connections towards the healthy hemisphere increased during movement attempts of the paretic

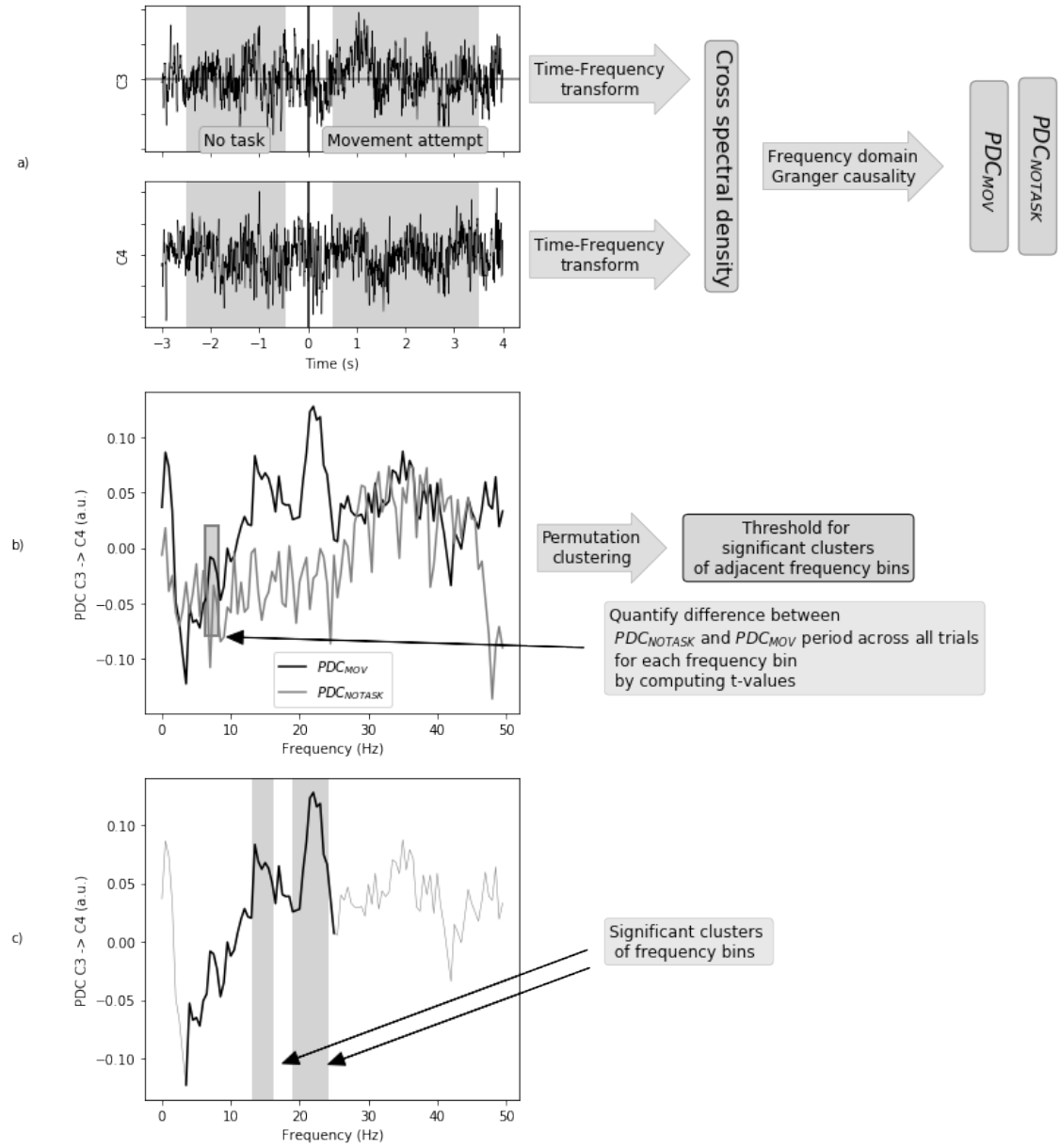

Figure 5.10: Procedure of parameter-free computation of Partial Directed Coherence and significance test
a) Time frequency transforms of data of each channel in the pairing for obtaining the cross spectral density matrix, from which the frequency domain Granger causality (i.e. Partial Directed Coherence) feature is computed for the two periods in the trials
b) Permutation clustering is applied to the difference between PDC during movement attempts and during the "notask" period. This procedure yields a threshold above which clusters of frequency bins are considered non-random contributors to PDC from one channel to the other
c) Significant clusters that are obtained after permutation clustering and subsequent thresholding

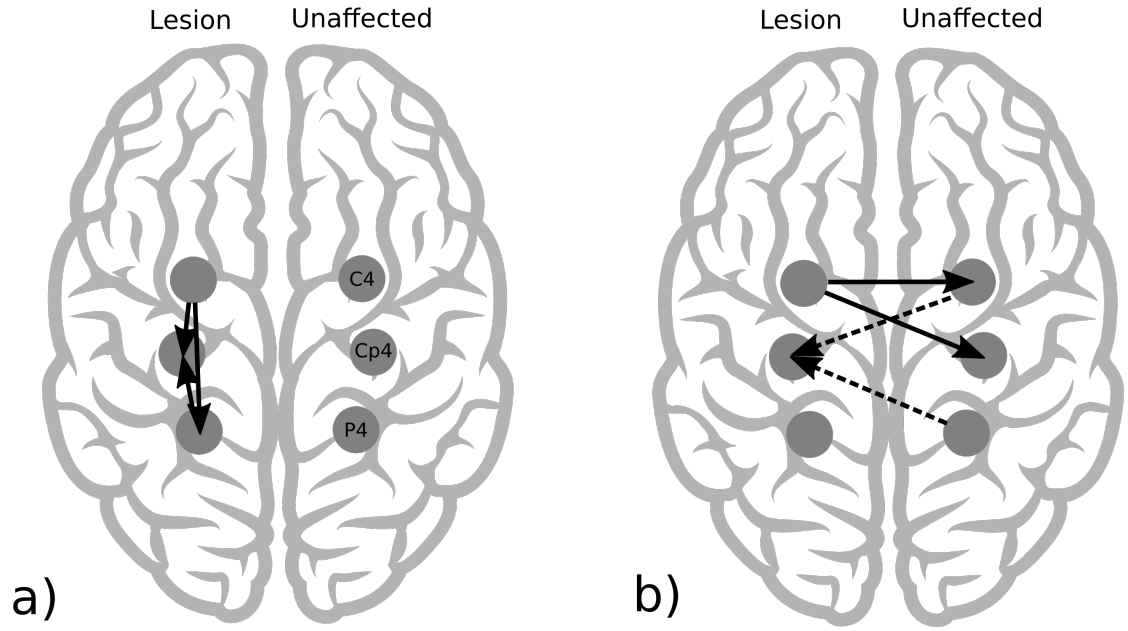

Figure 5.11: Connectivity metrics
Connectivity is quantified by three metrics:
a) Intrahemispheric connectivity within the hemisphere of the lesion is the number of channel pairs showing significant PDC divided by the total number of channel pairings (n = 6).
b) Interhemispheric connectivity is quantified by the number of channel pairs showing significant PDC from one hemisphere to the other divided by the total number of channel pairings (n = 9).

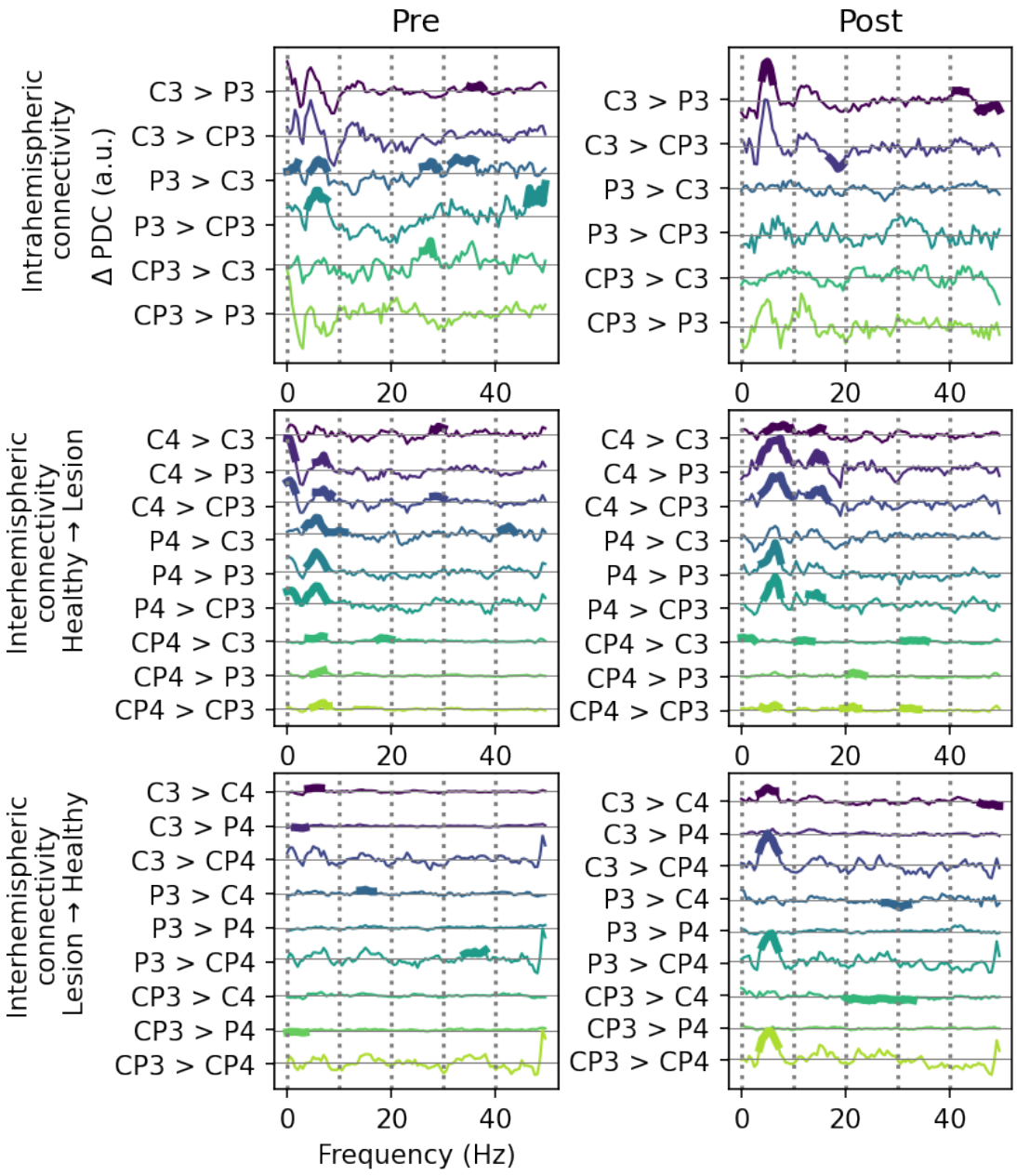

Figure 5.12: PDC and significant PDC values at *pre* and *post* for each channel pair of the connectivity measures for a representative subject. PDC was extracted between 0.1 and 50 Hz.

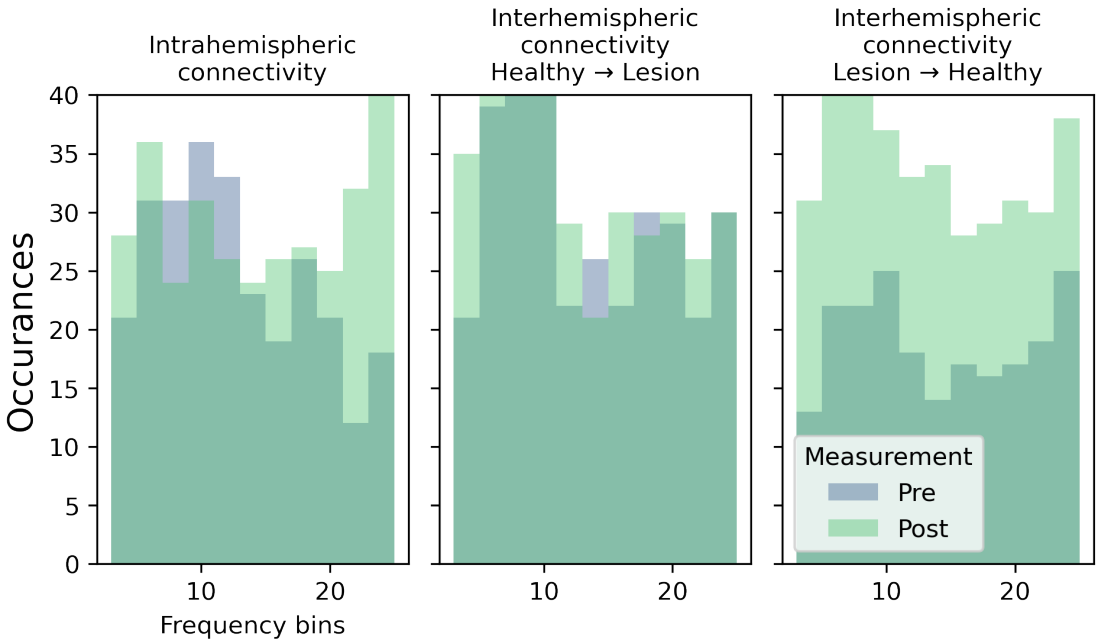

Figure 5.13: Histograms of frequencies that were part of significant clusters of partial direct coherence during attempted movement of the paretic limb (in all patients).The columns represent the three connectivity measures.
Each bar represents the number of frequency bins that were part of any significant cluster between two channels. The grey bars mark the number of bins at pre. The light green bars mark the number of bins at post. The dark green color represents the overlay between both conditions.

limb from the *pre* to the *post* measurement. The ratio of the contributions of the bands, α and upper β seems to stay similar for both. The largest increase of the number of significant clusters is in the α frequency range and in the high β range (fig. 5.13, panel on the right). This finding could mean that communication from the hemisphere of the lesion inscreases, indicating inhibition carried towards the healthy hemisphere and thus facilitating movements of the paretic limb controlled by the ipsilesional hemisphere.

5.4.2 Concluding remark

After discovering the pitfalls of the method that was implemented in section 5.2 the main focus of this work was implementing and testing a different valid approach for extracting (directed) connectivity measures while being able to assess significance of the strength of the connections. The first descriptive results obtained with the non-parametric processing pipeline encourage future research. Firstly, the general structure of the connections between the nodes (i.e. the channels) should be described at *pre* and *post* and potential

changes investigated. Secondly, potential changes should be quantified and tested statistically. Finally, a comparison between these patients and healthy volunteers performing the same task would underline significance of the changes found.

Chapter 6

Electromyographic indices of muscle fatigue in chronic stroke

This chapter was published as (Ray et al., 2019) (peer-reviewed four-page conference paper). Additional data has been recorded between publication and completion of this thesis. The results and conclusions of the paper have been updated accordingly in this chapter. Furthermore, some additional details on the experimental procedures have been added. For disclosure of contributions see section 8.2.

6.1 Introduction

Millions of stroke survivors live with chronically limited motor function or complete paralysis and depend on assistance (Feigin *et al.*, 2016a). Training based on Brain-Machine interfaces is an effective technique promoting motor recovery in these patients (Ramos-Murguialday *et al.*, 2013). Recent works aim at increasing the efficacy of these approaches by way of including non-invasive electromyographic signals (EMG) in the methodology. Decoding of (residual) muscle activity allows for controlling a rehabilitation exoskeleton in multiple degrees of freedom (Sarasola-Sanz *et al.*, 2017).

There are diverse non-physiological and physiological factors influencing the EMG signal and consequently the decoding and quality of the sensory feedback to the patient. A contingent link between neurophysiological signals and the proprioceptive and visual feedback, however, is key for the efficacy of rehabilitation. Muscle fatigue might have a detrimental effect on the EMG decoding accuracy and thus might diminish the quality of the feedback loop. This influence has been considered since the earliest works of BMI-based approaches that combine EEG and EMG for control of an exoskeleton (Enoka and Duchateau, 2008). None of the available works, however, have studied muscle fatigue within a rehabilitation framework for severely paralyzed chronic stroke victims.

Muscle fatigue is a physiological factor that changes the surface EMG signal during muscle contraction. The phenomenon is defined as exercise-induced reduction of the ability of a muscle to produce force (González-Izal *et al.*, 2012). Muscle fatigue may arise on the level of the nervous system, comprising all factors that lead to reduction of the numbers of recruited motor units. It may also arise on the level of the muscles.

During fatiguing contractions biological changes such as increases in metabolite concentrations and altered conduction velocity of the muscle fibers occur. Amplitude and power spectrum of the EMG are influenced by these changes (Sarasola Sanz *et al.*, 2015).

In the following, muscle fatigue in the Deltoid Anterior muscle during forward reaching is characterized. This movement is part of a rehabilitation intervention for chronic stroke patients with severe paralysis of the upper-limb. The change of EMG indices of muscle fatigue during performance of the specific movement used for the rehabilitation training in nine healthy subjects and four severely impaired chronic stroke patient is described. Subsequently, we investigate if the EMG activity of fatigued muscles of the healthy volunteers and the patients changes when performing the movement.

6.2 Methods

6.2.1 Rehabilitation environment

The rehabilitation environment comprises a set of neurophysiological sensors and a rehabilitation robot with 7 degrees of freedom that enables the patients to perform semi-functional multi-joint movements with arm and hand (for more details cf. Sarasola Sanz *et al.* (2015), section 7.2 and 1.3.1). There are multiple movement targets, a screen and a loudspeaker for presentation of stimuli. In this investigation the focus is on frontal reaching movements of the arm (fig. 1a). This type of movement consists of shoulder forward flexion and horizontal adduction as well as elbow extension. Besides Pectoralis Major and the Triceps, the most prominent muscle involved in successful performance of this movement within the training is the Deltoid Anterior muscle.

6.2.2 Muscle fatigue during dynamic contractions

Preparatory experiments confirmed that muscle fatigue indices of the EMG can be measured and quantified during dynamic contractions of the Biceps, replicating findings of others (Rogers and MacIsaac, 2013), (Komi and Tesch, 1979). The healthy volunteers were standing upright and held a dumbbell in their hands (approx. weight 4 Kg). The movement started with the elbow joint in a 90° angle. The lower arm was thus parallel to the floor. Then they initiated self-paced biceps contractions lifting the weight towards their shoulders and back to the starting position. The movement was repeated until exhaution (i.e. the participants could not lift the dumbbell to the shoulders anymore). Muscle activity was recorded from the biceps for data analysis. The movements were also recorded on video for later assessment of posture (compensatory movements), facial expression (indicator of exhaution) and quality of the weight lifting. Since the movements were uncued a moving average on the EMG amplitude was used to determine the beginning of a contraction (troughs in fig. 6.1).

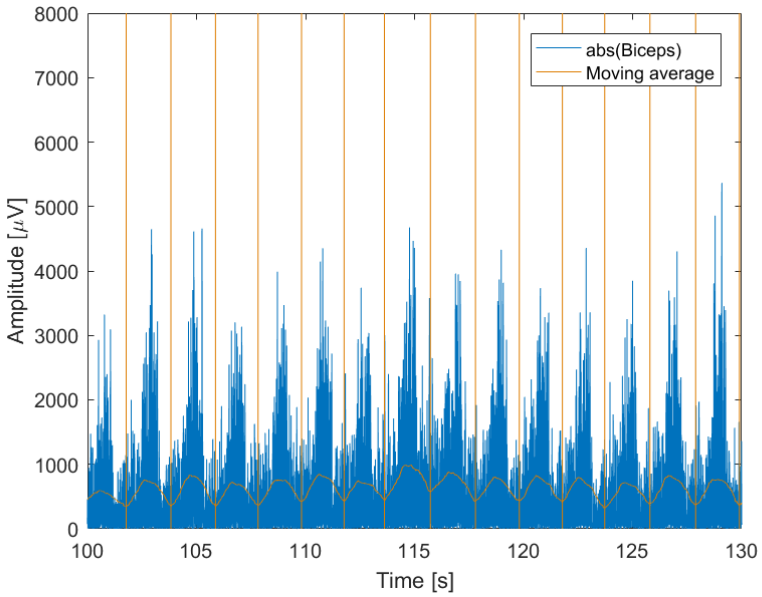

Figure 6.1: A sequence of single dynamic biceps contractions. A moving average filter was used to automatically determine the beginning of a contraction.

6.2.3 Inducing muscle fatigue during reaching movements

In order to investigate muscle fatigue during the rehabilitation exercise, a dynamic frontal reaching movement, a muscle-fatigue apparatus was designed (fig. 6.2). The nine healthy subjects (3 female, 6 male; age 26.8 $\pm$ 2.4, all right-handed, no neuromuscular disorders) performed ten repetitions of the reaching movement with the rehabilitation robot using their left arm. Afterwards they performed reaching movements using the fatiguing apparatus in a predefined frequency until they could not perform the movement anymore or until the maximum experimental time of 25 minutes was reached. The reaching movements with the rehabilitation robot were repeated immediately after muscle exhaustion to avoid recovery.

The chronically impaired patients presented very limited or no active arm and no active finger extension (Age: 52 $\pm$ 9, 1 female, 3 male, Fugl-Meyer score of arm and hand skills: 9.9 $\pm$ 2.9, time since stroke: 53 $\pm$ 98 months, locations of lesion: 2 L, 2 R). They underwent a Brain-Machine interface-based rehabilitation intervention in which they trained different multi-joint movements with their paretic left arm using a rehabilitation exoskeleton for 1 hour per session (cf. Ramos-Murguialday *et al.* (2013), Sarasola-Sanz *et al.* (2017) and section 7.2 as well as 1.3.1). Despite not being able to exert any arm or hand movement they produced residual EMG activity that was used to control the robot together with brain activity. The intervention consisted of twenty sessions of training. Before and after each training session the patients performed a compliant move-

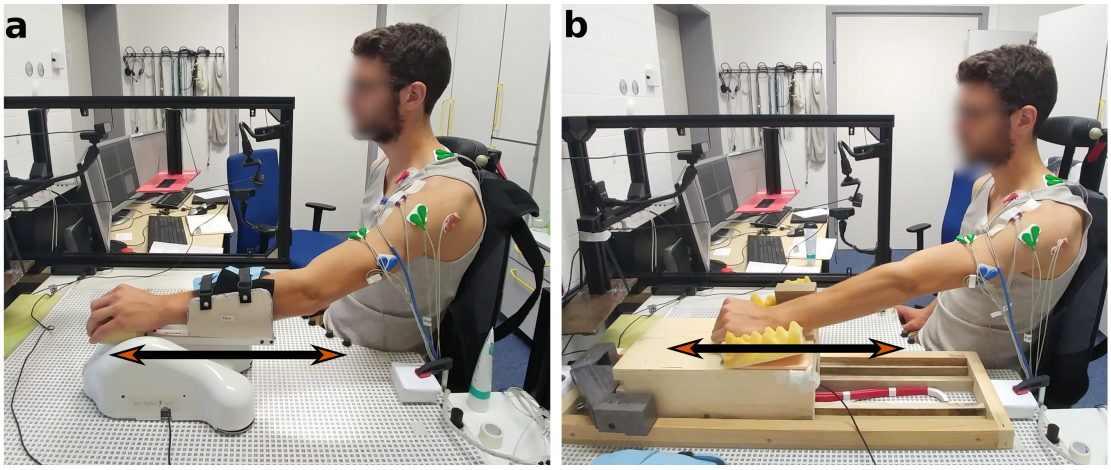

Figure 6.2: Experimental setup for the healthy subjects. (a) Frontal reaching movements with the rehabilitation exoskeleton. (b) Similar frontal reaching movement using the fatiguing apparatus. The moving block had to be pushed until maximum elongation of the arm using a handle against the force of a strong rubber band that pulled the block backwards. Maximum elongation was measured before and controlled by the experimenter during the experiment using a ruler attached to the apparatus. The frequency of the pushing movements was individually tuned to ensure challenging timing. The chair and seating position were fixed to avoid trunk movements.

ment session. During this part of the training the robot moved fully automatically to the predefined targets. The patients were asked to concentrate on the movement and try to actively follow it. Residual muscle activity for the specific movement of interest was thus recorded despite the complete paralysis.

In both cases the muscle activity of the main extensors and flexors of the arm was recorded using Bipolar EMG electrodes and a 16 channel Brain Products BrainAmp ExG amplifier system. The data were sampled at 1000 Hz. The movements in all experiments were cued by an auditory stimulus.

The EMG signal was filtered between 3 Hz and 250 Hz for the analysis. In the analysis of the data acquired during the fatiguing session the contractions of the Deltoid Anterior during each forward reaching movement were extracted automatically by finding the minima of a moving average of the rectified EMG signal (fig. 6.1). If no contraction was found the respective session was discarded from the analysis. For quantification of muscle fatigue two established markers were used. Firstly, the mean frequency of the spectrum: F_{mean} (equation (6.1)).

$$F_{mean} = \frac{\int_{f1}^{f2} f \cdot PS(f) \cdot df}{\int_{f1}^{f2} PS(f) \cdot df} \tag{6.1}$$

This index represents spectral parameters that reflect changes in conduction velocities

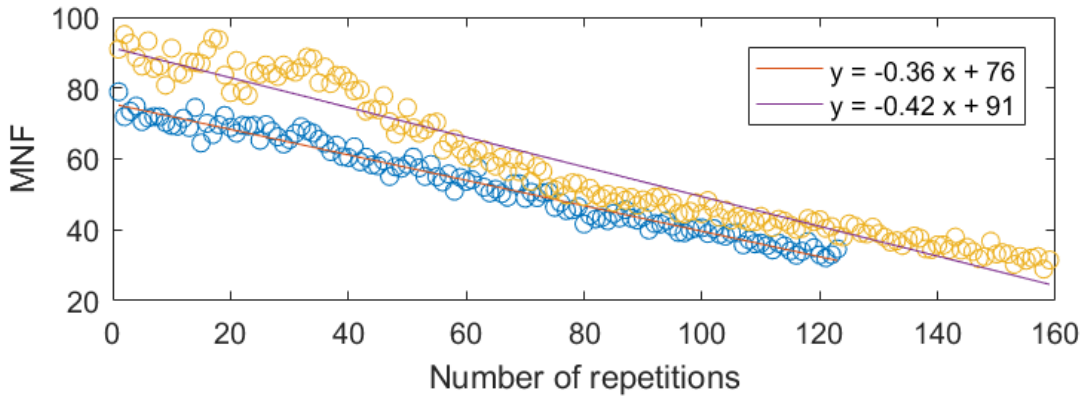

Figure 6.3: A sequence of fatiguing dynamic biceps contractions. The mean frequency of the muscle activity spectrum decreases linearly in two recordings of the same subject on different days (yellow and blue circles)

of muscle fibers, which lead to alterations of the waveforms of motor unit action potentials (Bigland-Ritchie *et al.*, 1981). Secondly, the Dimitrov spectral fatigue index F_{Insm5} (Dimitrov *et al.*, 2006) was used, which emphasizes increases in low frequencies and the decrease in high frequencies by employing moments -1 and 5 of the spectrum. This metric reflects increased negative after-potentials of motor units and increased duration of propagation of intracellular action potentials during fatigue (equation (6.2)).

$$F_{mean} = \frac{\int_{f1}^{f2} f^{-1} \cdot PS(f) \cdot df}{\int_{f1}^{f2} f^{5} \cdot PS(f) \cdot df} \tag{6.2}$$

All the results of the fatigue measures are presented as the percentage of decrease of the fatigue index from the *pre* to *post*.

6.3 Results

6.3.1 Dynamic fatiguing biceps contractions

Figure 6.3 shows mean frequency values of single dynamic biceps contractions of a healthy volunteer over time. Each circle represents one contraction. Blue and yellow circles are from two repetitions of the experiment on different days. Both recordings show a linear decrease of the mean frequency feature, indicating an increase of fatigue contraction by contraction. This increased fatigue is stable over multiple recording sessions.

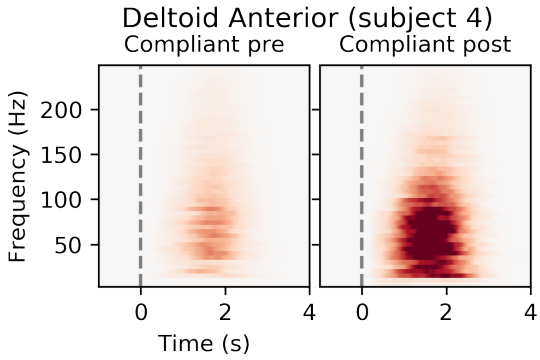

Figure 6.4: Time Frequency plot of EMG activity in subject 4 (representative healthy subject) before and after the fatiguing session. The color axis is in arbitrary units representing power in both plots.

Subject	F_{mean}	FI_{nsm5}
1	4.4%	-20.6%
2	-10.9%	49.4%
3	-6.9%	35.7%
4	-11.9%	77.3%
5	-1.7%	9%
6	-1.5%	- 8.5%
7	-0.8%	2.8%
8	-4.1%	0.6%
9	9.4%	-37.1%
Mean	-2.3%	12.1%

Table 6.1: Deltoid Anterior fatigue in healthy participants

6.3.2 Deltoid Anterior fatigue in the healthy participants

Fig. 6.4 shows a time-frequency plot of activations of the Deltoid Anterior muscle during the frontal reaching movements of a representative healthy participant (subject 4). The belly of the power spectrum of the EMG activity, which is common in dynamic contractions, is clearly visible before (PRE) and after (POST) using the fatiguing apparatus. The percentage change of the two fatigue indices for all patients are shown in table 6.1.

The difference of the means from zero was tested using a one-sided t-test. For F_{mean}: $t = -1.0$; $df = 8$; $p = 0.34$ and FI_{nsm5}: $t = -1.0$; $df = 8$, $p = 0.34$. Even though both measures indicated fatigue in the majority of the healthy subjects, i.e. a reduction in F_{mean} and an increase of FI_{nsm5}, the test did not reveal a clear difference of the means from zero for either index.

To further investigate fatigue in the Deltoid Anterior muscle and to understand the dif-

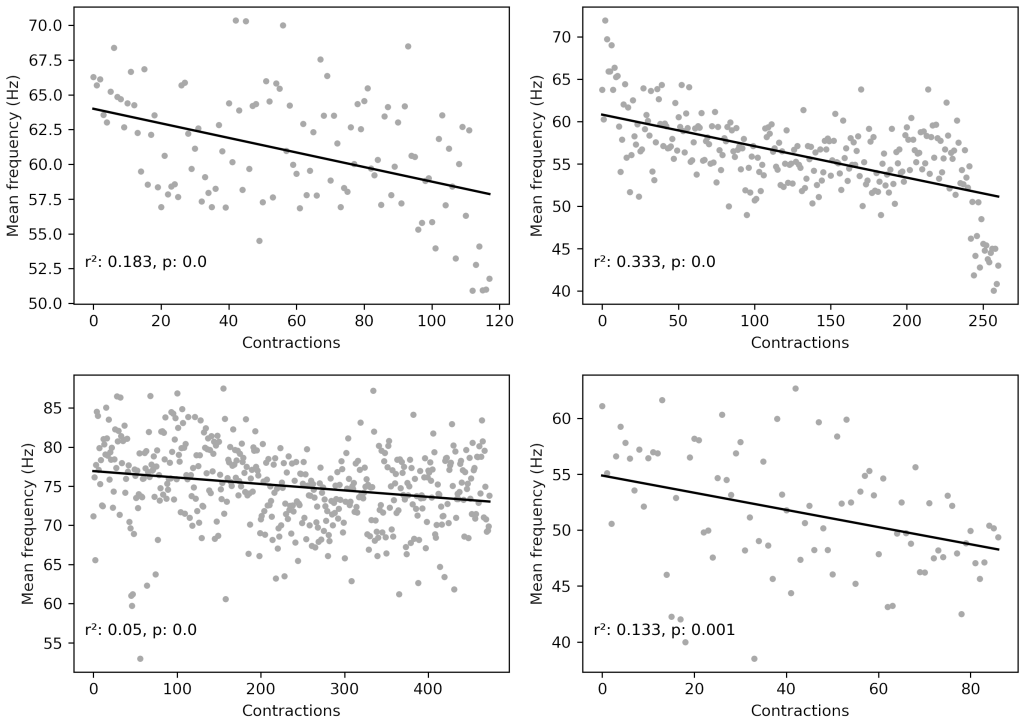

Figure 6.5: Regressions of F_{mean} of the EMG power spectrum per contraction. The four participants show a decrease of the fatigue index indicating induced muscular fatigue.

ferences between subjects the EMG of the dynamic contractions recorded during use of the fatiguing apparatus was analyzed. After segmenting the contractions we computed the fatigue indices for each segment. The figures show the evolution of the F_{mean} index of the healthy volunteers. Half of the subjects showed a continuous decrease of the mean frequency of the spectrum, indicating increasing muscle fatigue (fig. 6.5). The other subjects do not show a similar linear decrease (fig. 6.6). Two of those subjects were exceptionally well trained and did not reach a self-reported state of fatigue after the maximum duration of the session of 20 minutes (around 500 contractions). Another explanation of not reaching (self-reported) fatigue could have been exertion of involuntary compensatory movements with the shoulder or the trunk that could not be prevented by instruction or detected by the experimenter.

6.3.3 Deltoid Anterior fatigue in the patients

Fig. 6.7 shows a representative time-frequency plot of activations of the Deltoid Anterior muscle during the compliant frontal reaching movements of the patient in one of the sessions of patient P2. The patient shown was not able to elicit activity in the Deltoid

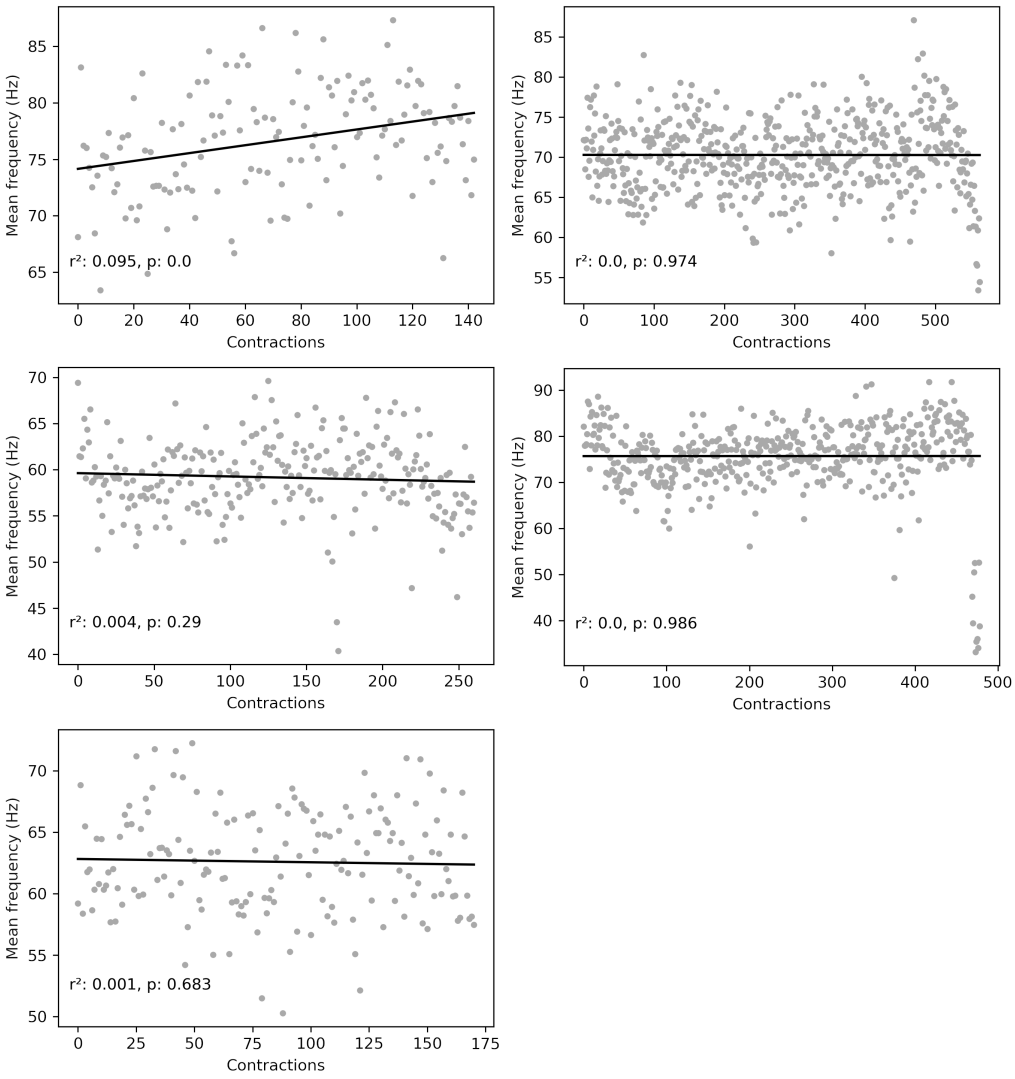

Figure 6.6: Regressions of F_{mean} of the EMG power spectrum per contraction. The five participants show no change of the fatiuge index indicating no muscular fatigue.

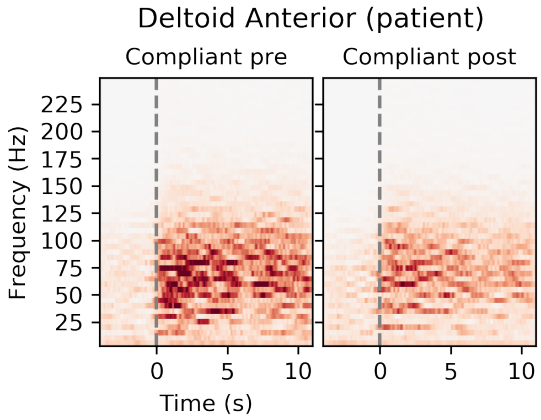

Figure 6.7: Time Frequency plot of EMG activity in the stroke patient before and after the training session; compliant movement (0s is the movement onset). The color axis is in arbitrary units representing power in both plots.

Anterior muscle in every trial exactly after the auditory cue because of the paralysis. For this reason the zero line is aligned to the movement onsets, which were manually determined for each repetition. In the plot the activity is stretched along the time axis more than in the healthy participants because the compliant reaching movements the patient performed had a longer duration than the reaching movements the healthy participants performed. The bandwidth of the spectrum, however, is similar.

Figure 6.8 shows fatigue as measured by the Mean Frequency of Spectrum index for each of the patients. The distribution of the fatigue index of each session is shown before the training (light grey) and after (dark grey). Patients P1 and P2 show an increase of the fatigue index after the session. P3 and P4 do not show a difference.

6.4 Discussion and conclusions

In this study we investigated how EMG features of muscle fatigue develop and progress in the setting of a semi-functional multi-joint movement within a rehabilitation paradigm for chronic stroke patients with severe paralysis of the upper-limb.

The Deltoid Anterior muscle is recruited during forward reaching movements as investigated here. Moreover, many paralyzed stroke patients show relatively more control in proximal than in distal muscles. Hence, the investigation was focused on this muscle in the present work. We found that fatigue could be induced and tracked using common EMG indices in healthy individuals during dynamic biceps contractions. These findings were transferred into a fatiguing task as closely related to the movements of the rehabilitation paradigm as possible. In the test with healthy participants muscle fatigue was induced using the fatiguing apparatus. The statistical test did not reveal a general sim-

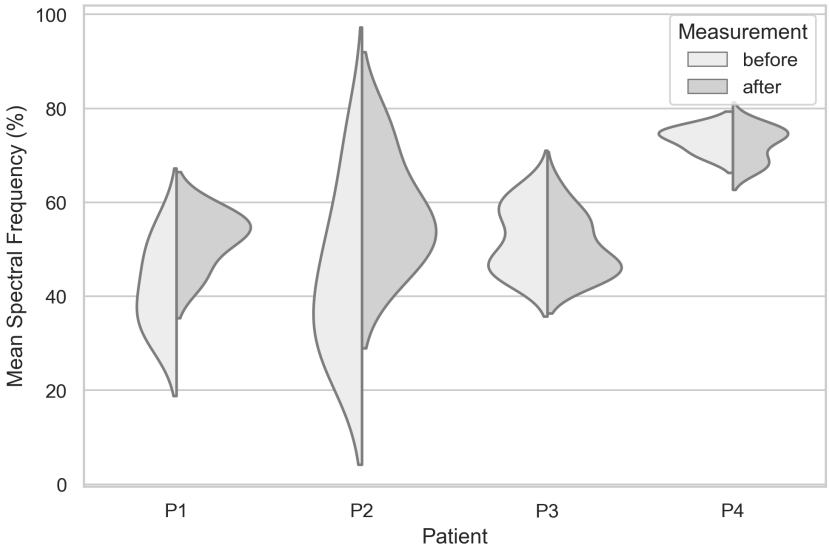

Figure 6.8: Distribution of the fatigue index measurements of each session before and after the training. The fatigue index is directly derived from the mean spectrum and normalized to a range of 0 to 100 in order to be comparable between subjects.

ilar change in all participants. Some participants, however, showed a distinct reduction in the mean frequency of the EMG power spectrum from the *pre* measurement to the *post* measurement. These subjects also showed a linear reduction of this fatigue feature during the fatiguing session, which is an effect that has been observed before (Komi and Tesch, 1979). In some participants the changes of the fatigue features in the Deltoid Anterior muscle were very small and thus a significant mean change for all subjects was not found. Even though elongation of the arm, repetition speed of the fatiguing movement and the strength of the rubber band were controlled, the subjects might have used compensatory strategies for completing the task unintentionally, e.g. using the trunk for the beginning of the movement and thus relieving the Deltoid Muscle. Such movements are hard to control in the described setting that required a lot of force. Monitoring trunk and neck muscles as well as contralateral muscles could help to further increase the number of controlled factors. Moreover, the different levels of fitness of the participants may have influenced the results as trained muscles recover more quickly and they may have partially recovered during the backwards movement of the fatiguing exercise or when switching from the fatiguing apparatus to the exoskeleton for the *post* measurement, which, however, only took a few seconds. The setup for the healthy participants could be further enhanced by stratifying subjects according to their level of fitness and adjusting the amount of resistance of the device accordingly. Furthermore, ways to constrain shoulder movements could be devised in order to limit compensatory movements and force fatigue in the target muscles.

In the severely paralyzed stroke patients the fatigue features did not show a consistent

pattern. On average, patient P1 and P2 showed a relative increase of the mean frequency index, which would indicate no or even less muscle fatigue. A reason for this effect could be that the training session actually activated the muscles of the patients rather than fatiguing them. The dimitrov index showed a similar anti-correlated pattern (not shown here).

Judging from the time-frequency plots, the bandwidth of the EMG power spectrum is similar to the one of the healthy participants, ranging from around 10 Hz to between 150 and 200 Hz. This indicates that comparison of muscle activity between both populations is possible, even though EMG amplitudes are much lower in the stroke patient.

The investigation of muscle fatigue in the stroke patients was performed under the assumption that the training task is fatiguing for the patient since he cannot perform the task normally and the Deltoid Anterior muscle is weak and easily fatiguable due to prolonged non-use. In the training the patient is forced to activate the muscle to trigger the movement of the exoskeleton. However, it may have been the case that the task was not fatiguing for the patient at the peripheral (i.e. the muscle) level. It has been shown some decades ago that healthy individuals with higher percentage of slow-twitch fibers (ST) show smaller changes in the EMG spectrum (Komi and Tesch, 1979). In paretic muscles of stroke survivors an increased number of slow twitch muscle fibers is innervated (Riley and Bilodeau, 2002). On top of that, it has been shown that the number of slow-twitch fibers is generally increased in the elderly (Campbell *et al.*, 1973). The muscles of the patients might thus be less susceptible to fatigue and may express less changes in the EMG spectrum.

We conclude from this investigation that if fatigue in the Deltoid Anterior muscle is induced during forward reaching movements within the described rehabilitation framework in healthy participants the measured EMG activity is altered. In the stroke patients no clear evidence was found that the fatigue features in the same muscles during a similar movement alter the EMG activity in a consistent way. The present experimental results of the measurement with the stroke patients thus hint at no or a negligible influence of the movements performed in the training on EMG fatigue features which might rule out the influence of this factor on EMG decoding. On the contrary, the training might even have a positive (”activating”) effect on the muscle activation. Further recordings of data of paralyzed stroke patients and investigation of potentially more sensitive EMG indices of muscle fatigue may provide more evidence toward either direction. Another merit of this work is the provision of a device and methodology to induce fatigue during dynamic forward reaching movements, often used in rehabilitation exercises.

Chapter 7

Increasing engagement and enhancing feedback

7.1 Introduction

Learning a motor skill requires the trainee to perform a movement, integrate feedback from various senses and use the feedback to improve the movement, i.e. reduce errors of movement kinematics (speed and geometry) and movement dynamics (forces) (Krakauer, 2006). This process entails three levels of learning: Hebbian learning, supervised learning and unsupervised learning. On the physiological Hebbian level connections between neurons are strengthened depending on their contingent activity. Supervised learning takes place on a higher cognitive level. It requires feedback on errors or potential for optimizing the task. In contrast, reinforcement learning does not necessarily punish errors but rewards optimal movements (Reinkensmeyer *et al.*, 2016).

There is an ongoing debate if in chronic stroke patients motor learning can actually lead to reversal of the impairment or does only entail compensation (i.e. learning of alternative strategies to achieve a movement goal) (Krakauer and Carmichael, 2017). The main goals of the studies from which the data was analyzed in this thesis (Dataset 1 and Dataset 2) were to explore a new kind of enhanced sensory feedback to the patient supporting learning on all three levels: Brain-Machine interfaces. The principle is that the intention to move (thought), which does not reach the muscle any more (in adequate strength) after stroke, is reconnected to the movement (action) via external pathways. In the studies under investigation modulation of the Sensorimotor Rhythm is detected via EEG and translated into movements of an exoskeleton that moves the arm of the patient. The sensation of the arm moving travels back to the brain via undamaged afferent sensory pathways (proprioception, vision). The second study (Dataset 2) improved the feedback by including an additional modality: the muscle activity. The exoskeleton used in that study is able to move in seven degrees of freedom. The effects on the training are twofold: Firstly, the feedback to the patients is enriched. Secondly, they are more engaged in the task. Both effects support motor learning (Krakauer, 2006; Blank *et al.*, 2014).

In the next section I provide an introduction to the setup and movements performed in the hBMI study followed by a description of the development of a software program for

improving the visual feedback to the patient in the study. The last section focusses on the AMoRSA project, which targeted increased engagement in the training and long-term motivation.

7.2 The Hybrid BMI study and setup

This pilot study was conducted at the Institute of Medical Psychology and Behavioral Neurobiology in Tübingen from 2016 to 2019. The goal was to implement and test a novel BMI-based neurorehabilitation training paradigm for stroke patients with chronic severe upper-limb paresis. The patients were seated and an exoskeleton was donned on their paralyzed arm and hand. The exoskeleton, built by Tecnalia, San Sebastián, Spain, allows movements in 7 degrees of freedom (xy-plane, xy-yaw, wrist angle, angle of thumb, index finger and the remaining three fingers together). It was designed for this experiment. The robot operates on a mat on a table with QR-codes for precise location (fig. 7.1). The patients control the movements of the robot using their brain activity and residual muscle activity. These neurophysiological signals are captured using 32 EEG channels and 14 bipolar EMG electrodes. A python-based laboratory program acquires, preprocesses and interprets the signals and connects a control system for the experimenter, the exoskeleton and a visualization program (see next section). Kinematics of the exoskeleton were controlled via two components: an assistive component and a component controlled by the patient. Speed and trajectory of the assistive component were derived by computing the speed of the robot following an ideal trajectory towards a defined target. This speed was linearly combined with mappings of the patient's muscle activity to the velocity of the appropriate degrees of freedom. However, the exoskeleton was only activated whenever the EEG classifier detected the intention to move in the brain. Thus, a biologically-inspired control flow was established. More details on the technical implementation can be found in the conference publication of our work group (Sarasola-Sanz *et al.*, 2017).

The training consisted of two phases. In each of them the patients practised in ten training sessions on consecutive days with exception of the weekends. Before and after each phase screening sessions took place. In these sessions the state of the patient was characterized: The behavioral state (the degree of paralysis) on multiple clinical scales, extent and volume of the lesion in the MRI, the neurophysiological state using EEG, EMG and MEP assessments and the psychological state using questionnaires. In the sessions the individual control parameters for the training sessions were determined. These comprised the individual sensorimotor frequency band being most discriminative of the two experimental conditions *Resting* and *Movement*. Moreover, the range of motion and the locations for the four movement targets were set (fig. 7.2). The targets were defined in all seven degrees of freedom and resembled movements that are relevant for day-to-day activities. The three forward movements were given a color that marked the approximate xy goal position on the experimental table and were also used as auditory

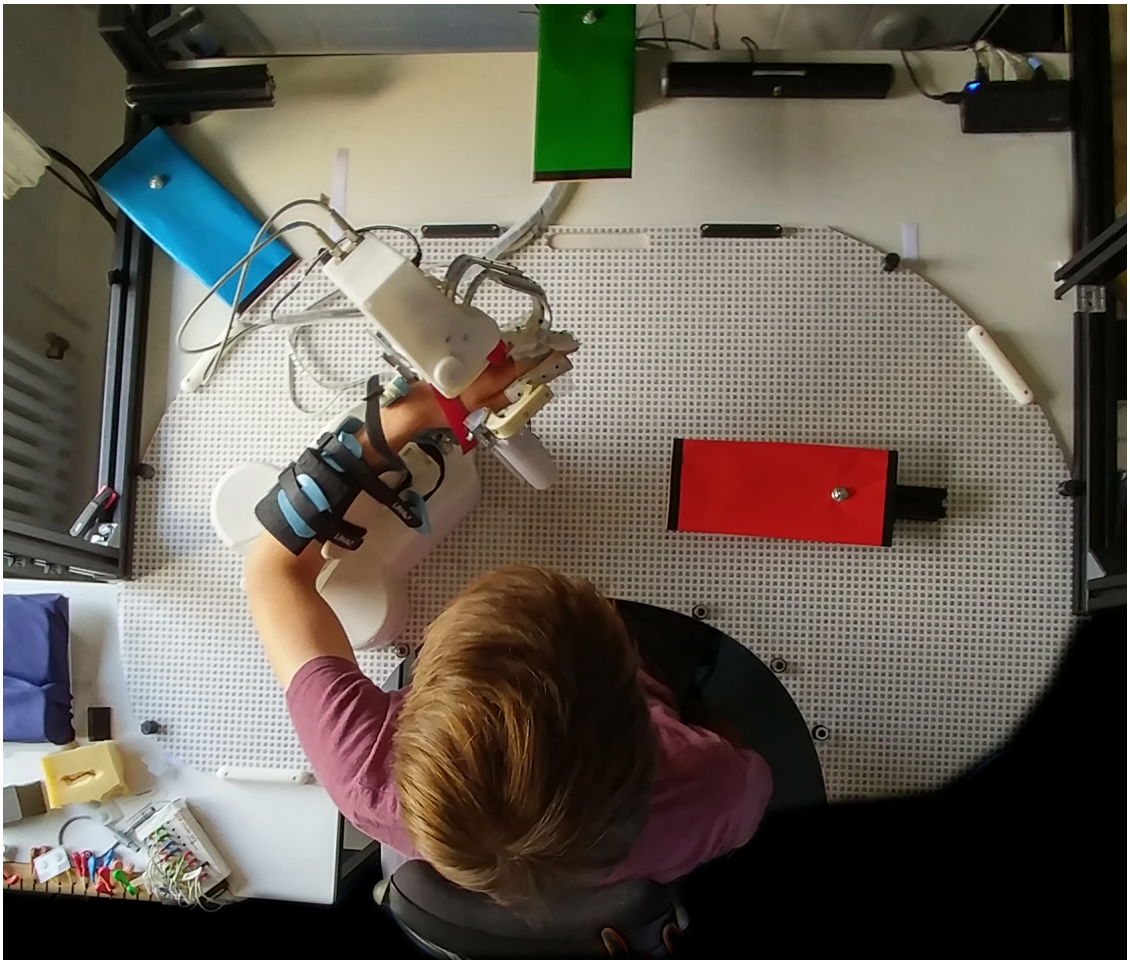

Figure 7.1: The experimental table seen from above. The subject is seated in the experimental chair. The exoskeleton is donned to arm and hand of the subject. It moves on the mat with the QR codes. The colored panels indicate the goal positions of the movements. EEG and EMG sensors are not attached in this figure for clarity.

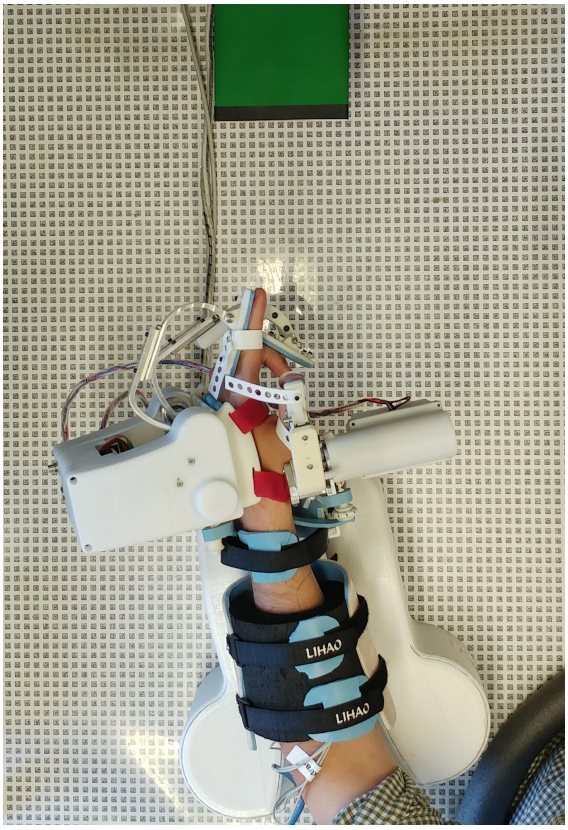

Figure 7.2: Target position *Grün zeigen*: The arm is extended towards the green target panel in the center. The index finger and the thumb are extended and the three other fingers are flexed. The wrist is rotated such that the plain spanned by the palm of the hand forms a 90° angle with the experimental table.

cue. The backward origin position did not have an associated color. If we assume a paresis of the right limb, the target *Rot greifen* was associated with a movement towards the left while pronating the wrist and grasping (i.e. trying to clench the fingers into fist). The target *Grün zeigen* was central and as far away from the patient as he or she could extend the arm. The patients were also asked to extend their index finger and thumb while flexing all other fingers. The target *Blau öffnen* was a movement towards the right side of the body while extending all fingers and supinating the wrist. After each movement or a timeout the patients had to move back to the origin position, a comfortable position of the robot just beside the torso in which all muscles were able to relax (vice versa if paresis affected the other side of the body).

A training session consisted of various measurements: EEG recordings during rest before the training and movements compliant with the movements of the exoskeleton (the exoskeleton moved automatically and the patient tried to follow the movement without influencing the trajectory) before and after the training. The training itself entailed a

series of runs in which all three movement targets were announced in random order and the task of the patients was to move the exoskeleton towards these targets using their brain and muscle activity and after reaching the goal (or a timeout when not reaching the goal) moving back to the origin.

7.3 Improving visuo-proprioceptive feedback: Interactive 3D visualization of the orthosis

During the training the patients face two potential challenges. Firstly, the movements of the fingers could be very subtle, which might hamper proprioception. Patients have reduced distal sensation and thus rely more on their vision. However, viewing the hand is not always possible in all positions during the movements. The view might be obstructed by the motors of the robot in certain positions and angles and the patients cannot move freely because of the constraints imposed by the EEG recording (fig. 7.3). Secondly, each movement that the patients train has a goal position defined in seven dimensions (all degrees of freedom). This position is defined individually for each patient. Even though the robot supports the patients in moving towards the target, it proved challenging for them to remember the multi-dimensional goal position. This could have negative psychological effects because the patients might get frustrated when not receiving the reward ("movement fully completed") repeatedly. For learning this could have a negative effect, too. The patients might just not activate the desired muscles because they are simply not able to tell where to go.

In order to overcome both problems I developed a program that enables patients to locate the movement target exactly. Moreover, the distance to the target in all degrees of freedom is also visualized.

The patients have a large screen in front of them at the far end of the rehabilitation table. The display shows two virtual three-dimensional representations of the exoskeleton (fig. 7.3).

The experimental control computer sends information on the current task to the visualization program. The target that is currently active will be displayed at the given location and yaw in the virtual space and the desired rotation of the wrist DOF and angles of thumb and fingers. The exoskeleton glows in the color of the real-world target (one of red, green or blue). The second exoskeleton visible represents location and angles of the real exoskeleton. Whenever the intention to move is detected the movement trajectory and angular velocities decoded from the neurophysiological signals are sent to the real exoskeleton and to the virtual one in real-time at an update frequency of 20 Hz. The real exoskeleton and the virtual one move contingently. While the patients move the two exoskeletons they can try to match location and angles of the virtual exoskeleton they control and the virtual target (fig. 7.3, 7.4).

The visual design is sparse on purpose. It does not show many details or special ef-

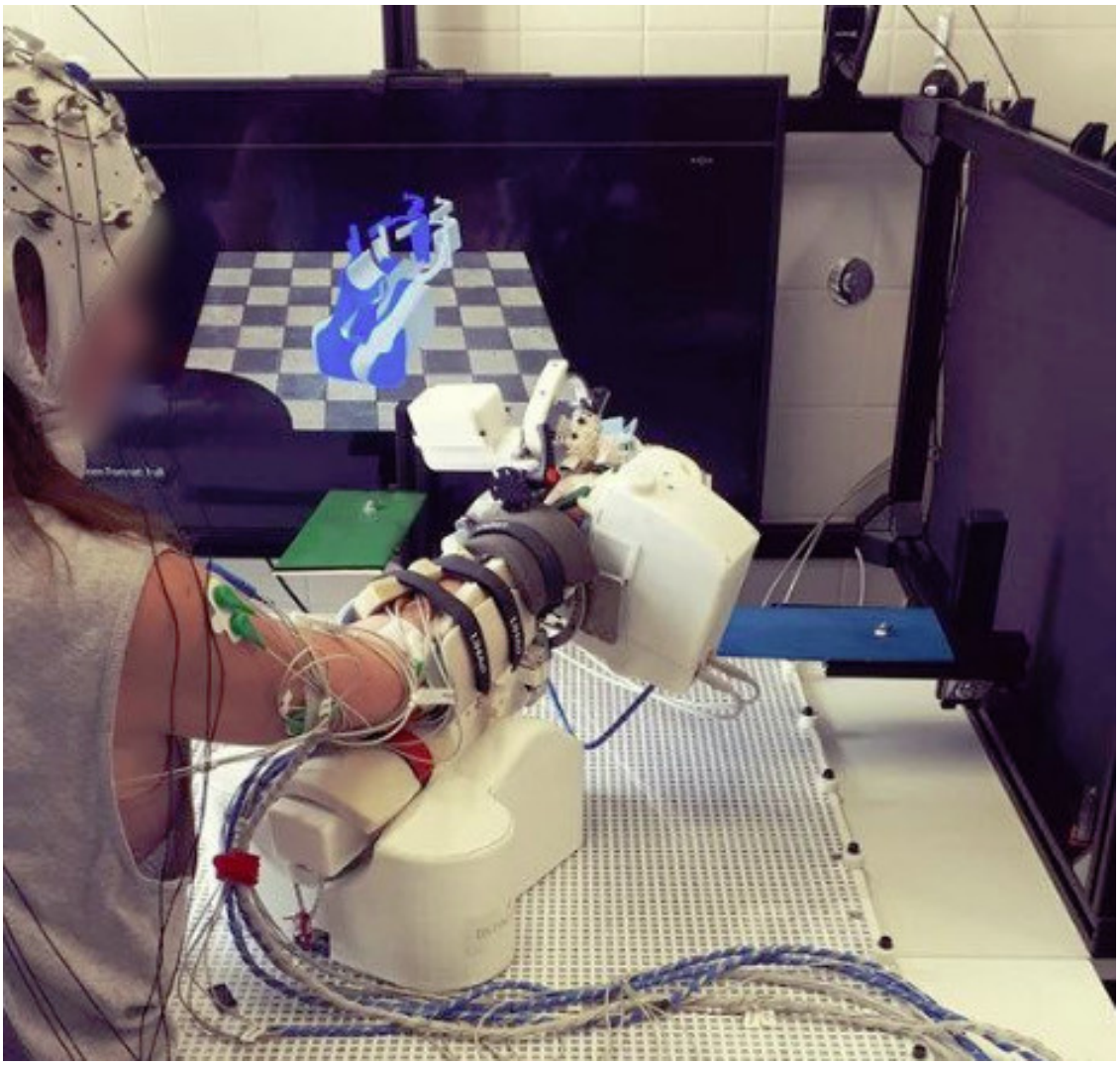

Figure 7.3: Full experimental setup. The exoskeleton is donned to hand and arm of the subject. EMG and EEG electrodes are attached. The visual feedback is shown on the screen at the far end of the experimental table. The subject is trying to perform the movement towards target *Blau öffnen*.

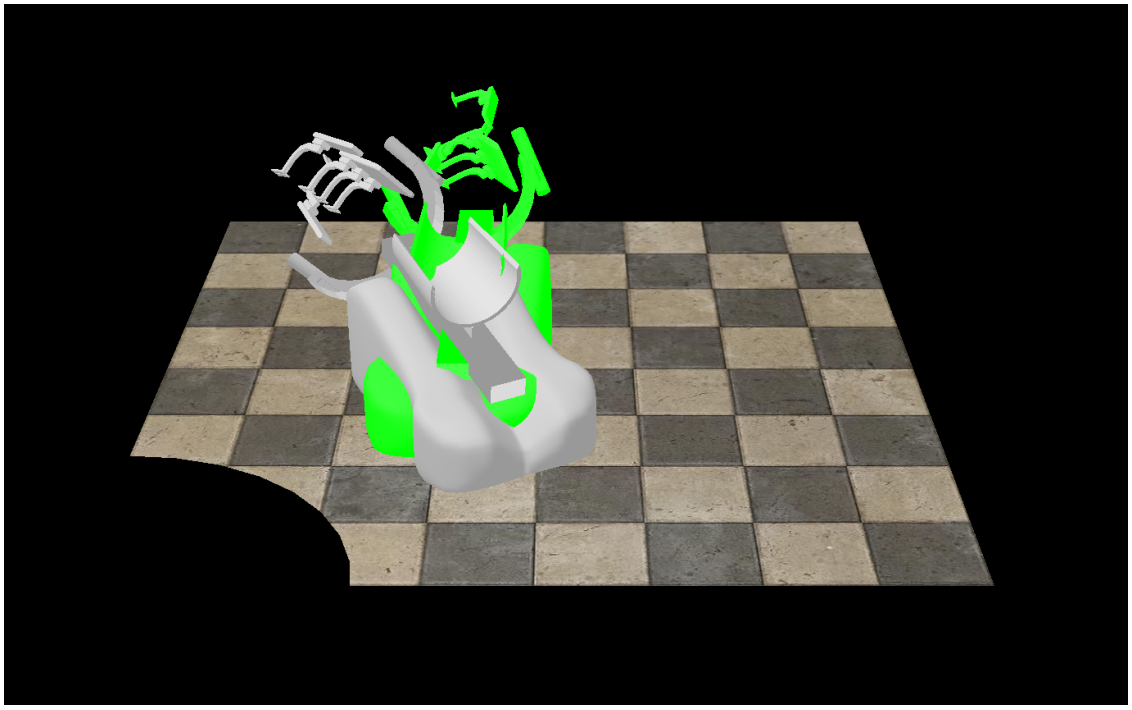

Figure 7.4: Screenshot of the visualization that the patients see on the experimental screen. The grey exoskeleton model is a representation of the actual state of the real exoskeleton. The green model is the the representation of the target (*Grün zeigen*). The subjects are able to reach the goals in all DOFs more precisely with the help of this visualization.

fects in order not to distract the patients. Their main focus should be on proprioception of their real hand throughout the training. The display is also concrete in the sense that it depicts reality as closely as possible (i.e. an exoskeleton moving). Another possibility would have been to show a virtual hand moving or other more abstract representations of trajectories and angles. However, the intention was to reduce the need for abstraction, which would have introduced an unnecessary (and possibly detrimental) layer of cognition for the sensory integration task at hand.

The feedback of the patients was collected informally and was positive overall. All patients who participated had the impression that the visual guidance helped them operate the system.

7.3.1 Technical details

The 3D visualization is programmed entirely in python using the Panda3D open-source engine developed at Carnegie Mellon University, Pittsburgh, PA, USA. It is lightweight and cross-platform by default. Software built with the engine can be packaged into a single file executed in a runtime environment. Deployment is thus user-friendly both for developers and end-users.

Once the program is running interaction takes place via a TCP interface that allows invoking all commands programmatically. An unlimited number of virtual exoskeletons can be spawned and individually controlled, including all DOFs and appearance. Each representation is linked to a unique string identifier that is passed on to the invoking program (e.g. the experimentation computer). This identifier is used to steer and remove the exoskeleton from the scene via simple chained string commands (see section 8.1.10 for details on the commands). Furthermore, the virtual robots can also be added, removed and controlled by the user directly using the keyboard.

Due to the simple interface the program can be integrated into any laboratory environment and controlled via TCP packages locally or via the network. On top of that, the system can be used for instruction, e.g. for showing the patients the target movements virtually and simulation of movements, e.g. for playback of previously recorded trajectories and angular velocities. These can be included in videos for scientific publications, presentations and other demonstrations.

7.4 Improving immersion and training motivation: The AMoRSA setup

The work presented in this section is multidisciplinary and could only be realized by collaboration. For disclosure of contributions see section 8.2.

Engagement in the training task and long-term motivation lead to high repetition rates

which are essential for the success of training. In chronic stroke patients progress is very slow. The results of the first BMI study (Dataset 1) show that after four weeks of training there is motor improvement measurable in terms of clinical scales but the changes are too small to have large impact on day-to-day activities (Ramos-Murguialday *et al.*, 2013). During the training the patients might not experience any immediate effects, even though there are neurophysiological changes such as of muscle activity, the ERD (e.g. chapter 2), brain connectivity (e.g. chapter 5) and low-frequency oscillations (e.g. chapter 4). As shown in this thesis these evolve throughout the intervention. Therefore, they could potentially be used to give patients feedback during the training, especially when behavioral effects are not visible.

The AMoRSA project was initiated to tackle the issue of engagement and motivation. In that project a serious game was to be embedded in the rehabilitation environment of the hBMI study. A serious game, actually a tautology - "serious fun", aims primarily at teaching and training through mechanisms of play rather than recreation (Zyda, 2005). Serious games have become popular in health, military, education and also in companies for in-house training or to guide transformation processes (Susi *et al.*, 2007).

In medical applications serious games could facilitate immersion, which would help patients to be virtually transferred out of clinical settings into a more enjoyable environment. Their sensations could be refocussed from pain and discomfort towards more pleasant feelings mediated by the game. Mechanisms of games such as winning points, shaping environments, defeating opponents, collaboration, experience of a story and exploration of virtual worlds not only lead to immersion but also to a shift of focus: The player concentrates on the task they are trying to achieve. Serious games blend these mechanisms with the learning or training target and while the user plays they learn and train the superordinate task. Furthermore, the progress in the game is related to the progress in the task, e.g. a therapy. Thus the gaming environment provides long-term feedback of the progress in the real-world. This could help the patient, for example, establish a sense of achievement and keep up motivation.

7.4.1 The game design

The theme of the game of AMoRSA is a virtual ethereal garden. At the beginning of the game (the therapy) the garden is completely empty (7.5). The patients can navigate their avatar to various spots within the garden by performing a movement of the rehabilitation training. They can plant trees and flowers or place decorative items (7.6).

These items cost points that the patients earn by performing the training movements. The patient announces the movement they would like to perform to the therapist. The therapist activates the target accordingly. The interaction between therapist and patient is important. The therapist can give the patient instructions and feedback but they also control the "weight of the targets", i.e. how many points the patient gets for performing one of the movements (7.7). The therapist can give the patients more points for more difficult movements, thus motivating the patient to train that task more often. Moreover,

Figure 7.5: The ethereal garden in an empty state at the beginning of the game. The glowing green globe is the avatar of the subject.

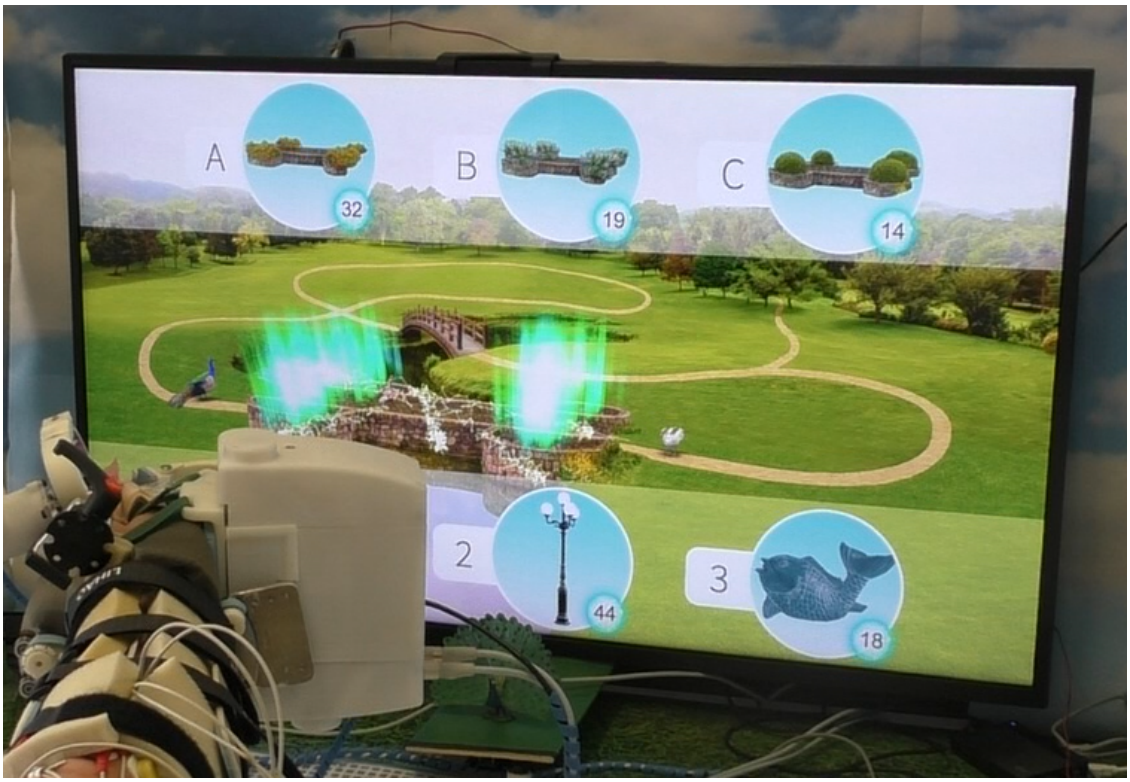

Figure 7.6: The matrix of plants and decorative elements the patients can choose at a specific position in the garden. The active garden position is marked by glowing green energy fields. The numbers next to the elements show the points (in-game currency) they need to be able to place the element.

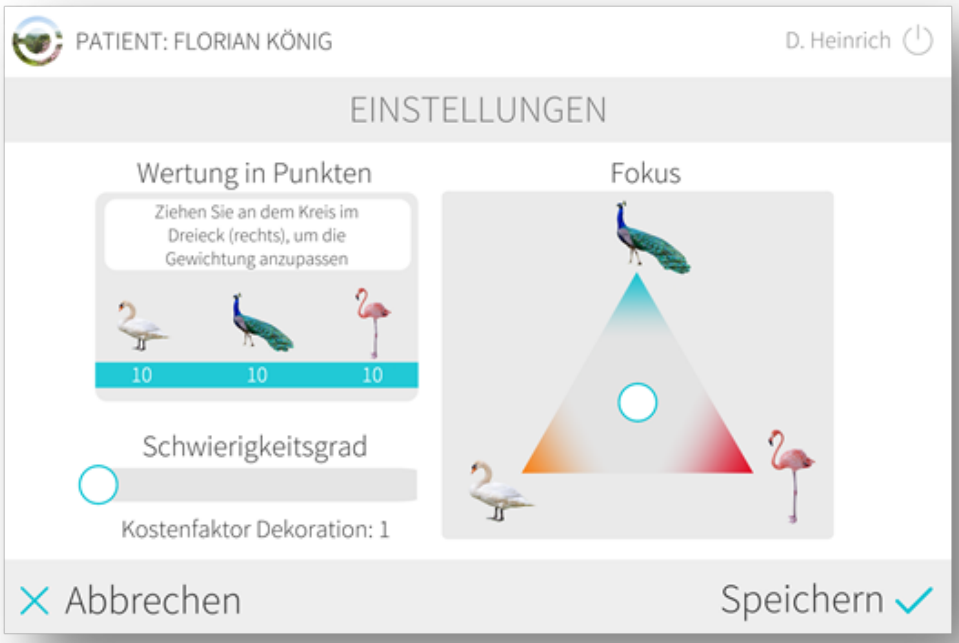

Figure 7.7: The interface for the therapists: The position of the circle in the ”Fokus” triangle specifies the ratio of points for the successful performance of each trained movement. The trained movements are represented by the three birds. If the circle is moved towards the swan, for example, these movements would be rewarded by relatively more points than movements towards the other targets. The ”Schwierigkeitsgrad” reduces the overall amount of points received for any movement.

the patients receive bonus points for performing the task well, e.g. reaching the goal position very quickly or with a smooth trajectory.

In the light of the insights from the previously presented 3D visualization project several elements have been included providing real-time feedback to the patient such as a distance marker and expansion and retraction of the avatar while performing the movement in order to give them immediate feedback (7.8).

The feedback to the patients is thus enhanced during the task. In addition to that the virtual environment also gives the patients an intuitive perception of progress. Every movement that they performed counts and is reflected in the plants and the decoration. The game was balanced such that the garden could only be completely explored and filled after several weeks of daily training. And even after that the garden could be shaped further by replacing items. There are hundreds of possible combinations of items. In the case of severely paralyzed chronic stroke patients, where progress is little and mostly

Figure 7.8: The patient has chosen planting (upper left corner) and a decorative element (upper right corner) and initiated a movement towards the peacock target. The peacock will yield a reward of 8 points plus potential bonus points for good performance. The green arrow in the lower center of the screen points towards the goal position. It is surrounded by a gray and green circle that displays the distance to the target position and angles. With great distance the circle is mainly grey and while getting closer, the circle becomes green. The avatar has expanded (sizzling white lines over the bridge), which also conveys a sense of distance to the target.

Figure 7.9: A stroke patient playing the AMoRSA game in the final setup of the game. The ethereal garden that is almost fully explored.

invisible in the beginning, the long-term feedback visualized as the garden can also help to carry them over periods of frustration (7.9).

The merit of this work is two-fold. Firstly, the existing rehabilitation paradigm was combined with a serious game. A questionnaire and interviews with patients and therapists helped understand the needs of the patients. They were carefully taken into consideration and a game concept was derived together with aspects of demographics and the pathophysiology. The age of the patients and mixed gender ratio and respective preferences encouraged a virtual world that did not have fantastic elements (e.g. a fairy-tale world or a science ficition-world). Moreover, the pathophysiology of severe stroke and the concentration necessary for performing the training tasks demanded a game that was not fast-paced, e.g. no activity dependent on reaction time. Psychologically, a virtual world supporting creation rather than destruction (e.g. a shooter game) would support the rehabilitation process. These premises lead to the concept of game based around the creation of a garden. A virtual world the patients certainly could identify themselves with. The theme is purely creative and positive as elements are only added but nothing is destroyed. Furthermore, the garden theme does not distract the patients from their actual task. Secondly, the technological integration of the game into the laboratory environment was designed and implemented. This included design of interfaces between acquisition hardware (EEG and EMG), actuators (the exoskeleton), the game, the exper-

imentation interface and the therapists interface. Furthermore, new programs, extensions of existing code and a database were implemented for representing the game logic in the experimentation interface.

The subjective feedback of five patients who played the game was positive. They liked the theme and enjoyed playing the game. They reported finding the game more attractive than just the rehabilitation training. All of the patients playing the game underestimated the actual playing time by more than 20 minutes. Their perceived playing time was much shorter, which underlines the impact of the immersive effect.

Chapter 8

Materials, contributions and meta information

8.1 Materials

This section provides additional materials and supporting information for the thesis. First, the general ogranization of the code and implementation procedures are described. Afterwards, details of specific parts of the code are shown and finally, the software development project Multicam is explained. Due to data privacy regulations not all of the code produced for the analyses in this thesis can be made publicly available because various parts of most analyses directly refer to identifiers and demographic information that potentially could lead to de-pseudonymization of the participants. Nonetheless, the intention for writing this section was to provide enough information for the reader to understand how the code was implemented for repeating the analyses.

8.1.1 Introduction to the code implemented for the analyses

For the final versions of the analyses presented only open source software was used. This guarantees that other researchers can easily reimplement and reproduce scientific evaluations. At the beginning of the PhD project (i.e. chapter 2) Matlab was used as a framework (MATLAB, 2020). The code of the analyses was based on the widely used Fieldtrip toolbox, which is also open source (Oostenveld *et al.*, 2010). Soon after starting the analyses, it became clear that Matlab is a suboptimal framework for neuroscientific analyses. It is bulky and proprietary. One always needs to be connected to the internet (or be able to reach Mathworks' registration server). Distributed computing does not work out of the box. I decided to switch to Python for all other implementations (i.e. chapters 3 through 6 and partly chapter 7) (Van Rossum and Drake, 2009). The MNE toolbox is an excellent collection of neuroscientific tools accessible in Python (Gramfort *et al.*, 2013). It is open source software that is actively maintained and continues to be expanded. The features include opening and managing practically all data formats of neural recordings, time-frequency decomposition, connectivity analysis, preprocessing and filtering, a vast set of visualization tools and many more features.

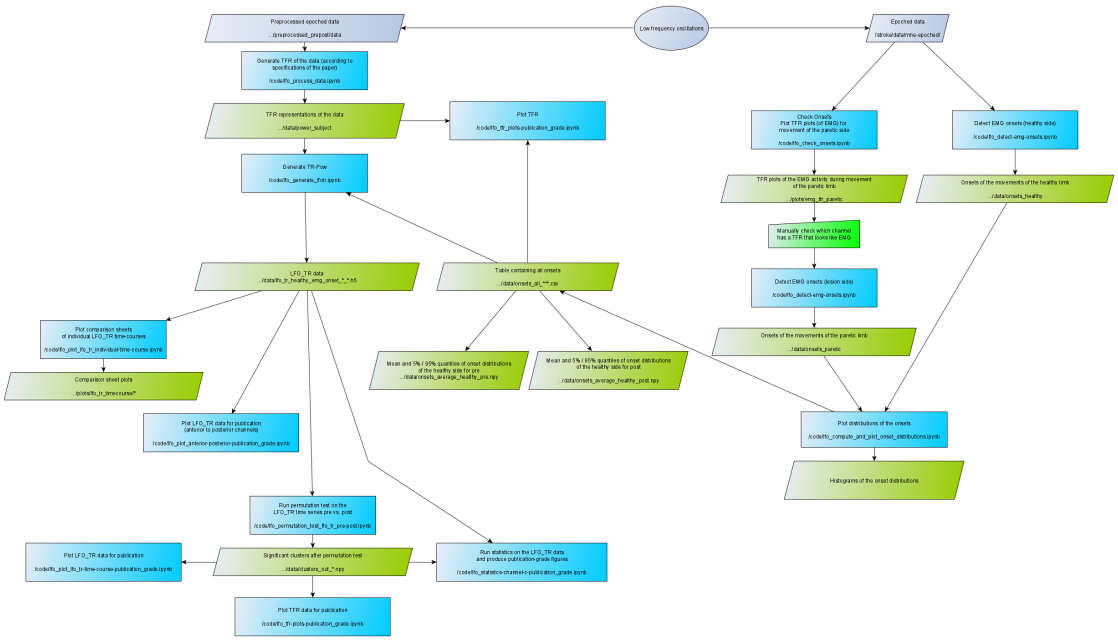

Figure 8.1: Flow chart of the ”processing tree” of an analysis performed on the data (this example refers to the analysis in chapter 4)

The methodology for implementing the analyses presented here is based upon the following four components:

1. Analysis plan and data flow
2. Configuration of analysis parameters and meta parameters
3. Implementation and organization of the analysis code
4. Running and logging the analysis

8.1.2 Planning of an analysis and data flow

Each analysis, especially those as complex as some presented here, consists of one or more series of processing steps that conceptually span a “processing tree”. At the root of the tree lie the source data and the leafs represent various results, such as tables, statistical tests or plots. For planning my analyses and for visualizing the steps taken I generated flow charts such as figure 8.1.

In the flow charts the analysis starts at the top with the name of the analysis and the source data files. Each data file is represented by a rhombus. The rectangles represent the processing steps. The connections between these elements, the arrows, represent the flow of data and the sequence of steps. The example shows the analysis performed and

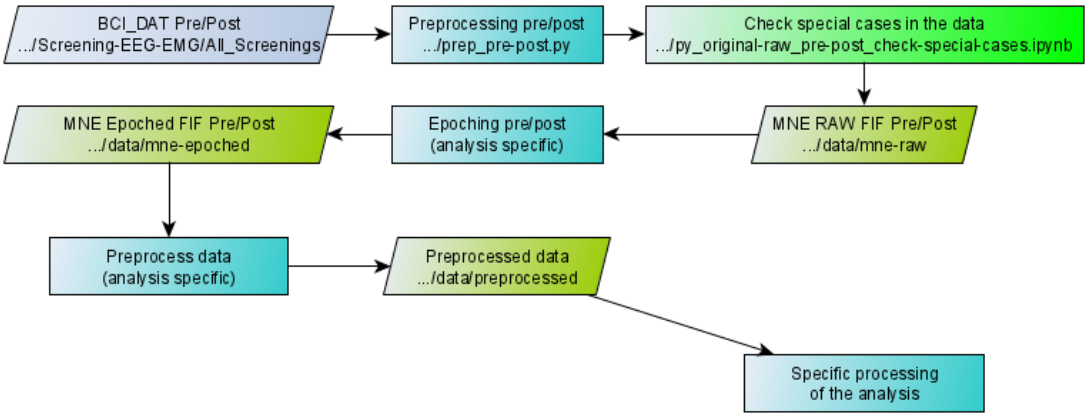

Figure 8.2: Flow chart of the ”processing tree” of steps of data preprocessing performed on the raw data.

presented in chapter 4. There are two levels of source data included. The left branch focusses on the EEG data and the branch on the right focusses on the EMG. Each processing step is implemented in its own Jupyter Notebook file (see below), the name of which is noted in the corresponding rectangle (Project Jupyter, 2020). The target directory of the resulting data is also noted in the flow chart. After multiple processing steps the two separate branches are joined and the analysis continues until it yields the desired results, such as the “TFR data for publication”. In the example processing of the data began with data that had already been preprocessed. The full processing pipeline actually starts with the raw data (fig. 8.2) of the experiments, e.g. Dataset 1 (section 1.3.1). The data comprises continuous recordings of EEG and EMG in the data format of the acquisition system. The preprocessing routines check the raw data and apply corrections were applicable. These comprise technical problems with the recording, such as broken EEG channels, or mislabelled EMG channels, for example. The corrected raw data is then transformed into the general data format of the MNE toolbox. Afterwards, the data is broken up into smaller components, so-called epochs. These units of the data contain neurophysiological data recorded during specific behavioral states such as periods of resting or periods of movement. The last step before starting the actual analysis is a basic preprocessing step where band-pass filters and a notch filter are applied.

8.1.3 Configuration of analysis parameters and meta parameters

The analysis often comprises many parameters that define the procedures such as the period used for baseline correction of the EEG or the lower and upper bound of a band-pass filter. In all analyses these settings are stored in a configuration file based on the YAML markup language (Yaml, 2020). The advantage of this configuration language is the easy integration into python code and human readability. Listing 1 shows a shortened

example of a configuration file. The configuration has three main sections: "meta", "script" and "processing". The first section contains meta information about the analysis, such as a machine readable name and description (which is important for automated logging). The script section contains information about the data flow, such as the source folder of the data and target folder for the plots. The processing section defines the actual parameters for the analysis such as the names of the EEG channels to be processed and the frequencies of interest for the analysis. Defining these parameters in a separate file has obvious advantages. There is no need for including ("hard coding") such values in the code, which helps reducing mistakes. Moreover, this procedure also supports modularity of the code as it can be used directly with different sets of parameters. For explorational analyses, for example, various sets of parameters can be evaluated without changing a single line of code.

8.1.4 Implementation and organization of the analysis code

The code for the analyses was usually organized in separate Jupyter Notebook files for each block in the analysis pipeline. Jupyter Notebook is an ideal choice for these kinds of analyses as it enables meaningful encapsulations of pieces of code. These "cells" can be run separately. The output (text and figures) is shown and stored directly in the browser and the code can be documented using markdown (including Latex for mathematical formulae). Jupyter Notebook runs in the browser. The execution of the code, however, can be run locally or remotely. The GIT version control system was used with all code in order to keep track of changes and for storing the code in a central repository.

Listings 2 through 8 show the code of the standard preprocessing pipeline for EEG data of the work group that was used in most analyses (López-Larraz *et al.*, 2018b).

The code for the analyses and projects presented here was written in Python to the greatest part. Some aspects were also written in Linux Shell script, YAML and Matlab. The Python modules *pymatreader* and *oct2py* were used to build a bridge between Python and Matlab. In some cases data from older analyses, which were implemented in Matlab, had to be included using these modules.

8.1.5 Performing analysis and logging

The analysis was mostly run on a computation cluster at the Center for Integrative Neurosciences at the University of Tübingen. A *jupyter notebook* daemon was activated on that cluster and ports were forwarded to the local computer using SSH. The Jupyter Notebooks could then be accessed, programmed and run via the local web browser. The execution, however, took place on the cluster with direct (and fast) access to the data and much larger computational power. Parts of the analyses were very demanding, especially the permutation tests that have been used in the analyses presented in chapters 4 and 5. Mathematical computations had to be repeated 1000 times per experimental unit of interest, which could easily amount to more than 4m computations (e.g. 1000

```
meta:
    - name: analysis_description
    description: Full pipeline for the LFO analysis (v1.3)
    data: lfo_standard_pipeline

script:
    - name: source_root_folder
    description: Root folder of the source files
    data: /.../preprocessed_prepost/data
    - name: target_plots_folder
    description: Root folder for the result files and plots
    data: /.../standard/plots

processing:
    - name: eeg
    description: Configuration of the EEG filtering
    data: {
        highpass: 1,
        lowpass: 22,
        channels: [4,5,6,7,10,11],
        channels_for_plots: ['C3','C4','CP3','CP4','P4','P3'],
        fs: 500
    }

    - name: analysis
    description: Items related to defining analysis and output
     ↪  (with respect to estimated EMG onset)
    data: {
        period_of_interest_plot_start: -1,
        period_of_interest_plot_end: 1,
        period_of_interest_mean_start: -0.2,
        period_of_interest_mean_end: 0.4,
        frequencies_of_interest_l: 3,
        frequencies_of_interest_u: 5,
        decim: 1
    }
```

Listing 1: Example configuration file (shortened for clarity). The three sections *meta*, *script* and *processing* contain information and definitions for logging, loading and saving data and processing the data, respectively

```
### Function definition for preprocessing EEG data for the
 ↪ coherence analysis (part 1)
# Custom packages
import config_utils as cu # Utilities for reading configuration
 ↪ files
import subject_info_utils as siu # Utilities for retrieving
 ↪ demographic data on subjects
# Toolset of the workgroup
import tools
# External packages
import mne
import os
import numpy as np
import datetime

def process(subject, measurement, condition, cfg, pat_info,
 ↪ run_emg_rejection, slogger):
    """
    Processes an epoched fif file using the RamosLAB pipeline
 ↪ and stores the result as a fif file.

    Arguments:
        subject (string): The pseudonym of the patient
        measurement (string): One of pre2 or post1 (the
 ↪ measurements before and after the intervention)
        condition (string): The behavioral state of the patient
 ↪ (performing a movement of the healthy arm, a movement
 ↪ attempt of the paretic arm or being at rest)
        cfg (dict): Configuration dictionary
        pat_info (dict): The patient information (a YAML file
 ↪ containing all demographic and other data of the patients)
        run_emg_rejection (bool): Determines if rejection of
 ↪ trials is also based on the EMG activity
        slogger (object): Instance of the logging mechanism
    """
```

Listing 2: Example of a processing script used in many analyses presented: The general processing pipeline for EEG data.

```
### Function definition for preprocessing EEG data for the
 ↪  coherence analysis (part 2)
# Open the source file (based on the configuration and using
 ↪  MNE)
try:
    source_dir = "{}/{}/{}/{}".format(cu.val(cfg['script'],
     ↪  'source_root_folder'), subject, measurement, condition)
    source_file = os.listdir(source_dir)[0]
    epochs = mne.read_epochs("{}/{}".format(source_dir,
     ↪  source_file))
except FileNotFoundError as e:
    print("Could not find file: {}".format(e))
    return

# Retrieve information on the patient
_, channels_healthy_arm, channels_paralyzed_arm =
 ↪  siu.get_feedback_channels(subject, pat_info)
lesion_side = siu.get_lesion_side(subject, pat_info)

# Pipeline preparation
eeg_channels_for_filter =
 ↪  ['C3','C4','P3','P4','T7','T8','F3','F4','Cz']
try:
    # Filter EEG
    pick_eeg = mne.pick_types(epochs.info, eeg=True)
    epochs.filter(cu.val(cfg['processing'],'eeg')['highpass'],
     ↪  cu.val(cfg['processing'], 'eeg')['lowpass'],
     ↪  picks=pick_eeg)

    # Filter EMG
    pick_emg = mne.pick_types(epochs.info, emg=True)
    epochs.filter(cu.val(cfg['processing'],'emg')['highpass'],
     ↪  None, picks=pick_emg)

    # Correct for EOG artifacts
    slogger.write_entry(datetime.now(), 'INFO', source_file,
     ↪  'Started EOG artifact correction')
    data_eeg_corrected, surrogate_EOG_used =
     ↪  tools.correct_for_eog_artifacts_epochs(epochs)
```

Listing 3: Example of a processing script used in many analyses presented (continued)

```
### Function definition for preprocessing EEG data for the
 ↪  coherence analysis (part 3)
# Replace EEG data with filtered data in current epochs array
chan_idc_emg = mne.pick_types(epochs.info,emg=True)
chan_idc_eeg = mne.pick_types(epochs.info,eeg=True)
chan_idc_eog = mne.pick_types(epochs.info,eog=True)
chan_idc_misc = mne.pick_types(epochs.info,misc=True)

all_types = []
all_types.extend(chan_idc_eeg)
all_types.extend(chan_idc_emg)
all_types.extend(chan_idc_eog)
all_types.extend(chan_idc_misc)

# Create new array with filtered EEG/EMG/EOG
if surrogate_EOG_used:
    args = (data_eeg_corrected, epochs.get_data()[:,
     ↪  chan_idc_emg, :])

    slogger.write_entry(datetime.now(), 'INFO', source_file,
     ↪  'Used frontal channels for artifact correction')

    # Prepare creation of new info dict. Misc channels are
     ↪  ignored
    ch_names = []
    ch_names.extend(list(np.array(
        epochs.info['ch_names'])[chan_idc_eeg]))
    ch_names.extend(list(
        np.array(epochs.info['ch_names'])[chan_idc_emg]))

    ch_types = []
    ch_types.extend(['eeg' for i in range(len(chan_idc_eeg))])
    ch_types.extend(['emg' for i in range(len(chan_idc_emg))])
```

Listing 4: Example of a processing script used in many analyses presented (continued)

```
### Function definition for preprocessing EEG data for the
 ↪  coherence analysis (part 4)
# (If proper EOG channels are present) Create new array with
 ↪  filtered EEG/EMG/EOG
else:
    data_eog = epochs.get_data()[:, chan_idc_eog, :]
    args = (data_eeg_corrected, epochs.get_data()[:,
     ↪  chan_idc_emg, :], data_eog)

    slogger.write_entry(datetime.now(), 'INFO', source_file,
     ↪  'Used EOG channels for artifact correction')

    # Prepare creation of new info dict. Misc channels are
     ↪  ignored
    ch_names = []
    ch_names.extend(list(
        np.array(epochs.info['ch_names'])[chan_idc_eeg]))
    ch_names.extend(list(
        np.array(epochs.info['ch_names'])[chan_idc_emg]))
    ch_names.extend(list(
        np.array(epochs.info['ch_names'])[chan_idc_eog]))

    ch_types = []
    ch_types.extend(['eeg' for i in range(len(chan_idc_eeg))])
    ch_types.extend(['emg' for i in range(len(chan_idc_emg))])
    ch_types.extend(['eog' for i in range(len(chan_idc_eog))])

new_info = mne.create_info(ch_names=ch_names, ch_types=ch_types,
 ↪  sfreq=epochs.info['sfreq'])
data_all_channels = np.concatenate(args, axis=1)

epochs_out = mne.EpochsArray(data=data_all_channels,
 ↪  info=new_info, events=epochs.events,
 ↪  tmin=cu.val(cfg['processing'],
 ↪  'timing_dict')['t_start_trial'])
epochs_out.set_montage(
    mne.channels.make_standard_montage("standard_1020"))

# Log errors (on ValueError and OSError exception) [omitted for
 ↪  brevity]
```

Listing 5: Example of a processing script used in many analyses presented (continued)

```
### Function definition for preprocessing EEG data for the
 ↪  coherence analysis (part 5)

# Continue preprocessing if at least one epoch remains
if len(epochs_out) > 0:
    if run_emg_rejection:
        # Run EMG rejection
        try:
            drop_log = tools.rejection_emg(
                epochs_out,
                channels_paralyzed_arm,
                channels_healthy_arm,
                cu.val(cfg['processing'], 'emg')['winsize'],
                cu.val(cfg['processing'], 'emg')['winstep'],
                cu.val(cfg['processing'], 'timing_dict'),
                cu.val(cfg['processing'],
                 ↪  'emg')['stdthreshold_artifacts'],
                cu.val(cfg['processing'],
                 ↪  'emg')['stdthreshold_movements'],
                cu.val(cfg['processing'],
                 ↪  'emg')['threshold_rejection_duration'],
                active_condition = condition
            )

            # Log dropped trials
            tools.store_drop_logs(drop_log, cu.val(cfg['script'],
             ↪  'target_root_folder') + '/drop_logs/',
             ↪  "{}-{}".format(subject, fuid), 1,
             ↪  len(epochs_out),
             ↪  np.hstack([channels_paralyzed_arm,
             ↪  channels_healthy_arm]))

# Log errors (on ValueError and OSError exception) [omitted for
 ↪  brevity]
```

Listing 6: Example of a processing script used in many analyses presented (continued)

```
### Function definition for preprocessing EEG data for the
 ↪  coherence analysis (part 6)
# Run EEG rejection
if len(epochs_out) > 0:

    try:
        slogger.write_entry(datetime.now(), 'INFO', source_file,
         ↪  'Started EEG rejection')

        drop_log = tools.rejection_eeg(
            epochs_out,
            eeg_channels_for_filter,
            cu.val(cfg['processing'],'eeg')['f_delta'],
            cu.val(cfg['processing'],'eeg')['f_gamma'],
            cu.val(cfg['processing'],'timing_dict'),
            cu.val(cfg['processing'],'eeg')['stdthreshold'],
        )

        tools.store_drop_logs(drop_log, cu.val(cfg['script'],
         ↪  'target_root_folder')+'/drop_logs/',
         ↪  "{}-{}".format(subject, fuid), 1, len(epochs_out),
         ↪  np.hstack([channels_paralyzed_arm,
         ↪  channels_healthy_arm]))
# Log errors (on ValueError and OSError exception) [omitted for
 ↪  brevity]
else:
    slogger.write_entry(datetime.now(), 'ERROR', source_file,
     ↪  'All epochs rejected due to EMG')
```

Listing 7: Example of a processing script used in many analyses presented (continued)

```
### Function definition for preprocessing EEG data for the
 ↪  coherence analysis (part 7)
    # Save preprocessed data
    target_folder = cu.val(cfg['script'], 'target_root_folder')
    out_folder = "{}/data/{}/{}/{}".format(target_folder,
     ↪  subject, measurement, condition)
    if not os.path.isdir(out_folder):
        os.makedirs(out_folder)

    fname_out = "{}/{}_{}-epo.fif".format(out_folder, subject,
     ↪  fuid)

    epochs_out.save(fname_out)
    slogger.write_entry(datetime.now(), 'FILE', source_file,
     ↪  'Created file')

# If all epochs have been dropped by the preprocessing
 ↪  procedure --> log
else:
    slogger.write_entry(datetime.now(), 'WARNING', source_file,
     ↪  'No epochs remained in current session')
```

Listing 8: Example of a processing script used in many analyses presented (continued)

permutations * 68 trials * 2 measurements * 30 subjects). I used two approaches to distributed computing in the analyses. At first, the Torque framework was used. The Torque server accept jobs submitted via the *qsub command* and distributes the workload among the available cores and balances fairly among different users. In the later stages of the analysis a framework based on an implementation of a message queue on Redis was used because it could be integrated into the existing python code more easily. RQ allows easy management of workers and failed jobs via a network interface. Both run directly from docker containers which reduces effort for the implementation of the approach on a distributed cluster. Listing 9 shows the typical pipeline in a Jupyter Notebook to run an analysis on the cluster using RQ. In cell [1] the necessary modules are loaded; "rl_prepost" contains the process that performs the actual analysis. After loading of necessary demographic information and configuration details (cell [1]) and instantiation of the logger in cell [2], the task queue that accepts processing jobs is initialized in cell [3]. Cell [4] specifies which conditions, measurements and subjects are to be processed. The job "rl_prepost.process" is dispatched to the job queue in cell [5] using the input parameters explained in listing 2.

In complex analyses such as the one on coherence presentend in chapter 5 the pipeline creates many intermediate results and files that are stored and loaded again in later processing steps. In this analysis these are thousands of files. In order to keep track of all files created I developed a **logging mechanism** ("slogger" in the above listings). The instance of slogger is called whenever a file is written to disk. For each file a unique identifier is generated that is added to the filename on disk. The creation of the file is logged in an Sqlite database. There are also other events that are logged in the database such as the starting time of execution of a specific part of the code (e.g. for determining computation time afterwards or errors during computations). Each entry contains the following fields:

- **Datetime**: The date and time (of the server) of creation of a file / entry
- **Caller**: The name of the script calling the logger
- **Level**: The "severity" level of the information, such as *INFO*, *FILE*, *WARNING*, *ERROR*
- **Context**: The context of the computation, usually the source file of the data being processed
- **Content**: The description of the event being logged
- **Comment**: A comment string
- **Config**: The configuration dictionary used for the computation
- **Fuid**: The unique file identifier generated for the output file

```
# CELL 1: Imports [ommited for brevity]

# Load config and patient information
pat_info = subject_info_utils.load_subject_info(
    '.../data/subjects_data_v191204.yaml')
cfg = config_utils.load_config(
    'config_coherence_pre-post_preprocessing.yml')
```

```
# CELL 2: Instantiate and initialize log
slogger = log_utils.Slogger('preprocess_prepost_RL',
↪  '.../slogging/slogging.db', cfg)
slogger.init_config(datetime.now())
```

```
# CELL 3: Initialize task queue
q_jobs = rq.Queue(name='jobs', connection=redis.Redis())
```

```
# CELL 4: Configure dispatching
conditions = ['paretic', 'rest', 'healthy']
measurements = ['pre1', 'pre2', 'post1', 'post2']
subjects = subject_info_utils.get_all_subjects(pat_info)
```

```
# CELL 5: Dispatch the jobs
for sub in subjects:
    for cond in conditions:
        for time in measurements:
            q_jobs.enqueue(rl_prepost.process, sub, time, cond,
            ↪  cfg, pat_info, True, slogger)
```

Listing 9: Example for a Jupyter notebook used to run part of an analysis on the computing cluster.

This logging procedure allows the user to recheck the "genesis" of each file after the analysis has completed. During the analysis this approach is helpful in order to track errors. However, one of the weaknesses of the methodology was that if too many jobs tried to access the sqlite file at the same time slogger would block execution and thus slow down the computation. Implementation of an SQL-based server with higher performance would mitigate this problem.

8.1.6 Details on the neurophysiological recordings of Dataset 1 (section 1.3.1)

Partly taken from Ray et al. (2020) and Ramos-Murguialday et al. (2013)

The EEG signals of the patients were sampled from the sixteen EEG channels (FP3, FP4, Fz, F3, F4, C3, C4, Cz, CP3, CP4, P3, P4, Pz, T7, T8, Oz) at 500 Hz. EMG data was recorded from four channels on each arm (forearm – flexor and extensor, upper-arm – biceps and triceps). The amplifier was a BrainAmp 32 by Brain Products GmbH, Munich, Germany. The ground electrode was placed at AFz and the reference at FCz. Furthermore, EOG electrodes for detection of vertical and horizontal eye movements were used.

Patients underwent a total of 17 $\pm$ 1.85 training sessions. Each session comprised 11 trial runs (totalling 165$\pm$19.5 trials). Upon hearing an auditory cue, patients had 2 seconds to get ready to try to move the paretic limb. Another auditory cue announced the beginning of a 5 second period, in which the patients could control the robotic exoskeleton using their brain signals. After this period a random inter-trial interval of between 5 and 7 seconds followed before the presentation of the next "ready" cue. All cues were auditory. The arm orthosis was a ReoGo rehabilitation robot (Motorika, Cesarea, Israel). We used a robotic orthotic system developed in-house to exert hand movements.

The neurophysiological recordings at the *pre* and *post* screenings were structured similarly. After a break of between 4 and 5 seconds the patients were cued to open their healthy hand, to try to open their paretic hand or to rest and relax all muscles. They had 5 seconds to perform and repeat the movement at their own pace. Afterwards the next break of 3 to 4 seconds was announced. The order of the trials was random and there were at minimum 17 repetitions of each trial type.

8.1.7 Implementation details of section 2.2.4

Listing 10 shows the R code that models longitudinal relative power. The dependent variable *relative power in alpha* (lesion_alpha_relative) is predicted by *time* (Session) and *subject* (Subject). This prediction assumes correlated random intercept and slope, which means that the slope can vary with the intercept. For this reason the formula contains the intercept term ("1 + Session") twice.

```
# Fit linear mixed effects models
lmem.alpha_lesion = lmer(lesion_alpha_relative ~ 1 + Session +
 ↪  (1 + Session | Subject),data=mydata)

# Retrieve coefficients from linear mixed model
cf.alpha_lesion = coef(lmem.alpha_lesion)$Subject

# Aggregate delta_fma and add to coefficients table (change of
 ↪  the clinical scale from pre to post)
cf.alpha_lesion$delta_arm = aggregate(delta_arm ~ Subject,
 ↪  mydata, mean)$delta_arm
cf.alpha_lesion$delta_hand = aggregate(delta_hand ~ Subject,
 ↪  mydata, mean)$delta_hand
cf.alpha_lesion$delta_combined = aggregate(delta_combined ~
 ↪  Subject, mydata, mean)$delta_combined
```

Listing 10: Mixed effects modeling for the longitudinal event-related power data and retrieval of the modeled coefficients.

Listing 11 shows the R code that models the coefficients that are extracted from the linear mixed-effects model. The dependent variable *change of impairment* (delta_combined) is predicted by *time* (Session) and *initial relative alpha power* (Intercept). Session and Intercept might interact, meaning that the progression of power over the course of the training might vary with the initial power.

```
# Fit linear model from coefficients
lin_m.alpha_lesion <- lm(delta_combined ~ Session * Intercept,
 ↪  data=cf.alpha_lesion)
```

Listing 11: Linear modeling of the coefficients extracted before relating the progression of relative alpha power throughout the training and the change of the clinical scale.

8.1.8 Implementation details of section 5.2

Generation of data for the MVAR process

Listings 12 and 13 show the code with which the data used in the examples in section 5.2 was generated.

Implementation details on the significance threshold paradigm

Listing 14 shows an example of an expensive computation necessary for arriving at the significance threshold of the parametric approach. This code is not making extensive use of numpy vectorization. However, it is optimized for use with the *numba* module which compiles the code just-in-time and speeds up computation that way.

8.1.9 The Multicam project

Multicam is a combination of specific computer hardware and software that enables recording of video and audio from multiple webcams. I started the Multicam project after having performed several experimental sessions of the hBMI study (see dataset 2 in section 1.3.1 and section 7.2). The intention of the work group was to record all experiments performed with patients on video. This is particularly useful to check unexpected events in the data during analysis and to confirm and prove that the subjects were actually performing the tasks that they were asked to do in retrospect.

The goal of this project was to have a plug-and-play solution for recording audio and video from multiple sources such as webcams using a graphical user interface and a programmatic interface.

Hardware

The core of the Multicam system is an Odroid XU4 single-board computer. It is housed in a self-made case that leaves enough room for a 3,5 “ hard disk drive and openings for the connectors for webcams, the network and other devices (fig. 8.3 and fig. 8.4). The Odroid single-board computer is powerful enough to capture h264-compressed video from up to four webcams at 720p resolution.

Software

The operating system used is ARCH Linux (on ARM) in a very basic configuration. It provides access to the harddisk and starts the Multicam daemon on bootup.

The Multicam software is implemented in Google’s *GO* language, which is ideally suited for network applications (The Google Go Project, 2020). The webcams are configured and controlled via GStreamer (The GStreamer Project, 2021). The software implements its own task queue that accepts tasks (such as “Start recording on webcam 2”)

```
### Generate samples of a multivariate auto-regressive process
# Imports [omitted for brevity]
# Definitions of the MVAR process
max_t = 4 # the model order
n_vecs = 5 # the number of the equations in the equation system
N = 50000 # the number of samples
# Generate normally distributed random variables
x = np.concatenate([np.random.normal(0, 1, (n_vecs,max_t)),
 ↪  np.zeros((n_vecs, N-max_t))], 1)
# Generate noise with identity covariance
noise = np.random.multivariate_normal(np.zeros(n_vecs),
 ↪  np.identity(n_vecs), N).T
# The coefficients of the equation system defined in the paper
 ↪  by Schelter and colleagues
original_coefs = np.array([
       [[ 0.6 ,  0.  ,  0.  ,  0.  ,  0.  ],
        [ 0.  ,  0.5 ,  0.  ,  0.6 ,  0.  ],
        [ 0.  ,  0.  ,  0.8 ,  0.  ,  0.  ],
        [ 0.  ,  0.  ,  0.  ,  0.5 ,  0.  ],
        [ 0.  ,  0.  ,  0.2 ,  0.  ,  0.7 ]],

       [[ 0.  ,  0.65,  0.  ,  0.  ,  0.  ],
        [ 0.  , -0.3 ,  0.  ,  0.  ,  0.  ],
        [ 0.  ,  0.  , -0.7 ,  0.  ,  0.  ],
        [ 0.  ,  0.  ,  0.9 ,  0.  ,  0.  ],
        [ 0.  ,  0.  ,  0.  ,  0.  , -0.5 ]],

       [[ 0.  ,  0.  ,  0.  ,  0.  ,  0.  ],
        [ 0.  ,  0.  ,  0.  ,  0.  ,  0.  ],
        [ 0.  ,  0.  ,  0.  ,  0.  , -0.1 ],
        [ 0.  ,  0.  ,  0.  ,  0.  ,  0.  ],
        [ 0.  ,  0.  ,  0.  ,  0.  ,  0.  ]],

       [[ 0.  ,  0.  ,  0.  ,  0.  ,  0.  ],
        [ 0.  ,  0.  , -0.3 ,  0.  ,  0.  ],
        [ 0.  ,  0.  ,  0.  ,  0.  ,  0.  ],
        [ 0.  ,  0.  ,  0.  ,  0.  ,  0.  ],
        [ 0.  ,  0.  ,  0.  ,  0.  ,  0.  ]]])
```

Listing 12: Generation of the data defined by the MVAR process.

```
### Generate samples of a multivariate auto-regressive process

# Compute a solution
for t in range(max_t, N):
    x[0,t] = .6 * x[0,t-1] + .65 * x[1,t-2] + noise[0,t]
    x[1,t] = .5 * x[1,t-1] - .3 * x[1,t-2] - .3 * x[2,t-4] + .6 *
     ↪  x[3,t-1] + noise[1,t]
    x[2,t] = .8 * x[2,t-1] - .7 * x[2,t-2] - .1 * x[4,t-3] +
     ↪  noise[2,t]
    x[3,t] = .5 * x[3,t-1] + .9 * x[2,t-2] + .4 * x[4,t-2] +
     ↪  noise[3,t]
    x[4,t] = .7 * x[4,t-1] - .5 * x[4,t-2] - .2 * x[2,t-1] +
     ↪  noise[4,t]
```

Listing 13: Generation of the data defined by the MVAR process (continued).

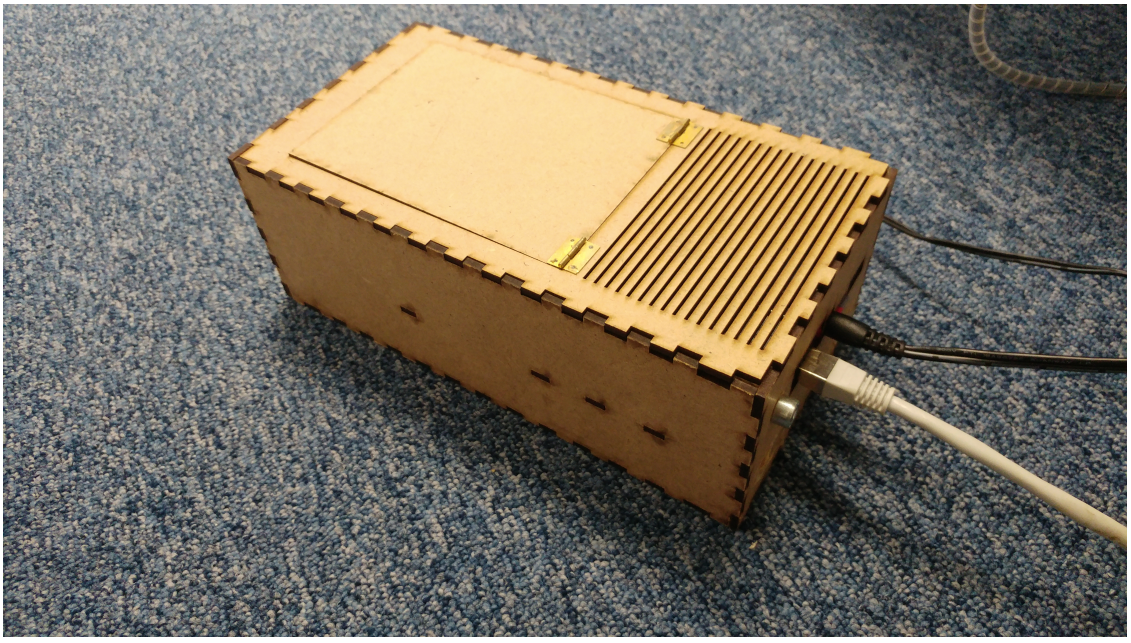

Figure 8.3: Case of the *Multicam* system. There are several connectors in the back such as DC power, Ethernet and USB. The back plate is removable in case the harddisk needs to be replaced.

```
jit(nopython=True)
def compute_matrix_C_ineff(H,p,nchan,SIGMA,N,f_ix):
    """ Compute the matrix Cij for a given frequency bin
    ↪  (Schelter et al eq. 13)
        This is the inefficient non-vectorized version
↪   optimized for just-in-time compilation with Numba

        Arguments:
            H (numpy ndarray): The matrix H
            p (int): The order of the VAR model
            nchan (int): Number of channels (i.e. number of
↪   vectors in the AR model)
            SIGMA (numpy ndarray): The covariance of the noise
↪   of the VAR model at time lag 0
            N: (int): The number of data points in the original
↪   data
            f_ix (int): The index of the frequency bin of
↪   interest

        Returns:
            Numpy ndarray: The matrix Cij for a given frequency
↪   bin
    """

    C = np.zeros((nchan, nchan))
    for ch1 in range(nchan):
        for ch2 in range(nchan):
            B = np.zeros((p, p))
            for k in range(p):
                for l in range(p):
                    B[k,l] = H[ch2+k*nchan, ch2+l*nchan]
                    ↪  *(np.cos((k+1) * f_ix) * np.cos((l+1) *
                    ↪  f_ix) + np.sin((k+1) * f_ix) *
                    ↪  np.sin((l+1) * f_ix))

            C[ch1,ch2] = SIGMA[ch1, ch1] * np.sum(B)
    return C
```

Listing 14: Computation of matrix C for retrieving the significance threshold using the parametric approach

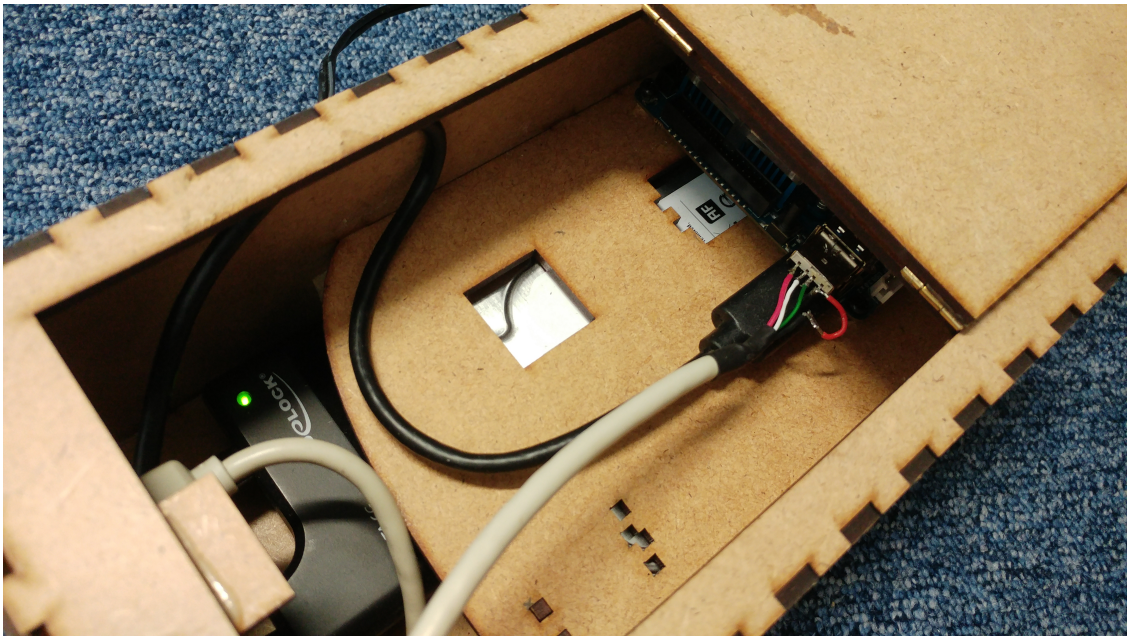

Figure 8.4: Interior of the case of the *Multicam* system. The harddisk is housed below the Odroid XU4 (right side).

from a TCP/IP command interface and via HTTP requests. Furthermore, I implemented a webserver that serves the user interface via the network and relays requests to the task queue (fig. 8.5).

The first section displays status information of the server such as date and time and free disk space. The second section shows captured images of the active webcams and the the names of the microphones that are active. In the third section the user can configure the system. For example, cameras and microphones can be included in the recording, the recording directory can be changed and the ID or name of the subject can be added. The current settings are displayed via the green bars below the cameras and in the list of microphones. The bars indicate which devices will be active during the recording. The last section allows the user to control the system manually. Here, the recording can be started or stopped and triggers can be sent to the server. These triggers are stored in a subtitle file that is displayed when the corresponding video is played back after recording. This functionality is useful for noting events during the experiment in the video file.

Once the recording is set up, it may be started manually or programmatically from any other application. In our experiments the recording was set up via the user interface and it was initiated by the experimental software. The experimental software can also send trigger information to the Multicam server directly in order to capture events down to a precision of 100 ms (such as cues being displayed to the patients).

All software was compiled into an image that can be readily copied to an SD card and that runs immediately on an Odroid XU4 computer.

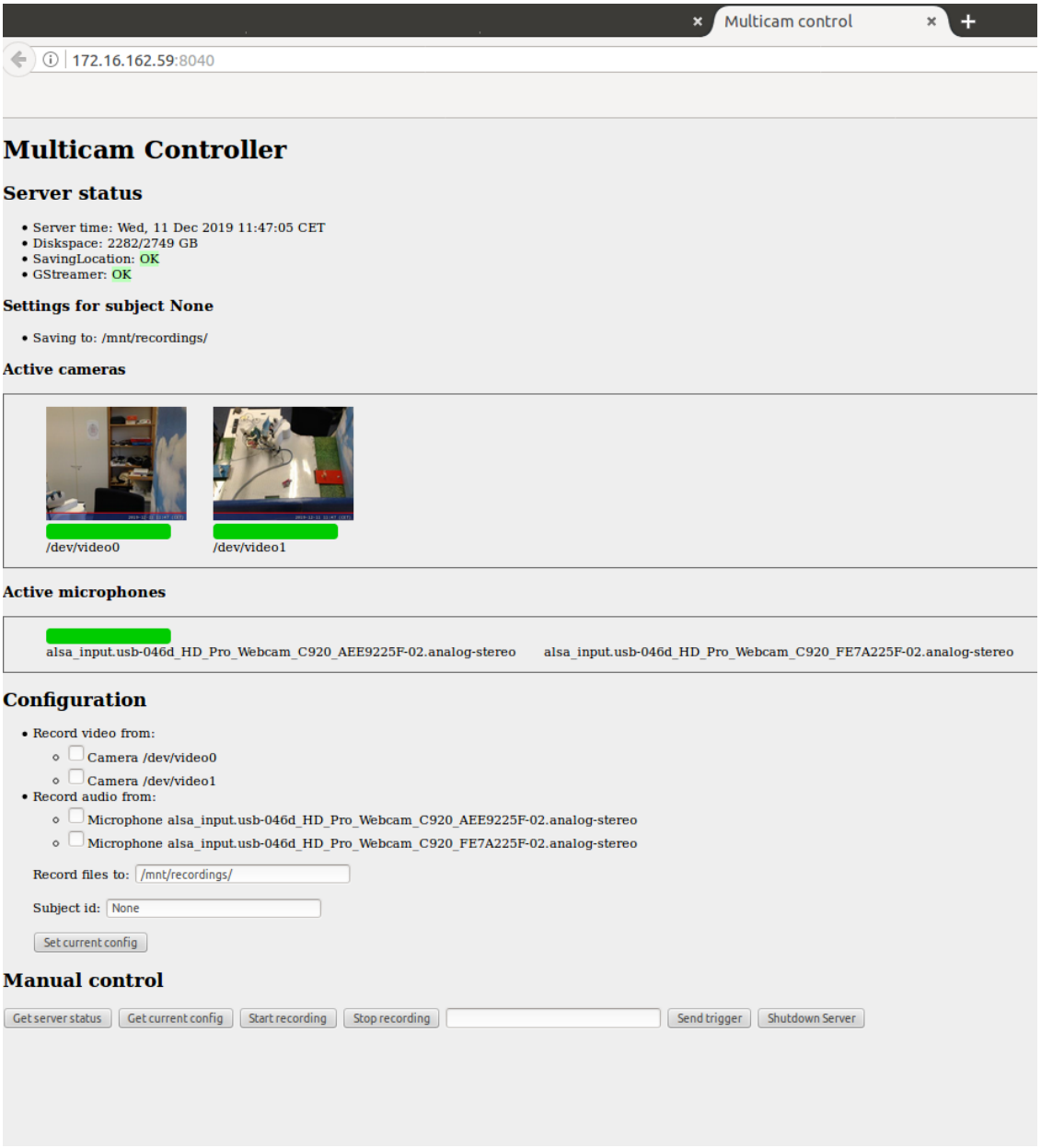

Figure 8.5: Screenshot of the user interface of the Multicam Server

The software is freely available on Github: www.github.com/ramoslab/multicam.

Multicam was used throughout the hBMI experiment (dataset 2) and during other experiments of our work group. It is a great tool complementing the usual documentation and protocols of each experiment.

8.1.10 Interactive 3D visualization of the orthosis

This is the specification of the protocol for sending commands to the interactive 3D visualization through the TCP connection (see chapter 7). All commands are strings. All commands have to end with two colons. Commands may be chained in one string.

Example

This is a valid command sent via TCP:

"ADDEXO EXOSTATIC 1,0,20::TOGGLEMAT RIGHT::ROTATECAMERA 120::"

The command would create a new static exoskeleton at x position 1 and y position 0 rotated by 20 degrees. Afterwards it would flip the configuration of the mat towards the right and rotate the camera by 120 degrees.

Command list

ADDEXO
Add a new exosekeleton.
Command structure:
ADDEXO EXOTYPE HANDEDNESS PARAMETERS
Parameters:

- Exotype - String that specifies the type of the exo to be added
- Handedness - String (either "left" or "right") that specifies the type of arm that should be added
- Parameters - Parameters needed by that exo type

DELETE
Delete an exoskeleton.
Command structure:
DELETE EXOID
Parameters:

- Exoid - Id of the exo to be removed

DATA
Send data to the exoskeletons.

Command structure:
DATA EXOID PARAMETERS
Parameters:

- Exoid - The unique Id of the exo
- Parameters - Parameters of the degrees of freedom, like for the EXOSTATIC type: BaseXpos,BaseYpos,BaseHeading,PronoRoll,IndexHeading,GroupHeading,ThumbHeading

SETCOLORBASE
Set the color of an exosekeleton.
Command structure:
SETCOLORBASE EXOID TARGET COLOR
Parameters:

- Exoid - The unique id of the exo
- Target - The part of the base to be colored. One of ”BASE” or ”ARMREST”
- Color - An RGB color in the format red,green,blue (values from 0 to 1)

SETCOLORHAND
Set the color of an exoskeleton.
Command structure:
SETCOLORHAND EXOID TARGET COLOR
Parameters:

- Exoid - The unique id of the exo
- Target - The part of the hand to be colored. One of ”SUPPRO” (Pronation/supination arc), ”THUMB”, ”FINGERGROUP”, or ”INDEX”.
- Color - An RGB color in the format red,green,blue (values from 0 to 1)

TOGGLETRANSPARENCY
Toggle transparency of an exoskeleton.
Command structure:
TOGGLETRANSPARENCY EXOID
Parameters:

- Exoid - The unique id of the exo

TOGGLEMAT
Add or change the orientation of the mat (for experiments with left or right hand).
Command structure:
TOGGLEMAT SIDE
Parameters:

- Side - Specifies which hand is being trained ('LEFT' or 'RIGHT')

SETBGCOLOR
Set the color of the background.
Command structure:
SETBGCOLOR COLOR
Parameters:

- Color - An RGB color in the format red,green,blue (values from 0 to 1)

ROTATECAMERA
Rotate the camera by some degrees around the center of the mat.
Command structure:
ROTATECAMERA ANGLE
Parameters:

- Angle - An angle in degrees

EXIT
End visualisation (close Panda3D).
Command structure:
EXIT

LOADCONFIG
Load a configuration profile file (.yml). The configuration profile can be used to set initial positions and angles of the DOFs of the exoskeleton, e.g. to individualize the visualization for the patients.
Command structure:
LOADCONFIG FILENAME
Parameters:

- Filename - The filename (without the file ending after the ".") of the calibration profile

SETCONFIG
Assign the current configuration profile to an exosekeleton.
Command structure:
SETCONFIG EXOID
Parameters:

- Exoid - The unique id of an existing exo

Exotypes

This section describes the different types of exoskeleton models available in the 3D visualisation.

EXOSTATIC

An exosekeleton that stays at a static position.
Parameters: List of positions and parameters, separated by commas.

- x-Position of the base,
- y-Position of the base,
- heading of the base,
- roll of the pronation module,
- heading of the index finger,
- heading of the finger group,
- heading of the thumb

Explanation:
This exoskeleton stays at the specified position until it is removed from the scene or the program ends. It can be used for specifying the target position the patients have to reach.

EXOKEYBOARD

An exo that is controlled by the keyboard
Parameters: - none -
Explanation: Focus the window that shows the 3D visualisation (e.g. move the mouse to the window that shows the feedback and click). All keyboard controlled exoskeletons are controlled by the keyboard. Arrow keys control heading and movement direction of the base. Pronation and supination are controlled by ”r” and ”f”, index, finger group and the thumb are controlled by ”q” and ”a”, ”w” and ”s” and ”e” and ”r”, respectively.
The function keys ”F8” through ”F12” have functionality, too. ”F8” toggles the mat, ”F9” adds a keyboard-controlled BASE, ”F10” and ”F11” add keyboard-controlled EXOs for left and right hand configuration. ”F12” removes the exos and bases in the opposite order of their creation.
The ”Escape” button exits the visualization.

EXOREALTIME

An exoskeleton that listens to data coming from a tcp connection.
Parameters: Depending on the plant type (exoseletons with hand or base only) there are 7 or 3 parameters to initialize the realtime exoskeleton.
For the exo with hand these parameters are:

- x-Position of the base,

- y-Position of the base,
- heading of the base,
- roll of the pronation module,
- heading of the index finger,
- heading of the finger group,
- heading of the thumb

For the exo with the base only these parameters are:

- x-Position of the base,
- y-Position of the base,
- heading of the base

Explanation: This exoskeleton is initialised with the specified values and controlled via tcp using the DATA command.

8.2 Contributions

This section provides detailed information on the contributions others have made to parts of this thesis.

8.2.1 Chapter 2

A great part of this chapter has been published in a peer-reviewed journal publication with contributions of co-authors as detailed below.

Title: Brain oscillatory activity as a biomarker of motor recovery in chronic stroke
Status: published as Ray *et al.* (2020). Contributions: Table 8.1.

Author	Author position	Scientific ideas	Data generation	Analysis and interpretation	Paper writing
Andreas Ray	1	50%	0%	70%	80%
Thiago Figueiredo	2	10%	0%	10%	5%

Eduardo López-Larraz	3	10%	0%	5%	0%
Niels Birbaumer	4	10%	20%	5%	5%
Ander Ramos-Murguialday	last	20%	80%	10%	10%

Table 8.1: Contributions to the scientific publication

Parts of section 2.5 have been published in a peer-reviewed conference paper with contributions of co-authors as detailed below.

Title: Movement-related brain oscillations vary with lesion location in severely paralyzed chronic stroke patients Status: published as: Ray *et al.* (2017). Contributions: Table 8.2.

Author	Author position	Scientific ideas	Data generation	Analysis and interpretation	Paper writing
Andreas Ray	1	50%	0%	80%	80%
Eduardo López-Larraz	2	10%	0%	5%	10%
Thiago Figueiredo	3	10%	0%	5%	5%
Niels Birbaumer	4	10%	20%	5%	0%
Ander Ramos-Murguialday	last	20%	80%	5%	5%

Table 8.2: Contributions to the scientific publication

8.2.2 Chapter 3

Data from multiple studies and experiments was pooled in order to produce the results. Apart from me, Dr. Ander Ramos-Murguialday, Carlos Bibián-Nogueras, Florian Helmhold, Ainhoa Insausti Delgado, Dr. Elaina Bolinger and Prof. Dr. Niels Birbaumer

contributed to data generation.

8.2.3 Chapter 4

My colleagues Dr. Ander Ramos-Murguialday, Prof. Dr. Niels Birbaumer, Carlos-Bibián Nogueras and Florian Helmhold supported analysis and interpretation in various discussions and review of the chapter.

8.2.4 Chapter 5

My colleagues Dr. Ander Ramos-Murguialday and Dr. Thiago Da Cruz Figueiredo contributed to developing the scientific ideas of this chapter. Both researchers also contributed to drafting the introduction. The first part of the analysis (section 5.2) was at first developed by Dr. Figueiredo and me and later I continued the work on my own.

8.2.5 Chapter 6

Parts of this paper have been published as a peer-reviewed conference paper with contributions of co-authors as detailed below.

Title: Electromyographic indices of muscle fatigue of a severely paralyzed chronic stroke patient undergoing upper limb motor rehabilitation Status: published as Ray *et al.* (2019). Contributions: Table 8.3.

Author	Author position	Scientific ideas	Data generation	Analysis and interpretation	Paper writing
Andreas Ray	1	50%	40%	55%	85%
Aurélien Maillot	2	20%	50%	30%	5%
Wala Jaser Mahmoud	3	10%	10%	5%	0%
Eduardo López-Larraz	4	0%	0%	5%	5%
Ander Ramos-Murguialday	last	20%	0%	5%	5%

Table 8.3: Contributions to the scientific publication

8.2.6 Chapter 7, section 7.4

Andreas Ray designed and implemented a survey for patients, caregivers and therapists, contributed to the development of the the game concept, software implementation and database design. He also collected / recorded experimental data. Florian Helmhold contributed to software implementation, database design, data collection and the development of the game concept. Dr. Ander Ramos-Murguialday was the project leader. Promotion Software GmbH contributed to the development of the game concept and implemented the game and the therapist's interface.

8.3 Descriptive statistics on the thesis

Even though this dissertation spans a proud number of pages and the efforts disembogued in some interesting publications it is merely a brief summary of all the thought processes, discussions, hours of recording neurophysiological data in the laboratory and tens of thousands of lines of code produced during the almost six years of its creation. Here, as final section of the dissertation, I would like to present descriptive statistics of the "meta data" to put the pages written into the perspective of the amount of work behind them.

8.3.1 Hours of neurophysiological data produced and analyzed

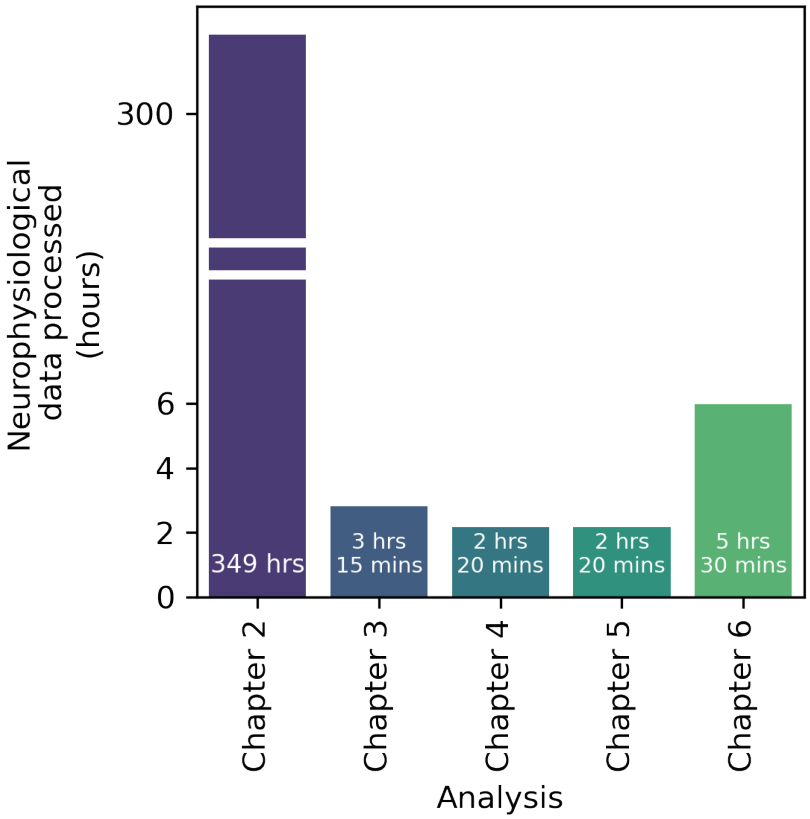

Figure 8.6: Hours of neurophysiological data processed per analysis

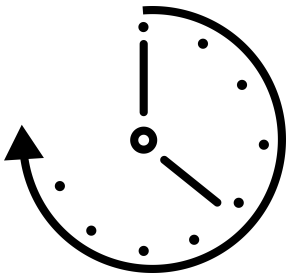

Figure 8.7: I was directly involved in or responsible for recording approximately 250 hours of neurophysiological data during 350 hours of experiments run in our laboratory.

8.3.2 Lines of code written

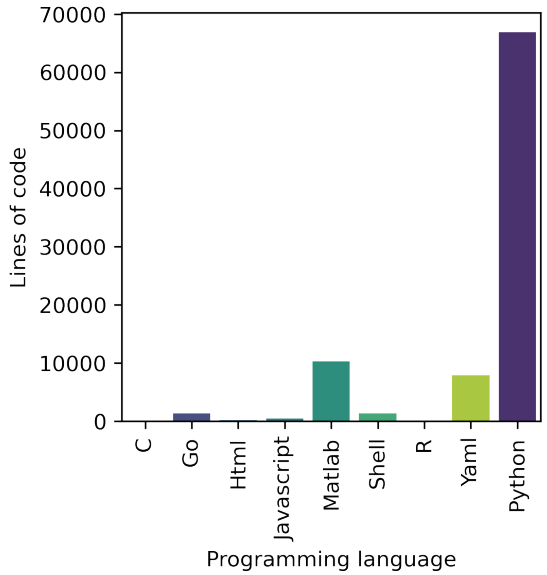

Figure 8.8: Total lines of code written for the analysis and programming projects presented in this thesis (including code of discarded analyses).

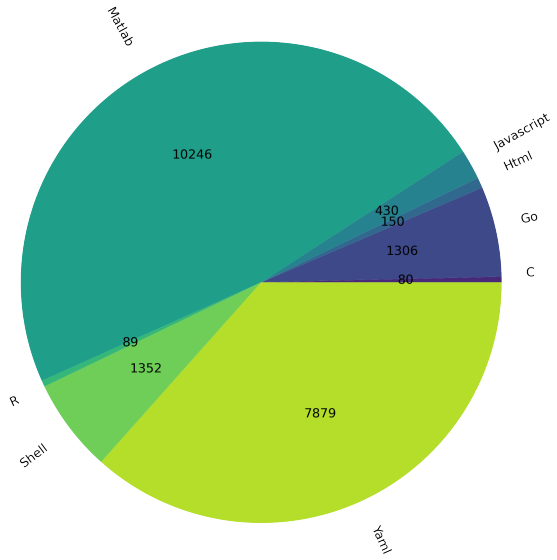

Figure 8.9: Lines of code written for the analyses and programming projects presented in this thesis in languages other than python.

8.3.3 Travel

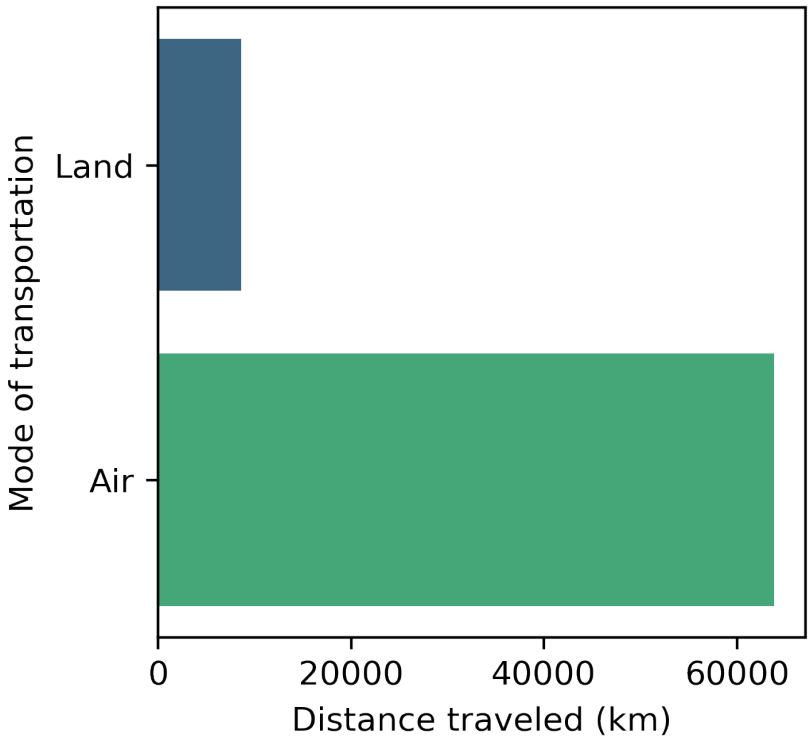

Figure 8.10: Distance traveled to conferences and scientific meetings related to this thesis.

Figure 8.11: Countries visited for conferences and scientific meetings related to this thesis.

8.3.4 Supervision

Figure 8.12: I supervised three students doing their Bachelor's or Master's thesis.

Abbreviations

ARAT	Action Research Arm Test
BMI	Brain-Machine interface
cFMA	The combined Fugl-Meyer score (a subset of the full Fugl-Meyer test only taking into account arm and hand movements)
ΔcFMA	Difference of the combined Fugl-Meyer score from before to after an intervention
DOF	Degrees of freedom
DTI	Diffusion tensor imaging
EEG	Electroencephalography
EMG	Eletromyography
ER	Emergency Room
ERD	Event-related Desynchronization
FMA	Fugl-Meyer Assessment
hBMI	Hybrid encephalographic and electromyographic Brain-Machine interface
ICU	Intensive Care Unit
LM	Linear model
MEG	Magnetoencephalography
MEP	Motor evoked potential
MRI	Magnetic resonance imaging
MVAR	Multivariate Autoregressive Model
NIHSS	National Institute of Health Stroke Scale
PDC	Partical Directed Coherence
pLC	Progressive laterality coefficient
SAFE	Shoulder abduction and finger extension (stroke scale)
SEP	Sensory evoked potential
SMR	Sensorimotor Rhythm
TCP	Transmission Control Protocol
TMS	Transcranial Magnetic stimulation

Bibliography

Aerts, H., Fias, W., Caeyenberghs, K., and Marinazzo, D. (2016). Brain networks under attack: robustness properties and the impact of lesions. *Brain*, **139**(12), 3063–3083.

Aiken, L. and West, S. (1991). *Multiple Regression: Testing and Interpreting Interactions*. SAGE.

Ang, K. K., Guan, C., Phua, K. S., Wang, C., Zhou, L., Tang, K. Y., Ephraim Joseph, G. J., Kuah, C. W. K., and Chua, K. S. G. (2014). Brain-computer interface-based robotic end effector system for wrist and hand rehabilitation: results of a three-armed randomized controlled trial for chronic stroke. *Frontiers in Neuroengineering*, **7**, 30.

Baccalá, L. A. and Sameshima, K. (2001). Partial directed coherence: a new concept in neural structure determination. *Biol. Cybern.*, **84**(6), 463–474.

Bansal, A. K., Vargas-Irwin, C. E., Truccolo, W., and Donoghue, J. P. (2011). Relationships among low-frequency local field potentials, spiking activity, and three-dimensional reach and grasp kinematics in primary motor and ventral premotor cortices. *Journal of Neurophysiology*, **105**(4), 1603–1619. PMID: 21273313.

Biasiucci, A., Leeb, R., Iturrate, I., Perdikis, S., Al-Khodairy, A., Corbet, T., Schnider, A., Schmidlin, T., Zhang, H., Bassolino, M., Viceic, D., Vuadens, P., Guggisberg, A. G., and Millán, J. d. R. (2018). Brain-actuated functional electrical stimulation elicits lasting arm motor recovery after stroke. *Nat. Commun.*, **9**(1), 2421.

Bigland-Ritchie, B., Donovan, E. F., and Roussos, C. S. (1981). Conduction velocity and EMG power spectrum changes in fatigue of sustained maximal efforts. *J. Appl. Physiol. Respir. Environ. Exerc. Physiol.*, **51**(5), 1300–1305.

Birbaumer, N. and Cohen, L. G. (2007). Brain-computer interfaces: communication and restoration of movement in paralysis. *The Journal of Physiology*, **579**, 621–636.

Birbaumer, N., Elbert, T., Canavan, A. G. M., and Rockstroh, B. (1990). Slow potentials of the cerebral cortex and behvior. *Physiological Reviews*, **70**(1), 41.

Blank, A. A., French, J. A., Pehlivan, A. U., and O'Malley, M. K. (2014). Current Trends in Robot-Assisted Upper-Limb Stroke Rehabilitation: Promoting Patient Engagement in Therapy. *Curr. Phys. Med. Rehabil. Rep.*, **2**(3), 184–195.

Bönstrup, M., Krawinkel, L., Schulz, R., Cheng, B., Feldheim, J., Thomalla, G., Cohen, L. G., and Gerloff, C. (2019). Low-Frequency Brain Oscillations Track Motor Recovery in Human Stroke. *Ann. Neurol.*, **86**(6), 853–865.

Bolinger, E., Cunningham, T. J., Payne, J. D., Bowman, M. A., Bulca, E., Born, J., and Zinke, K. (2019). Sleep's benefits to emotional processing emerge in the long term. *Cortex*, **120**, 457–470.

Boyd, L. A., Hayward, K. S., Ward, N. S., Stinear, C. M., Rosso, C., Fisher, R. J., Carter, A. R., Leff, A. P., Copland, D. A., Carey, L. M., Cohen, L. G., Basso, D. M., Maguire, J. M., and Cramer, S. C. (2017). Biomarkers of stroke recovery: Consensus-based core recommendations from the Stroke Recovery and Rehabilitation Roundtable. *International Journal of Stroke*, **12**(5), 480–493.

Breheny, P. and Burchett, W. (2016). visreg: Visualization of Regression Models. Technical report, University of Kentucky, Kentucky, USA. R package version 2.2-2.

Broetz, D., Del Grosso, N. A., Rea, M., Ramos-Murguialday, A., Soekadar, S. R., and Birbaumer, N. (2014). A new hand assessment instrument for severely affected stroke patients. *NeuroRehabilitation*, **34**, 409–427.

Buch, E., Weber, C., Cohen, L. G., Braun, C., Dimyan, M. A., Ard, T., Mellinger, J., Caria, A., Soekadar, S., Fourkas, A., and Birbaumer, N. (2008). Think to move: a neuromagnetic brain-computer interface (bci) system for chronic stroke. *Stroke*, **39**, 910–917.

Campbell, M. J., McComas, A. J., and Petito, F. (1973). Physiological changes in ageing muscles. *Journal of Neurology, Neurosurgery & Psychiatry*, **36**(2), 174–182.

Carroll, D. (1965). A quantitative test of upper extremity function. *J. Chronic Dis.*, **18**(5), 479–491.

Cauraugh, J. H. and Summers, J. J. (2005). Neural plasticity and bilateral movements: A rehabilitation approach for chronic stroke. *Prog. Neurobiol.*, **75**(5), 309–320.

Chan, D. Y. L., Chan, C. C. H., and Au, D. K. S. (2006). Motor relearning programme for stroke patients: a randomized controlled trial. *Clin. Rehabil.*, **20**(3), 191–200.

Chen, C.-C., Lee, S.-H., Wang, W.-J., Lin, Y.-C., and Su, M.-C. (2017). EEG-based motor network biomarkers for identifying target patients with stroke for upper limb rehabilitation and its construct validity. *PLoS One*, **12**(6), e0178822.

Cho, W., Vidaurre, C., Hoffmann, U., Birbaumer, N., and Ramos-Murguialday, A. (2011). Afferent and efferent activity control in the design of brain computer interfaces for motor rehabilitation. In *Proceedings of the 2011 Annual International Conference of the IEEE Engineering in Medicine and Biology Society*, pages 7310–7315. IEEE.

Coupar, F., Pollock, A., Rowe, P., Weir, C., and Langhorne, P. (2011). Predictors of upper limb recovery after stroke: a systematic review and meta-analysis. *Clin. Rehabil.*, **26**(4), 291–313.

Crichton, S. L., Bray, B. D., McKevitt, C., Rudd, A. G., and Wolfe, C. D. A. (2016). Patient outcomes up to 15 years after stroke: survival, disability, quality of life, cognition and mental health. *J. Neurol. Neurosurg. Psychiatry*, **87**(10), 1091–1098.

Crow, J. L. and Harmeling-van der Wel, B. C. (2008). Hierarchical Properties of the Motor Function Sections of the Fugl-Meyer Assessment Scale for People After Stroke: A Retrospective Study. *PTJ*, **88**(12), 1554–1567.

Cruikshank, L. C., Singhal, A., Hueppelsheuser, M., and Caplan, J. B. (2012). Theta oscillations reflect a putative neural mechanism for human sensorimotor integration. *Journal of Neurophysiology*, **107**(1), 65–77. PMID: 21975453.

Daly, J. J. and Wolpaw, J. R. (2008). Brain-computer interfaces in neurological rehabilitation. *The Lancet Neurology*, **7**, 1032–1043.

Dhamala, M., Rangarajan, G., and Ding, M. (2008). Analyzing Information Flow in Brain Networks with Nonparametric Granger Causality. *NeuroImage*, **41**(2), 354.

Dimitrov, G. V., Arabadzhiev, T. I., Mileva, K. N., Bowtell, J. L., Crichton, N., and Dimitrova, N. A. (2006). Muscle fatigue during dynamic contractions assessed by new spectral indices. *Medicine & Science in Sports & Exercise*.

Dubovik, S., Pignat, J.-M., Ptak, R., Aboulafia, T., Allet, L., Gillabert, N., Magnin, C., Albert, F., Momjian-Mayor, I., Nahum, L., Lascano, A. M., Michel, C. M., Schnider, A., and Guggisberg, A. G. (2012). The behavioral significance of coherent resting-state oscillations after stroke. *Neuroimage*, **61**(1), 249–257.

Eden, U. and Kramer, M. (2020). Spectral connectivity toolbox. Software package. https://github.com/Eden-Kramer-Lab/spectral_connectivity [Online; accessed 20. Dec. 2020].

Enoka, R. M. and Duchateau, J. (2008). Muscle fatigue: what, why and how it influences muscle function. *J. Physiol.*, **586**(1), 11–23.

Feigin, V. L., Roth, G. A., Naghavi, M., Parmar, P., Krishnamurthi, R., Chugh, S., Mensah, G. A., Norrving, B., Shiue, I., Ng, M., Estep, K., Cercy, K., Murray, C. J. L., and Forouzanfar, M. H. (2016a). Global burden of stroke and risk factors in 188 countries, during 1990–2013: a systematic analysis for the Global Burden of Disease Study 2013. *Lancet Neurol.*, **15**(9), 913–924.

Feigin, V. L., Norrving, B., George, M. G., Foltz, J. L., Roth, A., and Mensah, G. A. (2016b). Prevention of stroke: a strategic global imperative. *Nature Reviews Neurology*, **107**, 501–512.

Finnigan, S. and van Putten, M. J. A. M. (2013). Eeg in ischaemic stroke: Quantitative eeg can uniquely inform (sub-)acute prognoses and clinical management. *Clinical Neurophysiology*, **124**(1), 10–19.

Florian, G. and Pfurtscheller, G. (1995). Dynamic spectral analysis of event-related EEG data. *Electroencephalogr. Clin. Neurophysiol.*, **95**(5), 393–396.

Frolov, A. A., Mokienko, O., Lyukmanov, R., Biryukova, E., Kotov, S., Turbina, L., Nadareyshvily, G., and Bushkova, Y. (2017). Post-stroke Rehabilitation Training with a Motor-Imagery-Based Brain-Computer Interface (BCI)-Controlled Hand Exoskeleton: A Randomized Controlled Multicenter Trial. *Front. Neurosci.*, **11**, 400.

Fugl-Meyer, A. R., Jääskö, L., Leyman, I., Olsson, S., and Steglind, S. (1975). The post-stroke hemiplegic patient. A method for evaluation of physical performance. *Scand. J. Rehabil. Med.*, **7**(1), 13–31.

Gerloff, C., Bushara, K., Sailer, A., Wassermann, E. M., Chen, R., Matsuoka, T., Waldvogel, D., Wittenberg, G. F., Ishii, K., Cohen, L. G., and Hallett, M. (2006). Multimodal imaging of brain reorganization in motor areas of the contralesional hemisphere of well recovered patients after capsular stroke. *Brain*, **129**(3), 791–808.

González-Izal, M., Malanda, A., Gorostiaga, E., and Izquierdo, M. (2012). Electromyographic models to assess muscle fatigue. *Journal of Electromyography and Kinesiology*, **22**(4), 501–512.

Gramfort, A., Luessi, M., Larson, E., Engemann, D. A., Strohmeier, D., Brodbeck, C., Goj, R., Jas, M., Brooks, T., Parkkonen, L., and Hämäläinen, M. (2013). MEG and EEG data analysis with MNE-Python. *Front. Neurosci.*, **7**.

Grefkes, C., Nowak, D. A., Eickhoff, S. B., Dafotakis, M., Küst, J., Karbe, H., and Fink, G. R. (2008). Cortical connectivity after subcortical stroke assessed with functional magnetic resonance imaging. *Ann. Neurol.*, **63**(2), 236–246.

Gunkelman, J. D. and Johnstone, J. (2005). Neurofeedback and the Brain. *J. Adult Dev.*, **12**(2-3), 93–98.

Halder, S., Bensch, M., Mellinger, J., Bogdan, M., Kübler, A., Birbaumer, N., and Rosenstiel, W. (2007). Online artifact removal for brain-computer interfaces using support vector machines and blind source separation. *Computational Intelligence and Neuroscience*, **2007**, 10.

Haller, M., Donoghue, T., Peterson, E., Varma, P., Sebastian, P., Gao, R., Noto, T., Knight, R. T., Shestyuk, A., and Voytek, B. (2018). Parameterizing neural power spectra. *bioRxiv*.

Hatem, S. M., Saussez, G., Della Faille, M., Prist, V., Zhang, X., Dispa, D., and Bleyenheuft, Y. (2016). Rehabilitation of Motor Function after Stroke: A Multiple Systematic Review Focused on Techniques to Stimulate Upper Extremity Recovery. *Front. Hum. Neurosci.*, **10**.

Horwitz, B. (2003). The elusive concept of brain connectivity. *Neuroimage*, **19**(2), 466–470.

Hughes, S. W. and Crunelli, V. (2005). Thalamic mechanisms of eeg alpha rhythms and their pathological implications. *Neuroscientist*, **11**(4), 357–372.

Irastorza-Landa, N., Sarasola-Sanz, A., Insausti, A., Orthego-Isasa, I., Mahmoud, W., Ray, A., Helmhold, F., Bibian, C., López-Larraz, E., and Ramos-Murguailday, A. (2021). *Springer Handbook of Neuroengineering*, chapter Neural control of body actuators for upper limb rehabilitation in stroke patients. Springer. (forthcoming).

Jones, E. G. (2002). Thalamic circuitry and thalamocortical synchrony. *Philosophical transactions of the Royal Society London B*, **357**, 1659–1673.

Kaiser, V., Daly, I., Pichiorri, F., Mattia, D., Müller-Putz, G. R., and Neuper, C. (2012). Relationship between electrical brain responses to motor imagery and motor impairment in stroke. *Stroke*, **43**, 2735–2740.

Kim, T., Kim, S., and Lee, B. (2016). Effects of actioobservational training plus brain-computer interface-based functional electrical stimulation on paretic arm motor recovery in patient with stroke: A randomized controlled trial. *Occupational Therapy International*, **23**, 39–47.

Kirschstein, T. and Köhling, R. (2009). What is the Source of the EEG? *Clin. EEG Neurosci.*, **40**(3), 146–149.

Klimesch, W., Sauseng, P., and Hanslmayr, S. (2007). Eeg alpha oscillations: The inhibition-timing hypothesis. *Brain Research Reviews*, **53**(1), 63–88.

Komi, P. V. and Tesch, P. (1979). EMG frequency spectrum, muscle structure, and fatigue during dynamic contractions in man. *Europ. J. Appl. Physiol.*, **42**(1), 41–50.

Krakauer, J. W. (2006). Motor learning: its relevance to stroke recovery and neurorehabilitation. *Current Opinion in Neurology*, **19**(1).

Krakauer, J. W. and Carmichael, S. T. (2017). *Broken Movement*, volume 1. MIT Press.

Krauth, R., Schwertner, J., Vogt, S., Lindquist, S., Sailer, M., Sickert, A., Lamprecht, J., Perdikis, S., Corbet, T., Millán, J. D. R., Hinrichs, H., Heinze, H.-J., and Sweeney-Reed, C. M. (2019). Cortico-Muscular Coherence Is Reduced Acutely Post-stroke and Increases Bilaterally During Motor Recovery: A Pilot Study. *Front. Neurol.*, **10**, 126.

Kuhlman, W. N. (1978). Functional topography of the human mu rhythm. *Electroencephalography and Clinical Neurophysiology*, **44**(1), 83–93.

Lang, C. E., MacDonald, J. R., Reisman, D. S., Boyd, L., Jacobson Kimberley, T., Schindler-Ivens, S. M., Hornby, T. G., Ross, S. A., and Scheets, P. L. (2009). Observation of Amounts of Movement Practice Provided During Stroke Rehabilitation. *Arch. Phys. Med. Rehabil.*, **90**(10), 1692–1698.

Lang, C. E., Strube, M. J., Bland, D., Waddell, K. J., Cherry-Allen, K. M., Nudo, R. J., Dromerick, A. W., and Birkenmeier, R. L. (2016). Dose response of task-specific upper limb training in people at least 6 months poststroke: A phase ii, single-blind, randomized, controlled trial. *Annals of Neurology*, **80**, 342–354.

Leeb, R., Biasiucci, A., Schmidlin, T., Corbet, T., Vuadens, P., and del R. Millán, J. (2016). Bci controlled neuromuscular electrical stimulation enables sustained motor recovery in chronic stroke victims. In *Proceedings of the 6th International Brain-Computer Interface Meeting*. Proceedings of the 6th International Brain-Computer Interface Meeting.

Lindenberg, R., Renga, V., Zhu, L. L., Nair, D., and Schlaug, G. (2010). Bihemispheric brain stimulation facilitates motor recovery in chronic stroke patients. *Neurology*, **75**(24), 2176–2184.

Lo, A. C., Guarino, P. D., Richards, L. G., Haselkorn, J. K., Wittenberg, G. F., Federman, D. G., Ringer, R. J., Wagner, T. H., Krebs, H. I., Volpe, B. T., Bever, C. T., Bravata, D. M., Duncan, P. W., Corn, B. H., Maffucci, A. D., Nadeau, S. E., Conroy, S. S., Powell, J. M., Huang, G. D., and Peduzzi, P. (2010). Robot-Assisted Therapy for Long-Term Upper-Limb Impairment after Stroke. *N. Engl. J. Med.*, **362**(19), 1772–1783.

López-Larraz, E., Montesano, L., Gil-Agudo, n., Minguez, J., and Oliviero, A. (2015). Evolution of EEG Motor Rhythms after Spinal Cord Injury: A Longitudinal Study. *PLoS One*, **10**, 7.

López-Larraz, E., Sarasola-Sanz, A., Irastorza-Landa, N., Birbaumer, N., and Ramos-Murguialday, A. (2018a). Brain-machine interfaces for rehabilitation in stroke: A review. *NeuroRehabilitation*, **43**(1), 77–97.

López-Larraz, E., Figueiredo, T. C., Insausti-Delgado, A., Ziemann, U., Birbaumer, N., and Ramos-Murguialday, A. (2018b). Event-related desynchronization during movement attempt and execution in severely paralyzed stroke patients: An artifact removal relevance analysis. *NeuroImage: Clinical*, **20**, 972–986.

Luengo-Fernandez, R., Violato, M., Candio, P., and Leal, J. (2019). Economic burden of stroke across Europe: A population-based cost analysis. *European Stroke Journal*, **5**(1), 17–25.

Mane, R., Chew, E., Phua, K. S., Ang, K. K., Robinson, N., Vinod, A. P., and Guan, C. (2019). Prognostic and Monitory EEG-Biomarkers for BCI Upper-limb Stroke Rehabilitation. *IEEE Transaction on Neural System Rehabilitation Engineering*.

Maris, E. and Oostenveld, R. (2007). Nonparametric statistical testing of EEG- and MEG-data. *J. Neurosci. Methods*, **164**(1), 177–190.

MATLAB (2020). *Matlab*. The MathWorks Inc., Natick, Massachusetts.

Mima, T., Toma, K., Koshy, B., and Hallett, M. (2001). Coherence Between Cortical and Muscular Activities After Subcortical Stroke. *Stroke*, **32**(11), 2597–2601.

Mokienko, O., Lyukmanov, R., Chernikova, L., Suponeva, N., Piradov, M., and Frolov, A. (2016). Brain-computer interface: the first clinical experience in russia. *Human Physiology*, **42**, 31–39.

Mollazadeh, M., Aggarwal, V., Davidson, A. G., Law, A. J., Thakor, N. V., and Schieber, M. H. (2011). Spatiotemporal Variation of Multiple Neurophysiological Signals in the Primary Motor Cortex during Dexterous Reach-to-Grasp Movements. *J. Neurosci.*, **31**(43), 15531–15543.

Murase, M., Duque, J., Mazzocchio, R., and Cohen, L. G. (2004). Influence of interhemispheric interactions on motor function in chronic stroke. *Ann Neurol.*, **55**(3), 400–409.

Murphy, T. H. and Corbett, D. (2009). Plasticity during stroke recovery: from synapse to behaviour. *Nat. Rev. Neurosci.*, **10**(12), 861–872.

Naros, G. and Gharabaghi, A. (2015). Reinforcement learning of self-regulated β-oscillations for motor restoration in chronic stroke. *Front. Hum. Neurosci.*, **9**.

Nicolo, P., Rizk, S., Magnin, C., Pietro, M. D., Schnider, A., and Guggisberg, A. G. (2015). Coherent neural oscillations predict future motor and language improvement after stroke. *Brain*, **138**(10), 3048–3060.

Niedermeyer, E. and Lopes da Silva, F., editors (2005). *Electroencephalography: basic principles, clinical applications, and related fields*. Lippincott Williams & Wilkins, 5th edition.

Nielsen, J. B. and Conway, B. A. (2008). Reduction of common motoneuronal drive on the affected side during walking in hemiplegic stroke patients. *Clinical Neurophysiology*, **119**, 2813–2818.

NIH Fact Sheet authors (2020). Post-stroke rehabilitation fact sheet. Research report, National Institute of Health.

Ono, T., Shindo, K., Kawashima, K., Ota, N., Ito, M., Ota, T., Mukaino, M., Fujiwara, T., Kimura, A., Liu, M., and Ushiba, J. (2014). Brain-computer interface with somatosensory feedback improves functional recovery from severe hemiplegia due to chronic stroke. *Frontiers in Neuroengineering*, **7**, 19.

Oostenveld, R., Fries, P., Maris, E., and Schoffelen, J.-M. (2010). FieldTrip: Open Source Software for Advanced Analysis of MEG, EEG, and Invasive Electrophysiological Data. *Comput. Intell. Neurosci.*, **2011**.

Park, W., Kwon, G. H., Kim, Y.-H., Lee, J.-H., and Kim, L. (2016). Eeg response varies with lesion location in patients with chronic stroke. *Journal of NeuroEngineering and Rehabilitation*, **13**(1), 21.

Pellegrino, G., Tomasevic, L., Tombini, M., Assenza, G., Bravi, M., Sterzi, S., Giacobbe, V., Zollo, L., Guglielmelli, E., Cavallo, G., Vernieri, F., and Tecchio, F. (2012). Interhemispheric coupling changes associate with motor improvements after robotic stroke rehabilitation. *Restor. Neurol. Neurosci.*, **30**(6), 497–510.

Perrin, F., Bertrand, O., and Pernier, J. (1978). Scalp Current Density Mapping: Value and Estimation from Potential Data. *IEEE Trans. Biomed. Eng.*, **BME-34**(4), 283–288.

Perrin, F., Pernier, J., Bertrand, O., and Echallier, J. F. (1989). Spherical splines for scalp potential and current density mapping. *Electroencephalogr. Clin. Neurophysiol.*, **72**(2), 184–187.

Pfurtscheller, G. (2003). Induced Oscillations in the Alpha Band: Functional Meaning. *Epilepsia*, **44**(s12), 2–8.

Pfurtscheller, G. and Lopes da Silva, F. (1999). Event-related eeg/meg synchronization and desynchronization: basic principles. *Clinical Neurophysiology*, **110**, 1842–1857.

Philips, G. R., Daly, J. J., and Príncipe, J. C. (2017). Topographical measures of functional connectivity as biomarkers for post-stroke motor recovery. *J. NeuroEng. Rehabil.*, **14**(1), 67.

Pichiorri, F., Morone, G., Petti, M., Toppi, J., Pisotta, I., Molinari, M., Paolucci, S., Inghilleri, M., Astolfi, L., Cincotti, F., and Mattia, D. (2015). Brain–computer interface boosts motor imagery practice during stroke recovery. *Ann. Neurol.*, **77**(5), 851–865.

Pichiorri, F., Petti, M., Caschera, S., Astolfi, L., Cincotti, F., and Mattia, D. (2017). An eeg index of sensorimotor interhemispheric coupling after unilateral stroke: clinical and neurophysiological study. *The European journal of neuroscience*, **47**, 158–163.

Pineiro, R., Pendlebury, S. T., Smith, S., Flitney, D., Blamire, A. M., Styles, P., and Matthews, P. M. (2000). Relating MRI Changes to Motor Deficit After Ischemic Stroke by Segmentation of Functional Motor Pathways. *Stroke*, **31**, 672–679.

Pivik, R. T., Broughton, R. J., Davidson, R. J., Fox, N., and Nuwer, M. R. (1993). Guidelines for the recording and quantitative analysis of electroencephalographic activity in research contexts. *Psychophysiology*, **30**, 547–558.

Platz, T., Kim, I.-H., Engel, U., Kieselbach, A., and Mauritz, K.-H. (2002). Brain activation pattern as assessed with multi-modal eeg analysis predict motor recovery among stroke patients with mild arm paresis who receive the arm ability training. *Restorative Neurology and Neuroscience*, **20**, 21–35.

Platz, T., Pinkowski, C., van Wijck, F., Kim, I.-H., di Bella, P., and Johnson, G. (2005). Reliability and validity of arm function assessment with standardized guidelines for the Fugl-Meyer Test, Action Research Arm Test and Box and Block Test: a multicentre study. *Clin. Rehabil.*, **19**(4), 404–411.

Project Jupyter (2020). Juypter. Software package. [https://jupyter.org/index.html; Online; accessed 20. Dec. 2020].

Rabiller, G., He, J.-W., Nishijima, Y., Wong, A., and Liu, J. (2015). Perturbation of brain oscillations after ischemic stroke: A potential biomarker for post-stroke function and therapy. *International Journal of Molecular Sciences*, **16**(10), 25605–25640.

Ramanathan, D. S., Guo, L., Gulati, T., Davidson, G., Hishinuma, A. K., Won, S.-J., Knight, R. T., Chang, E. F., Swanson, R. A., and Ganguly, K. (2018). Low-frequency cortical activity is a neuromodulatory target that tracks recovery after stroke. *Nat. Med.*, **24**(8), 1257–1267.

Ramos-Murguialday, A. and Birbaumer, N. (2015). Brain oscillatory signatures of motor tasks. *J Neurophysiology*, **113**, 3663–3682.

Ramos-Murguialday, A., Soares, E., and Birbaumer, N. (2010). Upper limb emg artifact rejection in motor sensitive bcis. In *Proceedings of the 2010 Anual International Conference of The IEEE Engineering in Medicine and Biology*. IEEE.

Ramos-Murguialday, A., Schürholz, M., Caggiano, V., Wildgruber, M., Caria, A., Hammer, E. M., Halder, S., and Birbaumer, N. (2012). Proprioceptive Feedback and Brain Computer Interface (BCI) Based Neuroprostheses. *PLoS One*, **7**(10), e47048.

Ramos-Murguialday, A., Broetz, D., Rea, M., Läer, L., Yilmaz, O., Brasil, F. L., Liberati, G., Curado, M., Garcia-Cossio, E., Vyziotis, A., Cho, W., Agostini, M., Soares, E., Soekadar, S., Caria, A., Cohen, L. G., and Birbaumer, N. (2013). Brain-machine interface in chronic stroke rehabilitation: A controlled study. *Annals of Neurology*, **74**(1), 100–108.

Ramos-Murguialday, A., Curado, M., Broetz, D., Yilmaz, z., Brasil, F., Liberati, G., Garcia-Cossio, E., Cho, W., Caria, A., Cohen, L., and Birbaumer, N. (2019). Brain-machine-interface in chronic stroke: Randomised trial long-term follow-up. *Neurorehabilitation and Neural Repair*, **33**, 188–198.

Ray, A., Maillot, A., Helmhold, F., Jaser Mahmoud, W., López-Larraz, E., and Ramos-Murguialday, A. (2019). Electromyographic indices of muscle fatigue of a severely paralyzed chronic stroke patient undergoing upper limb motor rehabilitation. In *2019 9th Annual International IEEE EMBS Conference on Neural Engineering*, pages 126–129. © 2022 IEEE. Reprinted, with permission.

Ray, A. M., López-Larraz, E., Figueiredo, T. C., Birbaumer, N., and Ramos-Murguialday, A. (2017). Movement-related brain oscillations vary with lesion location in severely paralyzed chronic stroke patients. In *Proceedings of the 2017 39th Annual International Conference of the IEEE Engineering in Medicine and Biology Society (EMBC)*, pages 1664–1667. © 2022 IEEE. Reprinted, with permission. peer-reviewed.

Ray, A. M., López-Larraz, E., Birbaumer, N., and Ramos-Murguialday, A. (2018). Stability of the individual alpha oscillations in severely paralyzed stroke patients undergoing brain-machine interface training. In *11th FENS Forum of Neuroscience*.

Ray, A. M., Figueiredo, T. D. C., López-Larraz, E., Birbaumer, N., and Ramos-Murguialday, A. (2020). Brain oscillatory activity as a biomarker of motor recovery in chronic stroke. *Human Brain Mapping*, **41**, 1296–1308.

Rehme, A. K., Eickhoff, S. B., Wang, L. E., Fink, G. R., and Grefkes, C. (2011). Dynamic causal modeling of cortical activity from the acute to the chronic stage after stroke. *NeuroImage*, **55**(3), 1147–1158.

Reinkensmeyer, D. J., Burdet, E., Casadio, M., Krakauer, J. W., Kwakkel, G., Lang, C. E., Swinnen, S. P., Ward, N. S., and Schweighofer, N. (2016). Computational neurorehabilitation: modeling plasticity and learning to predict recovery. *Journal of NeuroEngineering and Rehabilitation*, **13**, 42.

Ribary, U., Doesburg, S. M., and Ward, L. M. (2014). Thalamocortical Network Dynamics: A Framework for Typical/Atypical Cortical Oscillations and Connectivity. *Magnetoencephalography*, pages 429–449.

Riley, N. A. and Bilodeau, M. (2002). Changes in upper limb joint torque patterns and EMG signals with fatigue following a stroke. *Disabil. Rehabil.*, **24**(18), 961–969.

Rodgers, H., Bosomworth, H., Krebs, H. I., van Wijck, F., Howel, D., Wilson, N., Aird, L., Alvarado, N., Andole, S., Cohen, D. L., Dawson, J., Fernandez-Garcia, C., Finch, T., Ford, G. A., Francis, R., Hogg, S., Hughes, N., Price, C. I., Ternent, L., Turner, D. L., Vale, L., Wilkes, S., and Shaw, L. (2019). Robot assisted training for the upper limb after stroke (RATULS): a multicentre randomised controlled trial. *The Lancet*, **394**(10192), 51–62.

Rogers, D. R. and MacIsaac, D. T. (2013). A comparison of EMG-based muscle fatigue assessments during dynamic contractions. *J. Electromyogr. Kinesiol.*, **23**(5), 1004–1011.

Rossiter, H. E., Boudrias, M.-H., and Ward, N. S. (2014). Do movement-related beta oscillations change after stroke. *Journal of Neurophysiology*, **119**, 2053–2058.

Saes, M., Meskers, C. G. M., Daffertshofer, A., de Munck, J. C., Kwakkel, G., and van Wegen, E. E. H. (2019). How does upper extremity Fugl-Meyer motor score relate to resting-state EEG in chronic stroke? A power spectral density analysis. *Clinical Neurophysiology*, **130**(5), 856–862.

Sakkalis, V. (2011). Review of advanced techniques for the estimation of brain connectivity measured with EEG/MEG. *Comput. Biol. Med.*, **41**(12), 1110–1117.

Sarasola Sanz, A., Irastorza Landa, N., Shiman, F., López-Larraz, E., Spüler, M., Birbaumer, N., and Ramos-Murguialday, A. (2015). Emg-based multi-joint kinematics decoding for robot-aided rehabilitation therapies. In *2015 IEEE International Conference on Rehabilitation Robotics (ICORR)*.

Sarasola-Sanz, A., Irastorza-Landa, N., López-Larraz, E., Bibián, C., Helmhold, F., Broetz, D., Birbaumer, N., and Ramos-Murguialday, A. (2017). A hybrid brain-machine interface based on EEG and EMG activity for the motor rehabilitation of stroke patients. *2017 International Conference on Rehabilitation Robotics (ICORR)*, pages 895–900.

Scally, B., Burke, M. R., Bunce, D., and Delvenne, J.-F. (2018). Resting-state EEG power and connectivity are associated with alpha peak frequency slowing in healthy aging. *Neurobiol. Aging*, **71**, 149–155.

Schelter, B., Winterhalder, M., Eichler, M., Peifer, M., Hellwig, B., Guschlbauer, B., Lücking, C. H., Dahlhaus, R., and Timmer, J. (2005). Testing for directed influences among neural signals using partial directed coherence. *J. Neurosci. Methods*, **152**(1), 210–219.

Schlögl, A., Keinrath, C., Zimmermann, D., Scherer, R., Leeb, R., and Pfurtscheller, G. (2007). A fully automated correction method of EOG artifacts in EEG recordings. *Clin. Neurophysiol.*, **118**(1), 98–104.

Schoffelen, J.-M., Oostenveld, R., and Fries, P. (2005). Neuronal Coherence as a Mechanism of Effective Corticospinal Interaction. *Science*, **308**(5718), 111–113.

Scott, S. H. (2004). Optimal feedback control and the neural basis of volitional motor control. *Nature Reviews Neuroscience*, **5**(7), 532–545.

Shetty, V., Morrell, C. H., and Najjar, S. S. (2009). Modeling a cross-sectional response variable with longitudinal predictors. *Journal of Applied Statistics*, **36**, 611–619.

Steriade, M., Gloor, P., Llinas, R. R., da Silva, F. L., and Mesulam, M.-M. (1990). Basic mechanisms of cerebral rhythmic activities. *Electroencephalography and Clinical Neurophysiology*, **76**(6), 481–508.

Stevens, E., Emmett, E., Wang, Y., McKevitt, C., and Wolfe, C. (2017). The burden of stroke in europe. Technical report, Stroke Alliance for Europe.

Stinear, C. M. (2017). Prediction of motor recovery after stroke: advances in biomarkers. *Lancet Neurol.*, **16**(10), 826–836.

Stinear, C. M., Byblow, W. D., Ackerley, S. J., Smith, M.-C., Borges, V. M., and Barber, P. A. (2017). PREP2: A biomarker-based algorithm for predicting upper limb function after stroke. *Ann. Clin. Transl. Neurol.*, **4**(11), 811–820.

Strimbu, K. and Tavel, J. A. (2010). What are Biomarkers? *Current opinion in HIV and AIDS*, **5**(6), 463.

Susi, T., Johannesson, M., and Backlund, P. (2007). *Serious Games : An Overview*. Institutionen för kommunikation och information.

Takemi, M., Masakado, Y., Liu, M., and Ushiba, J. (2015). Smr erd represents the excitability of human spiral motoneurons. *Neuroscience*, **297**, 58–67.

Tangwiriyasakul, C., Verhagen, R., Rutten, W. L. C., and van Putten, M. J. A. M. (2014). Temporal evolution of event-related desynchronization in acute stroke: A pilot study. *Clinical Neurophysiology*, **125**(6), 1112–1120.

Taub, E., Crago, J. E., Burgio, L. D., Groomes, T. E., Cook, E. W., DeLuca, S. C., and Miller, N. E. (1994). An operant approach to rehabilitation medicine: Overcoming learned nonuse by shaping. *Journal of the Experimental Analysis of Behavior*, **61**, 281–293.

Tedesco Triccas, L., Meyer, S., Mantini, D., Camilleri, K., Falzon, O., Camilleri, T., and Verheyden, G. (2019). A systematic review investigating the relationship of electroencephalography and magnetoencephalography measurements with sensorimotor upper limb impairments after stroke. *J. Neurosci. Methods*, **311**, 318–330.

The Google Go Project (2020). The Go Programming Language. Language reference, Google. https://golang.org [Online; accessed 20. Dec. 2020].

The GStreamer Project (2021). GStreamer: open source multimedia framework. Software package. https://gstreamer.freedesktop.org.

Thibaut, A., Simis, M., Battistella, L. R., Fanciullacci, C., Bertolucci, F., Huerta-Gutierrez, R., Chisari, C., and Fregni, F. (2017). Using Brain Oscillations and Corticospinal Excitability to Understand and Predict Post-Stroke Motor Function. *Front. Neurol.*, **8**.

Van der Meer, T., Te Grotenhuis, M., and Pelzer, B. (2010). Influential Cases in Multilevel Modeling: A Methodological Comment. *Am. Sociol. Rev.*, **75**(1), 173–178.

van Putten, M. J. A. M. (2007). The revised brain symmetry index. *Clinical Neurophysiology*, **118**, 2362–2367.

Van Rossum, G. and Drake, F. L. (2009). *Python 3 Reference Manual*. CreateSpace, Scotts Valley, CA.

van Wijk, B. C. M., Beek, P. J., and Daffertshofer, A. (2012). Neural synchrony within the motor system: what have we learned so far? *Front. Hum. Neurosci.*, **6**.

Verbeke, G. and Molenbergs, G. (2001). *Linear Mixed Models for Longitudinal Data*. Springer.

Ward, N. S., Brander, F., and Kelly, K. (2019). Intensive upper limb neurorehabilitation in chronic stroke: outcomes from the Queen Square programme. *J. Neurol. Neurosurg. Psychiatry*, **90**(5), 498–506.

Wendt, H. W. (1972). Dealing with a common problem in social science: A simplified rank-biserial coefficient of correlation based on the statistic.

Werner, W., Martin, D., Claus, F., and Gerhard, S. (2001). Onset Detection in Surface Electromyographic Signals: A Systematic Comparison of Methods. *EURASIP Journal on Advances in Signal Processing*, **2001**(2).

Whitall, J., Waller, S. M., Sorkin, J. D., Forrester, L. W., Macko, R. F., Hanley, D. F., Goldberg, A. P., and Luft, A. (2010). Bilateral and Unilateral Arm Training Improve Motor Function Through Differing Neuroplastic Mechanisms: A Single-Blinded Randomized Controlled Trial. *Neurorehabil. Neural Repair*, **25**(2), 118–129.

WHO (1993). Biomarkers and risk assessment: concepts and principles (EHC 155, 1993). Research report, World Health Organization. http://www.inchem.org/documents/ehc/ehc/ehc155.htm [Online; accessed 20. Oct. 2020].

WHO (2001). WHO International Classification of Functioning, Disability and Health (ICF). Research report, World Health Organization. https://www.who.int/classifications/icf/en [Online; accessed 20. Oct. 2020].

Wijngaarden, J. B. G. v., Zucca, R., Finnigan, S., and Verschure, P. F. M. J. (2016). The Impact of Cortical Lesions on Thalamo-Cortical Network Dynamics after Acute Ischaemic Stroke: A Combined Experimental and Theoretical Study. *PLOS Computational Biology*, **12**(8), e1005048.

Wolf, S. L., Catlin, P. A., Ellis, M., Archer, A. L., Morgan, B., and Piacentino, A. (2001). Assessing Wolf Motor Function Test as Outcome Measure for Research in Patients After Stroke. *Stroke*, **32**, 1635–1639.

Womelsdorf, T. and Fries, P. (2006). Neuronal coherence during selective attentional processing and sensory–motor integration. *J. Physiol.-Paris*, **100**(4), 182–193.

Wu, J., Quinlan, E. B., Dodakian, L., McKenzie, A., Kathuria, N., Zhou, R. J., Augsburger, R., See, J., Le, V. H., Srinivasan, R., and Cramer, S. C. (2015). Connectivity measures are robust biomarkers of cortical function and plasticity after stroke. *Brain*, **138**(8), 2359–2369.

Wu, J., Srinivasan, R., Burke Quinlan, E., Solodkin, A., Small, S. L., and Cramer, S. C. (2016). Utility of eeg measures of brain function in patients with acute stroke. *Journal of Neurophysiology*, **115**(5), 2399–2405. PMID: 26936984.

Wu, W., Sun, J., Jin, Z., Guo, X., Qiu, Y., Zhu, Y., and Tong, S. (2011). Impaired neuronal synchrony after focal ischemic stroke in elderly patients. *Clinical Neurophysiology*, **122**(1), 21–26.

Yaml (2020). The Official YAML Web Site. Language reference, The Yaml project. https://yaml.org [Online; accessed 20. Dec. 2020].

Yilmaz, O., Birbaumer, N., and Ramos-Murguialday, A. (2015). Movement related slow cortical potentials in severely paralyzed chronic stroke patients. *Frontiers in Human Neuroscience*, **8**.

Ziemann, U., Desideri, D., Belardinelli, P., and Zrenner, C. (2018). Brain-State Dependent Stimulation in Human Motor Cortex for Plasticity Induction Using EEG-TMS. In *Converging Clinical and Engineering Research on Neurorehabilitation III*, pages 1057–1060. Springer.

Zyda, M. (2005). From visual simulation to virtual reality to games. *Computer*, **38**(9), 25–32.